Universidad del País Vasco
Euskal Herriko Unibertsitatea

The Use of Mesenchymal Stromal Cells and Tissue-Engineered Blood Vessels for Seamless Implant Integration

Beatriz Hernaez Estrada
NanoBioCel Group, Laboratory of Pharmaceutics
University of the Basque Country (UPV/EHU)
Faculty of Pharmacy
Vitoria-Gasteiz 2021

ACKNOWLEDGEMENTS TO THE FINANCIAL SUPPORT

Beatriz Hernaez Estrada sincerely appreciates and acknowledges the predoctoral grant provided by the Basque Government. This doctoral thesis has been founded by the Spanish Ministry of Economy and Competitiveness (SAF2017-82292-R), Basque Government (Consolidated Groups IT907-16) and by the U.S National Institute of Health (NHLBI R01 HL130037).

The following chapter has already been submitted to international journal:

Immunomodulatory Biomaterials for Tissue Repair:

This chapter has been submited to Chemical Reviews
Manuscript ID: cr-2020-00895d

GLOSSARY

a**Hep^{-N}**	Heparin desulphated at the -N position
AT-MSC	Adipose Tissue-Derived Mesenchymal Stromal Cell
AT-RvD1	Aspirin-Triggered Resolvin D1
BCA	Bicinchoninic Acid Assay
BM	Bone Marrow
BSA	Bovine Serum Albumin
$CaSiO_3$-β-TCP	Calcium silicate/β-tricalcium Phosphate
CCL2	C–C Motif Chemokine Ligand 2
cDNA	Complementary Deoxyribonucleic Acid
CFSE	5,6-Carboxyfluorescein Diacetate *N*-Succinimidyl Ester
CG	Carboxymethyl chitosan hydrogel layer
Ch	Chitosan
CMCS	Carboxymethyl Chitosan
coll-nHA	Collagen-Nanohydroxyapatite
CSF1R	Colony Stimulating Factor Receptor 1
DAMPs	Damage Associated Molecular Patterns
DBM	Decellularized Bone Matrix
DCs	Dendritic Cells
dECM	Decellularized Extracellular Matrix
DM	Diabetes Mellitus
DMEM	Dulbecco´s Modified Eagle´s Medium
DMSO	Dimethyl Sulfoxide

DPBS	Dulbecco's Phosphate-Buffered Saline
DTT	Dithiothreitol
ECL	Enhanced Chemiluminescence
ECM	Extracellular Matrix
EDTA	Ethylenediaminetetraacetic Acid
FBGC	Foreign Body Giant Cells
FBR	Foreign Body Response
FBS	Fetal Bovine Serum
FcR	Fc Receptor
FDA	United States Food and Drug Administration
FGF	Fibroblast Growth Factor
FKN	Fractalkine
FlowSOM	Clustering Analysis
FUE	Follicular Unit Extraction
GAL9	Galectin 9
GFP	Green Fluorescent Protein
GvHD	Graft versus Host Disease
H&E	Hematoxylin & Eosin
HAMECs	Human Adipose Microvascular Endothelial Cells
HAp	Hydroxyapatite
HA-PEI	Hyaluronic acid-poly(ethyleneimine)
HF	Hair Follicle
HF-MSCs	Hair Follicle-Derived MSCs
HGF	Hepatocyte Growth Factor
HI-FCS	Heat-Inactivated Calf Serum
HRP	Horseradish Peroxidase
HS	Hyaluronan-Sulfate
IBD	Inflammatory Bowel Disease
IDO	Indoleamine 2,3-dioxygenase

IFNγ	Interferon gamma
IL-10	Interleukin-10
IL-13	Interleukin-13
IL-17	Interleukin-17
IL1RN	Interleukin-1-Receptor Antagonist
IL-4	Interleukin-4
iPSCs	Pluripotent Stem Cells
ISCT	International Society for Cellular Therapy
LPS	Lipopolysaccharide
MAA	Methacrylic Acid
MaFIA	Macrophage Fas-Induced Apoptosis
MCP-1	Monocyte Chemoattractant Protein-1
M-CSF	Macrophage Colony Stimulating Factor
MFI	Median Fluorescent Intensity
MHC-I	Major Histocompatibility Class I
MHC-II	Type-II Major Histocompatibility Complex
MI	Myocardial infarction
miRNAs	microRNAs
MS	Multiple Sclerosis
MSC	Mesenchymal Stem Cells
MVF	Tissue-Derived Microvascular Fragments
NETs	Neutrophil Extracellular Traps
NHG-MS	Nanofibrous heparin modified gelatin microsphere
NK Cells	Natural Killer Cells
ONF	Oronasal Fistula

OPTN/ SRTR	Organ Procurement and Transplantation Network/ Scientific Registry of Transplants Recipients
P(LLA-CL)	Poly(L-lactic acid-co-e-caprolactone)
PA	Polyacrylamide
PAMPs	Pathogen-Associated Molecular Patterns
PBMCs	Peripheral Blood Mononuclear Cells
PBS	Phosphate-Buffered Saline
PBT	Poly(butylene terephthalate)
PCA	Principal Component Analysis
PCBMA	Poly(carboxybetaine methacrylate)
PCL	Poly(ε-caprolactone)
PDL	Poly-D-lysine
PDMS	Poly(dimethyl siloxane)
PDO	Polydioxanone
PE	Polyethylene
PEEK	Polyetheretherketone
PEG	Poly(ethylene glycol)
PEGDA	Poly(ethylene glycol) diacrylate
PEOT	Poly(ethylene oxide terephthalate)
PET	Polyethylene terephthalate
PEU	Polyetherurethane
PFPE	Perfluoropolyether
PGA	Polyglycolide
pHEMA	Poly(2-hydroxyethyl methacrylate)
pHEMA-co-MMA	Poly(2-hydroxyethyl methacrylate-co-methacrylic) acid
PLA	Polylactic acid
PLAGA	Poly(lactic-co-glycolic-acid)
PLGA	Poly(D, L-lactide-co-glycolic) acid

PLGA-MSV	Poly(lactic-co-glycolic acid)-Multistage Silicon Particles
PLL	Poly-L-lysine
PLLA	Poly(L-lactic)
PMMA	Poly(methyl methacrylate)
PMPC	Poly(2-methacryloyloxyethyl phosphorylcholine)
PP	Polypropylene
PPFU	Poly (propylene fumarate) polyurethane
PRP	Platelet-Rich Plasma
PS	Phosphatidylserine
PTFE	Poly(tetrafluoroethylene)
PTGS2	Prostaglandin-endoperoxide synthase 2/ Cyclooxygenase 2
PUU-POSS	Poly(urea-urethane) and Polyhedral Oligomeric Silsesquioxane
PVA	Poly(vinyl alcohol)
RGD	Arginylglycylaspartic Acid
rHCI	Recombinant Human Collagen Type I
rHCIII	Recombinant Human Collagen Type III
RIPA	Radioimmunoprecipitation Assay
RNA	Ribonucleic Acid
RT-qPCR	Reverse Transcription Quantitative Polymerase Chain Reaction
S1P	Sphingosine 1-Phosphate Receptor

SASP	Senescence Associated Secretory Phenotype
SDF-1	Stromal Derived Factors
SHG	Second Harmonic Generation
T/DOP	Poly (dopamine) coated $Ti0_2$
TGF-β	Transforming Growth- β Factor
TGX	Greater Transfer Efficacy
Th17	T helper 17
THG	Third Harmonic Generation
TNF	Tumor Necrosis Factor
TNT	Titania Nanotube
TriMap	Dimensionality Reduction Algorithm
tSNE	t-Distribution Stochastic Neighborhood Embedding
UBM	Urinary Bladder Matrix
UMAP	Uniform Manifold Approximation and Projection
VEGF	Vascular Endotelial Growth Factor
α**SMA**	α-Smooth Muscle Actin
β**CaP**	Calcium Phosphate

Index

1

Introduction

This chapter has been submited to Chemical Reviews
Manuscript ID: cr-2020-00895d

Immunomodulatory Biomaterials for Tissue Repair

Ricardo Whitaker[1*], Beatriz Hernaez-Estrada[1,2*], Rosa Maria Hernandez[2,3,4] Edorta Santos-Vizcaino[2,3,4], Kara L. Spiller[1]

[1]School of Biomedical Engineering, Science, and Health Systems, Drexel University, Philadelphia, USA

[2]NanoBioCel Research Group, Laboratory of Pharmaceutics, School of Pharmacy, University of the Basque Country (UPV/EHU), Vitoria-Gasteiz, Spain

[3]Networking Research Centre of Bioengineering, Biomaterials and Nanomedicine (CIBER-BBN).

[4]Bioaraba, NanoBioCel Research Group, Vitoria-Gasteiz, Spain

*Equal Contribution

Abstract

All implanted biomaterials are targets of the host's immune system. With increasing understanding of the beneficial roles of immune cells in wound healing, in recent years it has become possible to leverage interactions with immune cells to improve the function and efficacy of biomaterials intended to augment tissue repair. In this review we will discuss the major immune cells that mediate the inflammatory response to biomaterials, with a focus on how biomaterials can be designed to modulate immune cell behavior to promote biomaterial-tissue integration. In particular, the intentional activation of immune cells with controlled timing and modulation of their interactions with other cell types involved in wound healing have emerged as key strategies to improve biomaterial efficacy. To this end, biomaterial structure can be designed to manipulate immune cell phenotype, and controlled release of immunomodulators can maximize a wound healing response. Finally, we discuss current challenges, such as limitations in the use of *in vitro* studies to model the immune response, and future directions for understanding and controlling the biomaterial-immune system interface, including the application of new imaging tools, the discovery of new cellular targets, and novel techniques for immune cell reprogramming.

Graphical Abstract

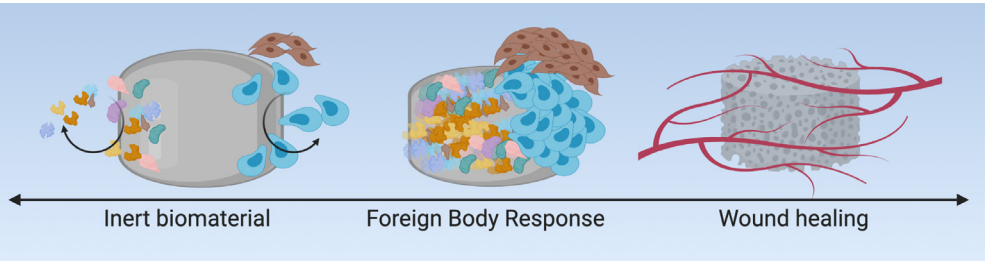

1. Introduction

Besides the need to ensure proper functionality of the device, biomaterials must address the immediate and aggressive response from the innate immune system upon implantation. An uncontrolled inflammatory response to implants results in fibrous encapsulation, which can lead to implant failure. However, the inflammatory response is also essential for wound healing and tissue repair, making it critical for biomaterial-tissue integration. Understanding the differences in these inflammatory responses is key to designing successful biomaterials. Here, we will review these two main types of inflammatory response to biomaterials (foreign body response and biomaterial-tissue integration) (Figure 1), with a focus on design strategies to promote beneficial interactions with the innate immune system.

Although we will briefly touch on the role of the adaptive immune system in these processes, the adaptive immune response to biomaterials, including its modulation for the development of vaccines and other immunotherapies, is considered to be outside the scope of this article.

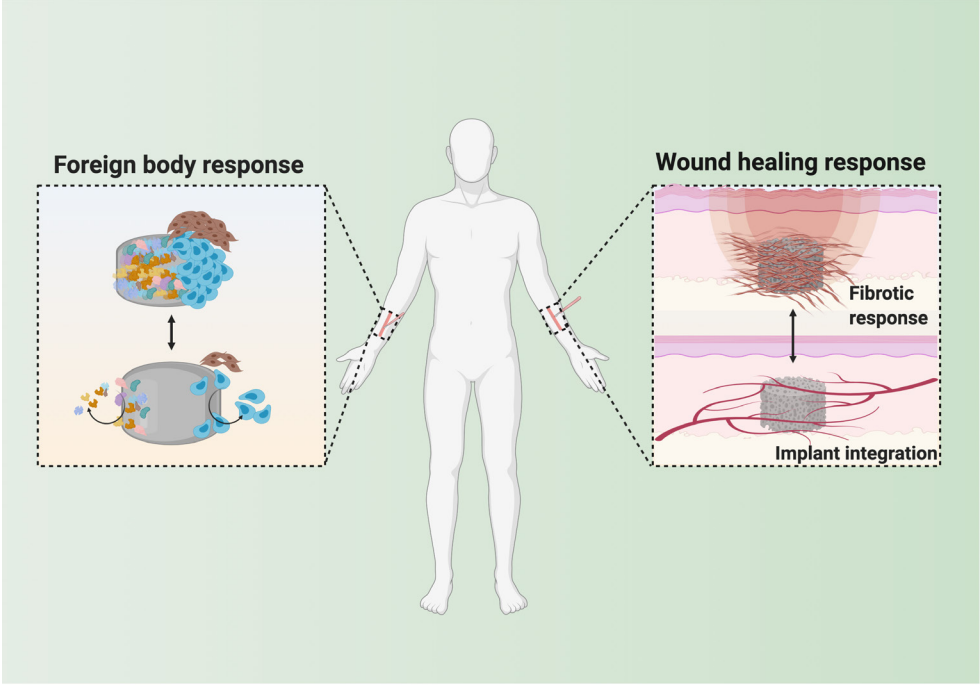

Figure 1: Overview. The two main types of inflammatory responses to implanted biomaterials include the foreign body response and biomaterial-tissue integration.

2. The Foreign Body Response

All implanted biomaterials trigger the foreign body response (FBR) to a certain extent, which is characterized by protein adsorption, the recruitment of innate immune cells like neutrophils, monocytes, and macrophages, fusion of macrophages into foreign body giant cells (FBGCs), and ultimately the formation of a fibrous capsule by FBGCs and/or fibroblasts that isolates the implant from the surrounding tissue. This process is generally considered detrimental for most biomaterials, and therefore numerous strategies have been developed to interfere with one or more steps, with the level of success measured in terms of either reduction in fibrous capsule thickness or vascularization and integration, depending on the intended purpose of the implant (Figure 2). Vascularization and integration are considered a wound healing-type response and will be covered in detail later in this review.

2.1. Major cells and steps of the FBR

2.1.1. Protein adsorption

The first step in the FBR is the adsorption of serum proteins to the surface of the biomaterial, which creates a chemoattractant gradient for neutrophils and macrophages. This process is called opsonization. Among the numerous proteins capable of signaling foreign objects, the most potent is the complement protein family, especially C3 and C5, which fragment to coat the foreign material and to recruit circulating immune cells — for a thorough review, see reference [1] —. Additional opsonins include albumin, globulins, and fibronectin, among others.

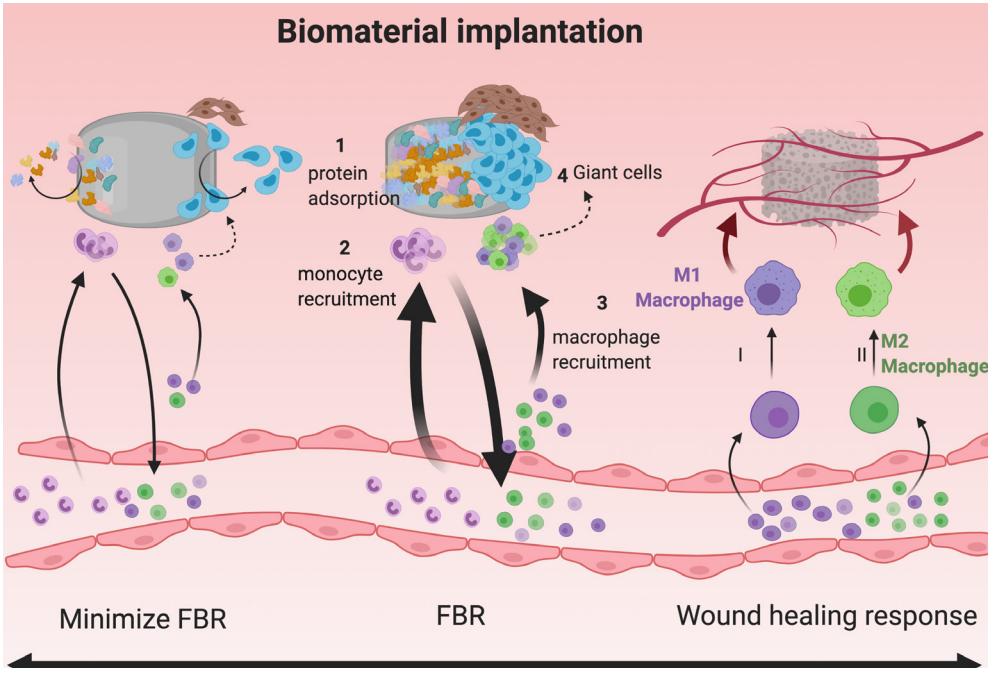

Figure 2: Continuum of the foreign body response to implants, which ranges from minimal interactions (left), to fibrous encapsulation (center), to biomaterial-tissue integration (right).

In general, higher levels of protein adsorption lead to increased cell adhesion and, therefore, increased fibrous encapsulation. As a result, a common strategy to reduce fibrous encapsulation of biomaterials is to coat them with non-fouling polymers. For example, zwitterionic polymers, which adsorb very low levels of proteins due to their highly hydrophilic nature and neutral charge, have shown promise for minimizing the FBR [2-7]. Zhang et al. prepared zwitterionic hydrogels from poly(carboxybetaine methacrylate) (PCBMA) and compared them to poly(2-hydroxyethyl)methacrylate (pHEMA) hydrogels implanted subcutaneously in mice for up to three months [7]. The fibrous capsule surrounding the zwitterionic hydrogels was much thinner and had lower collagen density compared to the pHEMA hydrogels. Liu et al. extended this strategy to minimize the FBR to hydrogels containing transplanted islet cells for the treatment of type 1 diabetes [6]. The group found that conjugation of zwitterionic moieties to alginate hydrogel particles resulted in less cell adhesion and improved survival of the transplanted islets in a diabetic mouse model and in larger animal models.

However, several studies have added complexity to this dogma. For example, fibronectin is a serum protein that is critical for cell adhesion. Therefore, if increased cell adhesion always resulted in increased fibrous capsule thickness, then biomaterials implanted in the absence of fibronectin would be expected to result in thinner fibrous capsules. In contrast, Keselowski and colleagues found increased fibrous encapsulation of polyethylene terephthalate (PET) discs implanted subcutaneously in mice that were genetically deficient for fibronectin [8]. These mice also showed a threefold increase in multinucleated cell formation around the implant compared to wild type controls, despite no differences in leukocyte recruitment. In another study, Swartzlander et al. showed that poly(ethylene glycol) (PEG)-based hydrogels conjugated with RGD, the major cell-binding motif found in fibronectin, were encapsulated in thinner fibrous capsules compared to controls without RGD, even though they adsorbed similar levels of protein and supported higher levels of macrophage adhesion *in vitro* and *in vivo* [9]. Thus, although reduced protein adsorption is generally associated with lower levels of fibrous capsule formation, future studies are needed to elucidate the complexities of the system with respect to specific proteins.

2.1.2. Neutrophil recruitment

Neutrophils, the most abundant cell type of the innate immune system, develop mainly within the bone marrow, where they mature and are released into the blood stream under healthy conditions. Under inflammatory conditions, including an injury or implantation of a biomaterial, this process is potentiated, leading to greater extravasation to affected tissues. Neutrophils are phagocytic cells and are capable of degrading foreign objects up to a certain volume [10]. While in a healthy wound neutrophils are generally cleared within a few days, they have been shown to persist for several weeks around implanted biomaterials [11]. The consequences of this persistence are poorly understood. To investigate the role of neutrophils in the FBR, Jhunjhunwala et al. implanted five different microparticles poly(lactic-co-glycolic acid) or PLGA, glass, polystyrene, poly(methyl methacrylate) or PMMA, and alginate of different sizes and shapes into the peritoneal cavity of mice [11]. While under homeostatic conditions the peritoneum is comprised mostly of resident macrophages, B cells, and T cells, the implantation of these materials provoked a 30- to 500-fold increase in the neutrophil population to around 8-35 % of the total

cell population, depending on the implanted material. Further evaluation of PMMA, polystyrene and alginate microparticles demonstrated that neutrophils deposited extracellular material on these implants resembling neutrophil extracellular traps (NETs), or tangles of protein and chromatin that neutrophils use to kill invading pathogens. To investigate the implications of NET formation in the FBR, Fetz et al. examined the response of neutrophils to electrospun scaffolds of poly(dimethyl siloxane) (PDO) of two different fiber sizes with or without collagen incorporation *in vitro* and *in vivo* [12]. *In vitro* studies with human neutrophils showed that the degree of NETosis, regardless of fiber size, was decreased in collagen-containing scaffolds. In addition, scaffolds with larger fibers (1-2 μm) stimulated less NETosis compared to those with smaller fibers (0.25-0.35 μm). When implanted subcutaneously in rats, the smaller fiber scaffolds resulted in fibrous encapsulation, while the larger diameter fiber scaffolds led to partial tissue integration, suggesting that NETosis propagates the FBR and hinders biomaterial-tissue integration.

On the other hand, a study by Doloff et al. suggested that neutrophils do not play a major role in fibrous capsule formation [13]. The authors depleted mice of neutrophils using a Ly6G-neutralizing antibody and then implanted alginate microparticles. Fibrous encapsulation was unaffected, although the alginate microparticles did appear to clump together more, which the team had previously found to be associated with fibrous encapsulation of other biomaterials [14]. These results suggest that neutrophils do play some role in the immune response to implants, although their precise functions are still poorly understood.

2.1.3. Macrophages and foreign body giant cells

Concurrent with neutrophils, monocytes and macrophages are also recruited to the site of injury, where they play indispensable and complex roles in the ensuing steps of the FBR. Monocytes, the precursors of macrophages, are formed and matured inside the bone marrow until they are released into the blood stream in response to injury. Monocytes are recruited to sites of injury via chemoattractive factors released from dying cells, and they differentiate into macrophages upon extravasation into the injured tissue. In addition to these blood-derived monocytes, long-lived tissue-resident macrophages are also recruited to sites of injury [15], although their specific role in the FBR is not yet known. Monocytes and macrophages are highly plastic, existing as numerous distinct phenotypes. Some phenotypes may

be more detrimental or beneficial than others, but the exact roles of each distinct phenotype in the FBR are still poorly understood — for review, see [16] —. While regulated macrophage activity is critical for biomaterial-tissue integration, which will be discussed in detail later in this review, macrophage fusion into foreign body giant cells (FBGCs) and their role in the propagation of fibrous capsule formation are hallmarks of the FBR.

In addition to many studies noting the prevalence of macrophages within the fibrous capsule surrounding biomaterials, several studies have shown that depletion of monocytes/macrophages via administration of clodronate liposomes inhibits fibrous encapsulation of biomaterials [13, 17, 18]. Pharmacologic inhibition of the major receptor responsible for macrophage maturation, CSF1R, also inhibited macrophage recruitment and the ensuing FBR [13]. However, one study suggested that the mechanism of macrophage depletion may directly impact the results, because macrophage depletion in macrophage fas-induced apoptosis (MaFIA) mice actually increased fibrous encapsulation surrounding subcutaneously implanted collagen scaffolds [19], even though a previous study in the same mouse strain showed the opposite effects when alginate microparticles were implanted intraperitoneally [14]. The discrepancies between these studies strongly suggest that the method of macrophage depletion has an as-yet poorly understood effect on macrophage behavior.

The FBR's requirement of macrophage fusion into FBGCs has also been challenged. Kyriakides and colleagues analyzed the impact of macrophage fusion on the fibrous encapsulation of subcutaneously implanted poly(vinyl alcohol) (PVA) sponges in mice genetically deficient for CCL2 (aka monocyte chemoattractant protein 1, MCP-1), which reduced macrophage fusion around the implants without affecting the total numbers of monocytes or macrophages [20]. Despite the reduction in macrophage fusion, collagen deposition and the thickness of the fibrous capsules surrounding the implants did not differ between groups, although scaffolds implanted in CCL2-null mice were 50 % more intact compared to wild-type mice, indicating a role for FBGCs in biomaterial degradation. Together, these results suggest that while macrophages and their fusion into FBGCs do mediate fibrous capsule formation, there must be redundancy in the system such that fibrous encapsulation can occur without these steps.

In addition to fusing into FBGCs to mediate biomaterial degradation, macrophages may also play a direct role in extracellular matrix deposition during the fibrous capsule formation process. Using MacGreen transgenic mice in which macrophages fluoresce green, Mooney et al. found that macrophages participating in the fibrous encapsulation of cubes of boiled egg whites implanted intraperitoneally accounted for 80 % of the cells expressing α-smooth muscle actin (αSMA), a typical fibroblast marker, and further suggested that these cells should be classified as "fibroblastoid" macrophages [18]. Similarly, Kuehlmann et al. analyzed the cellular composition of the fibrous capsule surrounding silicone implants in human and mice, and found that myeloid cells and not fibroblasts were the main depositors of extracellular matrix [21]. In summary, macrophages are indispensable for formation of the fibrous capsule, but their exact functions are still being elucidated.

2.1.4. Other innate immune cells

Mast cells, another type of innate immune cell that is critical for wound healing, have been sparsely investigated for their effects on the FBR. Mast cells are distributed throughout connective tissues and in close proximity with blood vessels. Their activation results in release of their α-granules, stimulating recruitment of neutrophils and macrophages. Farrugia et al. investigated the infiltration of mast cells into chitosan or cellulose sponges subcutaneously implanted in rats [22]. Immunohistochemical analysis of mast cell markers confirmed their presence around blood vessels and within the fibrous capsule, depending on the material type. However, other studies have questioned the importance of mast cells in the FBR, because the fibrous capsules surrounding PEG-PLGA, polyetherurethane (PEU), or polyethylene terapthalate (PET) implants were unaffected in mast cell-deficient mice [23, 24]. Similarly, natural killer (NK) cells, another innate immune cell that is important in wound healing, appear to be dispensable for the FBR [24], although this effect has not been widely studied.

It is also not clear to what extent dendritic cells (DCs) play a role in the FBR. DCs are considered the messengers between the innate and adaptive immune systems. One study found no evidence of DC presence in the fibrous capsules surrounding nylon meshes implanted subcutaneously in mice [25], while another showed that DCs were present in the fibrous capsule surrounding ECM scaffolds implanted subcutaneously in mice [26]. Another study retrieved DCs from

PVA sponges implanted subcutaneously in rats, finding that these cells accounted from 5-38 % of total inflammatory cells within the sponge and that their capacity to promote T cell activation decreased over time of implantation [27]. It may be that DCs do not typically reside in fibrous capsules, but instead interact with biomaterials and then migrate to lymph nodes, where they activate T cells, which further influence the FBR (for review of DC-biomaterial interactions, see references [28, 29]). This process is the main reason why DCs are considered detrimental for the survival of allogenic or xenogeneic cell-based therapies [30]. Biomaterial-mediated modulation of DC behavior is an active area of investigation for immunotherapies targeting the adaptive immune system, such as vaccines and cancer treatments [31, 32]. Collectively, these studies suggest that several innate immune cells that are clearly involved in wound healing may be less important in the fibrous encapsulation process of the FBR.

2.1.5. Adaptive immune cells

Lymphocytes, including T cells and B cells, are part of the adaptive immune system and provide delayed and specific responses to invading pathogens. Their role in the FBR is a subject of debate. Some reports show that adaptive immune cells contribute to the formation of fibrous capsules, while others report minimal effects. For example, Rodriguez and colleagues investigated the FBR to elastane 80A (PEU), silicone rubber, and PET samples implanted subcutaneously in nude (T cell-deficient) Balb/c mice [33]. Leukocyte recruitment, FBGC formation, and cytokine levels were similar in immunocompetent and nude mice, although fibrous capsules were not measured. On the other hand, Doloff et al. showed that fibrosis surrounding subcutaneously injected alginate microparticles was increased in mice genetically depleted of B cells (IghM-/-), while it was decreased in mice deficient for both B and T cells (Rag2-/-) compared to wild type mice, although these effects may have resulted from concomitant effects on macrophage behavior [13]. Sadtler and colleagues showed that the immune cell profile in response to ECM scaffolds differed in Rag1-/- mice, which are also deficient for B and T cells [26]. In particular, ECM scaffolds injected into Rag1-/- mice recruited higher levels of macrophages ($CD11b^+$ $F4/80^+$) within one week compared to wild-type mice. Therefore, it appears likely that the role of adaptive immune cells in the FBR is mediated through actions on macrophages, but further investigation in this area is needed and could provide new insights into how biomaterials can be tailored to control the FBR.

2.2. Effect of biomaterial properties on the FBR

Given the importance of the FBR for dictating the success or failure of implanted biomaterials, many studies have investigated how microstructure, surface chemistry, surface coating and topography of implants affect the FBR. In general, there are two main and very different goals behind decreasing fibrous encapsulation: 1) to minimize interactions with surrounding tissue, which would be desirable for removable biomaterial implants like sensors, and 2) to increase neovascularization and tissue integration, which is important for biomaterials intended to promote tissue repair (Figure 2).

2.2.1. Minimizing the FBR

With respect to inhibiting the FBR in order to minimize interactions with surrounding tissue, the general approach has been to decrease protein adsorption via coating with non-fouling polymers, as previously described in section 2.1.1. On the other hand, coating biomaterials with poly(ethylene glycol) (PEG), which generally decreases protein adsorption, has resulted in mixed effects, with some reporting decreased fibrous capsule thickness [34, 35] and others reporting increased fibrous capsules [36] or no effects [37]. For a thorough review on the use of PEG to modulate fibrous capsule formation, see reference [38].

Studies have shown that fibrous capsule formation can be reduced through physicochemical alterations of implants, including chemical and topographical modifications and polymer coatings, ultimately resulting in more inert biomaterials (Table 1). Other strategies to decrease fibrous encapsulation via promoting integration with surrounding tissue, which are generally applied to macroporous biomaterials, will be discussed in detail in section 2.2.2.

Table 1. Studies that investigated the effects of structural or surface modifications of biomaterials on minimizing the FBR.

Type	Animal Model	Polymer	Modification	Outcome	Ref.
Molded Substrate	Sprague Dawley Rats Subcutaneous	Silicone	Surface Modification	Ta-Si implant significantly reduced fibrous capsule thickness compared to bare silicone	[41]
	Goats Subcutaneous	PLA / Silicone	Topography	Compared to smooth control, microgrooves promoted thicker capsules, while roughened surfaces reduced fibrous capsule thickness	[43]
	Swiss Webster Mice Subcutaneous	PTFE	Topography	Substrates with greatest internodal distance reduced fibrous capsule thickness	[45]
Films	BALB/c Mice Subcutaneous	PP	Surface Modification	-CF and -COOH reduced fibrous capsule thickness compared to -OH and -NH_2	[42]
Scaffolds	Sprague Dawley Rats Subcutaneous	PCL	Topography	Aligned fibers reduced fibrous capsule thickness compared to random fibers group and film control	[44]
Hydrogel	Sprague Dawley Rats Intraperitoneally	PLL / PEG	Surface Coating	PEG-coated PLL particles reduced inflammatory response and fibrous capsule formation compared to uncoated PLL particles	[46]
Membrane	Minipig Intramuscular	Cellulose	Surface Coating	Cellulose-coated pacemakers reduced fibrous capsule thickness compared to uncoated controls	[47]
Medical Grade Silicone	Sprague Dawley Rats Subcutaneous	Silk / Silicone	Surface Coating	Silk-coated implants reduced fibrous capsule thickness compared to uncoated controls	[48]
Medical Grade Silicone	Sprague Dawley Rats Subcutaneous	PMPC / Silicone	Surface Coating	PMPC-coated group reduced fibrous capsule thickness compared to uncoated controls	[49]

TPP = Polypropylene. PLA = Poly(lactic acid). PCL = Poly(ε-caprolactone). PTFE = Poly(tetrafluoroethylene). PEG = Poly(Ethylene Glycol). PLL = Poly(l-Lysine). PMPC = Poly(2-methacryloyloxyethyl phosphorylcholine)

Some biomaterials have been discovered that result in such low levels of fibrous capsule formation that they appear nearly inert. Veiseh et al. showed that relatively simple design considerations such as implant shape and size have strong effects on the FBR [14]. They implanted alginate hydrogel spheres intraperitoneally in mice using eight groups with diameters ranging from 0.3 mm to 1.9 mm. Increasing sphere size resulted in reduced cell adhesion and formation of fibrous tissue, as measured by staining for α-SMA and F-actin and gene expression analysis of fibrosis-associated genes. Remarkably, this effect held true for a wide range of biomaterials, including hydrogels, ceramics, metals, and plastics. In addition, the reduced fibrous encapsulation around alginate hydrogel spheres of 1.5 mm diameter compared to 0.5 mm was confirmed following subcutaneous implantation for 14 days in non-human primates.

Another approach sought to discover polymer modifications that reduced the FBR via a high throughput, unbiased screen. Vegas et al. created a library of 774 chemical modifications to alginate hydrogels, implanted them subcutaneously in mice, and used a fluorescent probe for cathepsin activity to identify those that caused the least activity of this inflammatory marker [39]. The top ten performers were then implanted subcutaneously and intraperitoneally in mice for 14 days and analyzed for cell adhesion and fibrous capsule thickness, finally yielding three analogs that resulted in minimal cell adhesion and collagen deposition. The three candidates, all of which contained triazole groups, were further tested in primates for six months. All three modified alginates performed significantly better compared to unmodified alginate controls and had minimal fibrous capsule formation over six months as demonstrated by insignificant levels of α-SMA and collagen deposition, common indicators of the FBR. In corroboration with this study, Liu et al. demonstrated that triazole-containing pHEMA hydrogels decreased collagen deposition when subcutaneously implanted in mice compared to controls [5].

Other researchers have taken advantage of naturally occurring polymers to develop less reactive materials. For example, Yan and colleagues crosslinked the natural mucus biopolymer that covers the epithelium into hydrogels through the addition of tetrazine and norbornene [40]. The mucin hydrogels were surrounded by much lower collagen and cellular content compared to alginate hydrogels after 14 and 21 days of intraperitoneal implantation in mice.

2.2.2. Biomaterial-tissue integration

While the end result of inhibiting fibrous encapsulation may be the development of relatively more inert biomaterials, the goal of other strategies is to promote biomaterial-tissue integration. In general, porous biomaterials show lower levels of fibrous encapsulation and higher levels of implant integration compared to nonporous biomaterials [45, 50, 51], with larger pore sizes (~5-100 μm and higher) allowing for higher levels of cell infiltration and expansion of neovascular networks [52-54]. Adjustments to pore morphology, including size and shape, and microstructure also affect the balance between fibrous encapsulation and tissue integration. Madden et al. demonstrated the importance of pore size of microtemplated poly(2-hydroxyethyl methacrylate-co-methacrylic acid) (pHEMA-co-MMA) hydrogels when implanted in cardiac tissue [51]. Hydrogels with pores of 30 or 60 μm in diameter allowed for more neovascularization after 4 weeks compared to nonporous hydrogels and those with 20 μm pores. Interestingly, fibrous capsules were thicker around nonporous hydrogels and those with 60 μm pores compared to hydrogels with 20 or 30 μm pores, showing that neovascularization and fibrous encapsulation can occur concurrently. However, these results may depend on the specific application, the site of implantation, type of polymer, and animal model [55-57]. Newly developed techniques have allowed for more precise and controlled mechanisms to control the architecture of porous structures. For example, Thorson and colleagues used a PEG-based hydrogel with a highly organized and interconnected porous structure created through bicontinuous interfacially jammed emulsion jet (bijels) to evaluate tissue integration compared to other hydrogels [58]. When implanted subcutaneously in athymic mice, these bijels PEG hydrogels were better vascularized and integrated than particle-templated and non-templated PEG hydrogels.

Various surface modifications have also been shown to decrease fibrous capsule formation while increasing biomaterial-tissue integration. Among these modifications are the addition of functional groups to alter surface properties such as ionic charge and wettability [59], as well as coating with other polymers [35] or bioactive moieties to mimic the natural tissue environment [60]. For example, the incorporation of RGD or other ECM- or growth factor-derived peptides decreases fibrous encapsulation [9, 61-63], probably through as-yet unknown effects on the inflammatory response.

The work mentioned within this session exemplifies that physicochemical modifications to biomaterials can not only hinder fibrous capsule formation, but also guide the cells involved in this process to promote integration with surrounding tissues. With increasing understanding of how inflammatory cells modulate tissue repair, it has become possible to direct their behavior for the enhancement of biomaterial-tissue integration, which will be discussed in more detail in section 3.

2.2.3. Strategies to increase the FBR

A final consideration to discussion of the FBR, prior to moving on to strategies designed to actively promote biomaterial-tissue integration via modulation of the inflammatory response, is that some biomaterials are actually designed to augment the FBR for specific medical applications. For example, biomaterials and their ensuing fibrous capsules are used as embolic agents for the treatments of cardiovascular aneurysms, thinning of the blood vessel wall, which if ruptured would cause hemorrhage and stroke. Jung et al. investigated the usage of PVA particles as such an embolic agent in canine models with normal renal segmental arteries and aneurysms of the carotid wall [64]. PVA polymer coils were prepared by crosslinking them with tantalum particles. Complete occlusion of the segmental arteries occurred in all animals on day one and in 75 % of animals by four weeks. Researchers noted increasing numbers of inflammatory cells and progressive thrombus formation over time.

A similar strategy is used for the treatment of uterine fibroids, or leiomyomata, which are benign uterine tumors that cause significant morbidity in the United States. A common treatment is the use of polymeric microparticles (less than 1mm in diameter) of the uterine arteries in order to block the blood supply to the tumors, with the primary mechanism being the FBR [65]. These microparticles can be synthetic (PVA) or naturally derived (gelatin). PVA is not degradable so this effect is considered to be permanent. No significant differences were noted in the safety or effectiveness of these different materials in a study of 100 patients over three months [66]. In a five-year follow-up study of 200 patients, 73 % of patients treated with PVA occlusion reported symptom control [67]. Histologic studies of embolized uterine arteries removed for reasons other than complications due to embolization have noted long-term FBR, including the presence of macrophages and FBGCs,

with no adverse effects on surrounding tissue [68, 69]. However, in a study of eight patients presenting with complications believed to result from the PVA embolization, evidence of necrosis of nearby endometrial tissue was found in five of the eight cases [68].

Others have even leveraged the FBR to enhance tissue regeneration. For example, the healing of non-union bone fractures can be augmented by first implanting a PMMA block in the bone until a fibrous capsule forms, and then replacing the block with a bone autograft, in a surgical procedure known as the Masquelet technique [70]. As another example, researchers have shown that the fibrous tissue that forms around a polymeric tube implanted in the abdomen can be surgically removed and used successfully as an autologous blood vessel graft in animal models [71]. Rothuizen et al. implanted poly(ethylene oxide terephthalate) (PEOT) and poly(butylene terephthalate) (PBT) rods, with dimensions similar to the carotid artery, subcutaneously in pigs for four weeks [72]. Rods, together with surrounding fibrous capsules, were explanted and then implanted as vascular grafts in the carotid artery. Four weeks after vascular implantation, the grafts did not fail and underwent thorough alterations at the cellular and protein levels. Collagen, αSMA and desmin significantly increased and macrophage content significantly decreased post grafting, and a heavy capillary network was formed.

In summary, polymeric biomaterials typically elicit the FBR, which can be modulated to be minimal or robust as desired through chemical and structural modifications.

3. Biomaterial-Tissue Integration and Tissue Repair

Many studies have shown that inhibiting the FBR can lead to more inert biomaterials with minimal interactions with surrounding tissue. This outcome is ideal for removable biomaterials like sensors, but it is not desirable for biomaterials that need to integrate with surrounding tissue, as is the case for all biomaterials intended to support tissue repair. For these biomaterials, success is measured in terms of cellular infiltration, neovascularization, and the development of functional tissue. Successful biomaterials tend to promote an inflammatory response that is reminiscent of the normal wound healing process. In order to understand how biomaterials can be designed to promote such a beneficial inflammatory response,

it is helpful to first review how the inflammatory response proceeds in normal wound healing.

3.1. Inflammatory Response in Wound Healing

Any tissue injury initiates inflammation, which triggers the wound healing process. The recruitment of inflammatory cells is induced in response to damage associated molecular patterns (DAMPs, or alarmins) released from damaged cells and pathogen-associated molecular patterns (PAMPs) released from microbes [73]. The first step of inflammation is protein adsorption, followed by platelet adhesion, activation, and initiation of the blood-clotting cascade. A provisional fibrin matrix forms in the injury site, providing a scaffold for the infiltration of cells. Platelets release a multitude of growth factors and cytokines that activate and recruit inflammatory cells to the injury site [74]. Neutrophils are the first cells that are recruited, where they clear the wound of bacteria and foreign particles via enzymes and reactive oxygen species and by phagocytosis [74]. Neutrophil activation stimulates the release of monocyte-recruiting signals to the injury site. After 1-3 days, monocytes arrive at the site of injury and differentiate into macrophages, which are crucial for coordinating both early and late events in the wound healing cascade [75]. Neutrophils undergo apoptosis and are removed via phagocytosis by infiltrating macrophages, a process called efferocytosis that serves to regulate macrophage behavior [76].

Macrophages are major regulators of all stages of tissue repair. During the normal healing process, distinct macrophage phenotypes emerge in at least two sequential phases. The initial phase is marked by the presence of mostly pro-inflammatory macrophages, whereas the second stage is characterized by macrophages with a distinct pro-regenerative phenotype [77, 78]. Pro-inflammatory macrophages are often referred to as classically activated or M1, while the second population of macrophages are referred to as alternatively activated or M2, although there is considerable debate over this nomenclature (for more information see Murray et al. [79] and Spiller and Koh [80]). In addition, it is now known that the M2 population in particular is quite diverse, with numerous physiologically relevant stimuli leading to phenotypically distinct behaviors, including those induced by interleukin-4 (IL-4), IL-10, and efferocytosis of apoptotic neutrophils [81, 82].

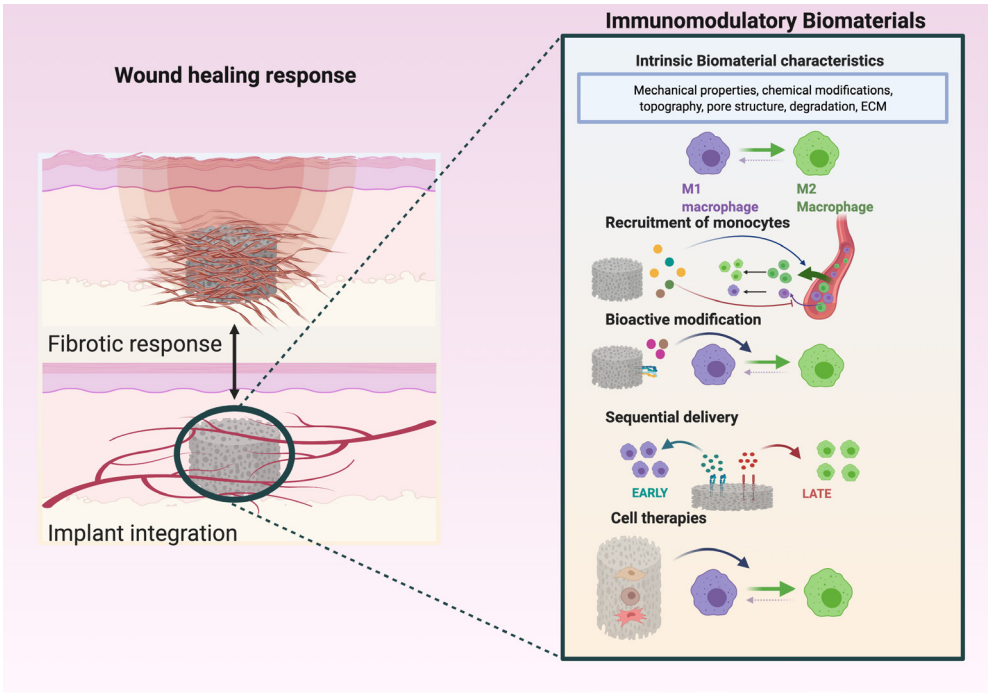

Figure 3: Design strategies for immunomodulatory biomaterials that achieve implant integration. Most strategies focus on manipulation of biomaterial-intrinsic properties, the addition of bioactive factors that mediate recruitment and/or the M1-to-M2 transition of macrophages, or the inclusion of immunomodulatory cell types

Moreover, M2-type macrophages may derive from the infiltration of newly arriving monocytes at later stages of wound healing, or they may derive from M1 macrophage repolarization [80, 83]. Finally, while most macrophages within an injury site are monocyte-derived, prenatally derived tissue-resident macrophages may play important roles at the early stages of the response to injury by recruiting monocytes and initiating inflammation [84].

Macrophages are critical regulators of angiogenesis, which is crucial for both wound healing and for biomaterial-tissue integration. While depletion of macrophages from wounds hinders angiogenesis [85], exogenous addition of macrophages promotes angiogenesis [81, 86]. However, the angiogenic effects of the dynamic changes in macrophage phenotype that normally occur over time are poorly understood. Recently, Graney et al. used a tissue-engineered

model of human blood vessel formation *in vitro* to interrogate macrophage-blood vessel interactions [81]. First, they showed that co-culture with M1 macrophages caused endothelial cells to upregulate genes associated with the early stages of angiogenesis, such as sprouting, while multiple M2-type phenotypes caused endothelial cells to upregulate genes associated with later stages of angiogenesis, such as regulation of pericyte differentiation. Then, they demonstrated that M1 macrophages stimulated angiogenesis in a three-dimensional (3D) triculture model of human blood vessel network formation, but only if their presence was short-term (1 day). These results, in combination with numerous other studies, suggest that M1 and M2-type macrophages act sequentially to regulate angiogenesis — for review see, [80] —. While the detailed mechanisms regulating macrophage functions during tissue healing are still poorly understood, their critical roles in both the response to biomaterials and in tissue repair marks them as a primary target when designing regenerative strategies.

Recent studies have highlighted the importance of adaptive immune cells, especially T cells, in biomaterial-mediated tissue repair. For example, Sadtler et al. showed that extracellular matrix (ECM)-derived scaffolds enhanced recovery from volumetric muscle loss injury in mice, but not in mice genetically deficient for T cells [87]. This effect was likely mediated through macrophages, since M2 macrophages failed to develop in the T cell-deficient mice. While biomaterials that target T cell behavior are an exciting area of future direction, in this review we will continue to focus on the innate immune system, which has been widely manipulated through biomaterial design to promote tissue repair and regeneration. Because of the importance of macrophages for wound healing, they are by far the most targeted immune cell for immunomodulatory biomaterials designed to enhance tissue repair.

3.2. Biomaterials that Manipulate Macrophage Polarization

Design strategies for promoting tissue regeneration via immunomodulation are progressing in conjunction with understanding of the crosstalk between the immune components, stem/progenitor cells, and other cells involved in the tissue healing process, such as endothelial cells and fibroblasts. Injuries characterized by defective healing, such as chronic wounds and large traumatic tissue defects, are distinguished by impairment in the M1-to-M2 transition — for review [88] —. Thus, many studies have been directed towards understanding how biomaterial properties

affect macrophage phenotype, often with a focus on promoting M2 activation. Extending these findings, strategies to actively control immune cell behavior in order to promote biomaterial-tissue integration and tissue repair/regeneration generally focus on enhancing recruitment of M2-biased monocytes/macrophages, stimulating M2 phenotypes, and/or sequentially promoting M1 followed by M2. These effects have been achieved through manipulation of biomaterial properties, the addition of bioactive proteins or drugs, or the inclusion of immunomodulatory cell types (Figure 3).

3.2.1. Effects of biomaterial properties on macrophage polarization

Although it has long been known that macrophage behavior is critical for determining the success or failure of implanted biomaterials — for review, see [89] —, Badylak and colleagues were the first to introduce the importance of the M1/M2 paradigm to the biomaterials community [90]. In a series of studies characterizing macrophages surrounding biomaterials with varying levels of success at being "constructively remodeled," it was concluded that higher ratios of M2:M1 markers were predictive of a successful outcome [90-92]. Together with the well-characterized importance of M2 macrophages in wound healing, these studies spurred a new subfield of biomaterials research focused on promoting the M2 phenotype. However, it is important to remember that M2 macrophages can be detrimental for healing, and that M1 macrophages are also critical for healing, as described above. Indeed, many studies have found higher M2:M1 ratios to be associated with thicker fibrous capsules surrounding biomaterials [93-95], which may be linked to pro-fibrotic processes by M2-like macrophages — for review, see [96] —. For these reasons, it is essential to understand the effect of biophysical clues such as biomaterial stiffness, pore structure, degradation, and incorporation of natural biomaterials on macrophage phenotype and how these factors influence tissue repair (Table 2).

3.2.1.1. Biomaterial stiffness

Cells are able to sense physical properties of the surrounding biomaterial and respond accordingly, in a process called mechanotransduction. For example, macrophages are able to sense the deformation created by fibroblast contraction in fibrillar collagen matrices, migrating toward the source from a distance, in an $\alpha_2\beta_1$ integrin-dependent process [97]. Sridharan et al. showed that macrophage migration

speed was dependent on substrate stiffness and was related to the migration mode adapted by macrophages and also to macrophage phenotype, with stiffer polyacrylamide gels (323 kPa) promoting slower migration and priming macrophages towards a pro-inflammatory (M1) phenotype compared to softer gels (11 kPa and 88 kPa) that promoted faster migration and primed macrophages towards an M2-like phenotype (Figure 4A) [98]. Similarly, other studies have also shown that stiffer substrates lead to more M1 activation [98-101], and that M2 macrophages are more migratory than M1 macrophages [102]. One study showed that increasing stiffness of poly(ethylene glycol) PEG hydrogels modified with RGD from 130 to 840 kPa increased M1 related cytokine secretion when stimulated with LPS by a mouse macrophage RAW 264.7 cell line [101]. When implanted subcutaneously in mice for 4 weeks, stiffer gels were surrounded by thicker layers of macrophages. However, at least one study using porous gelatin hydrogel-based scaffolds reported decreasing M1 marker expression and increasing M2 marker expression with increasing stiffness both *in vivo* and *in vitro* [103], suggesting that the relationship between macrophage activation and substrate stiffness likely depends on the substrate.

Patel et al. linked substrate-dependent changes in macrophage phenotype to elasticity of the cells themselves [104]. First, they showed that pro-inflammatory (M1) activation of macrophages with LPS and IFNγ caused their elastic moduli to increase, as measured by optical magnetic twisting cytometry. Then, using soft (1.2 kPa) and stiff (150 kPa) polyacrylamide gels, they found that macrophages cultured on stiffer substrates increased their own elastic moduli and their propensity to phagocytose latex beads, but without clear effects on inflammatory cytokine secretion or gene expression. Wu et al. designed porous scaffolds with dynamic stiffness based on poly(urea-urethane) and polyhedral oligomeric silsesquioxane (PUU-POSS) using a 3D printing-guided thermally-induced phase separation technique (3D-TIPS) [105]. These scaffolds exhibited stiffness memory properties, with decreasing stiffness over time. When implanted subcutaneously in rats, these scaffolds were better vascularized than scaffolds with uniform stiffness, concomitant with increased numbers of macrophages expressing both M1 and M2 markers. Collectively, these results demonstrate the capacity of implant stiffness to influence macrophage behavior.

3.2.1.2. Pore structure and surface topography

Pore size has also been demonstrated to exert an effect on macrophage behavior and the host immune response *in vivo* [103, 106, 107], with larger pores generally enhancing expression of M2 phenotype markers [108, 109]. However, one study highlighted the importance of context dependence, reporting that pro-inflammatory macrophage responses to chitosan scaffolds were exacerbated when pore size was increased [110].

In a recent study, Jiang et al. independently modulated pore size and stiffness of gelatin scaffolds to analyze the effects on macrophage and fibroblast behavior both *in vivo* and *in vitro* [103]. Different concentrations of glutaraldehyde were used to adjust stiffness, while different concentrations of dimethyl sulfoxide (DMSO) were used to regulate pore size by ice crystal formation during cryogelation. They found that increasing pore size from 30 to 80 μm decreased M1 marker expression and increased M2 marker expression by murine macrophages *in vitro*, with more pronounced effects on softer substrates 20 kPa compared to 70 and 90kPa). When implanted in cutaneous wounds in mice, softer scaffolds with smaller pores were more infiltrated by macrophages than stiffer scaffolds with larger pores, and the macrophages expressed higher levels of the antigen presentation-related marker MHC-II, although more commonly employed M1 and M2 markers were not assessed. Interestingly, softer scaffolds with larger pores achieved the most pronounced wound closure rate, suggesting that wound healing can be influenced by numerous cellular responses and different biomaterial properties [103] (Figure 4B).

More recent studies have focused on the shape of the pores, following a landmark study that showed that M2 macrophages were more elongated than M1 macrophages and that micropatterning could be used to promote M2 polarization via cell elongation [111] (Figure 4C). Even though this link between morphology and phenotype is true only for murine and not human macrophages [112], a recent study showed that primary human macrophages upregulated M2 markers when cultured on pHEMA scaffolds with an elongated pore structure [113]. In addition, another study screened drugs for those that promoted roundness of murine macrophages in order to find M1-promoting drugs for cancer treatment, and the selected drug also promoted M1 activation of human macrophages, despite a lack of effect on their morphology [114].

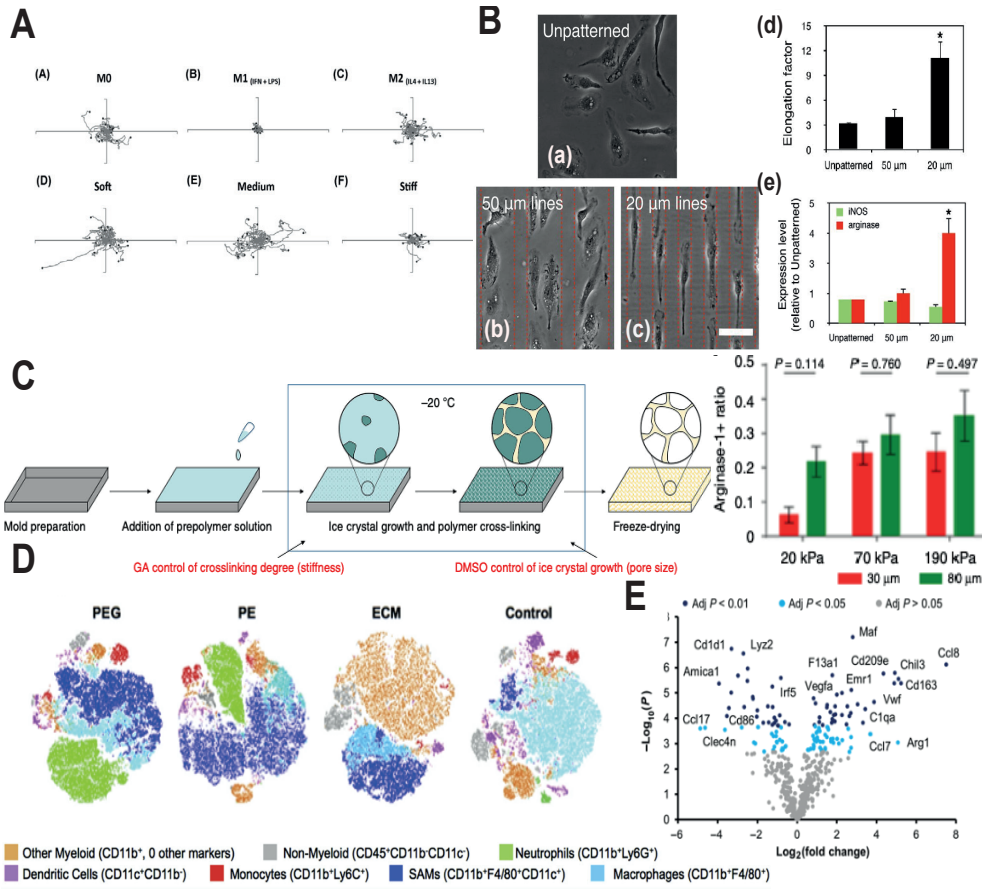

Figure 4: Intrinsic properties of biomaterials affect macrophage phenotype. (A) Macrophage motility is influenced by both phenotype and substrate stiffness. Reprinted and adapted with permission from reference [98]. Copyright 2019 Elsevier (B) Gelatin scaffolds were prepared with independent control over pore size and stiffness via the inclusion of cryoprotectant and crosslinkers, respectively. Quantification of macrophages expressing the M2 marker Arginase 1. Reprinted and adapted with permission from reference [103]. Licensed under a Creative Commons Attribution 4.0 International (CC BY 4.0) (C) Micropatterning was used to increase elongation of murine macrophages, which led to upregulation of M2 marker arginase. Reprinted from reference [111]. (D) Multidimensional parameter reduction of a 13-color flow cytometry panel to illustrate the heterogeneity of the immune cells infiltrating ECM and synthetic scaffolds. Reprinted from reference [119].Copyright 2019 Elsevier. (E) Volcano plot of up- and down-regulated genes by macrophages isolated from UBM-treated tumor microenvironment, highlighting their complex phenotype characterized by changes in both M1 and M2 markers compared to saline. Reprinted and adapted with permission from [118]. Copyright 2019 The American Association for the Advancement of Science.

As with 3D pore structure, macrophages also exhibit sensitivity towards surface topography. Bartneck et al. investigated the influence of different perfluoropolyether (PFPE) microstructures (lines, large cylindrical post, widespread cylindrical post, small posts, and concentrated small cylindrical posts) on the inflammatory activation of human macrophages. They showed that smaller posts separated by a shorter distance increased expression of M1 markers compared to those with a longer distance, while larger cylindrical posts mostly upregulated M2 markers [115].

3.2.1.3. Degradation

Another biomaterial characteristic that affects the inflammatory response is the degradation rate. For example, Zhang et al. investigated how the degradation rate of PGA scaffolds influenced the host response in a mouse subcutaneous model for 6 weeks [116]. Degradation rate was controlled by changing the crystallinity of the polymers via varying the fabrication process of the scaffolds between gas foaming and fiber formation. Fast-degrading scaffolds (50 % degradation in 1 week) increased the proportion of macrophages expressing the M1 marker CD86 compared to slow-degrading scaffolds (50 % degradation in 2 weeks), which were surrounded by macrophages expressing higher levels of the M2 marker CD163. These results corroborated previous findings that faster-degrading PLA/PEG scaffolds provoked a more pronounced inflammatory response and thicker fibrous capsules when implanted subcutaneously in rats compared to more slowly degrading formulations [117]. The effects of biomaterial degradation rate on macrophage activation are likely a combination of the degradation byproducts as well as effects on the macrophages' ability to clear the foreign body.

Table 2. Representative studies illustrating how biomaterial properties affect macrophage polarization

PROPERTY	STRATEGY	BIOMATERIAL	*IN VIVO/ IN VITRO*	OUTCOME	REF
MECHANICAL PROPERTIES	Stiffness	PA	*In vitro:* macrophages isolated from the femurs of C57BL/6 and TLR4-deficient mice	PA gels with ≥ 47 kPa stiffness increased M1 markers	[99]
	Stiffness	PA	*In vitro:* THP-1 cell line	Stiff gels increased M1 markers, while soft and medium stiffness gels increased M2 markers	[98]
	Stiffness	Agarose	*In vitro:* THP-1 cell line	Stiff substrates increased M1 markers, while soft substrates increased M2 markers	[100]
	Stiffness	PUU-POSS	*In vivo:* Subcutaneous implantation in rats	Scaffolds with dynamically decreasing stiffness increased vascularization and both M1 and M2 macrophage markers	[105]
CHEMICAL MODIFICATION	Enantiomer	PPFU / PLL / PDL	*In vivo:* Subcutaneous implantation C57BL/6 mice	PPFU-PDL increased M2 markers compared to PPFU-PLL	[107]
	Sulfonation	PEEK	*In vivo:* Mouse air punch model	Further sulfonation of PEEK increased M2 markers and decreased M1 markers	[125]
	Sulfonation	Collagen / HAp	*In vitro:* human macrophages	The matrix containing high-sulfated hyaluronan decreased M1 markers and increased M2 markers	[126]
	Biological Coating	PE / PRP / MVF	*In vivo:* Dorsal skinfold mice	PRP/MVF-coated and PRP-coated PE promoted M2 markers and accelerated vascularization	[113]

Hydroxyapatite (HAp), poly(urea-urethane) of terminated polyhedral oligomeric silsesquioxane (PUU-POSS), Polyacrylamide (PA), poly(propylene fumarate) polyurethane (PPFU), poly-L-lysine (PLL), poly-D-lysine (PDL), polyethylene (PE), tissue-derived microvascular fragments (MVF), platelet-rich plasma (PRP), Polydimethylsiloxane (PDMS), Perfluoropolyether (PFPE), Polydioxanone (PDO), Polycaprolactone (PCL), Poly(L-lactic acid-co-e-caprolactone) (P(LLA-CL)), poly(L-lactic) (PLLA), Polyetheretherketone (PEEK), Polylactic acid (PLA), Chitosan (Ch), poly(D,L-lactide-co-glycolide) (PLGA), Methacrylic acid (MAA), Poly(ethylene glycol) (PEG), Polyglycolide (PGA), extracellular matrix (ECM), decellularized extracellular matrix (dECM), Urinary bladder matrix (UBM)

Table 2 (continued)

PROPERTY	STRATEGY	BIOMATERIAL	*IN VIVO/ IN VITRO*	OUTCOME	REF
DEGRADATION	Different degradation rates	MAA-PEG	*In vivo:* Muscular injection in mice	Fast degrading group increased Arg1 (M2 marker), while slow group increased Fizz1 (another M2 marker), also decreasing M1 markers.	[134]
	Structural differences	PGA	*In vivo:* Subcutaneous implantation	Fast degrading increased M1 markers. Slow degrading increased M2 markers.	[116]
ECM	Formulation	dECM	*In vivo*: Rat periodontal defect model	dECM particles increased M1 markers, while gels increased M2 markers.	[135]
	Concentration	dECM	*In vivo*: Spinal cord injury model in rats	5mg/ml increased M2 markers compared to lower and higher concentrations.	[136]
	Tissue origin	Scaffolds prepared from intestinal submucosa, UBM, brain, esophagus, colon, skin, liver, skeletal muscle	*In vitro*: bone marrow derived C57bl/6 mice macrophages	Small intestinal submucosa, UBM, brain ECM, esophageal ECM, and colonic ECM increased M2 markers. Dermal ECM increased M1 markers. Skeletal muscle did not change expression of M1 or M2 markers.	[120]
	Synthetic vs ECM	PE / PEG / ECM	*In vivo*: Volumetric muscle loss model of C57BL/6	ECM increased M2 markers compared to synthetic scaffolds.	[119]
	Synthetic vs ECM	PCL / UBM	*In vivo*: muscle injury in mice	UBM scaffolds upregulated M2 markers. PCL-induced fibrosis was driven by IL17	[124]
	dECM vs Collagen I	Collagen I / dECM	Critical size calvarial defect model	dECM increased M2 markers	[137]

Table 2 (continued)

PROPERTY	STRATEGY	BIOMATERIAL	*IN VIVO/ IN VITRO*	OUTCOME	REF
TOPOGRAPHY	Surface roughness	PDMS	*In vitro*: murine bone marrow-derived macrophages	Micropatterned surfaces increased macrophage elongation, which enhanced M2 markers and inhibited M1 markers	[111]
	Surface roughness	PFPE	*In vitro*: Human macrophages	A microstructure of regular grooves and smaller posts with a shorter distance increased M1 marker. Larger cylindrical posts increased M2 markers.	[115]
	Surface roughness	PCL	*In vivo*: Subcutaneous implantation of C57BL/6 mice and Sprague-Dawley rats	Non-microchanneled scaffolds increased M1 markers. Microchanneled scaffold increased M2 markers.	[127]
PORE STRUCTURE	Pore size	PDO	*In vitro*: murine bone marrow derived macrophages	Increasing fiber/pore size increased M2 markers and decreased M1 markers.	[106]
	Pore size	PCL	*In vitro*: primary human macrophages	Scaffolds with smaller pores (40μm) and box shaped pores increased M2 macrophages markers.	[113]
	Pore size	Gelatin	*In vivo*: Subcutaneous implantation in Balb/c mice	Small and soft pores increased M1 markers. Larger and stiffer pores increased M2 markers.	[103]
	Pore size	pHEMA-co-MAA	*In vivo*: myocardial implantation in rats	40 and 80 μm pore size increased both M1 and M2 markers and vascularization	[128]
	Pore size	PCL	*In vivo*: replacement of rat aorta	Thicker fiber scaffolds increased M2 markers. Thinner fiber scaffolds increased M1 markers	[129]
	Pore size	PLA / Calcium phosphate glass / chitosan	*In vitro*: primary human macrophages	Chitosan increased M1 markers. PLA increased M2 markers	[130]

3.2.1.4. ECM scaffold

ECM scaffolds, which are prepared by decellularization of human or animal tissue, have been widely investigated for their immunomodulatory properties because of their widespread success at promoting tissue repair and regeneration in animal models and clinically [87, 118, 119]. The composition of the ECM scaffolds varies depending on its tissue origin [120-122]. Dziki et al. cultured murine macrophages on ECM scaffolds derived from eight different tissue sources [120]. They found that macrophages exposed to small intestinal submucosa, urinary bladder matrix (UBM), brain, esophageal and colonic ECM expressed higher levels of M2 markers and lower levels of M1 markers, while macrophages exposed to dermal ECM expressed higher levels of M1 marker and lower levels of M2 markers, and macrophages exposed to liver ECM and skeletal muscle ECM did not significantly change the expression of these markers [120]. Sadtler and colleagues performed detailed analyses of the immune cell response to ECM scaffolds derived from UBM, bone, or cardiac tissue and found that macrophages upregulated multiple M2 markers compared to macrophages infiltrating collagen or synthetic scaffolds prepared from PEG or PCL (Figure 4D) [87, 119, 123]. Interestingly, while M2 macrophages are typically believed to promote tumor progression, Wolf et al. showed that UBM scaffolds actually inhibited tumor formation, despite promoting increased expression of M2 macrophages markers (Figure 4E) [118]. Gene expression analysis of the macrophages showed that macrophages isolated from the UBM-treated tumor microenvironment were phenotypically distinct from traditional M2 cells and from classical tumor-associated macrophages. A recent study used single-cell RNA sequencing to further analyze macrophages sorted from UBM-treated muscle injuries compared to polycaprolactone (PCL), which led to a more pro-fibrotic response [124]. The authors found that macrophages infiltrating the ECM scaffolds did upregulate many M2 markers, but also highlighted the limitations of conventional M1/M2 markers for accurately separating pro-regenerative and pro-fibrotic behavior. They found that the PCL-induced fibrosis was driven by IL-17, and identified CD9 and CD301b as new cell surface markers to distinguish pro-regenerative from pro-fibrotic macrophages. These studies demonstrate that macrophage phenotypes are complex and caution against drawing broad conclusions about the role of M2 macrophages in tissue regeneration.

3.2.2. Design of immunomodulatory biomaterials

Beyond empirical investigations of how changes in biomaterial properties affect macrophage behavior and biomaterial-mediated tissue repair, the incorporation of immunomodulatory cytokines and drugs has contributed a great deal to our understanding of how immune cell behavior can be harnessed to promote tissue repair. Such immunomodulatory design strategies typically involve enhancing monocyte recruitment, promoting M2 polarization, or sequentially stimulating M1 and M2 activation (Table 3).

3.2.2.1. Biomaterials that recruit monocytes to the site of injury

Because monocytes are naturally recruited to sites of injury where they differentiate into macrophages, biomaterials that augment this process have been developed. Several studies have shown beneficial effects of biomaterials that enhance monocyte recruitment to a site of injury, especially if the monocytes quickly take on an M2 phenotype. For example, Kumar et al. designed multidomain peptide hydrogels that sequentially delivered MCP-1, to recruit monocytes, followed by IL-4, to promote M2 activation of the macrophages derived from those monocytes [138]. The hydrogels released 80 % of loaded MCP-1 in the first two days, while a much slower release of IL-4 occurred over the next sixteen days, with these divergent release profiles resulting from differences in diffusivities of MCP-1 and IL-4 as well as possible matrix-protein interactions. Subcutaneous implantation in rats confirmed that the sequential cytokine delivery increased the number of infiltrating monocytes and shifted the macrophage population towards M2.

Other studies have taken advantage of the fact that monocytes themselves exist as two different populations in the blood (three in humans), which appear to be biased towards M1 or M2 macrophages as they extravasate into tissues. The so-called classical or inflammatory monocytes are distinguished by the $Ly6C^{high}CX3CR1^{mid}CCR2^{+}(CD62L^{+}CD43^{low})$ surface receptor profile (in mice). Non-classical or alternative monocytes appear to be biased to become M2 macrophages, and are distinguished by $Ly6C^{low}CX3CR1^{high}CCR2^{-}(CD62L^{-}CD43^{high})$ [139] (for review see [140]). However, it is important to remember that classical monocytes can also be converted to non-classical monocytes, so the terms “M1-biased” and “M2-biased” may not always accurate [139]. Nonetheless, Awojoodu et al. showed

that M2-biased monocytes can be selectively recruited via the delivery of FTY720, a sphingosine 1-phosphate receptor (S1P) agonist, from PLGA thin films [141]. Implantation into a dorsal skinfold window chamber model in mice showed that the release of FTY720 increased the recruitment of alternative monocytes, resulting in higher numbers of M2 macrophages, lower inflammatory cytokine secretion, and increased microvascular density. This strategy was also shown to be effective at enhancing repair of skeletal muscle [142] and bone defects [143-145]. Similar effects on angiogenesis were achieved by preferentially recruiting alternative monocytes via controlled release of SDF-1α[146]. Kim et al. modified the release profiles of proteins from gelatin hydrogels by changing the isoelectric points of the hydrogels [147]. They incorporated SDF-1α and SEW2871, an SP1 agonist, which have both been shown in other studies to recruit alternative monocytes as well as other cells. The rapid release of SDF-1α combined with the sustained release of SEW2871 resulted in higher numbers of macrophages expressing M2 markers and faster wound closure when compared to sustained release of SDF-1α and rapid release of SEW2871 [147].

3.2.2.2. Bioactive modification with M2-promoting stimuli

A variety of techniques have been used to actively promote M2 polarization of macrophages responding to biomaterials. Biomaterials that release IL-4 and IL-10 in particular have been extensively investigated because of the potent effects of these cytokines on M2 polarization. For example, Hu et al. designed injectable heparin-modified gelatin microspheres to deliver IL-4 to macrophages within bone defects under diabetes mellitus (DM) conditions [148]. Because IL-4 has heparin-binding domains, the release of IL-4 was sustained for 3 weeks *in vitro* [149]. The system was able to increase the presence of macrophages expressing M2 markers and enhanced osteoblastic differentiation and bone regeneration in diabetic rats.

Another strategy to promote M2 polarization is using microRNAs (miRNAs). miRNAs are small (~22 nucleotides) non-coding RNAs that regulate translation of coding RNAs. Some miRNAs have been shown to regulate macrophage polarization and subsequently affect inflammation (for review see [150, 151]). A number of studies have determined miRNA expression profiles in M1- and M2-polarized human and murine macrophages using microarray and RT-qPCR arrays techniques, identifying potential targets for therapeutic manipulation. For example, Bejerano et

al. presented a new therapeutic strategy to manipulate macrophage phenotype using hyaluronan-sulfate (HS) nanoparticles loaded with miRNA-21, which promotes an M2 phenotype [152]. The nanoparticles were delivered intravenously to a murine model of myocardial infarction. The nanoparticles increased M2 polarization of macrophages in the infarcted zone, increased angiogenesis, and improved cardiac outcomes [152].

3.2.2.3. Mimicking efferocytosis

Considering another mechanism by which the M2 phenotype is generated *in vivo* is by efferocytosis, or the uptake of apoptotic neutrophils, some studies have sought to mimic this process using biomaterials. Apoptotic cells display phosphatidylserine (PS), which is a phospholipid typically hidden inside the cell membrane in non-apoptotic cells. The PS acts as an “eat me” signal for the macrophages, and the binding to this receptor triggers an anti-inflammatory phenotype in macrophages characterized by the secretion of IL-10, TGF-β and prostaglandins — for review, see [76] —. Huynth et al. were the first to propose the use of PS-containing liposomes to mimic apoptotic cells as a tool to promote the resolution of inflammation [153]. Harel-Adar et al. showed that PS-presenting liposomes promoted M2 polarization of cardiac macrophages after myocardial infarction in rats [154]. After PS-liposome uptake by macrophages *in vitro* and *in vivo*, macrophages secreted high levels of anti-inflammatory cytokines such as TFGβ and IL-10 and upregulated the M2 cell surface marker CD206 along with downregulation of proinflammatory markers such as TNFα and the M1 cell surface marker CD86. Finally, PS-liposomes have been shown to decrease inflammatory cytokine production and improve symptoms in a carrageenan-induced model of mouse hindpaw inflammation [155].

3.2.2.4. Biomaterials that promote sequential M1 then M2

Even though the precise roles of each population of macrophages in tissue repair is not fully understood, dysfunctional regulation of macrophage phenotype can impede proper healing. The early presence of M1 macrophages is key for the initiation of tissue regeneration, but chronic M1 activity could impede or prevent proper healing [156, 157]. On the other hand, uncontrolled M2 activation could lead to fibrosis [158-160]. Moreover, M1 and M2 macrophages appear to act sequentially

in their regulation of normal angiogenesis and wound healing, and improper activation in either phase is detrimental for healing (for review see [161]). For these reasons, numerous studies have recently reported the design of biomaterials that can promote sequential M1 and M2 activation of macrophages [80, 161-164].

One popular strategy to achieve sequential activation of M1 and M2 macrophages is the sequential release of a proinflammatory agent, such as IFNγ, which induces the M1 phenotype, followed by an M2-promoting cytokine or drug such as IL-4 or simvastatin [162-164]. This idea was first introduced by Spiller et al. using decellularized bone as a scaffold, with M1-promoting IFNγ released by desorption, with subsequent M2-promoting IL-4 released via biotin-avidin interactions [80]. This sequential release promoted the M1-to-M2 phenotypical change of primary human macrophages *in vitro* but failed to significantly enhance vascularization of bone scaffolds in a murine subcutaneous implantation model, an effect that was attributed to the overlapping of M1 and M2 phases at early time points. Following up on this study, Li et al. loaded IFNγ into calcium silicate/β-tricalcium phosphate scaffolds, so that IFNγ release would be followed by release of Si ions, which promote M2 polarization [165]. When the scaffolds were implanted subcutaneously in mice, the sequential delivery of IFNγ and Si ions upregulated M1 marker expression on day 3 and M2 marker expression on day 7 and increased the number of infiltrating blood vessels. Along similar lines, Alhamdi et al. designed a calcium phosphate (βCaP) drug delivery system to release IFNγ followed by the M2-promoting drug simvastatin, with release tied to the activity of macrophages, for a potentially self-regulating patient-specific biomaterial designed for bone repair [162]. Sequential M1-to-M2 activation was achieved in both a human monocyte cell line and in bone marrow-derived macrophages obtained from both young and old mice, although the expression of M1 and M2 gene markers was blunted in aged macrophages. Nonetheless the system showed potential applicability even for elderly patients, whose immune systems are compromised [162]. Externally controlled dual release of macrophage-modulating cytokines was achieved by Tolouei et al., who designed a two-compartment biomaterial system comprised of an outer gelatin scaffold and an inner biphasic ferrogel [164]. The outer porous gelatin layer was loaded with the IFNγ and the chemoattractant MCP-1, for rapid yet passive release via diffusion. In contrast, the inner compartment was composed of a biphasic ferrogel with an Fe_3O_4-laden region in the top half and a Fe_3O_4-free, porous, and deformable region on the bottom.

TARGET	STRATEGY	BIOMATERIAL	*IN VIVO/ IN VITRO*	EFFECTS ON MACROPHAGE	OUTCOME	REF
MONOCYTE RECRUITMENT	Delivery of AT-RvD1	PLGA	Murine dorsal skinfold window chamber	Increased the accumulation Ly6C^{low} monocytes and increased M2 macrophage markers.	Increased vascular remodeling. Limited neutrophil infiltration.	[166]
	Delivery of FTY720	PCL / PLAGA	Oronasal Fistula (ONF) C57BL/6 Model	Increased the accumulation of Ly6C^{low} monocytes and M2 macrophage markers.	Increased of ONF healing.	[167]
	Delivery of FTY720	PLAGA	Murine dorsal skinfold window chamber model	Increased the accumulation Ly6C^{low} monocytes.	Increased vascular remodeling.	[141]
	Entrapment of endogenous FKN into the scaffold	PEGDA	Skin injury mouse model	Increased the accumulation of Ly6C^{low} monocytes and increased M2 macrophage markers.	Increased FKN amount in the site of injury.	[168]
	Delivery of FKN	Agarose	Model of nerve regeneration in rat	Increased the accumulation Ly6C^{low} monocytes and increased M2 macrophage markers.	Increased in regeneration in the injury site	[169]
	Codelivery of FTY720 and SDF-1a	αHep^{-N} -PEG-DA	Murine partial thickness skin	Increased the accumulation of Ly6C^{low} monocytes and increased M2 macrophage markers.	Increased vascular remodeling.	[170]

Aspirin-triggered resolvin D1 (AT-RvD1), poly(D,L-lactide-co-glycolide) (PLGA), Oronasal fistula (ONF), Polycaprolactone (PCL), Poly(lactic-co-glycolic-acid) (PLAGA), Poly(ethylene glycol) (PEG), Fractalkine (FKN), Poly(ethylene glycol) diacrylate (PEGDA), Heparin desulphated at the -N position (aHep-N), poly(ethylene glycol) diacrylate (PEG-DA), recombinant human collagen type I (rHCI), recombinant human collagen type III (rHCIII), Hyaluronic acid-poly(ethyleneimine) (HA-PEI), Polypropylene (PP), Poly(lactic-co-glycolic acid)-multistage silicon particles (PLGA-MSV), Decellularized bone matrix (DBM),

Table 3 (Continued)

TARGET	STRATEGY	BIOMATERIAL	*IN VIVO/ IN VITRO*	EFFECTS ON MACROPHAGE	OUTCOME	REF
M2 PROMOTING AGENT	Viral IL-10 delivery	PLG	Intraperitoneal fat mice	Increased M2 macrophage markers	Decreased inflammation.	[172]
	IL-10 or IL-4 plasmid DNA	HA-PEI	Mice intraperitoneal injection	Increased M2 macrophage markers	Decreased inflammation.	[173]
	IL-4 cytokine release	Dermatan sulfate / chitosan / PP	Subcutaneous implantation in mice	Increased M2 macrophage markers	Improved tissue remodeling.	[174]
	IL-4 cytokine release	Collagen / PLGA-MSV	Rat subcutaneous model	Increased M2 macrophage markers	Improved wound healing	[175]
	IL-4 cytokine release	DBM	Large cranial bone defect in rats	Increased M2 macrophage marker. Decreased M1 macrophage markers	Promoted neo-vascularization and osteogenesis.	[176]
	IL-4 cytokine release	MHG-MS / heparin-modified gelatin	mandibular periodontal fenestration defect in a diabetic rat	Increased M2 macrophage markers	Enhanced osteoblastic differentiation and bone regeneration.	[148]
	IL-4 cytokine release	T/DOP nanotubes and CG layer	In vitro: RAW 264.7 murine	Increased M2 macrophage markers	Enhanced MSCs osteogenic differentiation.	[177]

Stromal derived factors (SDF-1), Mesenchymal stem cells (MSC), Interferon-gamma (IFNγ), Interleukin-4 (IL-4), Bone marrow (BM), Calcium silicate/β-tricalcium phosphate (CaSiO3-β -TCP), Titania nanotube (TNT), Chitosan (Ch), Carboxymethyl chitosan (CMCS),

Table 3 (Continued)

TARGET	STRATEGY	BIOMATERIAL	*IN VIVO/ IN VITRO*	EFFECTS ON MACROPHAGE	OUTCOME	REF
MONOCYTE RECRUITMENT	MCP-1 and IL-4	Multidomain peptides self-assembled into β-sheets	Subcutaneous implantation in Wistar rats	Increased M2 macrophage markers.	Allowed the formation of new blood vessels, as well as promoting an M2 macrophage phenotype	[138]
	SDF-1 and SEW2871	Gelatin	Skin wound defect in diabetic mice	Increased M2 macrophage markers.	Enhanced MSCs recruitment and wound closure	[147]
M1 TO M2 PROMOTIGN AGENTS	IFNγ (M1) and IL-4 (M2)	Decellularized bone	Murine subcutaneous implantation model	Promoted sequential M1 and M2 macrophage polarization	IFNγ scaffolds Increased vascularization.	[80]
	IFNγ (M1) and simvastatin (M2)	Biomimetic calcium phosphate	*In vitro*: THP-1 human monocyte line. Old mice BM derived macrophages	Promoted sequential M1 and M2 macrophage polarization	Sequential activation was also achieved in macrophages from old mice	[162]
	IFNγ (M1) and Si (M2)	$CaSiO_3$- β -TCP	Subcutaneous implantation of C57B1/6	Promoted sequential M1 and M2 macrophage polarization	Enhanced angiogenesis	[165]
	IFNγ (M1) and IL-4 (M2)	Ch / CMCS / TNT	*In vitro:* Mouse RAW 264.7 macrophage line	Promoted sequential M1 and M2 macrophage polarization	Macropahges cultured showed an earlier upregulation of TNFα and iNOS, and a late upregulation of IL-10 and Arg-1.	[163]

In the presence of a gradient magnetic field, the ferrogel physically deformed, releasing loaded IL-4 in a magnetically triggered fashion [164]. Although the bioactivity of this system was not assessed, it could be a promising approach to precisely control the release of macrophage-modulating cytokines, which would be useful for investigations of macrophage timing *in vitro* and *in vivo*

4. Biomaterial-Enabled Cell-Based Therapies for Immunomodulation

While the inclusion of macrophage-modulating cytokines has shown considerable promise, others have explored the delivery of cells with immunomodulatory properties, since they have the potential to respond to the changes in the local environment. While numerous attempts have been made to deliver macrophages themselves to sites of injury — for review, see [88] —, only recently have biomaterials been employed to support this strategy. For example, Hu et al. used pullulan-collagen hydrogels to deliver supraphysiologic numbers of inactivated macrophages to a murine cutaneous wound model [182] (Figure 5A). The transplanted cells survived for at least 7 days *in vivo*, migrated into the middle and lower dermis, and acquired mixed M1/M2 phenotypes. This treatment accelerated wound healing and angiogenesis. Interestingly, the authors showed that macrophages from diabetic mice also accelerated diabetic wound healing, and even transplantation of human diabetic monocytes accelerated wound healing in immunocompromised mice, although survival of the transplanted cells or their incorporation into the mouse tissue were not assessed.

Despite these encouraging results, the efficacy of monocyte/macrophage-based therapies has been limited due to inability to control the phenotype of exogenously administered macrophages, since their high plasticity causes them to take on the phenotype induced by microenvironmental stimuli at the injury site [183, 184]. To address this challenge, Wofford et al. designed a strategy to promote and preserve an anti-inflammatory macrophage phenotype through the use of intracellular microparticles [185].

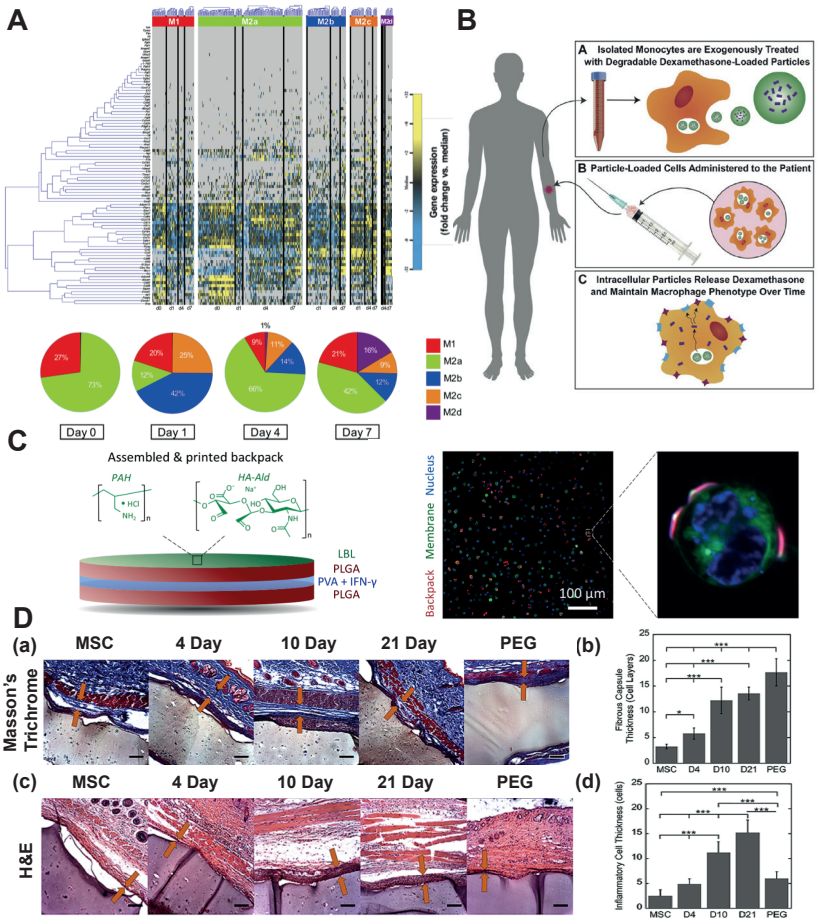

Figure 5: Cell therapies to promote wound healing response. (A) Macrophages delivered within hydrogels to cutaneous wounds took on complex phenotypic profiles. Reprinted and adapted, with permission from refernce [182]. Licensed under a Creative Commons Attribution 4.0 International (CC BY 4.0) (B) Strategy to control the phenotype of monocyte-derived macrophages by loading monocytes with drug-loaded microparticles, which release drug over time as the monocytes differentiate into macrophages. Reprinted with permission from [185]. Copyright 2020 Elsevier (C) Cytokine-loaded "backpacks" that adhere to the surface of macrophages and release cytokines to control their phenotype. Reprinted and adapted, with permission from reference [186]. Licensed under a Creative Commons Attribution-Non Commercial 4.0 International (CC BY-NC 4.0) (D) Ability of MSCs embedded within hydrogels to decrease fibrous capsule formation decreases with stage of differentiation. Reprinted and adapted with permission from reference [206]. Copyright 2015 Elsevier.

In this approach, monocytes would be isolated from patients, incubated with drug-loaded microparticles to allow their uptake by phagocytosis, and then re-administered back into the patient, so that the intracellular release of drug can maintain macrophages derived from those monocytes in an anti-inflammatory phenotype over time even in inflammatory environments [185] (Figure 5B). The authors showed that dexamethasone-loaded PLGA microparticles were retained within monocyte-derived macrophages for several weeks *in vitro*, inhibited expression and secretion of pro-inflammatory cytokines even in the presence of pro-inflammatory stimuli, and did not interfere with subsequent phagocytosis of tissue debris and bacteria [185].

Recently, Shields et al. described a strategy to lock macrophages in an M1 phenotype for cancer therapy [186] (Figure 5C). They designed discoidal shaped particles referred to as “backpacks”, whose anisotropical shape prevented phagocytosis by macrophages and instead promoted adhesion to their surfaces. Macrophages carrying IFNγ-releasing backpacks maintained a pro-inflammatory phenotype in the immunosuppressive environment of a murine breast cancer model, where they slowed tumor growth and reduced metastasis compared to control macrophages carrying blank backpacks. These studies demonstrate promising strategies to modify and maintain phenotypes of transplanted macrophages.

Mesenchymal stromal cells (MSCs) are a widely investigated cell source for diverse applications in regenerative medicine and have been used clinically for decades [187]. While originally touted for their ability to differentiate into multiple cell types in the mesenchymal lineage — e.g. bone and cartilage —, they are now even more widely used for their immunomodulatory properties — for review, see [188] —. In particular, they exhibit low immunogenicity even when transplanted allogenically, and they inhibit T cell proliferation. In addition, crosstalk of monocytes/macrophages with MSCs or MSC-derived conditioned media induces a unique macrophage phenotype sometimes referred to as MSC-educated macrophages [189-191]. As a result, MSC therapies have the potential to modulate macrophage phenotype for enhanced tissue repair. However, MSC transplantation suffers from poor survival *in vivo* and low cellular retention [192-194]. Therefore, biomaterials have been developed to protect MSCs in numerous applications (for review, see [195]). The inclusion of MSCs within hydrogels has been shown to reduce their fibrous encapsulation [196, 197], with the magnitude of this effect decreasing with

more differentiated cells (Figure 5D).

Recently, Clark et al. investigated how MSC functionality can be tuned by delivering them within hydrogels modified with different integrins [198]. PEG hydrogels were modified to present peptides capable of binding to different integrins expressed by MSCs. They compared GFOGER, derived from type I collagen, which has binding specificity for $\alpha_2\beta_1$ integrin, with RGD, which can be found in different ECM proteins, such as fibronectin, and which has binding specificity towards $\alpha\gamma\beta_3$, $\alpha\gamma\beta_1$ and $\alpha_5\beta_1$ integrins. GFOGER-presenting hydrogels prolonged MSC survival and caused them to upregulate numerous genes and cytokines associated with inflammation and enhanced their abilities to stimulate bone repair in a segmental defect model in mice.

In a wound healing environment, inflammatory cytokines prime MSCs to increase their immunomodulatory properties [199]. Recently, Gonzalez et al. took advantage of this finding to design immunomodulatory hydrogels for the delivery of MSCs [200]. The hydrogels consisted of an interpenetrating network of functionalized alginate and fibrillar collagen embedded with IFNγ-loaded heparin-coated beads. The inclusion of IFNγ-loaded beads prolonged the expression of immunomodulatory genes by bone marrow-derived primary human MSCs compared to 2D tissue culture.

Genetic modification of MSCs to amplify the expression of immunomodulatory factors is another promising strategy [201, 202]. Ueno et al. developed lentivirus-transduced IL-4 overexpressing MSCs (IL4-MSCs) to promote M2 polarization of macrophages [177]. IL4-MSCs were delivered in a microporous gelatin-based microribbon scaffold to critical-size long bone defects in mice. IL4-expressing MSCs increased M2 marker expression by surrounding macrophages without inhibiting M1 marker expression in the early stage and augmented macrophage migration into the scaffold, ultimately resulting in enhanced bone healing. Collectively, these studies show that biomaterials are useful delivery vehicles for immunomodulatory MSCs.

5. Future Directions

Designing new and more effective strategies to prevent the FBR and/or promote tissue repair and regeneration will undoubtedly require a greater understanding of the complex mechanisms that govern these processes. To that

end, researchers are exploring innovative avenues to study and manipulate the inflammatory response to biomaterials. At the same time, this is providing invaluable insight to identify hitherto unknown action points and new cellular targets.

5.1. Emerging tools and models for studying the inflammatory response to biomaterials

Typically, the FBR has been assessed by means of histopathological analysis of retrieved implants after staining with hematoxylin & eosin (H&E), Masson's trichrome and/or Sirius Red. The fibrous capsule can be analyzed via semiquantitative analysis for thickness, degree of fibrosis, and cell overgrowth. Supplementary methods include the use of gene expression analysis, cytokine arrays and multidimensional flow cytometry. However, the need for high-throughput, real-time, comprehensive, and biologically relevant data is leading researchers to the development of innovative ways to explore the FBR.

Multiphoton intravital microscopy can provide valuable information to unravel some of the still unknown complex and dynamic biological interactions driving the inflammatory response. This technique allows imaging living biological responses to materials implanted deep into the skin with excellent signal-to-background noise ratio and minimal photodamage (Figure 6A) [203]. Besides fluorescence detection, it is possible to exploit nonlinear processes such as second harmonic generation (SHG) and third harmonic generation (THG) [204]. In this vein, 3D porous electrospun PCL scaffolds implanted in the subcutaneous space of mice have been monitored by means of the generated THG signal, while following the deposition of SHG-positive collagen fibers and sprouting of red fluorophore-tagged neovessels (Figure 6B, C) [17]. Intravital microscopy is usually performed in transgenic mice, whose cells express fluorescent protein markers, to analyze kinetics of cell infiltrates [13].

In vivo molecular imaging techniques are also valuable tools, especially when combined with innovative strategies to conduct high throughput investigations. For example, by injecting 8 different polymer modifications subcutaneously into one mouse and using an injected imaging probe that fluoresces in proportion to the level of inflammation, researchers performed a rapid assessment of 774 variants of chemically modified alginates aimed at mitigating the FBR [39] (Figure 6D, E). Likewise, Yang et al. employed mice with a luciferase reporter gene to enable

real-time, non-invasive monitoring of expression of the pro-inflammatory cytokine interleukin-1β by bioluminescence imaging in response to subcutaneously implanted functionalized PLLA scaffolds [205]. Strategies that can combine these techniques with multiple reported outputs will be key to rapid advances in understanding the inflammatory response.

Along these lines, Witherel et al. examined the FBR to polypropylene sutures and polystyrene microparticles in zebrafish, which are optically translucent and genetically tractable model organisms that have been used extensively to study human disease [206]. By implanting these biomaterials in zebrafish with fluorescent macrophages and neutrophils, the dynamics of these immune cells interacting with model biomaterials could be visualized non-invasively and in real-time (Figure 6F). Zebrafish are amenable to numerous genetic and chemical modifications, which enables researchers to fluorescently label key cellular and molecular mediators including immune cells, pro-inflammatory signals and blood vessels, to evaluate the complex and multifaceted interplay between biomaterials and surrounding tissues [206-208].

Beyond animal testing, however, there are currently no reliable and accepted methods to assess the inflammatory response to biomaterials in a way that accurately represents the human response. Inter-species differences are well known to be a major reason that numerous therapies that appear promising in animal models ultimately fail in humans [209]. To address this problem and reduce the burden of experimental animals, some researchers direct their efforts towards the development of more clinically relevant *in vitro* models. These consist of human components intended to capture key aspects of the human inflammatory response. Whole blood assays have been used to replicate the transient contact of materials with the blood inherent to the surgical procedure [210, 211], while other assays are focused on the response of macrophages [212] and their interactions with other cell types like fibroblasts [213]. Jannasch et al. attempted to recapitulate the wound environment by exposing biomaterials — PTFE and titanium — to macrophages integrated in fibrin clots and co-culturing them with fibroblasts embedded within soft tissue-resembling 3D matrices — made of either collagen or fibrin — [214]. Their results generally agreed with pre-clinical and clinical studies described in the literature. With the development of more sophisticated “organ-on-a-chip” model systems, it may become possible to comprehensively evaluate the human response

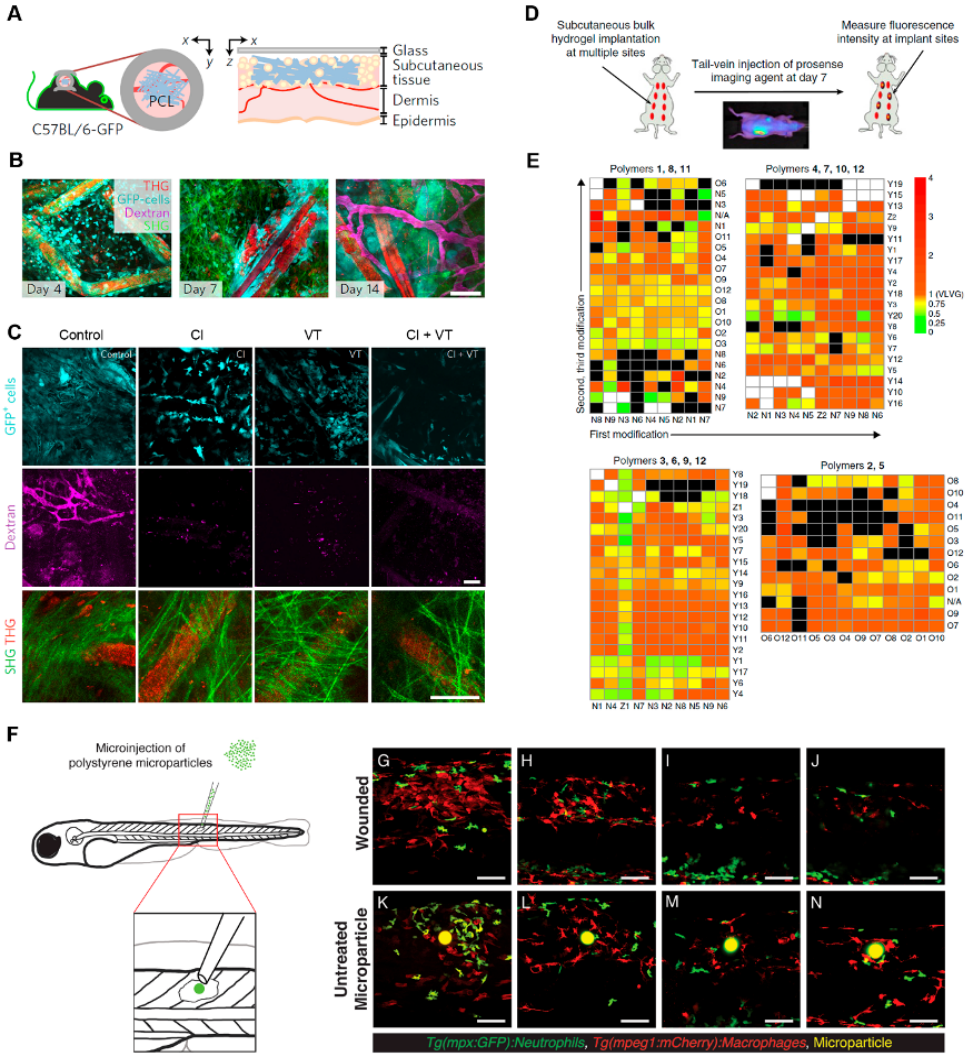

Figure 6. Representative examples of emerging tools for studying the inflammatory response to biomaterials. (A) Implantation of biomaterials in dorsal skinfold window chambers in transgenic mice to study the inflammatory response using intravital imaging. Reprinted by permission of reference [17]. Copyright 2016 Springer Nature. (B-C) Longitudinal intravital imaging of green fluorescent protein $(GFP)^+$ cells in combination with perfusion agent (dextran) and SHG and THG signals showing collagen fibril orientation. Reprinted by permission from [17]. Copyright 2016 Springer Nature. (D, E) High throughput evaluation of fluorescent inflammatory activity in response to a library of modified alginates injected subcutaneously into mice. (E) Heat map summarizing gelation and cathepsin activity of a library of 774 modifications to alginate. Reprinted with permission from [39]. Copyright 2016 Springer Nature. (F) Injection of fluorescent polystyrene microparticles into transgenic larval zebrafish with fluorescently labeled neutrophils and macrophages. Reprinted and adapted with permission from reference [206] Copyright (2018) American Chemical Society.

to biomaterials *in vitro* [215]. For example, the use of a FBR-on-a-chip platform combined with peripheral blood mononuclear cells (PBMCs) directly extracted from the patient has recently been proposed [216].

Such *in vitro* model systems may also help to address another major challenge in understanding the inflammatory response to biomaterials in humans, which is that patients may have very different responses based on their own clinical factors and medical history. It is generally not known how variations in the immunological profile of individuals related to age, sex or comorbidities affect the FBR or the ability of biomaterials to support tissue repair, although some studies are beginning to tackle these questions [217-219]. The effects of comorbidities in particular are especially difficult but important to consider because biomaterials are typically used to repair tissue in diseased sites. For example, the inflammatory response to dedrimer/dextran hydrogels was shown to vary greatly in healthy vs. pathologic models of colonic tissue [220]. These findings suggest that a personalized evaluation of the inflammatory response to biomaterials may be required.

5.2. Identification of new cellular targets

By harnessing spontaneous and knockout mutations or producing chemically-induced immune cell depletions in mice, it is possible to delete specific immune targets to study their role in the FBR and the inflammatory response to biomaterials [221, 222]. Using these models, independent studies targeting different immune mediators have arrived to similar conclusions: neutrophils [13, 26], mast cells [23, 24], natural killer cells (NK cells) [24], and T lymphocytes [33] seem to have little, if any, effect on fibrous capsule development. However, these cells do have major effects in wound healing, and T cells in particular have been demonstrated to be key regulators of biomaterial-mediated tissue repair [87]. Therefore, the similarities and differences between cellular regulation of the FBR and the wound healing response to biomaterials are still poorly understood.

A recent study by Chung et al. described so far overlooked potential therapeutic targets to reduce the FBR [223]. They analyzed the cellular components of fibrous capsules surrounding silicone breast implants in humans and identified IL17-producing $\gamma\delta^+$ T cells and T helper 17 (Th17) cells as well as senescent stromal cells. Senescent cells, which accumulate in aging and in chronic disease,

are non-proliferative cells that secrete numerous inflammatory cytokines as part of the senescence associated secretory phenotype (SASP). Clearance of these cells has been shown to ameliorate numerous diseases [224]. Using animal models, senescent cells were identified to be key mediators of the fibrotic response to PCL particles, inducing differentiation of Th17 cells and giving rise to IL-17-secreting antigen-dependent adaptive response [223]. This study opens the door to alternative therapeutic interventions aimed at blocking the IL-17-associated pathway in T cells and senescent stromal cells.

Still, macrophages have undeniable effects on regulating the FBR and biomaterial-mediated tissue repair [13, 17, 18]. Targeted and timely interventions in macrophage function represent a key area for future strategies to modulate the inflammatory response. For example, manipulation of specific macrophage signaling pathways, such as CSF1/CSF1R [13, 205] and CXCR7/CXCR4/CXCL12 [225], have been shown to ameliorate fibrous capsule development around biomaterials. The inflammasome of macrophages represents another valuable opportunity for therapeutic targeting. The inflammasome comprises a cytosolic multiprotein complex that assembles in response to the presence of danger signals and triggers the production of pro-inflammatory mediators such as IL-1β and IL-18 [226]. In a given moment, this complex can persist and develop a chronic inflammatory process, or it can take an alternative direction towards resolution of inflammation and tissue remodeling [227]. Gaining further insight into the biology of this mechanism may unveil key regulators of the innate response that can be modulated to enhance biomaterial integration.

Relatedly, future studies should direct efforts to overcome the limitations of many biomaterials' studies analyzing macrophage phenotype and overinterpretation of the M1/M2 paradigm. Most studies use a handful of typical M1 and M2 markers but fail to thoroughly characterize macrophage phenotype or extend the characterization to functional effects. In contrast, Sommerfeld et al. used single cell RNA sequencing to thoroughly characterize the phenotype of macrophages participating in the divergent responses to biologic — i.e., ECM scaffolds — or synthetic materials [228]. The team identified a particular combination of surface markers that discriminated between unique macrophage phenotype subsets in fibrotic or pro-regenerative environments. In addition, these populations did not necessarily converge with canonical M1/M2 markers, which reinforces the need for further investigation in this regard.

5.3. New strategies to modulate monocyte/macrophage behavior

Given the importance of macrophages in inflammatory disease and tissue repair, new strategies are needed to control their behavior. As an example, recent studies demonstrate how researchers have taken advantage of the natural behaviors of monocytes and macrophages to ameliorate excessive inflammation. When nanoparticles or microparticles are injected into the bloodstream, they are rapidly cleared from circulation by the reticuloendothelial system, which comprises circulating phagocytes — neutrophils and monocytes — and filtration organs like the liver, spleen, and kidney. While particle properties such as hydrophilicity, surface charge, size, shape, molecular weight, and even coating with biomimetic moieties affect their circulation time before they are cleared, all particles are eventually cleared from circulation within minutes to hours [135, 229-232].

While this rapid clearance is a major impediment to systemically delivered drug delivery systems, recently some researchers have turned it into an advantage. Because monocytes phagocytose particles in the blood stream and carry them to the liver and spleen, Getts et al. showed how this phenomenon can be leveraged to divert monocytes way from sites of inflammation, instead trafficking to the liver and spleen, thus reducing the number of monocytes at the inflammatory site and ameliorating disease in mouse models of myocardial infarction, multiple sclerosis, colitis, peritonitis, and West Nile virus [233]. The authors showed that negatively charged (-40 mV) particles of 0.5 μm in diameter and comprised of polystyrene, PLGA, or microdiamond were internalized by monocytes and quickly carried to the spleen. The effect was found to be more pronounced for negatively charged particles than neutral particles, and to be primarily mediated by the phagocytosis-related MARCO receptor on macrophages. Later, it was shown that the ability of the particles to promote monocyte redirection away from sites of injury also depended on PLGA molecular weight [234]. Finally, using a murine model of spinal cord injury, Park et al. extended this strategy to show that not only did negatively charged particles cause monocytes to redirect away from sites of inflammation, but the few remaining monocytes/macrophages at the injury site expressed higher levels of markers associated with tissue repair compared to controls [235]. While the mechanisms behind this finding remain to be determined, this study shows the potential for leveraging natural phenomena to ameliorate disease and promote tissue repair.

6. Conclusions

The host inflammatory response is a critical determinant of the success or failure of implanted polymeric biomaterials, with outcomes ranging from the foreign body response to biomaterial-tissue integration. Interdisciplinary studies at the intersection of biomaterials science and immunology have shown how these biomaterial outcomes can be influenced by modulating immune cell behavior. With increased understanding of how immune cells regulate tissue repair, it is increasingly possible to design biomaterials that harness the inflammatory response for beneficial effects

.

Acknowledgements

Research in the lab of KLS is supported by NHLBI HL130037 and NSF 1750788. BHE thanks the Basque Government (Dept. of Education, Universities, and Research) for PhD grant PRE_2019_2_0267. ESV and RMH thanks the project SAF2017-82292-R (MINECO) and the support from the Basque Country Government (Grupos Consolidados, No ref: IT907-16).

7. References

1. Holers, V.M., Complement and its receptors: new insights into human disease. Annu Rev Immunol, 2014. 32: p. 433-59.
2. Ladd, J., et al., Zwitterionic polymers exhibiting high resistance to nonspecific protein adsorption from human serum and plasma. Biomacromolecules, 2008. 9(5): p. 1357-61.
3. Li, B., et al., De novo design of functional zwitterionic biomimetic material for immunomodulation. Science Advances, 2020.
4. Li, G., et al., Ultra low fouling zwitterionic polymers with a biomimetic adhesive group. Biomaterials, 2008. 29(35): p. 4592-7.
5. Liu, Q., et al., Developing mechanically robust, triazole-zwitterionic hydrogels to mitigate foreign body response (FBR) for islet encapsulation. Biomaterials, 2020. 230: p. 119640.
6. Liu, Q., et al., Zwitterionically modified alginates mitigate cellular overgrowth for cell encapsulation. Nat Commun, 2019. 10(1): p. 5262.
7. Zhang, L., et al., Zwitterionic hydrogels implanted in mice resist the foreign-body reaction. Nat Biotechnol, 2013. 31(6): p. 553-6.
8. Keselowsky, B.G., et al., Role of plasma fibronectin in the foreign body response to biomaterials. Biomaterials, 2007. 28(25): p. 3626-31.
9. Swartzlander, M.D., et al., Linking the foreign body response and protein adsorption to PEG-based hydrogels using proteomics. Biomaterials, 2015. 41: p. 26-36.
10. Herant, M., V. Heinrich, and M. Dembo, Mechanics of neutrophil phagocytosis: experiments and quantitative models. J Cell Sci, 2006. 119(Pt 9): p. 1903-13.
11. Jhunjhunwala, S., et al., Neutrophil responses to sterile implant materials. PLoS One, 2015. 10(9): p. e0137550.
12. Fetz, A.E., et al., Electrospun template architecture and composition regulate neutrophil NETosis *in vitro* and *in vivo*. Tissue Eng Part A, 2017. 23(19-20): p. 1054-1063.
13. Doloff, J.C., et al., Colony stimulating factor-1 receptor is a central component of the foreign body response to biomaterial implants in rodents and non-human primates. Nat Mater, 2017. 16(6): p. 671-680.
14. Veiseh, O., et al., Size- and shape-dependent foreign body immune response to materials implanted in rodents and non-human primates. Nat Mater, 2015. 14(6): p. 643-51.
15. Davies, L.C., et al., Tissue-resident macrophages. Nat Immunol, 2013. 14(10): p. 986-95.
16. Witherel, C.E., et al., Macrophage and fibroblast interactions in biomaterial-mediated fibrosis. Adv Healthc Mater, 2019. 8(4): p. e1801451.
17. Dondossola, E., et al., Examination of the foreign body response to biomaterials by nonlinear intravital microscopy. Nat. Biomed Eng, 2016. 1(1): p. 1-10.
18. Mooney, J.E., et al., Cellular plasticity of inflammatory myeloid cells in the peritoneal foreign body response. Am J Pathol, 2010. 176(1): p. 369-80.
19. Bank, R.A., et al., Biomaterial Encapsulation Is Enhanced in the Early stages of the foreign body reaction during conditional macrophage depletion in transgenic macrophage Fas-induced apoptosis mice. Tissue Eng Part A, 2017. 23(19-20): p. 1078-1087.
20. Kyriakides, T.R., et al., The CC chemokine ligand, CCL2/MCP1, participates in macrophage fusion and foreign body giant cell formation. Am J Pathol, 2004. 165(6): p. 2157-66.
21. Kuehlmann, B.A., et al., Implant fibrosis is caused by a unique subgroup of collagen producing macrophages. Plast Reconstr Surg Glob Open, 2019. 7(4S): p. 92-93.
22. Farrugia, B.L., et al., The localisation of inflammatory cells and expression of associated proteoglycans in response to implanted chitosan. Biomaterials, 2014. 35(5): p. 1462-77.

23. Avula, M.N., et al., Foreign body response to subcutaneous biomaterial implants in a mast cell-deficient Kit(w-Sh) murine model. Acta Biomater, 2014. 10(5): p. 1856-63.
24. Yang, J., et al., *In vivo* quantitative and qualitative assessment of foreign body giant cell formation on biomaterials in mice deficient in natural killer lymphocyte subsets, mast cells, or the interleukin-4 receptorα and in severe combined immunodeficient mice. J Biomed Mater Res A, 2014. 102(6): p. 2017-23.
25. Higgins, D.M., et al., Localized immunosuppressive environment in the foreign body response to implanted biomaterials. Am J Pathol, 2009. 175(1): p. 161-70.
26. Sadtler, K., et al., The scaffold immune microenvironment: biomaterial-mediated immune polarization in traumatic and nontraumatic applications. Tissue Eng Part A, 2017. 23(19-20): p. 1044-1053.
27. Vasilijić, S., et al., Dendritic cells acquire tolerogenic properties at the site of sterile granulomatous inflammation. Cell Immunol, 2005. 233(2): p. 148-57.
28. Eslami-Kaliji, F., et al., Dendritic cells as targets for biomaterial-based immunomodulation. ACS Biomater Sci Eng, 2020. 6(5): p. 2726-2739.
29. Zhu, F.J., et al., Role of dendritic cells in the host response to biomaterials and their signaling pathways. Acta Biomater, 2019. 94: p. 132-144.
30. Hume, P.S., et al., Strategies to reduce dendritic cell activation through functional biomaterial design. Biomaterials, 2012. 33(14): p. 3615-25.
31. Wang, H. and D.J. Mooney, Biomaterial-assisted targeted modulation of immune cells in cancer treatment. Nat Mater, 2018. 17(9): p. 761-772.
32. Mora-Solano, C. and J.H. Collier, Engaging adaptive immunity with biomaterials. J Mater Chem B, 2014. 2(17): p. 2409-2421.
33. Rodriguez, A., et al., The foreign body reaction in T-cell-deficient mice. J Biomed Mater Res A, 2009. 90(1): p. 106-13.
34. Kim, Y., et al., Reduction of fibrous encapsulation by polyethylene glycol-grafted liposomes containing phosphatidylserine. Biomed Mater, 2020. 15(6); 065007
35. Spasojevic, M., et al., Reduction of the inflammatory responses against alginate-poly-L-lysine microcapsules by anti-biofouling surfaces of PEG-b-PLL diblock copolymers. PLoS One, 2014. 9(10): p. e109837.
36. Lynn, A.D., et al., Temporal progression of the host response to implanted poly(ethylene glycol)-based hydrogels. J Biomed Mater Res A, 2011. 96(4): p. 621-31.
37. Lee, H.C., et al., Foreign body response to intracortical microelectrodes is not altered with dip-coating of polyethylene glycol (PEG). Front Neurosci, 2017. 11: p. 513.
38. Vladkova, T.G.J.I.J.o.p.s., Surface engineered polymeric biomaterials with improved biocontact properties. International Journal of Polymer Science, 2010, p.1-22.
39. Vegas, A.J., et al., Combinatorial hydrogel library enables identification of materials that mitigate the foreign body response in primates. Nat Biotechnol, 2016. 34(3): p. 345-52.
40. Yan, H., et al., Immune-informed mucin hydrogels evade fibrotic foreign body response *in vivo*. Advanced Functional Materials, 2019. 29(46): p. 1902581.
41. Park, C., et al., Reduced fibrous capsule formation at nano-engineered silicone surfaces via tantalum ion implantation. Biomaterials Science, 2019. 7(7): p. 2907-2919.
42. Kamath, S., et al., Surface chemistry influences implant-mediated host tissue responses. J Biomed Mater Res A, 2008. 86(3): p. 617-26.
43. Parker, J.A., et al., Soft-tissue response to silicone and poly-L-lactic acid implants with a periodic or random surface micropattern. J Biomed Mater Res, 2002. 61(1): p. 91-8.
44. Cao, H., et al., The topographical effect of electrospun nanofibrous scaffolds on the *in vivo* and

in vitro foreign body reaction. J Biomed Mater Res A, 2010. 93(3): p. 1151-9.
45. Bota, P.C., et al., Biomaterial topography alters healing *in vivo* and monocyte/macrophage activation *in vitro*. J Biomed Mater Res A, 2010. 95(2): p. 649-57.
46. Sawhney, A.S., C.P. Pathak, and J.A. Hubbell, Interfacial photopolymerization of poly(ethylene glycol)-based hydrogels upon alginate-poly(l-lysine) microcapsules for enhanced biocompatibility. Biomaterials, 1993. 14(13): p. 1008-16.
47. Robotti, F., et al., Microengineered biosynthesized cellulose as anti-fibrotic *in vivo* protection for cardiac implantable electronic devices. Biomaterials, 2020. 229: p. 119583.
48. Zeplin, P.H., et al., Spider silk coatings as a bioshield to reduce periprosthetic fibrous capsule formation. Advanced Functional Materials, 2014. 24(18): p. 2658-2666.
49. Park, J.U., et al., Alleviation of capsular formations on silicone implants in rats using biomembrane-mimicking coatings. Acta Biomater, 2014. 10(10): p. 4217-25.
50. Brauker, J.H., et al., Neovascularization of synthetic membranes directed by membrane microarchitecture. J Biomed Mater Res, 1995. 29(12): p. 1517-24.
51. Madden, L.R., et al., Proangiogenic scaffolds as functional templates for cardiac tissue engineering. Proc Natl Acad Sci U S A, 2010. 107(34): p. 15211-6.
52. Rosengren, A. and L.M. Bjursten, Pore size in implanted polypropylene filters is critical for tissue organization. J Biomed Mater Res A, 2003. 67(3): p. 918-26.
53. Klinge, U., et al., Impact of polymer pore size on the interface scar formation in a rat model. J Surg Res, 2002. 103(2): p. 208-14.
54. Bashur, C.A., M.J. Eagleton, and A. Ramamurthi, Impact of electrospun conduit fiber diameter and enclosing pouch pore size on vascular constructs grown within rat peritoneal cavities. Tissue Eng Part A, 2013. 19(7-8): p. 809-23.
55. Chiu, Y.C., et al., The role of pore size on vascularization and tissue remodeling in PEG hydrogels. Biomaterials, 2011. 32(26): p. 6045-51.
56. Penk, A., et al., The pore size of PLGA bone implants determines the de novo formation of bone tissue in tibial head defects in rats. Magn Reson Med, 2013. 70(4): p. 925-35.
57. White, R.A., et al., Histopathologic observations after short-term implantation of two porous elastomers in dogs. Biomaterials, 1981. 2(3): p. 171-176.
58. Thorson, T.J., et al., Bijel-templated implantable biomaterials for enhancing tissue integration and vascularization. Acta Biomater, 2019. 94: p. 173-182.
59. Griffin, M., et al., Argon plasma improves the tissue integration and angiogenesis of subcutaneous implants by modifying surface chemistry and topography. Int J Nanomedicine, 2018. 13: p. 6123-6141.
60. Macdonald, M.L., et al., Tissue integration of growth factor-eluting layer-by-layer polyelectrolyte multilayer coated implants. Biomaterials, 2011. 32(5): p. 1446-1453.
61. Kantlehner, M., et al., Surface coating with cyclic RGD peptides stimulates osteoblast adhesion and proliferation as well as bone formation. Chembiochem, 2000. 1(2): p. 107-14.
62. Yu, J., et al., The effect of injected RGD modified alginate on angiogenesis and left ventricular function in a chronic rat infarct model. Biomaterials, 2009. 30(5): p. 751-756.
63. Flora, T., et al., Tethering QK peptide to enhance angiogenesis in elastin-like recombinamer (ELR) hydrogels. Journal of Materials Science: Materials in Medicine, 2019. 30(2): p. 30.
64. Jung, S.C., et al., Polymeric embolization coil of bilayered polyvinyl alcohol strand for therapeutic vascular occlusion: a feasibility study in canine experimental vascular models. J Vasc Interv Radiol, 2015. 26(1): p. 117-23.
65. Siskin, G.P., et al., Embolic agents used for uterine fibroid embolization. AJR Am J Roentgenol, 2000. 175(3): p. 767-73.

66. Spies, J.B., et al., Polyvinyl alcohol particles and tris-acryl gelatin microspheres for uterine artery embolization for leiomyomas: results of a randomized comparative study. J. Vasc Interv Radiol, 2004. 15(8): p. 793-800.
67. Spies, J.B., et al., Long-term outcome of uterine artery embolization of leiomyomata. Obstet Gynecol, 2005. 106(5): p. 933-939.
68. Colgan, T.J., et al., Pathologic features of uteri and leiomyomas following uterine artery embolization for leiomyomas. Am J Surg Pathol, 2003. 27(2): p. 167-177.
69. Siskin, G.P., et al., Pathologic findings in a uterine leiomyoma after bilateral uterine artery embolization. J Vasc Interv Radiol, 1999. 10(7): p. 891-894.
70. Tarchala, M., E.J. Harvey, and Barralet, J, Biomaterial-stabilized soft tissue healing for healing of critical-sized bone defects: the Masquelet technique. Adv Healthc Mater, 2016. 5(6): p. 630-640.
71. Campbell, J.H., J.L. Efendy, and G.R.J.C.r. Campbell, Novel vascular graft grown within recipient's own peritoneal cavity. Circ Res, 1999. 85(12): p. 1173-1178.
72. Rothuizen, T.C., et al., Development and evaluation of *in vivo* tissue engineered blood vessels in a porcine model. Biomaterials, 2016. 75: p. 82-90.
73. Julier, Z., et al., Promoting tissue regeneration by modulating the immune system. Acta Biomaterialia, 2017. 53: p. 13-28.
74. Grose, R. and S. Werner, Wound-healing studies in transgenic and knockout mice. Molecular Biotechnology, 2004. 28(2): p. 147.
75. Velnar, T., T. Bailey, and V. Smrkolj, The wound healing process: An overview of the cellular and molecular mechanisms. Journal of International Medical Research, 2009. 37(5): p. 1528-1542.
76. Boada-Romero, E., et al., The clearance of dead cells by efferocytosis. Nature Reviews Molecular Cell Biology, 2020. 21(7): p. 398-414.
77. Daley, J.M., et al., The phenotype of murine wound macrophages. Journal of Leukocyte Biology, 2010. 87(1): p. 59-67.
78. Kim, B.-S., et al., Characterization of adipose tissue macrophages and adipose-derived stem cells in critical wounds. PeerJ, 2017. 5: p. e2824.
79. Martinez, F.O., et al., Macrophage activation and polarization. Front Biosci, 2008. 13: p. 453-61.
80. Spiller, K.L., et al., Sequential delivery of immunomodulatory cytokines to facilitate the M1-to-M2 transition of macrophages and enhance vascularization of bone scaffolds. Biomaterials, 2015. 37: p. 194-207.
81. Graney, P.L., et al., Macrophages of diverse phenotypes drive vascularization of engineered tissues. Science Advances, 2020. 6(18)
82. Lurier, E.B., et al., Transcriptome analysis of IL-10-stimulated (M2c) macrophages by next-generation sequencing. Immunobiology, 2017. 222(7): p. 847-856.
83. Rao, A.J., et al., Revision joint replacement, wear particles, and macrophage polarization. Acta Biomaterialia, 2012. 8(7): p. 2815-2823.
84. Bajpai, G., et al., Tissue resident CCR2^{-} and CCR2^{+} cardiac macrophages differentially orchestrate monocyte recruitment and fate specification following myocardial injury. Circ Res, 2019. 124(2): p. 263-278.
85. Kubota, Y., et al., M-CSF inhibition selectively targets pathological angiogenesis and lymphangiogenesis. Journal of Experimental Medicine, 2009. 206(5): p. 1089-1102.
86. Hirose, N., et al., The local injection of peritoneal macrophages induces neovascularization in rat ischemic hind limb muscles:. http://dx.doi.org/10.3727/000000008783906919, 2008.
87. Sadtler, K., et al., Developing a pro-regenerative biomaterial scaffold microenvironment requires T helper 2 cells. Science, 2016. 352(6283): p 366-370.
88. Spiller, K.L. and T.J. Koh, Macrophage-based therapeutic strategies in regenerative medicine.

Advanced Drug Delivery Reviews, 2017. 122: p. 74-83.
89. Anderson, J.M. and K.M. Miller, Biomaterial biocompatibility and the macrophage. Biomaterials, 1984. 5(1): p. 5-10.
90. Badylak, S.F., et al., Macrophage phenotype as a determinant of biologic scaffold remodeling. Tissue Engineering Part A, 2008. 14(11): p. 1835-1842.
91. Brown, B.N., et al., Macrophage phenotype and remodeling outcomes in response to biologic scaffolds with and without a cellular component. Biomaterials, 2009. 30(8): p. 1482-1491.
92. Brown, B.N., et al., Macrophage phenotype as a predictor of constructive remodeling following the implantation of biologically derived surgical mesh materials. Acta Biomaterialia, 2012. 8(3): p. 978-987.
93. Yu, T., et al., Temporal and spatial distribution of macrophage phenotype markers in the foreign body response to glutaraldehyde-crosslinked gelatin hydrogels. Journal of Biomaterials Science, Polymer Edition, 2016. 27(8): p. 721-742.
94. Sussman, E.M., et al., Porous implants modulate healing and induce shifts in local macrophage polarization in the foreign body reaction. Annals of Biomedical Engineering, 2014. 42(7): p. 1508-1516.
95. van Putten, S.M., et al., Macrophage phenotypes in the collagen-induced foreign body reaction in rats. Acta Biomaterialia, 2013. 9(5): p. 6502-6510.
96. Witherel, C.E., et al., Macrophage and fibroblast interactions in biomaterial-mediated fibrosis. Advanced Healthcare Materials, 2019. 8(4): p. 1801451.
97. Pakshir, P., et al., Dynamic fibroblast contractions attract remote macrophages in fibrillar collagen matrix. Nature Communications, 2019. 10(1): p. 1-17.
98. Sridharan, R., et al., Material stiffness influences the polarization state, function and migration mode of macrophages. Acta Biomaterialia, 2019. 89: p. 47-59.
99. Previtera, M.L. and A. Sengupta, Substrate stiffness regulates proinflammatory mediator production through TLR4 activity in macrophages. PLOS ONE, 2015. 10(12): p. e0145813.
100. Okamoto, T., et al., Reduced substrate stiffness promotes M2-like macrophage activation and enhances peroxisome proliferator-activated receptor γ expression. Experimental Cell Research, 2018. 367(2): p. 264-273.
101. Blakney, A.K., M.D. Swartzlander, and S.J. Bryant, The effects of substrate stiffness on the *in vitro* activation of macrophages and *in vivo* host response to poly(ethylene glycol)-based hydrogels. Journal of Biomedical Materials Research Part A, 2012. 100A(6): p. 1375-1386.
102. Hind, L.E., et al., Effect of M1–M2 Polarization on the motility and traction stresses of primary human macrophages. cellular and molecular Bioengineering, 2016. 9(3): p. 455-465.
103. Jiang, S., et al., Cryoprotectant enables structural control of porous scaffolds for exploration of cellular mechano-responsiveness in 3D. Nature Communications, 2019. 10(1): p. 1-14.
104. Patel, N.R., et al., Cell elasticity determines macrophage function, in PLoS One. 2012.
105. Wu, L., et al., Cellular responses to thermoresponsive stiffness memory elastomer nanohybrid scaffolds by 3D-TIPS. Acta Biomaterialia, 2019. 85: p. 157-171.
106. Garg, K., et al., Macrophage functional polarization (M1/M2) in response to varying fiber and pore dimensions of electrospun scaffolds. Biomaterials, 2013. 34(18): p. 4439-4451.
107. Duan, Y., et al., Unsaturated polyurethane films grafted with enantiomeric polylysine promotes macrophage polarization to a M2 phenotype through PI3K/Akt1/mTOR axis. Biomaterials, 2020. 246: p. 120012.
108. Garg, K., et al., Macrophage functional polarization (M1/M2) in response to varying fiber and pore dimensions of electrospun scaffolds. Biomaterials, 2013. 34(18): p. 4439-51.
109. Wang, Z., et al., The effect of thick fibers and large pores of electrospun poly(epsilon-caprolactone) vascular grafts on macrophage polarization and arterial regeneration. Biomaterials, 2014. 35(22): p. 5700-10.

110. Almeida, C.R., et al., Impact of 3-D printed PLA- and chitosan-based scaffolds on human monocyte/macrophage responses: unraveling the effect of 3-D structures on inflammation. Acta Biomater, 2014. 10(2): p. 613-22.
111. McWhorter, F.Y., et al., Modulation of macrophage phenotype by cell shape. Proceedings of the National Academy of Sciences, 2013. 110(43): p. 17253.
112. Vogel, D.Y.S., et al., Human macrophage polarization *in vitro*: Maturation and activation methods compared. Immunobiology, 2014. 219(9): p. 695-703.
113. Später, T., et al., Biological coating with platelet-rich plasma and adipose tissue-derived microvascular fragments improves the vascularization, biocompatibility and tissue incorporation of porous polyethylene. Acta Biomaterialia, 2020. 108: p. 194-206.
114. Rodell, C.B., et al., TLR7/8-agonist-loaded nanoparticles promote the polarization of tumour-associated macrophages to enhance cancer immunotherapy. Nature Biomedical Engineering, 2018. 2(8): p. 578-588.
115. Bartneck, M., et al., Induction of specific macrophage subtypes by defined micro-patterned structures. Acta Biomaterialia, 2010. 6(10): p. 3864-3872.
116. Zhang, J., et al., A comparable study of polyglycolic acid's degradation on macrophages' activation. Materials Science and Engineering: C, 2020. 109: p. 110574.
117. Burdick, J.A., et al., An investigation of the cytotoxicity and histocompatibility of in situ forming lactic acid based orthopedic biomaterials. Journal of Biomedical Materials Research, 2002. 63(5): p. 484-491.
118. Wolf, M.T., et al., A biologic scaffold–associated type 2 immune microenvironment inhibits tumor formation and synergizes with checkpoint immunotherapy. Science Translational Medicine, 2019. 11(477).
119. Sadtler, K., et al., Divergent immune responses to synthetic and biological scaffolds. Biomaterials, 2019. 192: p. 405-415.
120. Dziki, J.L., et al., Solubilized extracellular matrix bioscaffolds derived from diverse source tissues differentially influence macrophage phenotype. Journal of Biomedical Materials Research Part A, 2017. 105(1): p. 138-147.
121. Beachley, V.Z., et al., Tissue matrix arrays for high-throughput screening and systems analysis of cell function. Nature Methods, 2015. 12(12): p. 1197-1204.
122. Sadtler, K., et al., Proteomic composition and immunomodulatory properties of urinary bladder matrix scaffolds in homeostasis and injury. Seminars in Immunology, 2017. 29: p. 14-23.
123. Sadtler, K., et al., The scaffold immune microenvironment: Biomaterial-mediated immune polarization in traumatic and nontraumatic applications. Tissue Engineering Part A, 2016. 23(19-20): p. 1044-1053.
124. Sommerfeld, S.D., et al., Interleukin-36γ–producing macrophages drive IL-17–mediated fibrosis. Science Immunology, 2019. 4(40).
125. Wei, R., J. Wu, and Y. Li, Macrophage polarization following three-dimensional porous PEEK. Materials science and engineering. C, Materials for biological applications, 2019. 104: p. 109948.
126. Franz, S., et al., Artificial extracellular matrices composed of collagen I and high-sulfated hyaluronan promote phenotypic and functional modulation of human pro-inflammatory M1 macrophages. Acta Biomaterialia, 2013. 9(3): p. 5621-5629.
127. Won, J.-E., et al., Hierarchical microchanneled scaffolds modulate multiple tissue-regenerative processes of immune-responses, angiogenesis, and stem cell homing. Biomaterials, 2020. 227: p. 119548.
128. Madden, L.R., et al., Proangiogenic scaffolds as functional templates for cardiac tissue engineering. Proceedings of the National Academy of Sciences, 2010. 107(34): p. 15211.

129. Wang, Z., et al., The effect of thick fibers and large pores of electrospun poly(ε-caprolactone) vascular grafts on macrophage polarization and arterial regeneration. Biomaterials, 2014. 35(22): p. 5700-5710.
130. Almeida, C.R., et al., Impact of 3-D printed PLA- and chitosan-based scaffolds on human monocyte/macrophage responses: Unraveling the effect of 3-D structures on inflammation. Acta Biomaterialia, 2014. 10(2): p. 613-622.
131. Jia, Y., et al., Nanofiber arrangement regulates peripheral nerve regeneration through differential modulation of macrophage phenotypes. Acta Biomaterialia, 2019. 83: p. 291-301.
132. Saino, E., et al., Effect of electrospun fiber diameter and alignment on macrophage activation and secretion of proinflammatory cytokines and chemokines. Biomacromolecules, 2011. 12(5): p 1900-11.
133. Bartneck, M., et al., Inducing healing-like human primary macrophage phenotypes by 3D hydrogel coated nanofibres. Biomaterials, 2012. 33(16): p. 4136-4146.
134. Carleton, M.M. and M.V. Sefton, Injectable and degradable methacrylic acid hydrogel alters macrophage response in skeletal muscle. Biomaterials, 2019. 223: p. 119477.
135. Casey, L.M., et al., Cargo-less nanoparticles program innate immune cell responses to toll-like receptor activation. Biomaterials, 2019. 218: p. 119333.
136. Hong, J.Y., et al., Decellularized brain matrix enhances macrophage polarization and functional improvements in rat spinal cord injury. Acta Biomaterialia, 2020. 101: p. 357-371.
137. Qiu, P., et al., Periosteal matrix-derived hydrogel promotes bone repair through an early immune regulation coupled with enhanced angio- and osteogenesis. Biomaterials, 2020. 227: p. 119552.
138. Kumar, V.A., et al., Self-assembling multidomain peptides tailor biological responses through biphasic release. Biomaterials, 2015. 52: p. 71-78.
139. Olingy, C.E., et al., Non-classical monocytes are biased progenitors of wound healing macrophages during soft tissue injury. Scientific Reports, 2017. 7(1): p. 1-16.
140. Ginhoux, F. and S. Jung, Monocytes and macrophages: developmental pathways and tissue homeostasis. Nature Reviews Immunology, 2014. 14(6): p. 392-404.
141. Awojoodu, A.O., et al., Sphingosine 1-phosphate receptor 3 regulates recruitment of anti-inflammatory monocytes to microvessels during implant arteriogenesis. Proceedings of the National Academy of Sciences, 2013. 110(34): p. 13785.
142. San Emeterio, C.L., et al., Selective recruitment of non-classical monocytes promotes skeletal muscle repair. Biomaterials, 2017. 117: p. 32-43.
143. Aronin, C.E.P., et al., FTY720 promotes local microvascular network formation and regeneration of cranial bone defects. Tissue Engineering Part A, 2010. 16(6): p. 1801-9.
144. Petrie Aronin, C.E., et al., The enhancement of bone allograft incorporation by the local delivery of the sphingosine 1-phosphate receptor targeted drug FTY720. Biomaterials, 2010. 31(25): p. 6417-6424.
145. Das, A., et al., Delivery of S1P receptor-targeted drugs via biodegradable polymer scaffolds enhances bone regeneration in a critical size cranial defect. Journal of Biomedical Materials Research Part A, 2014. 102(4): p. 1210-1218.
146. Krieger, J.R., et al., Spatially localized recruitment of anti-inflammatory monocytes by SDF-1α-releasing hydrogels enhances microvascular network remodeling. Biomaterials, 2016. 77: p. 280-290.
147. Kim, Y.-H. and Y. Tabata, Enhancement of wound closure by modifying dual release patterns of stromal-derived cell factor-1 and a macrophage recruitment agent from gelatin hydrogels. Journal of Tissue Engineering and Regenerative Medicine, 2017. 11(11): p. 2999-3013.
148. Hu, Z., et al., Immunomodulatory ECM-like microspheres for accelerated bone regeneration in diabetes mellitus. 2018.

149. Lortat-Jacob, H., et al., Human Interleukin-4 is a glycosaminoglycan-binding ptotein. Cytokine, 1997. 9(2): p. 101-105.
150. Essandoh, K., et al., MiRNA-mediated macrophage polarization and its potential role in the regulation of inflammatory response. Shock, 2016. 46(2).
151. Liu, G. and E. Abraham, MicroRNAs in Immune response and macrophage polarization. Arteriosclerosis, Thrombosis, and Vascular Biology, 2013. 33(2): p. 170-177.
152. Bejerano, T., et al., Nanoparticle delivery of miRNA-21 mimic to cardiac macrophages improves myocardial remodeling after myocardial infarction. Nano Letters, 2018. 18(9): p. 5885-5891.
153. Huynh, M.-L.N., V.A. Fadok, and P.M. Henson, Phosphatidylserine-dependent ingestion of apoptotic cells promotes TGF-β1 secretion and the resolution of inflammation. The Journal of Clinical Investigation, 2002. 109(1): p. 41-50.
154. Harel-Adar, T., et al., Modulation of cardiac macrophages by phosphatidylserine-presenting liposomes improves infarct repair. Proceedings of the National Academy of Sciences, 2011. 108(5): p. 1827.
155. Ramos, G.C., et al., Apoptotic mimicry: phosphatidylserine liposomes reduce inflammation through activation of peroxisome proliferator-activated receptors (PPARs) *in vivo*. British Journal of Pharmacology, 2007. 151(6): p. 844-850.
156. Paulina, K., et al., The role of macrophages in acute and chronic wound healing and interventions to promote pro-wound healing phenotypes. Frontiers in Physiology, 2018. 9.
157. Sindrilaru, A., et al., An unrestrained proinflammatory M1 macrophage population induced by iron impairs wound healing in humans and mice. The Journal of Clinical Investigation, 2011. 121(3): p. 985-997.
158. Moore, J.P., et al., M2 macrophage accumulation in the aortic wall during angiotensin II infusion in mice is associated with fibrosis, elastin loss, and elevated blood pressure. American Journal of Physiology-Heart and Circulatory Physiology, 2015. 309(5): p. H906-H917.
159. Bility, M.T., et al., Hepatitis B virus infection and immunopathogenesis in a humanized mouse model: Induction of human-specific liver fibrosis and M2-like macrophages. PLOS Pathogens, 2014. 10(3): p. e1004032.
160. Stahl, M., et al., Lung collagens perpetuate pulmonary fibrosis via CD204 and M2 macrophage activation. PLOS ONE, 2013. 8(11): p. e81382.
161. O'Brien, E.M., G.E. Risser, and K.L. Spiller, Sequential drug delivery to modulate macrophage behavior and enhance implant integration. Advanced Drug Delivery Reviews, 2019. 149-150: p. 85-94.
162. Alhamdi, J.R., et al., Controlled M1-to-M2 transition of aged macrophages by calcium phosphate coatings. Biomaterials, 2019. 196: p. 90-99.
163. Chen, J., et al., Macrophage phenotype switch by sequential action of immunomodulatory cytokines from hydrogel layers on titania nanotubes. Colloids and Surfaces B: Biointerfaces, 2018. 163: p. 336-345.
164. Tolouei, A.E., et al., A Magnetically responsive biomaterial system for flexibly regulating the duration between pro- and anti-Inflammatory cytokine deliveries. Advanced Healthcare Materials, 2018. 7(12): p. 1800227.
165. Li, T., et al., 3D-printed IFN-γ-loading calcium silicate-β-tricalcium phosphate scaffold sequentially activates M1 and M2 polarization of macrophages to promote vascularization of tissue engineering bone. Acta Biomaterialia, 2018. 71: p. 96-107.
166. Sok, M.C.P., et al., Aspirin-triggered resolvin D1-modified materials promote the accumulation of pro-regenerative immune cell subsets and enhance vascular remodeling. Acta Biomaterialia, 2017. 53: p. 109-122.
167. Ballestas, S.A., et al., Improving hard palate wound healing using immune modulatory

autotherapies. Acta Biomaterialia, 2019. 91: p. 209-219.
168. Enam, S.F., et al., Enrichment of endogenous fractalkine and anti-inflammatory cells via aptamer-functionalized hydrogels. Biomaterials, 2017. 142: p. 52-61.
169. Mokarram, N., et al., Immunoengineering nerve repair. Proceedings of the National Academy of Sciences, 2017. 114(26): p. E5077.
170. Ogle, M., et al., Dual affinity heparin-based hydrogels achieve pro-regenerative immunomodulation and microvascular remodeling. 2017.
171. McLaughlin, S., et al., Injectable human recombinant collagen matrices limit adverse remodeling and improve cardiac function after myocardial infarction. Nature Communications, 2019. 10(1): p. 1-14.
172. Gower, R.M., et al., Modulation of leukocyte infiltration and phenotype in microporous tissue engineering scaffolds via vector induced IL-10 expression. Biomaterials, 2014. 35(6): p. 2024-2031.
173. Tran, T.-H., et al., Modulation of macrophage functional polarity towards anti-inflammatory phenotype with plasmid DNA delivery in CD44 targeting hyaluronic acid nanoparticles. Scientific Reports, 2015. 5(1): p. 16632.
174. Hachim, D., et al., Shifts in macrophage phenotype at the biomaterial interface via IL-4 eluting coatings are associated with improved implant integration. Biomaterials, 2017. 112: p. 95-107.
175. Minardi, S., et al., IL-4 release from a biomimetic scaffold for the temporally controlled modulation of macrophage response. Annals of Biomedical Engineering, 2016. 44(6): p. 2008-2019.
176. Zheng, Z.-w., et al., Development of an accurate and proactive immunomodulatory strategy to improve bone substitute material-mediated osteogenesis and angiogenesis. Theranostics, 2018. 8(19): p. 5482-5500.
177. Li, M., et al., Synergistic regulation of osteoimmune microenvironment by IL-4 and RGD to accelerate osteogenesis. Materials Science and Engineering. C, Materials for Biological Applications, 2020. 109: p. 110508.
178. Kumar, M., et al., Immunomodulatory injectable silk hydrogels maintaining functional islets and promoting anti-inflammatory M2 macrophage polarization. Biomaterials, 2018. 187: p. 1-17.
179. Castaño, I.M., et al., Rapid bone repair with the recruitment of $CD206^{+}$M2-like macrophages using non-viral scaffold-mediated miR-133a inhibition of host cells. Acta Biomaterialia, 2020. 109: p. 267-279.
180. Kraynak, C.A., D.J. Yan, and L.J. Suggs, Modulating inflammatory macrophages with an apoptotic body-inspired nanoparticle. Acta Biomaterialia, 2020. 108: p. 250-260.
181. Gao, L., et al., Dual-inflammatory cytokines on TiO_2 nanotube-coated surfaces used for regulating macrophage polarization in bone implants. Journal of Biomedical Materials Research Part A, 2018. 106(7): p. 1878-1886.
182. Hu, M.S., et al., Delivery of monocyte lineage cells in a biomimetic scaffold enhances tissue repair. JCI Insight, 2017. 2(19).
183. Kigerl, K.A., et al., Identification of two distinct macrophage subsets with divergent effects causing either neurotoxicity or regeneration in the injured mouse spinal cord. The Journal of Neuroscience : the Official Journal of the Society for Neuroscience, 2009. 29(43): p. 13435-13444.
184. Cao, Q., et al., Failed renoprotection by alternatively activated bone marrow macrophages is due to a proliferation-dependent phenotype switch *in vivo*. Kidney International, 2014. 85(4): p. 794-806.
185. Wofford, K.L., et al., Biomaterial-mediated reprogramming of monocytes via microparticle phagocytosis for sustained modulation of macrophage phenotype. Acta Biomaterialia, 2020. 101: p. 237-248.
186. Shields, C.W., et al., Cellular backpacks for macrophage immunotherapy. 2020.
187. Squillaro, T., G. Peluso, and U. Galderisi, Clinical Trials with Mesenchymal Stem Cells: An Update. Cell Transplantation, 2016. 25(5): p. 829-848.

188. Le Blanc, K. and O. Ringdén, Immunomodulation by mesenchymal stem cells and clinical experience. Journal of Internal Medicine, 2007. 262(5): p. 509-525.
189. Eggenhofer, E. and M.J. Hoogduijn, Mesenchymal stem cell-educated macrophages. Transplantation Research, 2012. 1(1): p. 12.
190. Németh, K., et al., Bone marrow stromal cells attenuate sepsis via prostaglandin E2–dependent reprogramming of host macrophages to increase their interleukin-10 production. Nature Medicine, 2009. 15(1): p. 42-49.
191. de Witte, S.F.H., et al., Immunomodulation by therapeutic mesenchymal stromal Cells (MSC) is triggered through phagocytosis of MSC by monocytic cells. Stem Cells, 2018. 36(4): p. 602-615.
192. Levit Rebecca, D., et al., Cellular encapsulation enhances cardiac repair. Journal of the American Heart Association. 2(5): p. e000367.
193. Ishihara, A., Effect of intra-medullar and intra-venous infusions of mesenchymal stem cells on cell engraftment by *in vivo* cell tracking and osteoinductivity in rabbit long bones: A pilot study. Orthopedic & Muscular System, 2014. 03(03).
194. Gronthos, S., et al., Integrin-mediated interactions between human bone marrow stromal precursor cells and the extracellular matrix. Bone, 2001. 28(2): p. 174-181.
195. Marquardt, L.M. and S.C. Heilshorn, Design of injectable materials to improve stem cell transplantation. Curr Stem Cell Rep, 2016. 2(3): p. 207-220.
196. Swartzlander, M.D., et al., Immunomodulation by mesenchymal stem cells combats the foreign body response to cell-laden synthetic hydrogels. Biomaterials, 2015. 41: p. 79-88.
197. Niu, Y., et al., Modulating the phenotype of host macrophages to enhance osteogenesis in MSC-laden hydrogels: Design of a glucomannan coating material. Biomaterials, 2017. 139: p. 39-55.
198. Clark, A.Y., et al., Integrin-specific hydrogels modulate transplanted human bone marrow-derived mesenchymal stem cell survival, engraftment, and reparative activities. Nature Communications, 2020. 11(1): p. 114.
199. Wang, Y., et al., Plasticity of mesenchymal stem cells in immunomodulation: pathological and therapeutic implications. Nature Immunology, 2014. 15(11): p. 1009-1016.
200. Gonzalez-Pujana, A., et al., Multifunctional biomimetic hydrogel systems to boost the immunomodulatory potential of mesenchymal stromal cells. Biomaterials, 2020. 257: p. 120266.
201. Nakamura, Y., et al., Enhanced wound healing by topical administration of mesenchymal stem cells transfected with stromal cell-derived factor-1. Biomaterials, 2013. 34(37): p. 9393-9400.
202. Nauta, A., et al., Adipose-derived stromal cells overexpressing vascular endothelial growth factor accelerate mouse excisional wound healing. Molecular Therapy, 2013. 21(2): p. 445-455.
203. Larson, A.M.J.N.P., Multiphoton microscopy. 2011. 5(1): p. 1-1.
204. Hoover, E.E. and J.A.J.N.p. Squier, Advances in multiphoton microscopy technology. Nature Photonics, 2013. 7(2): p. 93-101.
205. Yang, N., et al., Immobilized macrophage colony-stimulating factor (M-CSF) regulates the foreign body response to implanted materials. ACS Biomater, 2020. 6(2): p. 995-1007.
206. Witherel, C.E., et al., Host–Biomaterial interactions in zebrafish. ACS Bio mater Sci Eng, 2018. 4(4): p. 1233-1240.
207. Gurevich, D.B., et al., Live imaging of wound angiogenesis reveals macrophage orchestrated vessel sprouting and regression.EMBO J, 2018. 37(13): p. e97786.
208. Gurevich, D.B., et al., Live imaging the foreign body response in zebrafish reveals how dampening inflammation reduces fibrosis. J Cell Sci, 2019. 133(5): p. jcs236075.
209. Hackam, D.G. and D.A.J.J. Redelmeier, Translation of research evidence from animals to humans. JAMA, 2006. 296(14): p. 1727-1732.
210. Ørning, P., et al., Alginate microsphere compositions dictate different mechanisms of

complement activation with consequences for cytokine release and leukocyte activation. Journal of Controlled Release, 2016. 229: p. 58-69.
211. Gravastrand, C., et al., Alginate microbeads are coagulation compatible, while alginate microcapsules activate coagulation secondary to complement or directly through FXII. Acta Biomater, 2017. 58: p. 158-167.
212. Witherel, C.E., P.L. Graney, and K.L. Spiller, *In vitro* model of macrophage-biomaterial interactions, in biomaterials for Tissue Engineering. 2018, Springer. p. 161-176.
213. Zhou, G., et al., *In vitro* study of the host responses to model biomaterials via a fibroblast/macrophage co-culture system. Biomaterials Science, 2017. 5(1): p. 141-152.
214. Jannasch, M., et al., An *in vitro* model mimics the contact of biomaterials to blood components and the reaction of surrounding soft tissue. Acta Biomaterialia, 2019. 89(34): p. 227-241.
215. Ahadian, S., et al., Organ-on-a-chip platforms: A convergence of advanced materials, Cells, and Microscale Technologies. Adv Healthc Mater, 2018. 7(2).
216. Sharifi, F., et al., A foreign body response-on-a-chip platform. Advanced Healthcare Materials, 2019. 8(4): p. 1801425.
217. Liu, M., et al., Effect of age on biomaterial-mediated in situ bone tissue regeneration. Acta Biomater, 2018. 78: p. 329-340.
218. Dalu, A., et al., A comparison of the inflammatory response to a polydimethylsiloxane implant in male and female Balb/c mice. Biomaterials, 2000. 21(19): p. 1947-57.
219. Berger, M.B., et al., Human osteoblasts exhibit sexual dimorphism in their response to estrogen on microstructured titanium surfaces. Biol Sex Differ, 2018. 9(1): p. 30.
220. Oliva, N., et al., Regulation of dendrimer/dextran material performance by altered tissue microenvironment in inflammation and neoplasia. Sci Transl Med, 2015. 7(272): p. 272ra11.
221. Veiseh, O. and A.J.J.A.D.D.R. Vegas, Domesticating the foreign body response: recent advances and applications. Advanced Drug Delivery Reviews, 2019. 144: p. 148-161.
222. Saleh, L.S. and S.J.J.D.D.T.D.M. Bryant, *In vitro* and *in vivo* models for assessing the host response to biomaterials. Drug Discovery Today: Disease Models, 2017. 24: p. 13-21.
223. Chung, L., et al., Interleukin 17 and senescent cells regulate the foreign body response to synthetic material implants in mice and humans. Science Translational Medicine, 2020. 12(539).
224. Childs, B.G., et al., Cellular senescence in aging and age-related disease: from mechanisms to therapy. Nat Med, 2015. 21(12): p. 1424-1435.
225. Cai, X., et al., Identification of the CXCL12–CXCR4/CXCR7 axis as a potential therapeutic target for immunomodulating macrophage polarization and foreign body response to implanted biomaterials. Applied Materials Today, 2020. 18: p. 100454.
226. Malik, A.F., et al., Inflammasome components Asc and caspase-1 mediate biomaterial-induced inflammation and foreign body response. Proc Natl Acad Sci USA, 2011. 108(50): p. 20095-20100.
227. Vasconcelos, D.P., et al., The inflammasome in host response to biomaterials: Bridging inflammation and tissue regeneration. Acta Biomater, 2019. 83: p. 1-12.
228. Sommerfeld, S.D., et al., Interleukin-36γ–producing macrophages drive IL-17–mediated fibrosis. Sci Immunol, 2019. 4(40): p. eaax4783.
229. He, C., et al., Effects of particle size and surface charge on cellular uptake and biodistribution of polymeric nanoparticles. Biomaterials, 2010. 31(13): p. 3657-66.
230. He, Q., et al., *In vivo* biodistribution and urinary excretion of mesoporous silica nanoparticles: effects of particle size and PEGylation. Small, 2011. 7(2): p. 271-80.
231. Okuda, T., et al., Biodistribution characteristics of amino acid dendrimers and their PEGylated derivatives after intravenous administration. J Control Release, 2006. 114(1): p. 69-77.
232. Huang, X., et al., The shape effect of mesoporous silica nanoparticles on biodistribution,

clearance, and biocompatibility *in vivo*. ACS Nano, 2011. 5(7): p. 5390-5399.
233. Getts, D.R., et al., Therapeutic inflammatory monocyte modulation using immune-modifying microparticles. Sci Transl Med, 2014. 6(219): p. 219ra7.
234. Saito, E., et al., Designing drug-free biodegradable nanoparticles to modulate inflammatory monocytes and neutrophils for ameliorating inflammation. J Control Release, 2019. 300: p. 185-196.
235. Park, J., et al., Intravascular innate immune cells reprogrammed via intravenous nanoparticles to promote functional recovery after spinal cord injury. Proc Natl Acad Sci U S A, 2019. 116(30): p. 14947-14954.

2

Hypothesis and Objectives

In recent years, organ transplantation technology has made significant improvements regarding long-term survival, substantially decreasing the risk of graft rejection. However, with each passing year, the gap between available donors and the number of patients needing an organ transplant is steadily increasing. Consequently, there is a growing demand to create engineered tissues to minimize the need for organ transplantation. However, the rejection of engineered tissue implants has become a critical challenge today. Primarily, rejection occurs due to the crosstalk between immune cells and the engineered tissue structure. Therefore, it is important to be able to influence the immune cell milieu of the implantation site to achieve graft integration. With this perspective in mind, this doctoral thesis aims to provide two different strategies: 1) The use of human hair follicle derived mesenchymal stromal cells (HF-MSCs) for immunomodulation, and 2) The application of tissue engineered blood vessels to interact with different macrophage phenotypes and promote a tissue remodeling response around the implant.

The first strategy is based on the fact that MSC have the ability to secrete immunomodulatory factors which can then subsequently regulate both the adaptative and the innate immune response, thereby indirectly influencing the implant outcome. Since they were first described in 1968, MSCs have been isolated from nearly all tissues, with MSCs derived from bone marrow (BM-MSC) and adipose tissue (AT-MSC) being the most widely used. However, the isolation procedures of these origins are painful and invasive for patients. For that reason, this work proposes the use of a lesser-known source of MSCs: the hair follicle. The main advantages of the HF-MSCs are the easy accessibility, painless procedure and lower risk of viral infections. Therefore, we hypothesized that HF-MSCs could be a feasible alternative source of MSCs for immunomodulation regarding their accessibility and ease of harvesting and that they could have better or at least comparable immunomodulatory potential as AT-MSCs.

The second strategy relies on the addition of tissue-engineered blood vessels to the biomaterial prior to implantation. Implant failure occurs mainly due to the inability of the host tissue to rapidly vascularize the implanted engineered tissue, leading to lack of oxygen and nutrients, the consequent cell death and the eventual deterioration of tissue integration and function. To enhance vascularization, one of the strategies that has been recently explored is the pre-vascularization of

the engineered tissues. This could help to promote the anastomosis and subsequent perfusion to the implant. However, upon implantation, the engineered tissue will encounter the host's immune system. Macrophages, key regulators of wound healing and angiogenesis, are one of the first immune cells to reach the wound site. They are very plastic cells with the ability to switch phenotype depending on the milieu. In addition, it is well known that they have a principal role in determining the success or failure of the tissue-engineered integration. Thus, we hypothesized that learning about the crosstalk between macrophage and blood vessels could help to gain control over tissue integration.

Thus, the specific objectives of the present thesis are the following:

1. To isolate and characterize MSCs from the hair follicle. Specifically, describe their exact anatomical location, study their naïve phenotype, validate their stemness properties along the period of validity, and assess their immunoevasiveness.
2. To assess the immunomodulatory capacities of HF-MSCs, as compared to the most used AT-MSCs, when it comes to inhibiting the proliferation of peripheral blood mononuclear cells (PBMCs), inducing T regulatory phenotype and skewing macrophages towards a tissue remodeling phenotype (also referred as M2 phenotype).
3. To characterize the effects of tissue-engineered blood vessels on macrophage phenotype by forming a three-dimensional (3D) tri-culture system model comprising of endothelial cells, mesenchymal stromal cells and macrophages *in vitro*. The effects of tissue-engineered blood vessels on undifferentiated (M0), pro-inflammatory (M1) and regenerative (M2 and M1M2) macrophage phenotype will be assessed by flow cytometry. For a thorough characterization of the different macrophage populations, single cell analysis, specifically dimensionality reduction and clustering algorithms will be used.

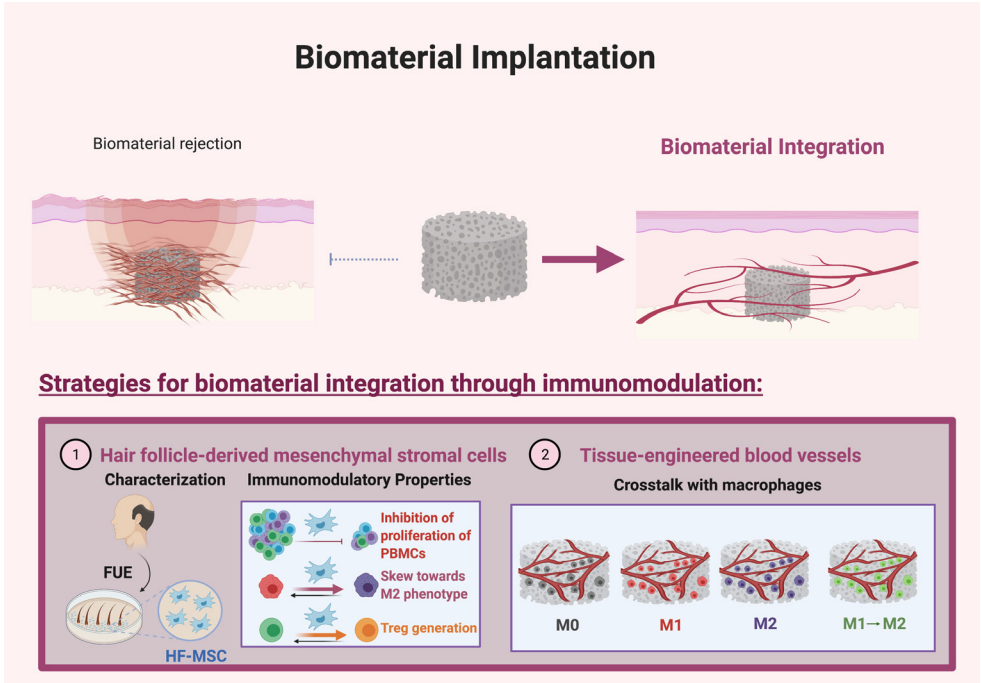

Figure 1: Schematic representation of the objectives of the doctoral thesis. FUE, follicular unit extraction. HF-MSCs, hair follicle derived mesenchymal stromal cells. PBMCs, peripheral blood mononuclear cells.Treg, Regulatory T lymphocytes

3

Human Hair Follicle-Derived Mesenchymal Stromal Cell from Lower Dermal Sheath as a Competitive Alternative for Immunomodulation

Abstract

Mesenchymal stromal cells (MSCs) have unique immunomodulatory capacities. Here, we investigate hair follicle-derived MSCs (HF-MSCs) from the lower dermal sheath, which are advantageous as an alternative source because of their relatively painless and minimally risky extraction procedure. These cells expressed neural markers upon isolation and maintained stemness for a minimum of 10 passages. Furthermore, HF-MSCs showed responsiveness to pro-inflammatory environments by expressing type-II major histocompatibility complex antigens (MHC)-II to a lesser extent than adipose tissue-derived MSCs (AT-MSCs). Regarding immunomodulation, HF-MSCs effectively inhibited the proliferation of peripheral blood mononuclear cells equivalently to AT-MSCs. Additionally, HF-MSCs reduced CD8 and CD19 lymphocyte populations and promoted the induction of $CD4^{+}CD25^{+}FOXP3^{+}$ regulatory T lymphocytes to the same extent as AT-MSCs. Finally, HF-MSCs, more so than AT-MSCs, skewed M0 and M1 macrophages towards M2 phenotypes, with upregulation of typical M2 markers CD163 and CD206 and downregulation of M1 markers such as CD64, CD86 and MHC II. Thus, we conclude that HF-MSCs are a promising source of MSCs for immunomodulation.

Grafical Abstract

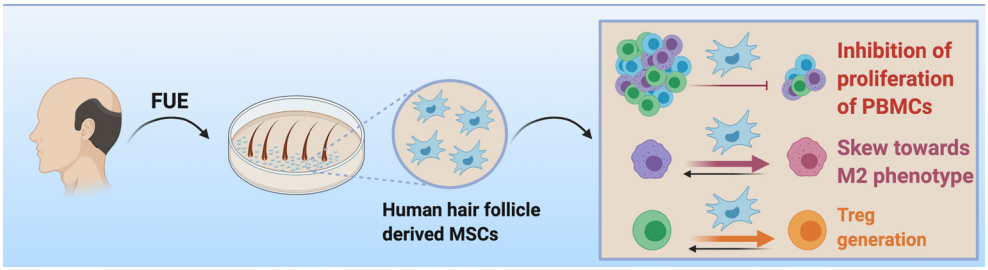

3.1. Introduction

Mesenchymal stromal cells (MSCs) are proliferative and multipotent cells that exist in most tissues of the body and show numerous therapeutic properties. As their immunomodulatory potential has become increasingly appreciated through hundreds of clinical trials — reviewed in Ref. (1) —, in recent years a number of MSC cell therapies have been approved for clinical use, including Temcell® for the treatment of steroid-refractory acute graft versus host disease (GvHD) in Japan. Alofisel® for Crohn's related enterocutaneous fistular disease in the European Union, and Remestemcel-L for pediatric steroid-refractory GvHD — reviewed in (1) and (2) —. In December 2020, the United States Food and Drug Administration (FDA) announced that they had granted Fast Track designation to Remestemcel-L to treat acute respiratory distress syndrome — which is the primary cause of death in COVID-19 patients— due to COVID-19 infection. This designation will speed up the phase three trial review process and its approval if the results are positive (1-3).

MSCs have two primary and important characteristics that make them an attractive therapeutic option for a wide range of inflammatory and immune-mediated diseases: immune evasion and immunomodulation. Their ability to evade immune rejection results from relatively low levels of major histocompatibility class I (MHC-I) expression and absence of type-II major histocompatibility complex antigens (MHC-II) and the co-stimulatory molecules CD40, CD80, or CD86 (4). The immunomodulatory abilities of MSCs are numerous, in that they regulate both adaptative and innate responses, relaying on paracrine factors and cellular contact for their function. In particular, MSCs inhibit the proliferation of lymphocytes, induce the generation of regulatory T lymphocytes and skew macrophage phenotype into a pro-regenerative and pro-tolerogenic one, among other immune cells (4-7). One of the main effectors in MSC-mediated immunomodulation in humans is indoleamine 2,3-dioxygenase (IDO), a metabolic enzyme that is secreted by MSCs upon exposure to inflammatory conditions (8). However, the clinical potential of MSCs remains limited by numerous obstacles, including (i) the invasive and painful harvesting procedure with possible complications; (ii) their gradual loss of "stemness" and immunomodulatory properties during *in vitro* expansion; and (iii) their loss of immune evasiveness in inflammatory environments (9).

Unlike many other cells that are tissue-specific, MSCs can be harvested

from almost every tissue at all developmental stages — fetal, young, adult, and aged — using their plastic-adherence properties. Historically, bone marrow was the first source from which MSCs were obtained (10). MSCs have since been isolated from other tissue sources, including but not limited to umbilical cord, placenta, adipose tissue, kidney, liver, lung and dental tissue — reviewed in (11) —. Of note, MSCs originating from diverse sources may present different properties and differentiation potentials (12). Recently, adipose tissue-derived MSCs (AT-MSCs) have been utilized to almost the same extent as bone marrow-derived MSCs (BM-MSCs) because they are easier to isolate in higher numbers (2, 13). However, the procedures to harvest the cells from both origins are still relatively harmful, painful, and invasive for the patient. Moreover, in the particular case of AT-MSCs, a recent study has demonstrated that these cells are dysfunctional and undergo early senescence when harvested from obese patients (14). Obesity, together with other pathological conditions, can also alter their "stemness" and secretory profiles, thus diminishing the immunomodulatory properties of these cells. For example, Serena et al. reported that AT-MSCs obtained from patients suffering from obesity or Type 2 diabetes were impaired in their abilities to suppress lymphocyte proliferation and promote M2 polarization of macrophages (15). Therefore, there is a need to evaluate the immunomodulatory potential of MSCs derived from other, more easily accessible cell sources.

The hair follicle is one of the main appendages of the skin and the source of two different types of multipotent cells: epidermal-origin stem cells and dermal-origin MSCs — HF-MSCs from now on — (16, 17). HF-MSCs can be obtained both from the dermal papilla region and from the dermal sheath (18). One of the main characteristics of the HF-MSCs is their possible neural differentiation capacity (19-22). This could be attributed to the hypothesis that these cells have their origin in the neural crest, as denoted by the possible presence of neural markers such as SOX-2, CD271 and CD56. So far, a few limited studies have demonstrated the potential of HF-MSCs. Hoogduijn et al. isolated HF-MSCs from the whisker hairs of Wistar rats and compared their characteristics to those isolated from the bone marrow (23). Wang et al. were able to induce pluripotent stem cells (iPSCs) from HF-MSCs obtained by direct plucking (24). Yu et al. demonstrated the transdifferentiation capacity of human HF-MSCs obtained by direct plucking into mature erythrocytes induced by the OCT4 gene (25). Ma et al. showed that human HF-MSCs were able to differentiate into chondrogenic, osteogenic, and adipogenic cells, and promoted wound healing

in a diabetic wound healing model (26). Lastly, Li et al. isolated MSCs from the outer root sheath of the epilated hair follicle and showed that HF-MSCs may display immunomodulatory potential, in that they reduced secretion of TNF and IL12p40 in cultures of pro-inflammatory macrophages, and increased secretion of IL10 and expression of the M2 macrophage marker CD163. However, the immunomodulatory potential of HF-MSCs has not yet been explored in detail, and whether they display the same capabilities of other sources of MSCs is not known (27).

In the present study, we sought to explore the immunomodulatory properties of primary HF-MSCs obtained from human donors undergoing hair transplant therapy. We first characterized their location within the hair follicle, their expression of neural phenotypic markers, and their stemness at both early and late passages *in vitro*. Subsequently, we evaluated the responsiveness of the HF-MSCs to interferon gamma (IFNγ) by measuring the increased production of IDO and the expression of MHC-II. The immunomodulatory capacity of HF-MSCs was further evaluated in comparison to AT-MSCs in terms of their ability to suppress proliferation of activated peripheral blood mononuclear cells (PBMCs), to stimulate induction of regulatory T cells, and to promote M2 polarization of macrophages. The results comprehensively demonstrate that HF-MSCs represent an effective and accessible source of MSCs with immunomodulatory potential comparable to that of AT-MSCs.

2. Material and Methods

2.1. Isolation of the different cell types

2.1.1. HF-MSCs

Hair follicles were obtained from occipital scalps of routine hair transplant procedures with the application of Follicular Unit Extraction technique (FUE) in which individual follicular grafts from androgenetic alopecia patients were harvested with the help of manual punches (Clínica Dermatológica Ercilla, Spain) following informed consent under an approved protocol (M30_2019_054, M10_2019_053). Each collection consisted of five hair follicles per patient. This procedure, which is minimally invasive, was performed under local anesthesia.

After removing the follicles, they were separated one by one, cleaned —

involving removal of the fat tissue and the capillaries— and rinsed with phosphate-buffered saline (PBS) (Gibco, Cat. No: 10010023). These hair follicles were then washed twice with PBS. Following this, they were transferred to a 24-well cell culture treated plate (Costar®, Cat. No: 3524) and incubated at 37 ºC in a humidified atmosphere containing 5 % CO_2 with 1 mL Dulbecco´s modified Eagle´s medium (DMEM) (Gibco, 11965092) supplemented with 30 % human serum and 10 % antibiotic/antimycotic solution (GIBCO, Cat No:15140-122).

For obtaining the HF-MSCs, the explant attachment method was used, which exploits the inherent ability of MSCs to adhere to the plastic. Briefly, the hair follicles were placed in a cell culture treated well plate, and the culture medium was carefully changed every 3-4 days until the HF-MSCs were released from the hair follicles around the 15th day. Then, the hair follicles were removed, and fibroblast-like cells were allowed to grow until 80 % of confluency was obtained. These cells were considered to be in passage 0. Subsequently, the cells were harvested using trypsin, plated in cell culture 175 cm^2 T-flasks (Corning Life Science, Cat No: 431080), and expanded as explained in section 2.2. To maintain consistency and for a thorough comparison, pools of no more than 5 different patients' cells were used. All the cells were grown up to passage 2 and passage 10 and all subsequent characterization experiments were performed using both passages 2 and 10. The experiments regarding immunomodulation of both HF-MSCs and AT-MSCs were performed within six passages.

2.1.2. PBMCs, T lymphocytes and macrophages

PBMCs were isolated from the blood of healthy donors (San Jose Medical Center, Vitoria-Gasteiz, Spain), following informed consent under a protocol approved by the Research Ethics Committee of the Basque Country and that of Txagorritxu University Hospital (CES-BIOEF 2017-26, CEIC Áraba Expte 2017-025). PBMCs were separated from the whole blood by a density gradient centrifugation method using Ficoll®-Paque premium (Sigma-Aldrich, Cat. No: GE17-5442-02). Then $CD4^+$ T lymphocytes and $CD14^+$ monocytes were purified from PBMCs using CD4 MicroBeads (Mitenyi Biotec, Cat No: 130-050-201) and CD14 MicroBeads (Mitenyi Biotec, Cat. no: 130-045-101) respectively, in a LS Column (Mitenyi Biotec, Cat. no: 130-042-401) of the QuadroMACS™ separator (Mitenyi Biotec, Cat. no:130-090-976) following manufacturer's instructions.

2.2. Expansion and preparation of HF-MSCs and AT-MSCs

MSCs were seeded in 175 cm^2 T-flasks and cultured in the corresponding medium for each cell type: AT-MSC were purchased from ATCC® (ATCC®, Cat. No: PCS-500-011™) and were cultured in Mesenchymal Stem Cell Basal Medium (ATCC®, Cat. No: PCS-500-030™) supplemented with the Mesenchymal Stem Cell Growth kit (ATCC®, Cat. No: PCS-500-040™) and 1 % antibiotic/antimycotic solution (GIBCO, Cat No:15140-122). HF-MSCs were grown in DMEM (Gibco, Cat. No: 11965092) supplemented with 10 % of Fetal Bovine Serum (FBS) (Gibco, Cat. No: 10270-106) and 1 % antibiotic/antimycotic solution (Gibco, Cat. No: 15140-122). Cells were maintained at 37 ºC, 5 % CO_2 and passaged when reaching 80 % confluency using 0.25 % trypsin ethylenediaminetetraacetic acid (EDTA) (ATCC® Cat. No: PCS-999-003™) and neutralized with Trypsin Neutralizing solution (ATCC® Cat. No: PCS-999-004™) (AT-MSCs) or DMEM containing 10 % of FBS (HF-MSCs), respectively. To generate IFNγ-licensed MSCs, cells were plated at the same density in complete HF-MSC media supplemented with 100 ng/mL recombinant human IFNγ (Sigma-Aldrich, Cat. No: I17001) for 72 h.

2.3. HF-MSCs characterization

2.3.1. Phenotype analysis

For the analysis of neural markers, freshly harvested hair follicles were washed with PBS and centrifuged at 600 x g for 5 minutes in order to remove the residual blood left from the surgery. Hair follicles were incubated in a PBS solution containing 0.2 mg/mL collagenase (Sigma-Aldrich, Cat. No: 9001-12-1) and 200 µg of calcium chloride (Sigma-Aldrich, Cat. No: C1016). Agitation was maintained in the incubator, at 37 ºC in a 5 % CO_2 air atmosphere for 90 minutes. After the incubation period, hair follicles were homogenized using gentleMACS™ Dissociator (Miltenyi Biotech, Cat. No: 130-093-235) and filtered with 70 µm cell strainer (Falcon®, Cat. No, 352340) to obtain a single cell suspension. Cells were resuspended in staining buffer — containing 0.5 % bovine serum albumin (BSA) (Sigma-Aldrich, Cat. No: A2153) and 2 mM EDTA (Sigma-Aldrich, Cat. No: E9884) in PBS —. The cell suspension was dyed for 15 minutes at 4 ºC in the dark with a dilution of 1:50 of the following antibodies: anti-CD271-APC (Miltenyi Biotech, Cat. No: 130-112-

791), anti-CD56-PE (Miltenyi Biotech, Cat. No: 130-113-874) and anti-CD90-PE-VIO770 (Miltenyi Biotech, Cat. No: 130-119-975), or with the corresponding isotype control antibodies, following manufacturer instructions. Subsequently, the cells were fixed and permeabilized using Intracellular Staining Buffer Set (Miltenyi Biotec, Cat No: 130-093-142). Cells were then stained with a dilution 1:50 of anti-SOX2-FITC (Miltenyi Biotech, Cat. No: 130-140-940) or with the corresponding isotype control following manufacturer instructions and analyzed by flow cytometry using the MACSQuant® Analyzer. Data was analyzed using FlowJo™ software (FlowJo™ 10.6.2 Software, TreeStar Inc., USA).

HF-MSCs were cultured until passage 2 and passage 10 in order to determine if the cells were able to maintain stemness even in late passages. Cells were trypsinized, collected, and re-suspended in a staining buffer. A suspension of $1x10^6$ cells was dyed for a span of 15 minutes at 4 ºC in the dark with a dilution of 1:20 with the following antibodies: Anti-CD14-PerCP, anti-CD20-PerCP, anti-CD34-PerCP, anti-CD45-PerCP, anti-CD73-APC, anti-CD90-FITC and anti-CD105-PE (MSC Phenotyping kit, Miltenyi Biotech, Cat No 130-095-198), anti-MHC-I-PeVio770 (Miltenyi Biotec, Cat. No: 130-120-573) and anti-MHC-II-VioBlue (Miltenyi Biotec, Cat. No:130-111-947) or corresponding isotype controls following the manufacturer's instructions. Anti-MHC-I and anti-MHC-II antibodies were also used after licensing the cells with IFNγ for 72 hours to determine if the pro-inflammatory environment altered the expression of MHC-I and MHC-II. After the incubation period cells were washed and resuspended in the staining buffer. Data was collected by flow cytometry using MACSQuant® Analyzer (Miltenyi Biotec, Germany). Data was analyzed using FlowJo™ software (FlowJo™ 10.6.2 Software, TreeStar Inc., USA).

.

2.3.2. Induction of osteogenic, chondrogenic and adipogenic differentiation

For the purpose of osteogenic and adipogenic differentiation, HF-MSCs — passage 2 and 10 — were seeded at a density of 2 x 10^5 cells/well in a cell culture treated 6-well plates (Costar®, Cat.No:3736) and cultured in basal medium: DMEM, supplemented with 10 % of FBS and 1 % antibiotic/antimycotic solution. When these cells reached 70 % of confluence, the basal medium was changed to differentiation medium. Osteogenic differentiation medium: Basal medium was supplemented with 0.05 mM L-ascorbic acid (Sigma-Aldrich, Cat. No: A8960), 20 nM β-glycerophosphate

(Sigma-Aldrich, Cat. No: G5422) and 100 nM dexamethasone (Sigma-Aldrich, Cat. No: D2915). Adipogenic differentiation medium: basal medium was supplemented with 0.5 µM dexamethasone (Sigma-Aldrich, Cat. No: D2915), 0.5 µM 3-isobutyl-1-methylxanthine (Sigma-Aldrich, Cat. No: I5879), and 50 µM indomethacin (Sigma-Aldrich, Cat. No: I7378). For chondrogenic differentiation, 2.5 x 10^5 cells were cultured in 15 mL conical tubes with 7 mL basal medium supplemented with 50 nM L-ascorbic acid (Sigma-Aldrich, Cat. No: A8960), 6.25 µg/mL bovine insulin (Sigma-Aldrich, Cat No: I0516) and 10 ng/mL of transforming growth- β factor (TGF-β) (Sigma-Aldrich, Cat. No: SRP0300). Each differentiation medium was replaced every 3-4 days for 3 weeks. After this time, cells were fixed with neutral buffered formalin solution at 10% (Sigma-Aldrich, Cat. No: 252931.1211) and stained with Alizarin Red S (Sigma-Aldrich, Cat. No: A5533) for osteogenic differentiation, Oil Red O (Sigma-Aldrich, Cat.No: O0625) for adipogenic differentiation and Alcian Blue (Sigma-Aldrich, Cat. No: B8438) for chondrogenic differentiation.

The results obtained with the microscope imaging were validated by reverse transcription quantitative polymerase chain reaction (RT-qPCR). Briefly, samples were collected at the end of each stage of differentiation. Cell pellets were resuspended in the ribonucleic acid (RNA) lysis buffer (RLT) from the RNeasy Mini Kit (Qiagen, Cat No:74104) and stored at -80 ºC until RNA extraction. RNA was extracted following the manufacturer´s recommendations. After extraction, total RNA was quantified with a SimpliNano nanodrop (GE Healthcare LifeScience, Iceland). For complementary deoxyribonucleic acid (cDNA) synthesis, 100 ng of total RNA was used. RT-qPCR was performed with StepOne™ Real-Time PCR system (Applied Biosystems Inc., Foster City, CA) by using specific TaqMan fluorescent probes (Applied Biosystem): Lipoprotein lipase (LPL) (Thermo Fisher, Hs00173425_m1) and Leptin (Thermo Fisher, Hs00174877_m1) for adipogenic differentiation; aggrecan (ACAN) (Thermo Fisher, Hs00153936_m1) and Collagen Type X Alpha 1 Chain (COL10A) (Thermo Fisher, Hs00166657_m1) for chondrogenic differentiation; and Osteopontin (SPP1) (Thermo Fisher, Hs00959010_m1) for osteogenic differentiation. 18 S was used as the housekeeping gene (Integrated DNA technologies). All samples were assayed in triplicate and normalized based on their constitutive 18 S ribosomal RNA.

2.3.3. IFNγ licensing by Western Blot

Cells were immersed in ice-cold radioimmunoprecipitation assay (RIPA)

Lysis and Extraction Buffer (Thermo Scientific, Cat. No: 89901) with Halt Protease inhibitors (Thermo Scientific, Cat. No: 78430). Following this, samples were maintained in agitation for 2 hours at 4 ºC. Afterwards, lysates were spun down at 12,000 x rpm for 20 minutes in a centrifuge at 4 ºC. Supernatants were collected and 30 µg protein quantified by Pierce Bicinchoninic acid assay (BCA) protein assay kit (Thermo Scientific, Cat. No: 23225) were mixed with 1/10 parts of dithiothreitol (DTT) (Sigma-Aldrich, Cat. No: 10197777001) and ¼ parts of 4 X Laemmle Sample Buffer (Bio-Rad, Cat. No: 161-0747). The mixture was heated at 85 ºC for 10 minutes and right after the mixture was cooled on ice for 3 minutes. Samples were run on 10 % Criterion™ greater transfer efficacy (TGX) Stain-Free™ Precast Gel (Bio-Rad, Cat. No: 567-8033) and transferred onto a Polyvinylidene fluoride (PVDF) membranes using the Trans-Blot®Turbo™Midi PVDF Transfer Packs (Bio-Rad, Cat. No:170-4157). Anti-IDO antibody (rabbit monoclonal, 1:1000 dilution) (Cell Signaling, Cat. No: 86630) and anti-β-actin antibody (mouse monoclonal, 1:4000 dilution) (Sigma Aldrich, Cat. No: A1978) as a loading control were used, followed by horseradish peroxidase (HRP)-conjugated Goat Anti-Rabbit (Bio-Rad, Cat. No:170-6515) and Goat Anti-Mouse (Bio-Rad, Cat. No: 170-6516) secondary antibodies (1:10000 dilution for both). Finally, Clarity™ Western enhanced chemiluminescence (ECL) Substrate (1:1) (Bio-Rad Cat. No: 170-5061) was added and blots were visualized using a ChemiDoc™ multiplex (MP) Imaging System (Bio-Rad, Cat. No:170-8280). Obtained band signals were processed for semi-quantitative analysis using Image Lab™ Software 4.0.1 (Bio-Rad, USA).

2.3.4. IFNγ licensing by RT-qPCR

The IDO expression was also analyzed at gene expression level by RT-qPCR. Briefly, after the IFNγ licensing, passage 2 and passage 10 HF-MSCs were collected in the RLT buffer from the RNeasy Mini Kit and stored at - 80 ºC until RNA extraction. RNA was extracted following the manufacturer´s recommendations of the RNeasy Mini Kit (Qiagen, Cat No:74104). Extracted total RNA was quantified with a SimpliNano nanodrop (GE Healthcare LifeScience, Iceland). For cDNA synthesis, 500 ng of total RNA was used. RT-qPCR was performed with StepOne™ Real-Time PCR system (Applied Biosystems Inc., Foster City, CA) by using specific TaqMan® IDO fluorescent probes (Thermo Fisher, Hs00984148_m1) and 18 S as the housekeeping gene (Integrated DNA technologies).

2.3.5. CD90 Immunohistochemistry

Freshly isolated hair follicles were fixed with 10 % formalin for 20 minutes. Fixed hair follicles were then blocked with 2 % BSA solution and 0.5 % Triton-X (Sigma-Aldrich, Cat.No: T8787) in PBS for 2 hours at room temperature. After rinsing with PBS, they were incubated with the primary antibody anti-CD90 (Abcam, Cat. No: ab189367) at a 6 μg/mL concentration overnight at 4 ºC in a solution containing PBS with 0.1 % BSA and 0.1 % Triton-X. This was followed by a subsequent incubation with the secondary antibody (Fisher Scientific, Cat. No: A11055) in PBS with 0.1 % BSA and 0.1 % Triton-X for 2h at room temperature. After toughly rinsing with PBS, the hair follicles were incubated with a 1:10,000 4,6-diamidino-2-phenylindole (DAPI): PSB solution for 20 minutes. After toughly rinsing with PBS, the hair follicles were washed and mounted on gelatin-coated slides and cover slipped with Fluoromount-GTM mounting medium (Thermo Fisher, Cat. No: 00-4958-02). Images were taken in the Zeiss Apotome 2 microscope (Jena, Germany).

2.4. Immunomodulatory properties of HF-MSCs

2.4.1. PBMC proliferation assay

The capacity of MSCs to suppress the activation and proliferation of stimulated PBMCs was assessed by means of a 5,6-carboxyfluorescein diacetate N-succinimidyl ester (CFSE)-based proliferation assay (Molecular Probes, cat no. C1157). Briefly, PBMCs were labeled with CFSE at a final concentration of 5 μM for 5 minutes at room temperature in a PBS solution, and then washed three times with PBS containing 5 % FBS. PBMCs were treated with 2.5 μg/mL of the stimulant Concanavalin A (Sigma-Aldrich, Cat. No: C0412) in the absence or presence of either HF-MSCs or AT-MSCs — with or without a 100 ng/mL IFNγ licensing — at PBMC:MSC different ratios for 5 days. On the fifth day, cells were collected, and resuspended in a staining buffer containing 0.5 % BSA (Sigma-Aldrich, Cat. No: A2153) and 2 mM EDTA (Sigma-Aldrich, Cat. No: E9884) in PBS (Gibco, Cat. No: 10010023). CFSE intensity was determined by flow cytometry using MACSQuant® Analyzer. Data was measured by FlowJo's proliferation tool (FlowJo 10.5.0 Software, TreeStar Inc.,USA).

2.4.2. PBMCs population change during MSCs co-culture

PBMCs were stimulated with 2.5 µg/mL Concanavalin A in the absence or presence of either HF-MSCs or AT-MSCs — with or without a 100 ng/mL IFNγ licensing— at PBMC:MSC 1:1 ratio for 5 days. Then, PBMCs were collected, and resuspended in a staining buffer containing 0.5 % BSA (Sigma-Aldrich, Cat. No: A2153) and 2 mM EDTA (Sigma-Aldrich, Cat. No: E9884) in PBS (Gibco, Cat. No: 10010023). A suspension of $1x10^6$ cells was dyed for 15 minutes at 4 ºC in the dark at 1:50 dilution with staining buffer with the following antibodies: Anti-CD3-VioGreen (Miltenyi Biotec, Cat.No: 130-113-704), anti-CD19-PEVio770 (Miltnyi Biotec, Cat.No: 130-114-173), anti-CD8-APC (Miltenyi Biotech, Cat. No: 130-113-716), or corresponded isotype controls. Data were collected by flow cytometry using MACSQuant® Analyzer. Data was analyzed using FlowJo™ software (FlowJo™ 10.6.2 Software, TreeStar Inc.,USA)

2.4.3. Induction of regulatory T lymphocytes and co-culture with HF-MSCs

For *in vitro* regulatory T lymphocyte induction, purified $CD4^+$ T cells were cultured in a complete medium containing RPMI medium, 10 % FBS and 1 % antibiotic/antimycotic solution. The wells of a cell culture treated 24-well plate were coated overnight with 1 µg/mL anti-CD3 monoclonal antibody (eBiosciences, Cat. No: 300437) at 4 °C. Purified $CD4^+$ T lymphocytes were seeded at $1×10^6$ cells/well and then stimulated with 25 µL of Dynabeads Human T-Activator CD3/CD28 (Gibco®, Cat No: 11161D), 5 ng/mL TGF-β and 0.1 µM/mL all-trans-retinoic acid (Sigma-Aldrich, Cat. No: R2625) for 2 days with T lymphocytes alone or in the presence of either HF-MSCs and AT-MSCs. MSCs were co-cultured with $CD4^+$ T lymphocytes at a ratio of 1:10 (MSCs: $CD4^+$).

After 2 days, $CD4^+$ T lymphocytes were removed by a thorough aspiration, as T lymphocytes are much less adherent to the plastic than the MSCs. Cell suspension was dyed for 15 minutes at 4 ºC in the dark with the following antibodies: Anti-CD4-VioBlue (Miltenyi Biotech, Cat. No: 130-113-820) and anti-CD25-PE (Miltenyi Biotech, Cat. No: 130-113-848) or with the corresponding isotype control antibodies. Then, cells were fixed and permeabilized using FoxP3 Staining Buffer Set (Miltenyi Biotech, Cat. No: 130-093-142). Finally, T lymphocytes were stained with anti-

FoxP3-APC (Miltenyi Biotech, Cat. No: 130-113-996) or with the corresponding isotype control antibodies and analyzed by flow cytometry using the MACSQuant® Analyzer. Data was analyzed using MACSQuantify® software and FlowJo Software (FlowJo 10.6.2 Software, TreeStar Inc.,USA)

2.4.4. Induction of differentiated macrophages and their co-culture with HF-MSCs

For *in vitro* macrophage induction, purified $CD14^+$ monocytes were cultured in a complete RPMI medium containing RPMI 1640 (Gibco BRL,11875101) supplemented with 10 % heat-inactivated calf serum (HI-FCS) (Sigma-Aldrich, Cat. No:C8056), 2 mM L-glutamine (Gibco, Cat. No: 25030081), 1 % antibiotic/ antimycotic solution and 100 ng/mL human Macrophage Colony-Stimulating Factor (M-CSF) (Miltenyi Biotec, Cat. No: 130-096-489) for 8 days. Afterwards, obtained M0 macrophages were polarized towards a pro-inflammatory (M1) phenotype by incubating them with 120 ng/mL of IFNγ and 10 ng/mL of Lipopolysaccharides (LPS) (Sigma-Aldrich, Cat.No: L4391) for 48 hours. Alternatively, M0 macrophages were polarized towards a pro-regenerative (M2) phenotype by incubating them with 2 µg/ mL recombinant human interleukin 4 (IL-4) (Prepotech, 200-04) for 48 hours. MSCs were co-cultured with either M0, M1 or M2 macrophages at a ratio of 1:1 (MSC: Macrophage).

After 2 days, the macrophages were removed from the culture and washed twice with in staining buffer. Macrophages were dyed for 15 minutes at 4 ºC in the dark with the following antibodies: anti-CD163-APC (Miltenyi-Biotech, Cat. No:130-097-630), anti-CD64-APC-Vio770 (Miltenyi-Biotech, Cat. No:130-100-449), anti-CD209-PE-Vio770 (Miltenyi-Biotech, Cat. No:130-109-591), anti-CD86-FITC (Miltenyi-Biotech, Cat. No:130-102-506), anti-MHC-I- PeVio770 (Mitenyi Biotec, Cat. No: 130-120-573), anti-CD206 VioBlue (Miltenyi-Biotech, Cat. No:130-100-034) or with the corresponding isotype control antibodies. Data was acquired by flow cytometry using the MACSQuant® Analyzer. Data was analyzed using MACSQuantify software and FlowJo Software (FlowJo 10.6.2 Software, TreeStar Inc.,USA).

To further confirm the capacity of HF-MSCs to modulate the differentiation of macrophages, RT-qPCR was conducted. Briefly, samples were collected after 48 h of the co-culture of the macrophages with the HF-MSCs. Cell pellets were

resuspended in the RLT buffer from the RNeasy Mini Kit (Qiagen, Cat No:74104) and stored at - 80 ºC until RNA extraction. RNA was extracted following the manufacturer´s recommendations. After extraction, total RNA was quantified with a SimpliNano nanodrop (GE Healthcare LifeScience, Iceland). For cDNA synthesis, 100 ng of total RNA was used. RT-qPCR was performed with StepOne™ Real-Time PCR system (Applied Biosystems Inc., Foster City, CA) by using specific TaqMan fluorescent probes (Applied Biosystem): IDO (Thermo Fisher, Hs00984148_m1), C-X-C motif chemokine ligand 11 (CXCL11) (Thermo Fisher, Hs00171138_m1), C-C Motif Chemokine ligand 19 (CCL19) (Thermo Fisher, Hs00171149_m1) and C-X-C motif chemokine ligand 10 (CXCL10) (Thermo Fisher, Hs00171042_m1) as M1 phenotype markers; and C-C Motif Chemokine ligand 13 (CCL13) (Thermo Fisher, Hs00234646), mannose receptor c-type (MRC) (Thermo Fisher, Hs00267207_m1), Fibronectin 1 (FN1) (Thermo fisher, Hs203717), fibrinogen like 2 (FGL2) (Thermo Fisher, Hs00173847_m1) and C-C chemokine receptor type 7 (CCR7) (Thermo Fisher, Hs01013469_m1) as M2 phenotype markers. All were normalized based on their constitutive 18 S ribosomal RNA.

2.5. Data analysis and statistics

The experiments have been done in triplicate at least and the results are shown as mean of at least 3 independent experiments ± SD for line and bar graphs. First the normal distribution of the data was determined using Shapiro-Wilk test. To detect statistical significances between two groups, t-test was performed in normally distributed data. The non-parametric Mann-Whitney U test was used if the data was non-normally distributed. For multiple comparisons, one-way ANOVA was used. In One-way ANOVA the Bartlett's or Levene test was performed to determine the homogeneity of variances. If homogeneous, the Tukey or Bonferroni post-hoc test was applied; if not, the Tamhane post-hoc test was used. All statistical analyses were performed by SPSS 23 (IBM SPSS, Chicago, IL) and Prism GraphPad (Prism 9, San Diego, CA) Software.

3. Results

3.1. Characterization of HF-MSCs

First, we characterized the HF-MSCs regarding their (i) localization and

neural crest-like phenotype; (ii) “stemness” properties; and (iii) responsiveness to pro-inflammatory stimulus. We explored all these characteristics with cells of passage 2 and passage 10 to detect any possible significant change in the quality of the cells throughout the recommended expansion range.

3.1.1. Isolation, localization and freshly harvested phenotype

Hair follicles from patients aged between 25-40 were harvested using Follicular Unit Extraction (FUE) technique and used for either immunohistochemical staining or flow cytometry analysis (Figure 1A). These experiments were performed with the objective of addressing the exact location of the HF-MSCs ($CD90^+$) (Figure 1A1) and analyzing whether these stromal cells showed expression of neural markers SOX2, CD56 and CD271 (Figure 1A2).

Thus, we first conducted an immunohistochemistry assay to detect CD90 in the explanted hair follicles. CD90 is one of the three markers that should be expressed by a cell to be considered MSC. $CD90^+$ cells were found only in the lower part of the hair follicles that is located in the dermal papilla and dermal cup/ lower dermal sheath (Figure 1B). One of the differential characteristics of HF-MSCs is their neural differentiation capacity and the expression of neural crest markers, which provide these cells with unique characteristics that are not observed in MSCs from other origins. To confirm our cells met these criteria, we dissociated the hair follicles to obtain single cell suspensions and conducted flow cytometry for three neural markers: CD271, SOX2 and CD56. To ensure that HF-MSCs exclusively were analyzed, only CD90 positive cells were considered (Figure 1C, Supplementary Figure 1).

The histograms showed remarkable differences in the percentages of neural marker expression between each patient, indicating the inter-patient variability (Figure 1C). However, as noticed in the three-dimensional (3D) density plot at least 96 % of $CD90^+$ cells were also positive for at least one of the assayed neural markers (Figure 1C). Of note, once the cells were cultured *in vitro*, CD271 expression decreased rapidly, whereas CD56 and SOX-2 were gradually lost over subsequent cell passages (Supplementary Figure 1).

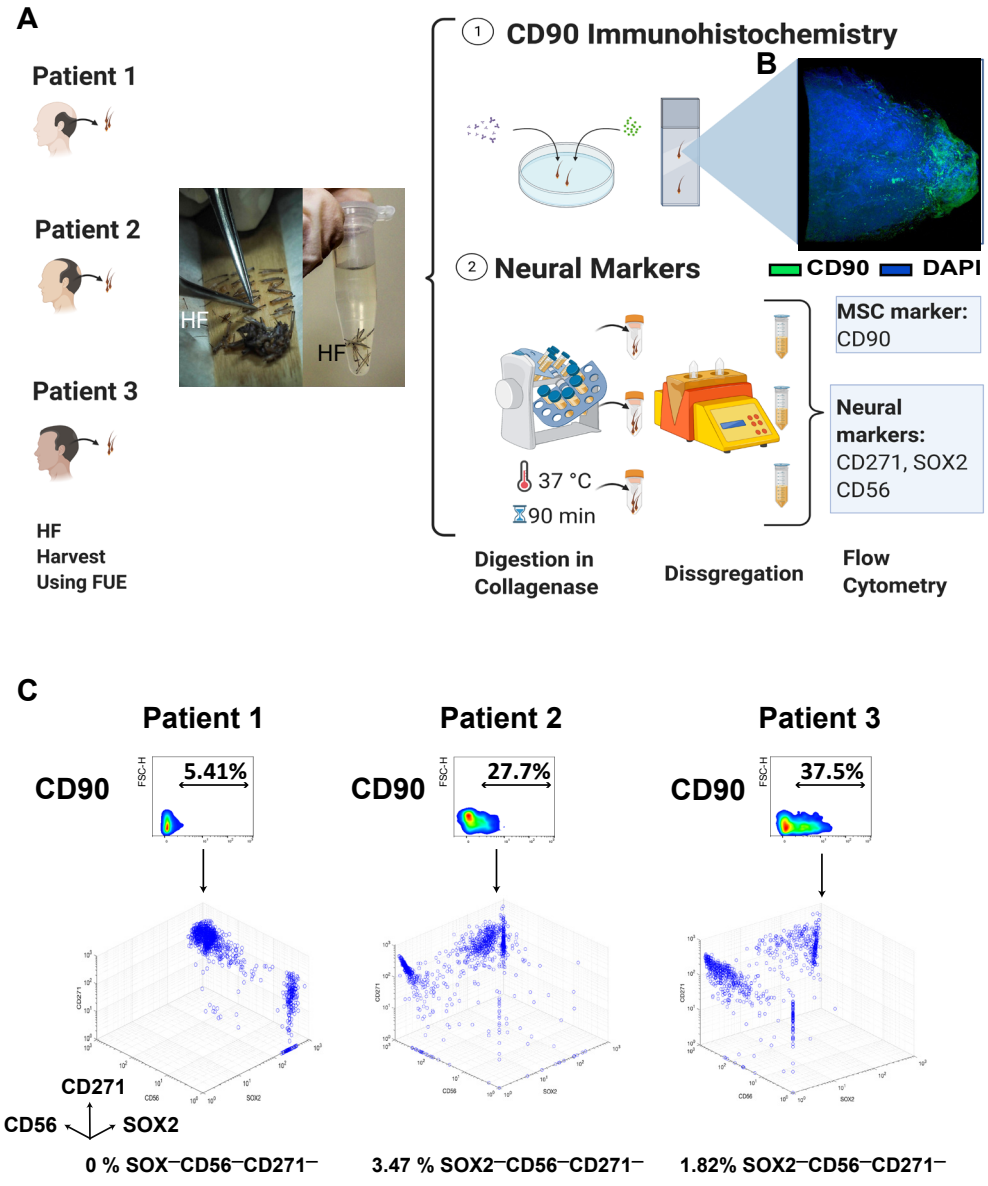

Figure 1. Isolation of HF-MSCs and neural origin characterization of freshly harvested HF-MSCs. (A) Hair follicle extraction using FUE technique from patients undergoing hair transplant therapy. After the extraction, the hair follicles were cleaned and used either for an (1) immunochemistry assay or digested and used for the (2) expression of neural markers (CD271, SOX2 and CD56) in freshly harvested cells. (B) Immunohistochemistry of the hair follicle showing the MSC marker CD90 in green and DAPI in blue. (2) Schematic representation of the procedure to obtain single cell suspension from freshly harvested hair follicles and subsequent staining of the HF-MSCs with neural markers. (C) Density plot representation of

(Figure 1 continued) the CD90 variation with respect to FSC-H for the three different patients and three-dimensional representations of the intensity of neural markers, SOX2 (x- axis), CD56 (y-axis) and CD271(z- axis) after the CD90 gating. FUE, follicular unit extraction. HF, hair follicle. MSC, mesenchymal stromal cells.

3.1.2. "Stemness" characterization

HF-MSCs were then characterized according to the 2006 International Society for Cellular Therapy (ISCT) criteria (Figure 2A) (28) at both early (passage 2) and late (passage 10) passages to assess the duration over which the cells are able to maintain "stemness" properties.

HF-MSCs displayed a high capacity to adhere to tissue culture treated plastic and to proliferate (Figure 2B). Similar to MSCs from other tissues, the attached cells showed a significant decrease in proliferation rate capacity when cells reached passage 10 (Figure 2C) (29, 30).

Subsequently, we analyzed the phenotype of HF-MSCs cultured at passage 2 and passage 10 by flow cytometry. Both passages met the criteria addressed by ISCT, with non-statistically significant differences in expression levels of the explored markers between MSCs from different passages (Figure 2D).

To demonstrate the differentiation potential of HF-MSCs, both passages were cultured under the conditions to induce chondrogenic, osteogenic, and adipogenic differentiation (Figure 2E-J). After 3 weeks of culture, chondrogenic differentiation was confirmed in both passages by Alcian blue staining, which stains proteoglycans (Figure 2E). To further confirm these results, expression of chondrogenic gene mRNAs COL10A and ACAN was evaluated. Both genes were highly expressed in passage 2 ($p < 0.001$ and $p < 0.01$ respectively compared to control), but only COL10A was expressed by cells at passage 10 ($p < 0.05$ compared control). (Figure 2F). Differentiation into the osteogenic lineage was characterized by the deposition of calcified nodules, as shown by Alizarin Red staining (Figure 2G). While at passage 2 the stain was visible all over the well, at passage 10 the stain was more sparse. To further confirm the results, the gene expression of SPP1, an osteogenic marker, was analyzed. SPP1 was highly expressed in passage 2 cells ($p < 0.001$ compared to control) but there was reduced expression in passage 10 cells

compared to passage 2 ($p < 0.01$), although expression was still significantly higher than the control ($p < 0.001$). Adipogenic differentiation of HF-MSCs was evaluated by staining the lipid vacuoles with Oil Red O (Figure 2I). The formation of lipid vacuoles was less prominent at passage 10 compared with passage 2. To further confirm adipogenic differentiation, the expression of LPL and LEPTIN genes was evaluated (Figure 2J). LEPTIN was highly expressed at both passage 2 and passage 10 ($p < 0.001$ compared to control), with no significant difference between passages ($p > 0.05$). However, the expression of LPL was only detected at passage 2 ($p < 0.001$ compared to control and $p < 0.01$ compared to passage 10).

These results suggested that *naïve* HF-MSCs fulfilled all commonly considered attributes of bona fide mesenchymal stem cells, but also that the cells gradually lost stemness properties in adaptation to culture.

3.1.3. Immunomodulatory responsiveness and maintenance of immunoevasiveness against pro-inflammatory stimulus

Two of the main characteristics of MSCs are their immunomodulatory and immunoevasiveness capacities. MSCs are able to secrete IDO, among other immunomodulatory molecules, in response to pro-inflammatory stimuli, which further modulates the phenotype of immune cells such as macrophages and T lymphocytes (Figure 3A). Thus, we examined if HF-MSCs were able to produce IDO in response to a pro-inflammatory signal. After licensing the HF-MSCs for 3 days with IFNγ (29, 30), a pro-inflammatory cytokine, we assessed IDO expression at both early and late passages by qRT-PCR (Figure 3B) and by western blot (Figure 3C, Supplementary Figure 3). IFNγ-treated HF-MSCs exhibited significantly higher IDO expression compared to the untreated cells at both the mRNA ($p < 0.001$ each passage compared to its control) and protein levels ($p < 0.001$ passage 2 compared to its control, and $p < 0.01$ passage 10 compared to its control), with no statistical differences ($p > 0.05$) between passages.

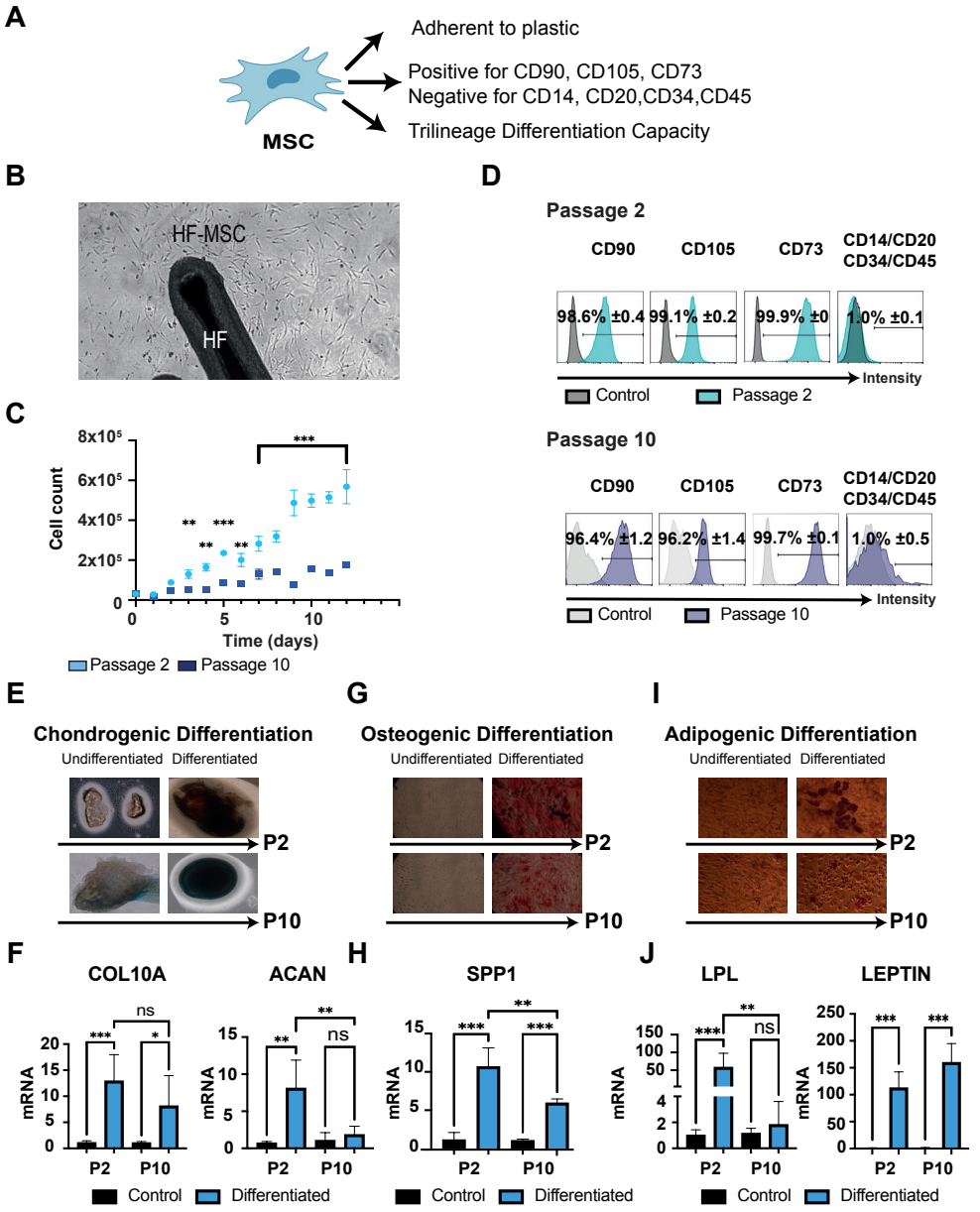

Figure 2. Characterization of minimal criteria to define MSCs. (A) A Schematic representation of the MSCs and their necessary properties**.** (B) Microscopic image representing the capacity of the HF-MSCs to adhere to plastic (C) Graphical representation of the proliferation potential of HF-MSCs at both passage 2 and passage 10. Each datapoint represents the mean for 3 biological replicates ± SD. Statistical significance: *** $p < 0.001$ ** $p < 0.01$, * $p < 0.05$. (D) Cells cultured at passage 2 and passage 10 were harvested and labelled with antibodies against the following cell surface proteins CD90, CD105, CD73,

(Figure 2 continued) CD14, CD20, CD34, CD45. Flow cytometry histograms of cells at P2 (teal) and P10 (dark blue) are shown. Gray histograms indicate isotype control for each antibody. Each datapoint represents the mean for 3 wells ± SD. (E-J) Trilineage differentiation of cells at both passage 2 and passage 10. (E) Chondrogenic differentiation capacity of HF-MSC after 21 days with the differentiation medium. Blue color represents the secretion of sulfated proteoglycans visualized with Alcian blue. (F) Chondrogenic differentiation was further confirmed by COL10A and ACAN gene expression. (G) Osteogenic differentiation capacity of HF-MSCs after 21 days with the differentiation medium. Deposition of calcified nodules was visualized by Alizarin Red staining. (H) Osteogenic differentiation was further confirmed by SPP1 gene expression. (I) Adipogenic differentiation capacity of HF-MSCs after 21 days with the differentiation medium. Red color indicates the staining of lipid vesicle-forming adipocytes by Oil Red staining. (J) Adipogenic differentiation was further confirmed by LPL and LEPTIN gene expression. Each datapoint represents the mean for at least 3 wells ± SD. Statistical significance: *** $p < 0.001$ ** $p < 0.01$, * $p < 0.05$. MSC, mesenchymal stromal cells. P2, passage 2. P10, passage 10. HF-MSC, hair follicle-derived mesenchymal stromal cell

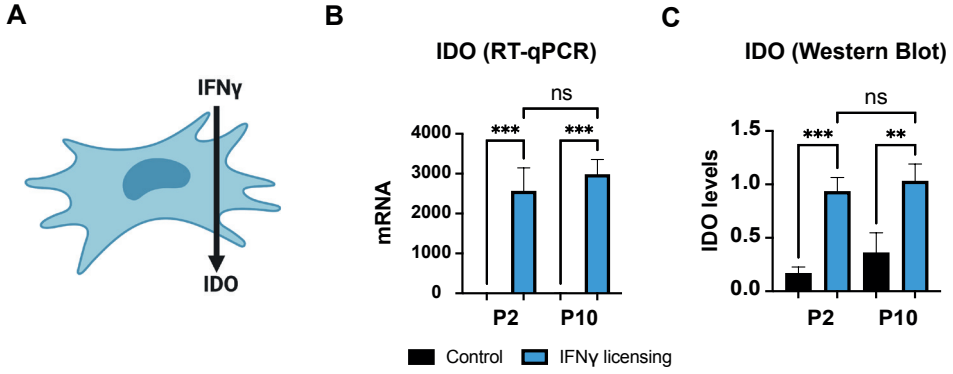

Figure 3: Effect of IFNγ licensing on HF-MSCs immunomodulatory responsiveness. (A) In humans, IFNγ induces expression of IDO in MSCs, which is a key molecule to drive their immunomodulatory capacity. (B,C) Histogram representation of IFNγ dependent relative IDO gene expression levels in HF-MSCs, as characterized by (B) qRT-PCR and (C) Western Blot. Each datapoint represents the mean for at least 3 biological replicates ± SD. Statistical significance: *** $p < 0.001$, ** $p < 0.01$, ns, no significant difference $p > 0.05$. IFNγ, interferon gamma. IDO, indoleamine 2,3-dioxygenase. RT-qPCR, reverse transcription quantitative polymerase chain reaction. P2, passage 2. P10, passage 10. mRNA, messenger ribonucleic acid.

It has been described that IFNγ induces expression of MHC-II in MSCs from different origins (Figure 4A), which could make MSCs lose their immunoevasiveness. To assess if this too influences our cells, we used IFNγ as a pro-inflammatory inducing agent and the MHC-II and MHC-I expression was compared, between HF-MSCs and AT-MSCs by means of flow cytometry (Figure 4). Interestingly, we observed that HF-MSCs, even though they started expressing MHC-II when treated with IFNγ, showed lower expression that AT-MSCs ($p < 0.001$), indicating that HF-MSCs may remain immunoevasive even when exposed to a proinflammatory environment (Figure 4B). Regarding MHC-I expression, when treated with IFNγ, HF-MSCs showed higher expression compared to AT-MSCs ($p < 0.01$) (Figure 4C).

3.2. Immunomodulatory potential of HF-MSCs

Having confirmed the “stemness” of the HF-MSCs and their responsiveness to pro-inflammatory cues, we next addressed the extent of their immunomodulatory potential. To this end, we evaluated their ability to inhibit the proliferation of activated human PBMCs and to induce regulatory phenotypes in both T lymphocytes and macrophages. We used AT-MSCs as a positive control because these cells exhibit strong immunomodulatory capacity.

3.2.1. PBMCs inhibitory potential

Initially, we analyzed the capacity of HF-MSCs to inhibit the proliferation of PBMCs (Figure 5). PBMCs were isolated from the blood of healthy volunteers by density gradient centrifugation. These PBMCs were then cultured alone or in the presence of either HF-MSCs or AT-MSCs at different MSC:PBMCs ratios — 1:1, 1:2, 1:5 and 1:10 — for 5 days in the presence of Concanavalin A to stimulate the PBMCs (Figure 5A). Proliferation was assessed by CFSE staining and flow cytometry.

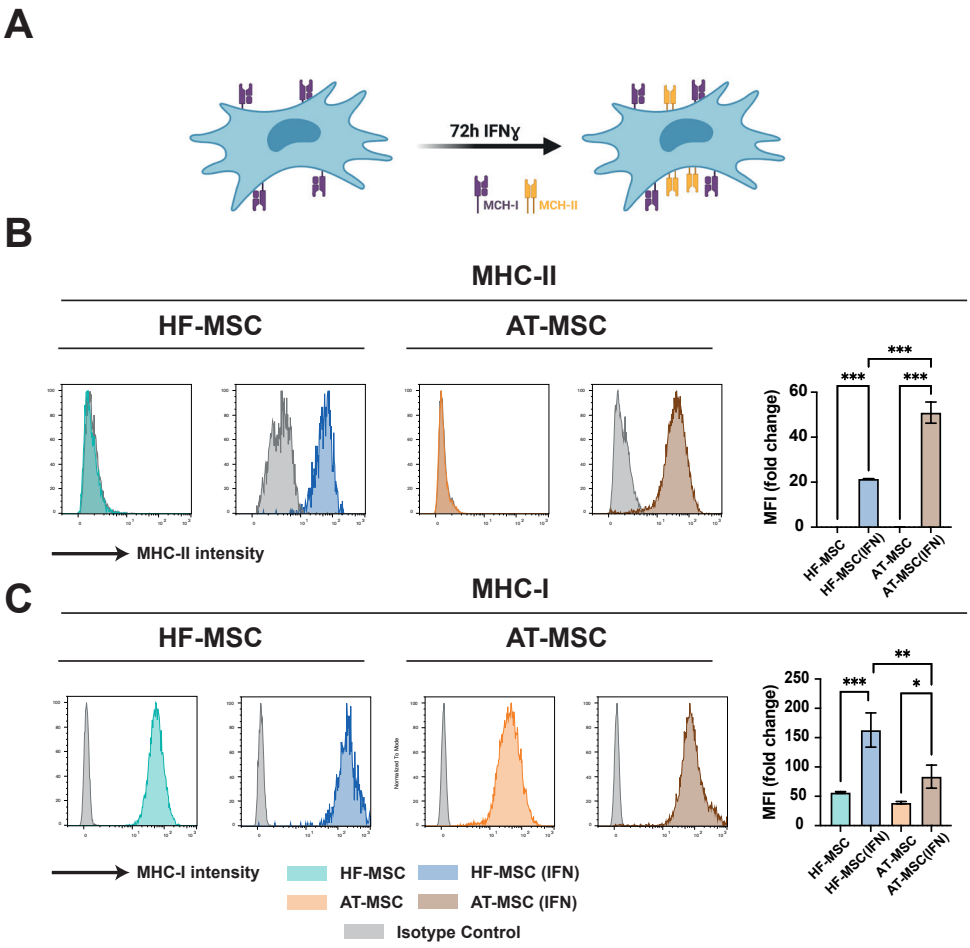

Figure 4. Effect of IFNγ licensing on HF-MSCs immunoevasiveness. (A) Schematic representation showing IFNγ-mediated upregulation of MHC-II expression in MSCs. (B,C) Histograms from flow cytometry assays depicting percentage of HF-MSCs positively stained for MHC-II (B) and MHC-I (C) on unstimulated and IFNγ-licensed HF-MSCs (light blue for unstimulated and dark blue for IFNγ-licensed and AT-MSCs (light orange for unstimulated and dark orange for IFNγ-licensed) Each datapoint represents the mean for at least 3 biological replicates ± SD. Statistical significance: *** $p < 0.001$ ** $p < 0.01$, * $p < 0.05$. IFNγ, interferon gamma. MHC-I, major histocompatibility class I molecule. MHC-II, major histocompatibility class II molecule. HF-MSCs, hair follicle-derived MSCs. AT-MSC, adipose tissue-derived MSCs.

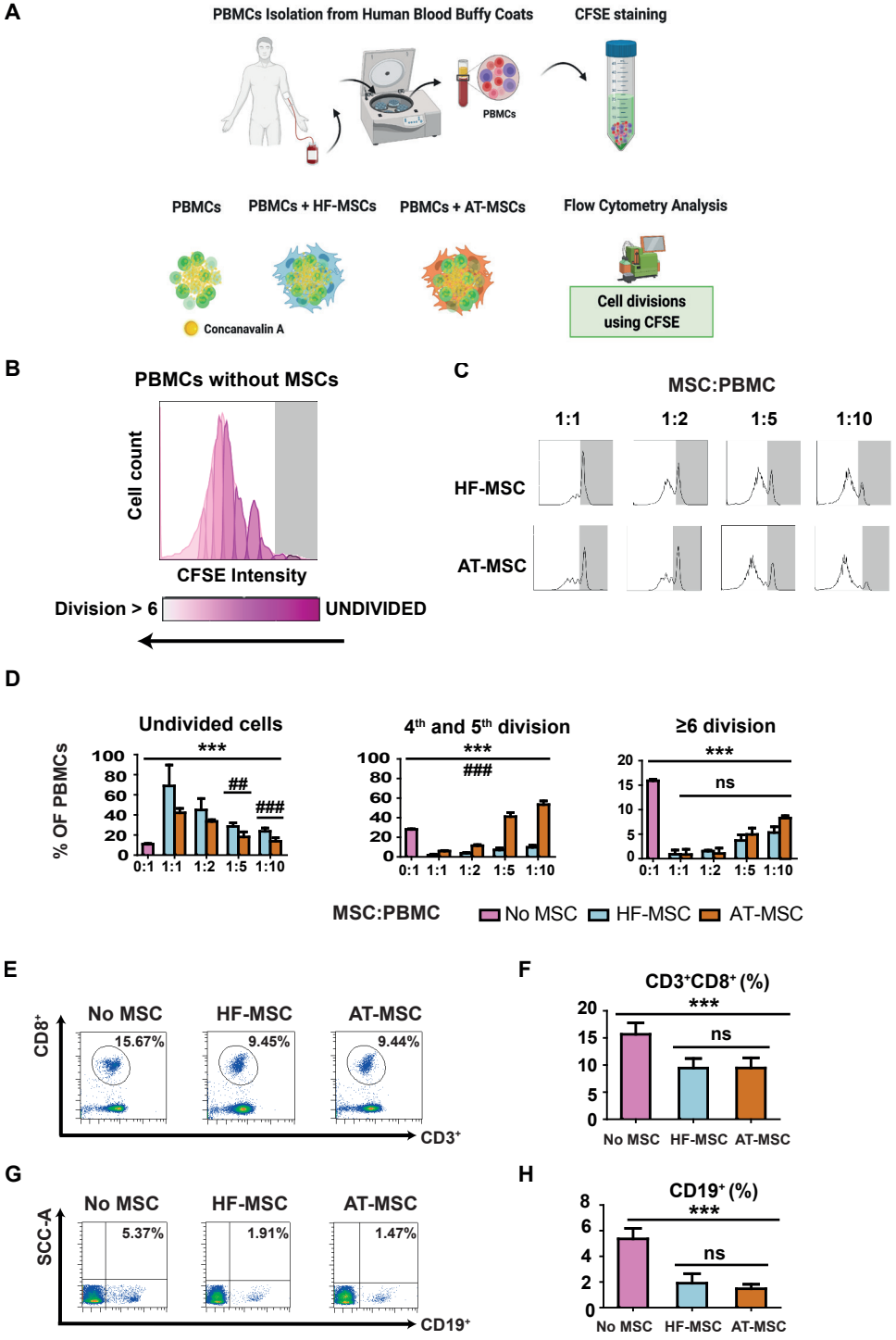
A
PBMCs Isolation from Human Blood Buffy Coats
CFSE staining
PBMCs
PBMCs
PBMCs + HF-MSCs
PBMCs + AT-MSCs
Flow Cytometry Analysis
Concanavalin A
Cell divisions using CFSE
B
PBMCs without MSCs
Cell count
CFSE Intensity
Division > 6
UNDIVIDED
C
MSC:PBMC
1:1
1:2
1:5
1:10
HF-MSC
AT-MSC
D
Undivided cells
4th and 5th division
≥6 division
% OF PBMCs
***
##
###
ns
0:1 1:1 1:2 1:5 1:10
MSC:PBMC
No MSC
HF-MSC
AT-MSC
E
No MSC
HF-MSC
AT-MSC
15.67%
9.45%
9.44%
CD8+
CD3+
F
CD3+CD8+ (%)
***
ns
No MSC HF-MSC AT-MSC
G
No MSC
HF-MSC
AT-MSC
5.37%
1.91%
1.47%
SCC-A
CD19+
H
CD19+ (%)
***
ns
No MSC HF-MSC AT-MSC

Figure 5. Immunomodulatory effects of HF-MSCs and AT-MSCs in concanavalin A-stimulated PBMCs. (A) PBMCs were isolated from the blood of human healthy donors and stained with CFSE to monitor their proliferation. (B) Flow cytometry histogram showing the proliferation profile of PBMCs without MSCs after 5 days of co-culture. Undifferentiated cells are represented by the vertical grey bars in the figure. (C) Flow cytometry histograms showing the proliferation profiles of the PBMCs after 5 days of co-culture with different ratios —1:1, 1:2, 1:5, 1:10 — of either AT-MSC or HF-MSCs. (D) Percentages of PBMCs remaining undivided, undergoing 4 and 5 division and undergoing more than or 6 divisions. Statistical significance: *** $p < 0.001$ and ** $p < 0.01$ when compared against PBMCs without MSCs; ### $p < 0.001$ and ## $p < 0.01$ when compared HF-MSCs with AT-MSCs; ns: not significant differences, $p>0.05$. (E-F) Flow cytometry dot plot depicting the populations of $CD3^+CD8^+$ T lymphocytes (E) and their relative percentages (F) when PBMCs were cultured alone (no MSCs), with HF-MSCs or with AT-MSCs. (G-H) Flow cytometry dot plot representing the populations of $CD19^+$ B lymphocytes (G) and their relative percentages (H) when PBMCs were cultured alone — no MSCs —, with HF-MSCs or with AT-MSCs. Each datapoint represents the mean for at least 3 wells ± SD. Statistical significance: *** $p < 0.001$ and ** $p < 0.01$ when compared with PBMCs without MSCs; ns: not significant differences, $p > 0.05$. CFSE, 5,6-carboxyfluorescein diacetate N-succinimidyl ester PBMCs, peripheral blood mononuclear cells. MSC, mesenchymal stromal cells. HF-MSCs, hair follicle-derived mesenchymal stromal cells. AT-MSCs, adipose tissue-derived mesenchymal stromal cells.

PBMCs alone showed a strong proliferative response (Figure 5B, D). In contrast, PBMCs demonstrated a significantly decreased proliferation when co-cultured with HF-MSCs and AT-MSCs in a dose-dependent manner ($p < 0.001$) (Figure 5C, D). Overall, few significant differences between HF-MSCs and AT-MSCs were observed. HF-MSCs stimulated considerably higher percentage of undivided cells for 1:5 ($p < 0.01$) and 1:10 ($p < 0.001$) ratios, and lower percentage of cells between four and five divisions ($p < 0.001$), compared to AT-MSCs. In addition, HF-MSCs pretreated with IFNγ did not elicit a stronger inhibitory response on PBMC proliferation than non-stimulated counterparts (Supplementary Figure 4). Finally, we examined whether MSCs were able to decrease the percentage of cytotoxic T cells ($CD3^+CD8^+$) (Figure 5E, F) and B cells ($CD19^+$) (Figure 5G, H) in a 1:1 PBMC:MSC ratio. Significant decreases in the percentages of both $CD3^+CD8^+$ and $CD19^+$ positive cells were observed when PBMCs were co-cultured with MSCs ($p < 0.001$). Both HF-MSCs and AT-MSCs showed similar immunosuppressive capacity ($p > 0.05$).

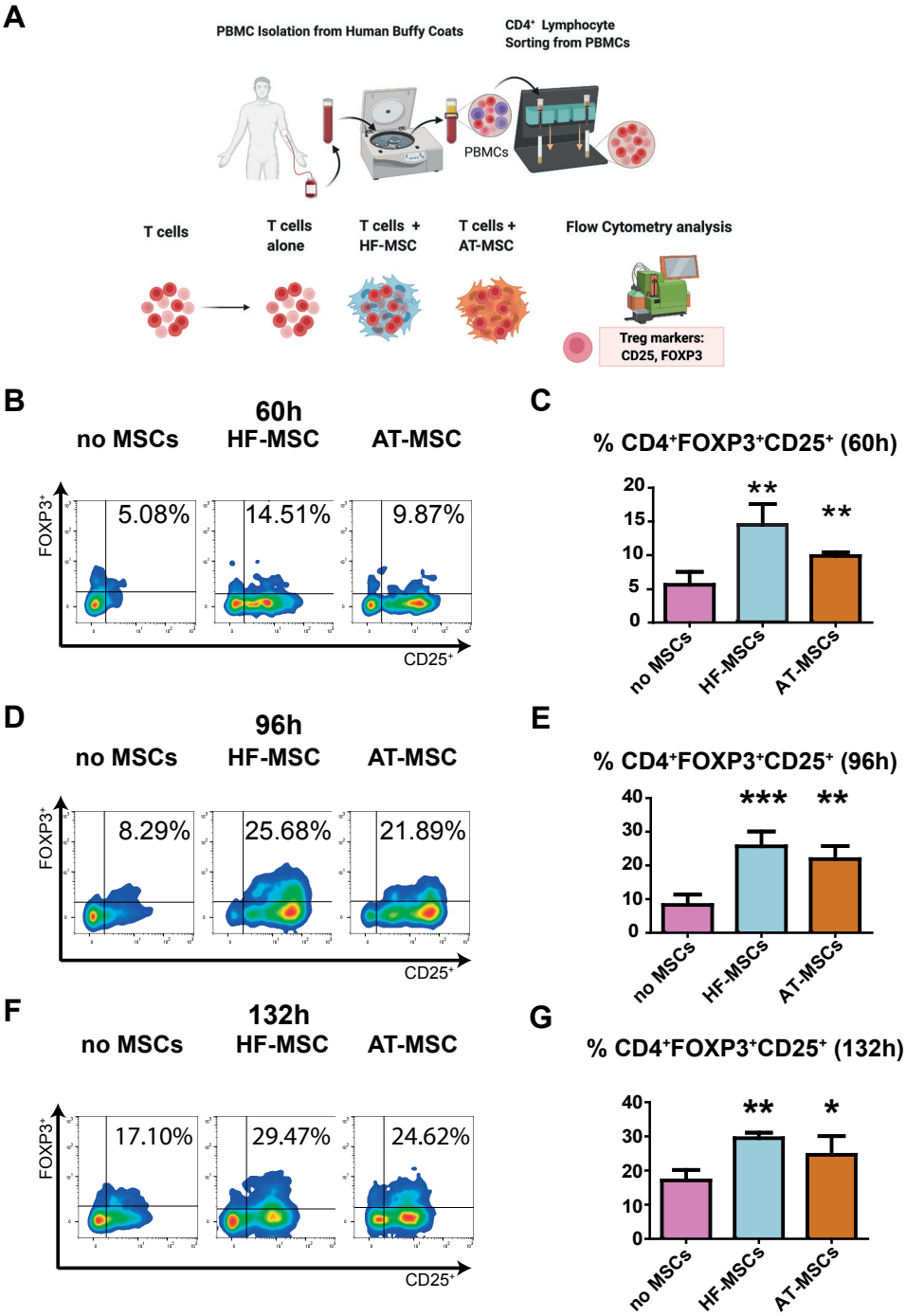

Figure 6. Effect of HF-MSC and AT-MSCs on induction of CD4⁺CD25⁺FOXP3⁺ T regulatory lymphocyte from CD4⁺ T lymphocytes (A) Schematic representation of the methods to obtain CD4⁺ T cells from the blood of human healthy donors and the ability of

(Figure 6 continued) MSCs to enhance induction of regulatory T lymphocytes in vitro. (B-G) Dot plots (B, D, F) and their bar-graph representations (C, E, G) exhibiting the percentages of $CD4^+CD25^+FOXP3^+$ cells under T regulatory induction conditions when cultured alone, with HF-MSCs or with AT-MSCs during (B, C) 60h, (D, E) 96h and (F, G) 132h. Each data point represents the mean for at least 3 wells ± SD. Statistical significance: *** $p < 0.001$, ** $p < 0.01$ and *$p < 0.05$ when compared against the control group without MSCs. PBMCs, peripheral blood mononuclear cells. MSC, mesenchymal stromal cells. HF-MSCs, hair follicle-derived mesenchymal stromal cells. AT-MSCs, adipose tissue-derived mesenchymal stromal cells.

3.2.2. Capacity to generate $CD4^+CD25^+FOXP3^+$ Regulatory T lymphocytes

We next evaluated the capacity of HF-MSCs to induce $CD4^+CD25^+FOXP3^+$ T regulatory differentiation as compared to AT-MSCs. To this end, $CD4^+$ T lymphocytes were obtained from healthy human blood by gradient centrifugation and subsequent sorting by positive magnetic isolation for CD4. Then, $CD4^+$ T lymphocytes were stimulated with anti-CD3, anti-CD28, $TGF\beta_1$ and all-trans-retinoic acid while co-culturing with or without MSCs for 60 h, 96 h and 132 h (Figure 6A). The number of cells exhibiting a T regulatory phenotype ($CD4^+CD25^+FOXP3^+$) was analyzed by flow cytometry (Figure 6B-G). As expected, there was a significant increase in $CD4^+CD25^+FOXP3^+$ T regulatory induction at all assayed time points when T lymphocytes were cocultured with MSCs, with peak induction at 96 h ($p < 0.001$ and $p < 0.01$ for HF-MSCs and AT-MSCs vs. the control group, respectively). No significant differences between HF-MSCs and AT-MSCs ($p > 0.05$) were observed throughout the experiments (Figure 6C, E, G).

3.2.3. Capacity to regulate macrophage phenotype

Macrophages are the primary cells of the inflammatory response, and they have long been recognized as one of the most crucial regulators of the healing process. In order for successful wound healing to occur, macrophages must switch their phenotype from pro-inflammatory — also called M1 — to an M2 phenotype associated with resolution of the healing process — reviewed in (31) —. MSCs have been previously shown to cause macrophages to reduce markers of the pro-inflammatory M1 phenotype and to increase expression of M2 markers *in vitro* and *in vivo* (32, 33). Based on the observation that MSCs are able to promote M2 macrophage polarization, we next investigated the effects of HF-MSCs and AT-MSCs on human

peripheral blood monocyte-derived macrophages *in vitro*. $CD14^+$ monocytes were sorted using positive magnetic isolation from PBMCs obtained from a buffy coat from healthy donors. Monocytes were differentiated towards macrophages through the addition of M-CSF for 8 days. Macrophages were consequently co-cultured with the MSCs and their phenotype marker expression was analyzed by flow cytometry after 48 hours (Figure 7).

Regarding M1 markers, macrophages cocultured with HF-MSCs and AT-MSCs showed significantly lower expression levels of CD86 ($p < 0.01$ and $p < 0.001$, respectively) and MHC-II ($p < 0.001$ and $p < 0.001$, respectively) than the M1 control group, reaching values similar to or even lower than the M2 control. Notably, HF-MSCs but not AT-MSCs caused macrophages to express lower levels of CD64 compared to the M1 control. For M2 markers, only HF-MSCs were able to express CD206 and CD163 to the same extent as the positive control M2 ($p > 0.05$), while AT-MSCs were not able to express these markers as much, exhibiting significant differences between them and the positive M2 control ($p < 0.05$ for CD206 and $p < 0.001$ for CD163).

To determine whether the macrophage pre-polarization state has an impact in the crosstalk between macrophages and MSCs, macrophages were further polarized towards M1 and M2 phenotypes through the addition of LPS and IFNγ or IL-4, respectively, prior to co-culture with MSCs (Figure 7A and Supplementary Figure 6A). Overall, when M1 macrophages were cocultured with the MSCs, they downregulated M1 markers and upregulated M2 markers (Figure 7C), although M1 macrophages showed less plasticity than did the M0 macrophages. Specifically, HF-MSCs and AT-MSCs were able to lower the expression of the M1 markers CD86 ($p < 0.001$ and $p < 0.05$ respectively) and HLA-DR ($p < 0.001$ and $p < 0.001$, respectively) as compared to the M1 control group. No major differences were observed in the downregulation of M1 markers between HF-MSC and AT-MSC groups, although the expression of CD64 was decreased to a greater extent by HF-MSCs than by AT-MSCs ($p < 0.05$ for the HF-MSC group and $p > 0.05$ compared to the M1 control). With respect to M2 markers, co-culture with HF-MSCs caused macrophages to upregulate CD163 and CD206 ($p < 0.01$), while co-culture with AT-MSCs had no significant effect ($p > 0.05$). However, such expression levels were not comparable to those of the M2 control group in any case.

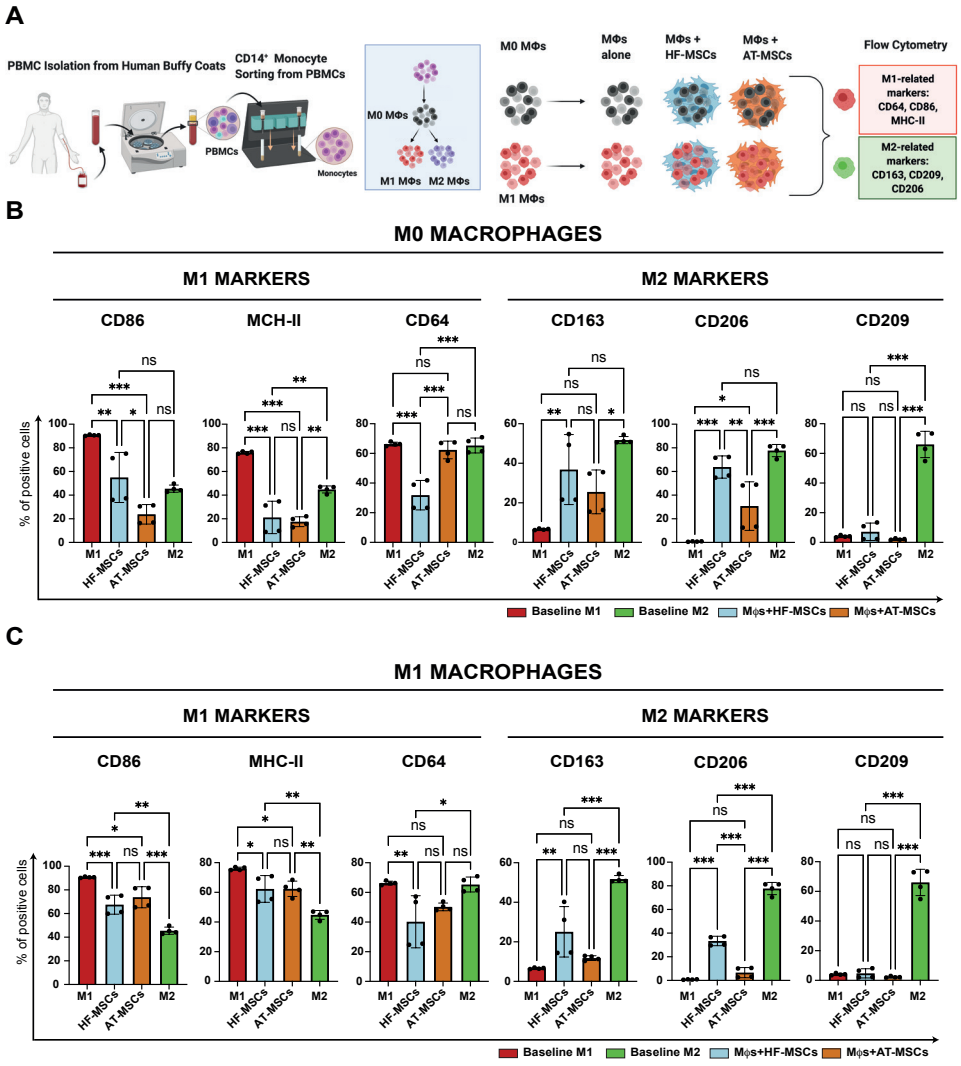

Figure 7. Effect of HF-MSCs and AT-MSCs on the modulation of macrophages phenotype. (A) CD14⁺ monocytes, obtained from blood samples of healthy donors were cultured with M-CSF for 8 days. Obtained M0 macrophages were either kept in M-CFS containing media or kept in M1 or M2 differentiation conditions for 48 hours. Once all the different types of macrophages were ready, it was followed by the addition of either HF-MSC or AT-MSC to the culture of M0 and M1 macrophages in 1:1 ratio for another 48 hours. Flow cytometry was performed to assess the phenotypical markers of M1 and M2 macrophages after either M0 or M1 macrophages were cocultured with the MSCs. M1 and M2 macrophages cultured without MSCs were used as a control. (B, C) Bar-graphs showing percentage of cells positive for either M1 related phenotypic markers CD86, MHC-II and CD64 or M2 related phenotypic markers

(Figure 7 continued) CD163, CD206 and CD209 expression when M0 macrophages (B) or M1 macrophages (C) were cocultured with HF-MSCs or AT-MSCs. Each datapoint represents the mean ± SD of 4 wells. Statistical significance: ***$p < 0.001$ and ** $p < 0.01$ and * $p < 0.05$ when compared with macrophages without MSCs ; ns: not significant differences, $p > 0.05$. PBMCs, peripheral blood mononuclear cells. Mϕs macrophages. HF-MSCs, hair follicle-derived mesenchymal stromal cells. AT-MSCs, adipose tissue-derived mesenchymal stromal cells.

Furthermore, the addition of HF-MSCs or AT-MSCs did not significantly alter M2 macrophages, with the exception of decreased CD209 and increased CD163 expressions (Supplementary Figure 6B). Indeed, when M2 were co-cultured with HF-MSCs, there was a significant increase in CD163 expression compared to AT-MSCs ($p < 0.01$). Additionally, gene expression analysis validated that ability of the HF-MSCs to skew macrophage phenotype towards an M2 phenotype (Supplementary Figure 7).

4. Discussion

In this study, we isolated and characterized MSCs from the human hair follicle. HF-MSCs showed immunomodulatory potential equal to or exceeding that of AT-MSCs, including inhibition of PBMC proliferation, suppression of cytotoxic T cell induction, promotion of regulatory T cell differentiation, and modulation of macrophage phenotype from M1 to M2. These results suggest that HF-MSCs should be considered a viable alternative to BM- and AT-MSCs for therapies that rely on their immunomodulatory potential.

Bone marrow and adipose tissue are the most studied sources of MSCs in clinical trials, with both of them being used with almost equal frequency (34, 35). However, there are substantial limitations in using these cells, mostly regarding the harvesting procedure and the patient situation. On the one hand, harvesting BM-MSCs from the bone marrow presents a high degree of viral and bacterial exposure and shows a significant decrease in cell number and proliferation/differentiation capacity with the increasing age of the donor (36, 37). On the other hand, the clinical utility of AT-MSCs is limited by the need to overcome certain challenges such as the extraction technique invasiveness, extraction limitations and the way this type of cells lose effectiveness if they have been extracted from obese patients or from patients with autoimmune pathologies such as diabetes (14, 15, 38). In contrast,

HF-MSCs can be obtained by means of a relatively painless, less invasive, and low risk harvesting procedure, which also presents a lower risk of viral and bacterial contamination.

The cells analyzed throughout this study came specifically from the hair follicle lower dermal sheath/dermal papilla, and these freshly isolated cells expressed the neural markers SOX2, CD271 and CD56. CD271 has been proposed as one of the most specific marker for the characterization and purification of different origin human mesenchymal stromal cells, such as, bone marrow- and adipose tissue-derived MSCs (39). Interestingly, CD271 expression is found in cells within human neural crest-derived tissues (40, 41). As the hair follicle has many different stem cell niches to focus on, an immunohistochemistry analysis was conducted to ensure that the cells that were being analyzed — CD90 positive cells — came from the mesenchymal niche of the hair. As expected, and in concordance of previous studies, most of the stained section were in the lower part of the hair follicle, where the dermal papilla/dermal cup is localized (Figure 1B) (42-44). The dermal papilla is a cluster of specialized mesenchymal cells. In addition to the dermal papilla, the mesenchyme of the follicle is also composed of a follicle smooth muscle known as the dermal sheath (45). Work conducted by Rahmani et al. showed the existence of dermal stem cells that are located in the hair follicle dermal sheath (46). They studied the crosstalk between the dermal sheath and dermal papilla, and they demonstrated the importance of these stem cells in the hair follicle regeneration. Some studies have suggested that a difference between HF-MSCs and other origin MSCs is the possible neural origin of the former one (Figure 1C) (21, 22). Our results showed that at least 96 % of the freshly harvested $CD90^{+}$ cells co-expressed a minimum of one of the neural markers. We also noticed that there was a lot of variability between donors (Supplementary Figure 1) and that these markers were lost at different rates when cells were cultured *in vitro* (Supplementary Figure 2).

HF-MSCs fulfilled all the requirements to be called MSCs for at least 10 passages (Figure 2) (28). First, the HF-MSCs were able to adhere to plastic and proliferate (Figure 2 B, C). Phenotypically, they were positive for the MSC markers and negative for the non-specific MSC-markers (Figure 2D). Finally, they possessed the capacity to differentiate into mesenchymal trilineage, which was proven by tissue-specific staining and expression of specific genes (Figure 2E-J). Interestingly, stemness — strictly interpreted from the minimum criteria defined by the ISCT —

and the immunomodulatory responsiveness capacity, were maintained even in passage 10, although the proliferation rate slowed significantly (Figure 2B) along with a decrease in differentiation potential. This could be an important feature as it has been described that MSCs lose their differentiation and immunomodulatory capacity earlier than passage 10 (29, 30). By taking advantage of aforementioned characteristics, HF-MSCs could be cultured until the needed yield is obtained without any concern of losing important MSC qualities.

HF-MSCs showed immunomodulatory responsiveness to pro-inflammatory signals for at least 10 passages. Immunomodulatory capacity of MSCs have been associated with the activity of IDO, among many other compounds of their secretome (9). However, it is known that this immunosuppressive potential of MSCs is not constitutive, but dependent on the inflammatory environment to which MSCs are exposed (47, 48). For example, it has been demonstrated that pretreatment of MSCs with IFNγ induces a robust expression of IDO, leading to subsequent inhibition of immune cell proliferation (49, 50). Thus, to assess the possible immunomodulatory capacity of the HF-MSCs, the cells were licensed for 3 days with IFNγ and then, expression of IDO was analyzed by RT-qPCR and Western Blot (Figure 3B and C, respectively). HF-MSCs showed a good responsiveness to pro-inflammatory stimulus, expressing comparable levels of IDO at both passage 2 and passage 10. This indicates that they did not lose their IDO responsiveness even when cultured for a long period *in vitro*.

HF-MSCs did not express MHC-II molecule when exposed to pro-inflammatory environments, even at late passages (Figure 3). An important characteristic of the MSCs is their immune evasiveness, namely the capacity of non-inducing an immune response. One of the main reasons for this — in addition to others explained in the introduction part— has been associated with the fact that they do not express MHC-II (51). However, it has been described that in inflammatory environments MSCs of diverse origins start expressing MHC-II molecules, thereby losing their characteristic evasiveness (52). We observed that both HF-MSCs and AT-MSCs expressed MHC-I class but not MHC-II class molecules. However, when exposed to pro-inflammatory environment there was an upregulation of the expression of both markers (Figure 4B,C). Importantly, we observed that HF-MSCs, even though they starting expressing MHC-II when treated with IFNγ, showed lower expression than AT-MSCs. This could be due to the hair being an immune privileged organ,

where physiologic processes are maintained by several mechanisms that merge to limit recognition of foreign antigens, deviate immune response to favor tolerance, and suppress immune-mediated inflammation (53, 54). Thus, considering the limited number of cells available for autologous use, HF-MSCs may be a suitable allogenic alternative for MSC-based cell therapy.

HF-MSCs suppressed the proliferation of PBMCs and reduced the populations of $CD8^+$ T lymphocytes and $CD19^+$ B cells at same extent as AT-MSCs (Figure 5). Once HF-MSCs were characterized and analyzed for their responsiveness to IFNγ and their immunoevasiveness, the next step was to assess their immunomodulatory reach. For such aim, AT-MSCs were used as a reference, because they are considered as the MSC type with the highest immunomodulatory potential (38). First, by means of co-culture experiments, the influence of both MSCs on the proliferation of Concanavalin A activated PBMCs was examined and compared (Figure 5B-D). The results demonstrated a dose-dependent suppressive effect with point differences between both groups. Interestingly, HF-MSCs exerted a more powerful inhibition than AT-MSCs when co-cultured at lower MSC:PBMC ratios (Figure 5D). The impact of these cells on specific lymphoid populations was further evaluated, and a significant reduction in the percentages of cytotoxic $CD3^+CD8^+$ T cells and $CD19^+$ B cells was observed, with no significant differences between both types of MSCs (Figure 6).

HF-MSCs induced the generation of $CD4^+CD25^+FOXP3^+$ T regulatory lymphocytes for over a period of 132 h to the same extent as AT-MSCs (Figure 6). $CD4^+CD25^+FOXP3^+$ T regulatory lymphocytes are a specialized suppressor T lymphocyte subpopulation that play a critical role in self-tolerance and immune homeostasis. Therefore, the ability of HF-MSCs to prompt T regulatory differentiation, and thus inhibit the response of activated B and T cells, makes this cell type a promising candidate for different immune-mediated diseases — such as graft-versus-host disease — where the adaptive immunity plays a critical role (55-57)

With respect to modulation of innate immune cells, HF-MSCs increased M2 polarization of M0 macrophages to a greater extent than AT-MSCs (Figure 7). MSCs have been reported to be able to influence M2 polarization of macrophages *in vivo* and *in vitro*, which is an important mechanism in resolution of inflammation or the induction of immune tolerance (11, 58-60). Specifically, a recent study has shown

that MSCs located in the outer root sheath of the hair follicle suppressed secretion of the proinflammatory cytokines TNFγ and IL-12p40 while stimulating the production of anti-inflammatory cytokine IL-10 and the expression of the M2 marker CD163 in M1 macrophages (27). Our findings that HF-MSCs promoted M2 polarization of primary human macrophages are in accordance with the work published by Cutler et al. and Witte et al. who showed that MSCs induced expression of the M2 markers CD163 and CD206 on monocytes (61, 62). Interestingly, when directly compared to AT-MSCs, HF-MSCs demonstrated a superior performance, as they were the only MSC type able to reduce significantly the CD64 M1 marker and increase CD163 and CD206 M2 markers to the same levels shown by the M2 control group.

HF-MSCs switched M1 macrophages into more M2-like regenerative phenotypes to an equal or greater extent than AT-MSCs. It was also desired to determine whether the pre-polarization state of the macrophages influenced the crosstalk with MSCs. M1 macrophages did not show as high plasticity as undifferentiated ones, at least with the markers used in this study. Although both MSC types caused downregulation of M1-related markers, only HF-MSCs caused upregulation of any M2 markers in the M1 macrophages. This is of great importance in chronic inflammatory conditions, as a transition from the pro-inflammatory phenotype M1 to the regenerative phenotype M2 is pivotal to overcome the pathological state and heal. A failure in this transition can cause poor healing, as in the case of chronic wounds (63). Indeed, recent studies have highlighted the importance of MSCs to modulate the macrophage phenotype from M0 and M1 to M2, to kickstart the wound healing process (32, 33, 59, 64-66). In this study we can notice that the addition of HF-MSCs results in macrophages moving towards an M2 phenotype. The fact that M1 macrophages were less plastic than M0 macrophages may suggest generation of a hybrid M1/M2 phenotype, which was recently shown to be associated with the production of less fibrotic extracellular matrix compared to a more predominant M2 macrophage phenotype (67).

5. Conclusions

In summary, the cells obtained from the lower dermal sheath/dermal papilla of human hair follicles expressed specific neural markers such as CD56, CD271 and SOX-2 upon extraction, which disappeared at different rates upon culture. In addition, HF-MSCs maintained sufficient stemness properties for at least 10

passages, including standard phenotypic markers, trilineage differentiation and proliferative capacity. These cells showed responsiveness to the pro-inflammatory cytokine IFNγ while retaining their immuno-privileged status, which makes allogenic HF-MSCs a feasible alternative source of stem cells. In addition, HF-MSC exhibited immunomodulatory properties comparable to or exceeding those of AT-MSCs with respect to crosstalk with cells of both the innate and adaptive immune systems. Together with the advantages of HF-MSC accessibility, such as easy accessibility, relatively painless procedures for donors and lower risk of possible infections, these results suggest that HF-MSCs may be a suitable alternative to AT-MSCs for the treatment of inflammatory disorders. Further studies will fully evaluate the immunogenic properties and immunomodulatory function of HF-MSCs *in vivo.*

6. References

1. Wu X, Jiang J, Gu Z, Zhang J, Chen Y, Liu X. Mesenchymal stromal cell therapies: immunomodulatory properties and clinical progress. Stem Cell Research & Therapy. 2020;11(1):345.
2. Yin JQ, Zhu J, Ankrum JA. Manufacturing of primed mesenchymal stromal cells for therapy. Nat Biomed Eng. 2019;3(2):90-104.
3. Galipeau J, Sensébé L. Mesenchymal stromal cells: clinical challenges and therapeutic opportunities. Cell Stem Cell. 2018;22(6):824-33.
4. Tse WT, Pendleton JD, Beyer WM, Egalka MC, Guinan EC. Suppression of allogeneic T-cell proliferation by human marrow stromal cells: implications in transplantation. Transplantation. 2003;75(3).
5. Corcione A, Benvenuto F, Ferretti E, Giunti D, Cappiello V, Cazzanti F, et al. Human mesenchymal stem cells modulate B-cell functions. Blood. 2006;107(1):367-72.
6. Selmani Z, Naji A, Zidi I, Favier B, Gaiffe E, Obert L, et al. Human leukocyte antigen-G5 secretion by human mesenchymal stem cells is required to suppress T lymphocyte and natural killer function and to induce $CD4^{+}CD25^{high}FOXP3^{+}$ regulatory T cells. Stem Cells. 2008;26(1):212-22.
7. YlÖstalo JH, Bartosh TJ, Coble K, Prockop DJ. Human mesenchymal stem/stromal cells cultured as spheroids are self-activated to produce prostaglandin E2 that directs stimulated macrophages into an anti-inflammatory phenotype. Stem Cells. 2012;30(10):2283-96.
8. Spaggiari GM, Capobianco A, Abdelrazik H, Becchetti F, Mingari MC, Moretta L. Mesenchymal stem cells inhibit natural killer–cell proliferation, cytotoxicity, and cytokine production: role of indoleamine 2,3-dioxygenase and prostaglandin E2. Blood. 2008;111(3):1327-33.
9. Martin I, Galipeau J, Kessler C, Le Blanc K, Dazzi F. Challenges for mesenchymal stromal cell therapies. Science Translational Medicine. 2019;11(480):eaat2189.
10. Friedenstein AJ, Chailakhjan RK, Lalykina KS. The development of fibroblast colonies in monolayer cultures of guinea-pig bone marrow and spleen cells. Cell Proliferation. 1970;3(4):393-403.
11. Andrzejewska A, Lukomska B, Janowski M. Concise review: mesenchymal stem cells: from roots to boost. Stem Cells. 2019;37(7):855-64.
12. Elahi KC, Klein G, Avci-Adali M, Sievert KD, MacNeil S, Aicher WK. Human mesenchymal stromal cells from different sources diverge in their expression of cell surface proteins and display distinct differentiation patterns. Stem Cells Int. 2016;2016:5646384.
13. Strioga M, Viswanathan S, Darinskas A, Slaby O, Michalek J. Same or not the same? comparison of adipose tissue-derived versus bone marrow-derived mesenchymal stem and stromal cells. Stem Cells and Development. 2012;21(14):2724-52.
14. Conley SM, Hickson LJ, Kellogg TA, McKenzie T, Heimbach JK, Taner T, et al. Human obesity induces dysfunction and early senescence in adipose tissue-derived mesenchymal stromal/stem cells. Frontiers Cell Dev Biology. 2020;8:197.
15. Serena C, Keiran N, Ceperuelo-Mallafre V, Ejarque M, Fradera R, Roche K, et al. Obesity and type 2 diabetes alters the immune properties of human adipose derived stem cells. Stem Cells. 2016;34(10):2559-73.
16. Rahmani W, Sinha S, Biernaskie J. Immune modulation of hair follicle regeneration. Npj Regen Medicine. 2020;5(1):9.
17. Purba TS, Haslam IS, Poblet E, Jiménez F, Gandarillas A, Izeta A, et al. Human epithelial hair follicle stem cells and their progeny: Current state of knowledge, the widening gap in translational research and future challenges. BioEssays. 2014;36(5):513-25.
18. Driskell RR, Clavel C, Rendl M, Watt FM. Hair follicle dermal papilla cells at a glance. Journal of Cell Science. 2011;124(8):1179.
19. Obara K, Tohgi N, Mii S, Hamada Y, Arakawa N, Aki R, et al. Hair-follicle-associated pluripotent

stem cells derived from cryopreserved intact human hair follicles sustain multilineage differentiation potential. Scientific Reports. 2019;9(1):9326.
20. Veraitch O, Mabuchi Y, Matsuzaki Y, Sasaki T, Okuno H, Tsukashima A, et al. Induction of hair follicle dermal papilla cell properties in human induced pluripotent stem cell-derived multipotent LNGFR(+) THY-1(+) mesenchymal cells. Scientific Reports. 2017;7(1):42777.
21. Etxaniz U, Pérez-San Vicente A, Gago-López N, García-Dominguez M, Iribar H, Aduriz A, et al. Neural-competent cells of adult human dermis belong to the schwann lineage. Stem Cell Reports. 2014;3(5):774-88.
22. Bharti D, Shivakumar SB, Park J-K, Ullah I, Subbarao RB, Park J-S, et al. Comparative analysis of human Wharton's jelly mesenchymal stem cells derived from different parts of the same umbilical cord. Cell Tissue Res. 2018;372(1):51-65.
23. Hoogduijn MJ, Gorjup E, Genever PG. Comparative characterization of hair follicle dermal stem cells and bone marrow mesenchymal stem cells. Stem Cells and Development. 2006;15(1):49-60.
24. Wang Y, Liu J, Tan X, Li G, Gao Y, Liu X, et al. Induced pluripotent stem cells from human hair follicle mesenchymal stem cells. Stem Cell Rev Rep. 2013;9(4):451-60.
25. Yu X, Sun P, Huang X, Chen H, Huang W, Ruan Y, et al. RNA-seq reveals tight junction-relevant erythropoietic fate induced by OCT4 in human hair follicle mesenchymal stem cells. Stem Cell Research & Therapy. 2020;11(1):454.
26. Ma D, Kua JE, Lim WK, Lee ST, Chua AW. In vitro characterization of human hair follicle dermal sheath mesenchymal stromal cells and their potential in enhancing diabetic wound healing. Cytotherapy. 2015;17(8):1036-51.
27. Li H, Masieri FF, Schneider M, Kottek T, Hahnel S, Yamauchi K, et al. Autologous, non-invasively available mesenchymal stem cells from the outer root sheath of hair follicle are obtainable by migration from plucked hair follicles and expandable in scalable amounts. Cells. 2020;9(9).
28. Dominici M, Le Blanc K, Mueller I, Slaper-Cortenbach I, Marini FC, Krause DS, et al. Minimal criteria for defining multipotent mesenchymal stromal cells. The International Society for Cellular Therapy position statement. Cytotherapy. 2006;8(4):315-7.
29. Pokrywczynska M, Maj M, Kloskowski T, Buhl M, Balcerczyk D, Jundził A, et al. Molecular aspects of adipose-derived stromal cell senescence in a long-term culture: A potential role of inflammatory pathways. Cell Transplant. 2020;29:0963689720917341.
30. Yang M, Lin J, Tang J, Chen Z, Qian X, Gao W-Q, et al. Decreased immunomodulatory and secretory capability of aging human umbilical cord mesenchymal stem cells in vitro. Biochem Bioph Res Co. 2020;525(3):633-8.
31. O'Brien EM, Risser GE, Spiller KL. Sequential drug delivery to modulate macrophage behavior and enhance implant integration. Adv Drug Deliver Rev. 2019;149-150:85-94.
32. Zhang Q-Z, Su W-R, Shi S-H, Wilder-Smith P, Xiang AP, Wong A, et al. Human gingiva-derived mesenchymal stem cells elicit polarization of M2 macrophages and enhance cutaneous wound healing. Stem Cells. 2010;28(10):1856-68.
33. François M, Romieu-Mourez R, Li M, Galipeau J. Human MSC suppression correlates with cytokine induction of indoleamine 2,3-dioxygenase and bystander M2 macrophage differentiation. Molecular Therapy. 2012;20(1):187-95.
34. Moll G, Hoogduijn MJ, Ankrum JA. Editorial: Safety, efficacy and mechanisms of action of mesenchymal stem cell therapies. Frontiers in Immunology. 2020;11(243).
35. Moll G, Ankrum JA, Kamhieh-Milz J, Bieback K, Ringdén O, Volk H-D, et al. Intravascular mesenchymal stromal/stem cell therapy product diversification: time for new clinical guidelines. Trends in Molecular Medicine. 2019;25(2):149-63.
36. Zaim M, Karaman S, Cetin G, Isik S. Donor age and long-term culture affect differentiation and

proliferation of human bone marrow mesenchymal stem cells. Annals of Hematology. 2012;91(8):1175-86.
37. Bruna F, Contador D, Conget P, Erranz B, Sossa CL, Arango-Rodríguez ML. Regenerative potential of mesenchymal stromal cells: age-related changes. Stem Cells Int. 2016;2016:1461648.
38. Rady D, Abbass MMS, El-Rashidy AA, Moshy SE, Radwan IA, Dörfer CE, et al. Mesenchymal stem/progenitor cells: the prospect of human clinical translation. Stem Cells Int. 2020;2020:1-45.
39. Álvarez-Viejo M, Menéndez-Menéndez Y, Otero-Hernández J. CD271 as a marker to identify mesenchymal stem cells from diverse sources before culture. World J Stem Cells. 2015;7(2):470.
40. Kasemeier-Kulesa JC, Kulesa PM. The convergent roles of CD271/p75 in neural crest-derived melanoma plasticity. Developmental Biology. 2018;444:S352-S5.
41. Brboric A, Vasylovska S, Saarimäki-Vire J, Espes D, Caballero-Corbalan J, Larfors G, et al. Characterization of neural crest-derived stem cells isolated from human bone marrow for improvement of transplanted islet function. Upsala Journal of Medical Sciences. 2019;124(4):228-37.
42. Fernandes KJL, McKenzie IA, Mill P, Smith KM, Akhavan M, Barnabé-Heider F, et al. A dermal niche for multipotent adult skin-derived precursor cells. Nature Cell Biology. 2004;6(11):1082-93.
43. Waters JM, Richardson GD, Jahoda CAB. Hair follicle stem cells. Seminars in Cell & Developmental Biology. 2007;18(2):245-54.
44. Owczarczyk-Saczonek A, Krajewska-Włodarczyk M, Kruszewska A, Banasiak Ł, Placek W, Maksymowicz W, et al. Therapeutic potential of stem cells in follicle regeneration. Stem Cells Int. 2018;2018:1049641.
45. Heitman N, Sennett R, Mok K-W, Saxena N, Srivastava D, Martino P, et al. Dermal sheath contraction powers stem cell niche relocation during hair cycle regression. Science. 2020;367(6474):161.
46. Rahmani W, Abbasi S, Hagner A, Raharjo E, Kumar R, Hotta A, et al. Hair follicle dermal stem cells regenerate the dermal sheath, repopulate the dermal papilla, and modulate hair type. Developmental Cell. 2014;31(5):543-58.
47. Gonzalez-Pujana A, Vining KH, Zhang DKY, Santos-Vizcaino E, Igartua M, Hernandez RM, et al. Multifunctional biomimetic hydrogel systems to boost the immunomodulatory potential of mesenchymal stromal cells. Biomaterials. 2020;257:120266.
48. Gonzalez-Pujana A, de Lázaro I, Vining KH, Santos-Vizcaino E, Igartua M, Hernandez RM, et al. 3D encapsulation and inflammatory licensing of mesenchymal stromal cells alter the expression of common reference genes used in real-time RT-qPCR. Biomaterials Science. 2020;8(23):6741-53.
49. Zimmermann JA, Hettiaratchi MH, McDevitt TC. Enhanced immunosuppression of T Cells by sustained presentation of bioactive interferon-γ within three-dimensional mesenchymal stem cell constructs. Stem Cells Translational Medicine. 2017;6(1):223-37.
50. Shi Y, Wang Y, Li Q, Liu K, Hou J, Shao C, et al. Immunoregulatory mechanisms of mesenchymal stem and stromal cells in inflammatory diseases. Nature Reviews Nephrology. 2018;14(8):493-507.
51. Ankrum JA, Ong JF, Karp JM. Mesenchymal stem cells: immune evasive, not immune privileged. Nature Biotechnology. 2014;32(3):252-60.
52. Gonzalez-Pujana A, Igartua M, Santos-Vizcaino E, Hernandez RM. Mesenchymal stromal cell based therapies for the treatment of immune disorders: recent milestones and future challenges. Expert Opin Drug Del. 2020;17(2):1-12.
53. Niederkorn JY. See no evil, hear no evil, do no evil: the lessons of immune privilege. Nature Immunology. 2006;7(4):354-9.
54. Bertolini M, McElwee K, Gilhar A, Bulfone-Paus S, Paus R. Hair follicle immune privilege and its collapse in alopecia areata. Experimental Dermatology. 2020;29(8):703-25.
55. Lee H-J, Kim S-N, Jeon M-S, Yi T, Song SU. ICOSL expression in human bone marrow-derived mesenchymal stem cells promotes induction of regulatory T cells. Scientific Reports. 2017;7(1):44486.

56. English K, Ryan JM, Tobin L, Murphy MJ, Barry FP, Mahon BP. Cell contact, prostaglandin E2 and transforming growth factor beta 1 play non-redundant roles in human mesenchymal stem cell induction of CD4+CD25Highforkhead box P3+ regulatory T cells. Clinical & Experimental Immunology. 2009;156(1):149-60.
57. Maccario R, Podesta M, Moretta A, Cometa A, Comoli P, Montagna D, et al. Interaction of human mesenchymal stem cells with cells involved in alloantigen-specific immune response favors the differentiation of CD4+ T-cell subsets expressing a regulatory/suppressive phenotype. Haematologica. 2005;90(4):516.
58. Park HJ, Oh SH, Kim HN, Jung YJ, Lee PH. Mesenchymal stem cells enhance α-synuclein clearance via M2 microglia polarization in experimental and human parkinsonian disorder. Acta Neuropathologica. 2016;132(5):685-701.
59. Németh K, Leelahavanichkul A, Yuen PST, Mayer B, Parmelee A, Doi K, et al. Bone marrow stromal cells attenuate sepsis via prostaglandin E2–dependent reprogramming of host macrophages to increase their interleukin-10 production. Nature Medicine. 2009;15(1):42-9.
60. Maggini J, Mirkin G, Bognanni I, Holmberg J, Piazzón IM, Nepomnaschy I, et al. Mouse Bone Marrow-Derived Mesenchymal Stromal Cells Turn Activated Macrophages into a Regulatory-Like Profile. PLOS ONE. 2010;5(2):e9252.
61. de Witte SFH, Luk F, Sierra Parraga JM, Gargesha M, Merino A, Korevaar SS, et al. Immunomodulation By Therapeutic Mesenchymal Stromal Cells (MSC) Is Triggered Through Phagocytosis of MSC By Monocytic Cells. Stem Cells. 2018;36(4):602-15.
62. Cutler AJ, Limbani V, Girdlestone J, Navarrete CV. Umbilical Cord-Derived Mesenchymal Stromal Cells Modulate Monocyte Function to Suppress T Cell Proliferation. The Journal of Immunology. 2010;185(11):6617.
63. Santos-Vizcaino E, Salvador A, Vairo C, Igartua M, Hernandez RM, Correa L, et al. Overcoming the Inflammatory Stage of Non-Healing Wounds: In Vitro Mechanism of Action of Negatively Charged Microspheres (NCMs). Nanomaterials (Basel). 2020;10(6).
64. Le Blanc K, Davies LC. Mesenchymal stromal cells and the innate immune response. Immunology Letters. 2015;168(2):140-6.
65. Melief SM, Schrama E, Brugman MH, Tiemessen MM, Hoogduijn MJ, Fibbe WE, et al. Multipotent stromal cells induce human regulatory T cells through a novel pathway involving skewing of monocytes toward anti-inflammatory macrophages. Stem Cells. 2013;31(9):1980-91.
66. Las Heras K, Igartua M, Santos-Vizcaino E, Hernandez RM. Chronic wounds: Current status, available strategies and emerging therapeutic solutions. Journal of Controlled Release. 2020;328:532-50.
67. Witherel CE, Sao K, Brisson BK, Han B, Volk SW, Petrie RJ, et al. Regulation of extracellular matrix assembly and structure by hybrid M1/M2 macrophages. Biomaterials. 2021;269:120667.

SUPPLEMENTARY TABLES AND FIGURES

Supplementary Table 1: PCR primers for RT-qPCR

Gene symbol	Gene Name	Prime ID
IDO	Indoleamine 2,3-dioxygenase 1	Hs00984148_m1
LPL	Lipoprotein lipase	Hs00173425_m1
Leptin	Leptin	Hs00174877_m1
ACAN	Aggrecan	Hs00153936_m1
COL10A	Collagen Type X Alpha 1 Chain	Hs00166657_m1
SPP1	Osteopontin	Hs00959010_m1
CXCL11	C-X-C motif chemokine ligand 11	Hs00171138_m1
CCL19	C-C Motif Chemokine ligand 19	Hs00171149_m1
CXCL10	C-X-C motif chemokine ligand 10	Hs00171042_m1
CCL13	C-C Motif Chemokine ligand 13	Hs00234646_m1
MRC	Mannose receptor c-type	Hs00267207_m1
FN1	Fibronectin 1	Hs203717_m1
FGL2	Fibrinogen like 2	Hs00173847_m1
CCR7	C-C chemokine receptor type 7	Hs01013469_m1
18S	18S ribosomal RNA	Hs.PT.39a.22214856

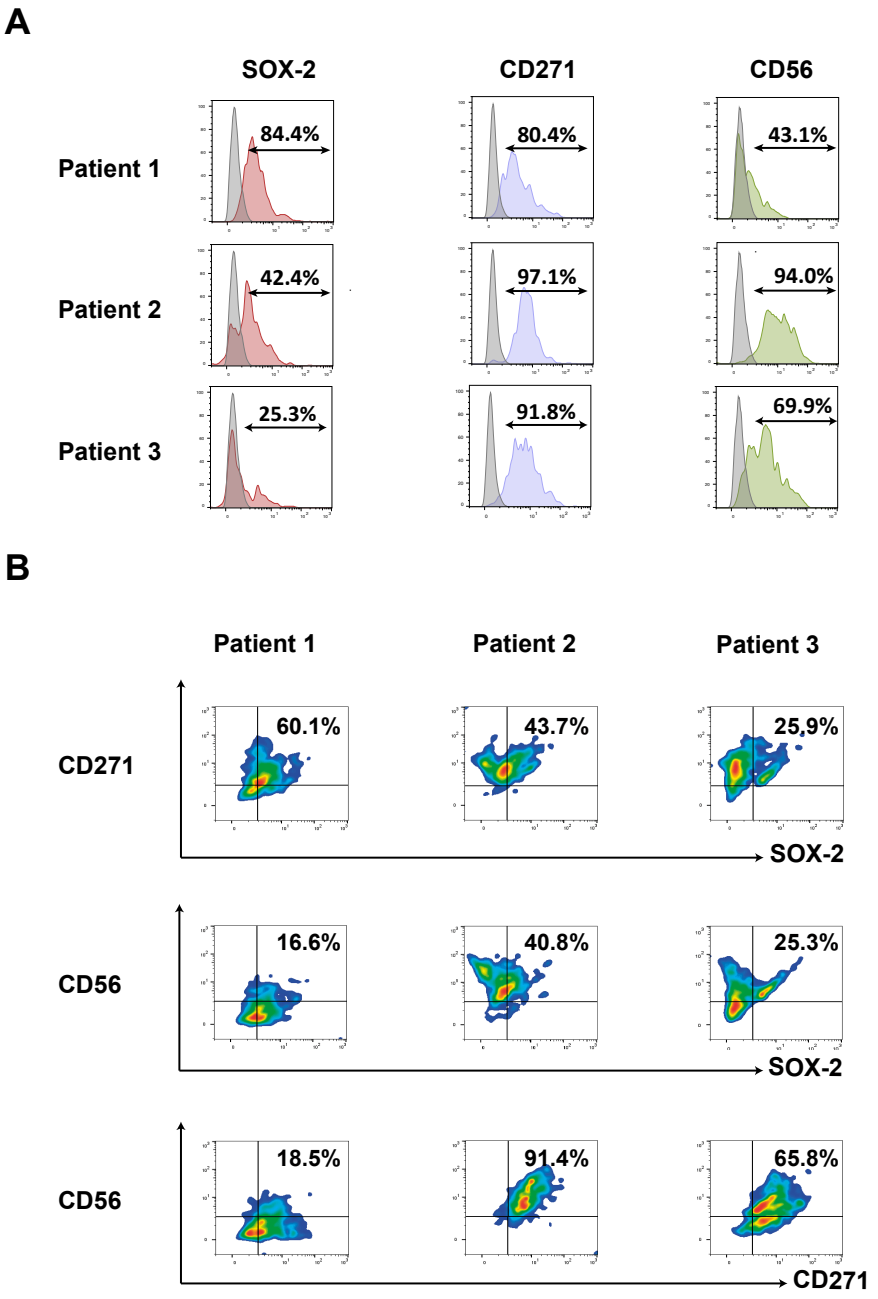

Supplementary Figure 1: Neural origin characterization of freshly harvested HF-MSCs. (A) Flow cytometry histograms representing the % of positive freshly isolated CD90+ HF-MSCs expressing SOX2, CD271 or CD56 neuronal marker in. (B) Flow cytometry density plots representing the percentage of positive cells co-expressing both of the neural markers.

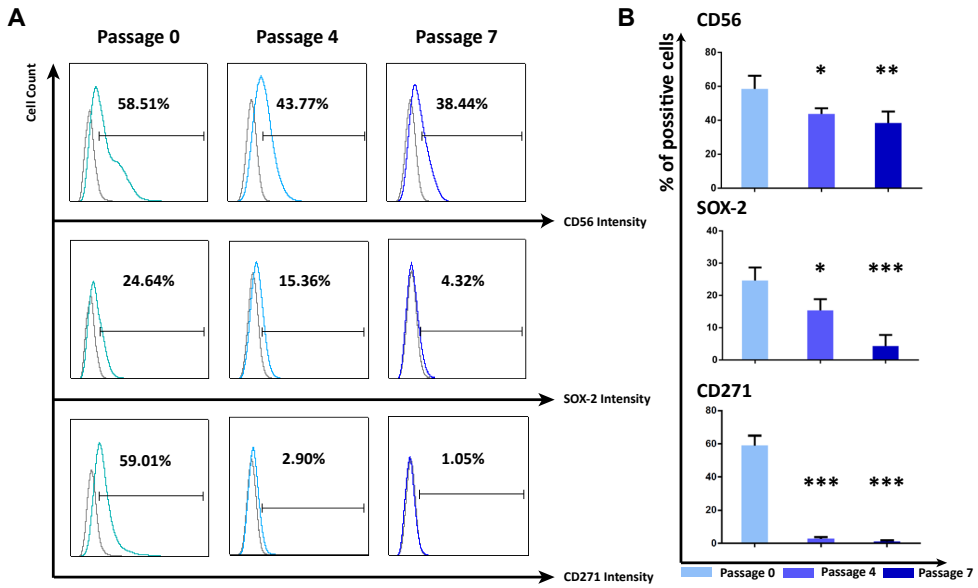

Supplementary Figure 2: Specific neural marker expression CD56, CD271 and SOX-2 disappeared when HF-MSCs were cultured in vitro. (A) Flow cytometry histograms representing the expression of CD56, SOX-2 and CD271 neuronal marker in HF-MSCs of passage 0, passage 4 and passage 7. (B) Graphical bars showing the percentage of positive HF-MSCs to CD56, SOX-2 or CD271 neuronal markers in passage 0, passage 4 or passage 7. The numbers represent means ± SD of the percentage of positive cells for each of the marker. Statistical significance: ***p < 0.001, ** p < 0.01 and * p < 0.05 when compared HF-MSCs in passage 4 and passage 7 to passage 0.

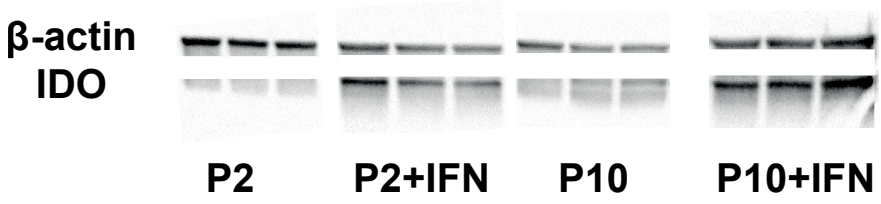

Supplementary Figure 3: Western Blot bands of the expression of indolamine 2,3-dioxygenase (IDO) and b-actin when hair follicle mesenchymal stromal cells (HF-MSCs) of passage 2 (P2) and passage 10 (P10) are licensed with interferon (IFN) (P2+IFN, P10+IFN) or without IFN licensing (P2, P10).

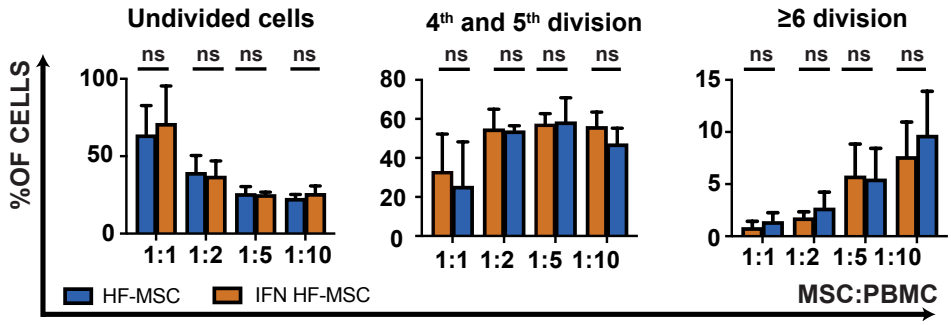

Supplementary Figure 4: Immunomodulatory effects of IFN-licensed HF-MSCs and AT-MSCs in Concanavalin A-stimulated PBMCs. (A) The proliferation profiles of the PBMCs after 5 days of co-culture with different ratios (1:1, 1:2, 1:5, 1:10) of either IFN-licensed AT-MSC or HF-MSCs by means of percentages of PBMCs remaining undivided, undergoing 4 and 5 division and undergoing more than or 6 divisions. The numbers represent means ± SD of the percentage of PBMCs in each division. Statistical significance: ns: not significant differences, $p > 0.05$. PBMCs, peripheral blood mononuclear cells. HF-MSCs, hair follicle-derived mesenchymal stromal cells. AT-MSCs, adipose tissue-derived mesenchymal stromal cells.

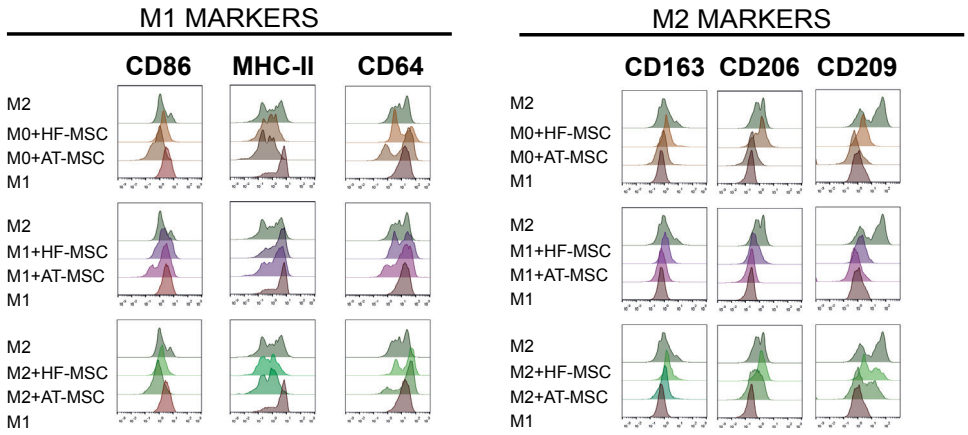

Supplementary Figure 5: Flow cytometry histograms showing either M2-related phenotypic markers (CD163, CD206 and CD209) or M1-related phenotypic markers (CD86, CD64 and MHC-II) expression when M0, M1 or M2 macrophages were co-cultured with HF-MSCs or AT-MSCs. HF-MSCs, hair follicle-derived mesenchymal stromal cells. AT-MSCs, adipose tissue-derived mesenchymal stromal cells.

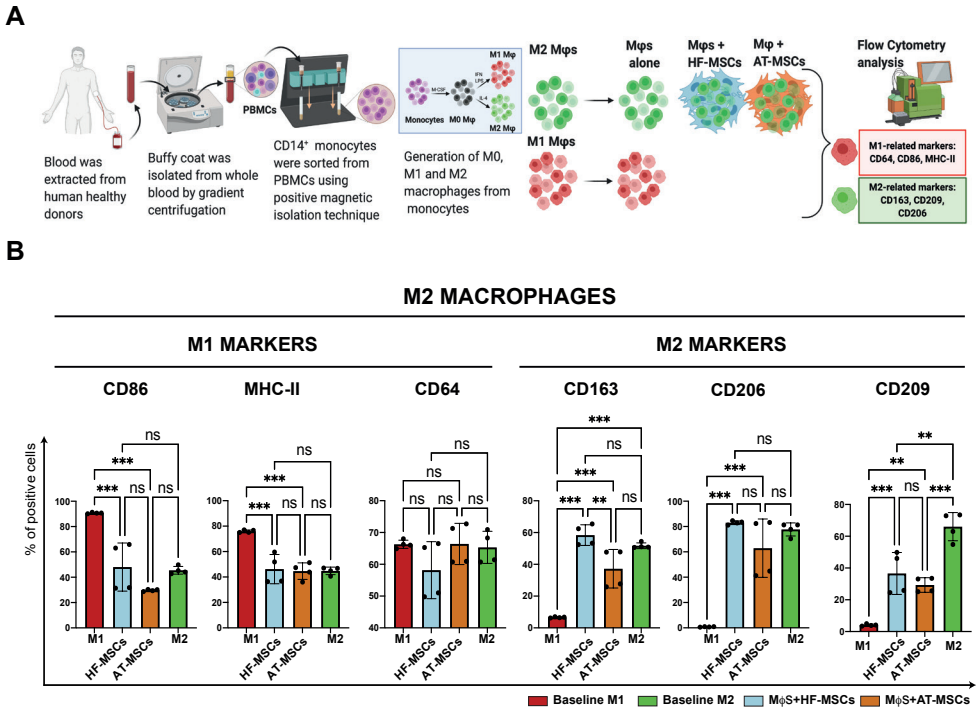

Supplementary Figure 6: Effect of HF-MSCs and AT-MSCs on the modulation of M2 macrophages phenotype. (A) CD14⁺ monocytes, obtained from blood samples of healthy donors were cultured with M-CSF for 8 days. Obtained M0 macrophages were kept in M1 or M2 differentiation conditions for 48 hours. Once all the different types of macrophages were ready, it was followed by the addition of either HF-MSC or AT-MSC to the culture of M2 macrophages in 1:1 ratio for another 48 hours. Flow cytometry was performed to assess the phenotypical markers of M1 and M2 macrophages after M2 macrophages were cocultured with the MSCs. M1 and M2 macrophages cultured without MSCs were used as a control. (B) Bar-graphs showing either M2 related phenotypic markers (CD163, CD209 and CD206) or M1 related phenotypic markers (CD64, CD86 and MHC-II) expression when M2 macrophages were co-cultured with HF-MSCs or AT-MSCs. (The numbers represent means ± SD of the percentage of positive cells for each of the marker. Statistical significance: ***p < 0.001 and ** p < 0.01 when compared with macrophages without MSCs; ns: not significant differences, p > 0.05. Mϕs macrophages. PBMCs, peripheral blood mononuclear cells. HF-MSCs, hair follicle-derived mesenchymal stromal cells. AT-MSCs, adipose tissue-derived mesenchymal stromal cells.

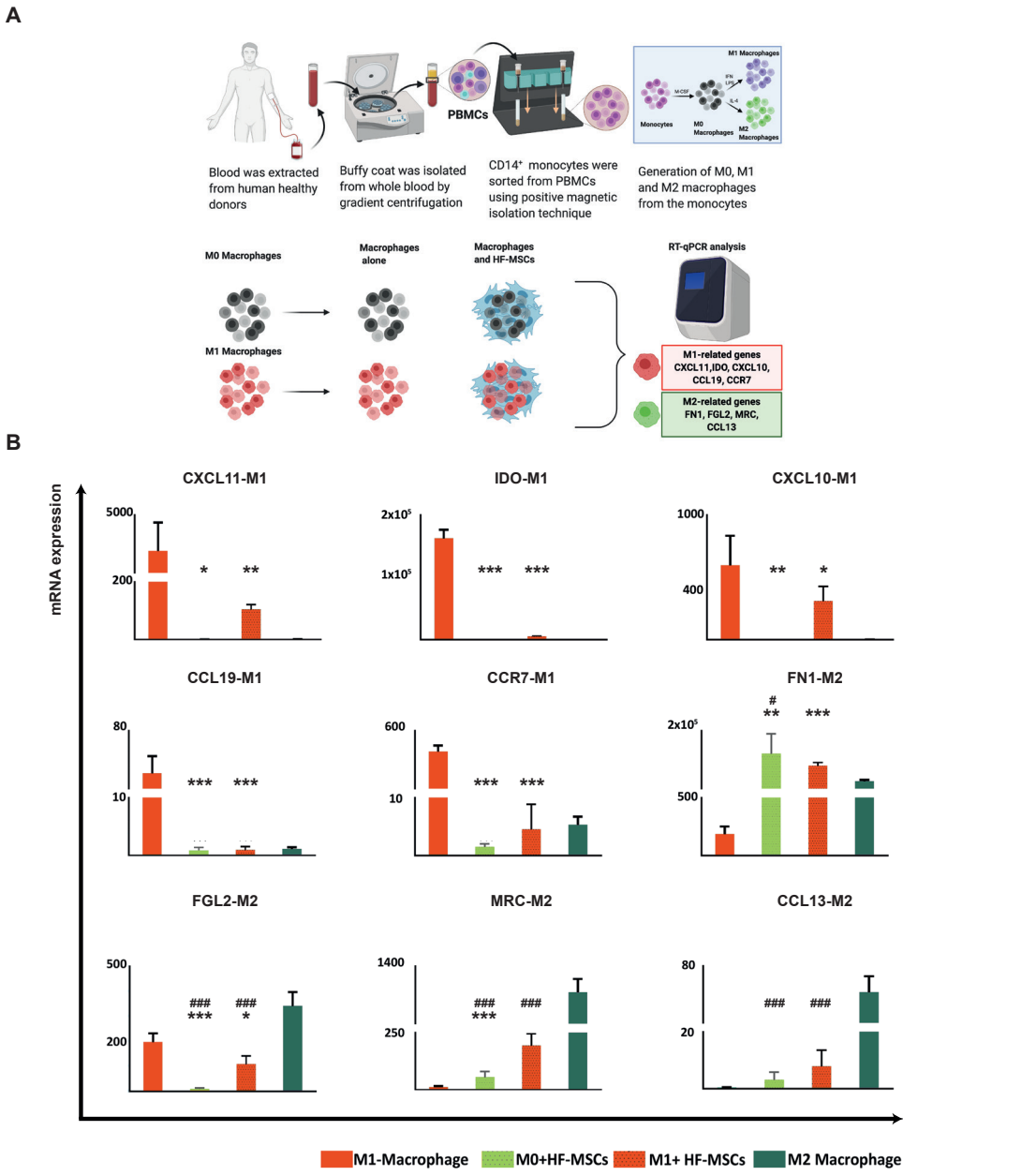

Supplementary Figure 7: Effect of HF-MSCs on the modulation of M0 and M1 macrophages gene expression. (A) CD14+ monocytes, obtained from blood samples of healthy donors were cultured with M-CSF for 8 days. Obtained M0 macrophages were kept in M1 or M2 differentiation conditions for 48 hours. Once all the different types of macrophages were ready, it was followed by the addition of HF-MSC to the culture of M0 and M1 macrophages in 1:1 ratio for another 48 hours. Flow cytometry was performed to assess the phenotypical markers of M1 and M2 macrophages after M0 and M1 macrophages were co-cultured with the

(Supplementary Figure 7 continue) HF-MSCs. M1 and M2 macrophages cultured without HF-MSCs were used as a control. (B) Bar-graphs showing either M1 related genes (CXCL11, IDO, CXCL10, CCL19 and CCR7) or M2 related genes (FN-1, FGL2, MRC and CCL13) expression when M0 or M1 macrophages were cocultured with HF-MSCs. The numbers represent means ± SD of the percentage of positive cells for each of the marker. Statistical significance: ***p < 0.001, ** p < 0.01 * p < 0.05 when compared with M1 control. ###p < 0.001, #p < 0.05 when compared with M2 control. PBMCs, peripheral blood mononuclear cells. HF-MSCs, hair follicle-derived mesenchymal stromal cells. AT-MSCs, adipose tissue-derived mesenchymal stromal cells.

4

Crosstalk with Tissue-Engineered Blood Vessels Alters Macrophage Phenotype

Abstract

Engineered tissues could be a promising strategy to regenerate unfunctional organs and tissues. However, the inability of the host tissue to vascularize its corresponding engineered counterpart significantly diminishes the overall tissue integration and function. Pre-vascularization of biomaterials could be a feasible strategy to overcome this hurdle. Nevertheless, engineered tissues will interact with the innate immune system upon implantation. Macrophages, the primary cells of the innate immune system are known to be important regulators during the whole process of wound healing. In early stages, pro-inflammatory —M1— macrophages are predominant whereas in later stages regenerative — M2— macrophages. However, how blood vessels, and engineered blood vessels, will interact with macrophages upon implantation it has not been studied in detail yet. Therefore, the goal of this study was to study the crosstalk between tissue-engineered blood vessels and undifferentiated and pre-polarized macrophages. For a thorough analysis, we used single cell analysis, specifically dimensionality reduction and clustering algorithms. The addition of tissue-engineered blood vessels to the biomaterial resulted in macrophages takin on a more regenerative, M2 phenotype. Furthermore, each pre-polarization state also upregulated distinct M1 markers, suggesting that the pre-polarization state does play a role in the crosstalk. To conclude, describing the phenotypical switch of macrophages when co-cultured with tissue-engineered blood vessels could help us in determining the exact implantation time of the tissue engineering construct to prevent implant rejection.

Grafical Abstract

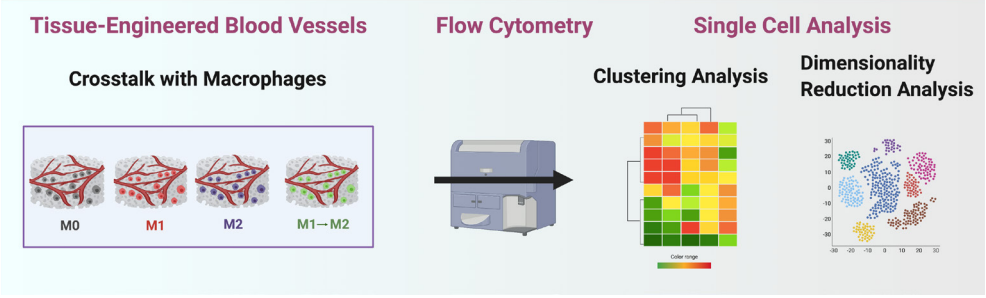

1. Introduction

In the past years, organ transplantation has accomplished major advances regarding long-term survival and substantially decreasing graft rejection risk. However, with every year, the gap between available donors and the number of patients needing organ transplantation gradually increases. Data from the annual report of the Organ Procurement and Transplantation Network/ Scientific Registry of Transplants Recipients (OPTN/ SRTR) states that, in 2019, in the United States alone, there were 19,267 donors, 39,718 transplants and 112,568 patients on the waiting list. As a possible solution to this problem, investigators have attempt to engineer *in vitro* every tissue and organ comprising the body by means of tissue engineering [1]. The main objective of tissue engineering is to repair and regenerate unfunctional organs and tissues by a combination of cells, tissue-inducing substances such as cytokines or growth factors, placed on or within a biomaterial. This scaffold or biomaterial serves as a support to guide tissue formation by creating an appropriate microenvironment that helps in the regeneration process. Unfortunately, the inability of the host tissue to quickly vascularize with the implanted engineered tissue or organ, leads to lack of oxygen and nutrients, subsequently leading to cell death and impaired tissue integration and function. As a first step towards this goal, Levenberg et al. showed the effectiveness of growing blood vessels *in vitro* as this helped accelerating anastomosis with surrounding vasculature and the following perfusion towards implant *in vivo* [2, 3]. However, like all biomaterials, engineered tissues will interact with the innate immune system upon implantation.

The primary cells of the innate immune response, macrophages, are known to be key regulators of wound healing and angiogenesis — reviewed in [4] —. The depletion of macrophages from wounds causes impaired angiogenesis, whereas the addition of macrophages stimulates it [5, 6]. In the wound healing response, the monocytes that first arrive to the wound site mostly differentiate into pro-inflammatory —also called M1— macrophages. In the resolution phase of wound healing, macrophages dramatically change their phenotype to a more pro-regenerative type commonly referred to as M2. However, the M2 descriptor has been expanded to include numerous different subtypes, and the extent of the diversity of this group is not known. Notably, M2-type macrophages can be differentiated from arriving monocytes, or they can be produced by a transition from the M1 macrophages presented in the wound site. *In vitro* studies of M1-to-M2 switching has shown

that M1-derived M2 macrophages —or M1-M2— display many similarities to M2 macrophages derived directly from inactivated (or M0) macrophages —referred as M2— at least on the gene level [7], although some key differences have been observed [8, 9]. M1, M2, and M1-M2 phenotypes can be modeled *in vitro* through the addition of Th1 or Th2 stimuli. While the addition of lipopolysaccharide (LPS) with or without interferon gamma (IFNγ) polarizes macrophages towards the M1 phenotype, interleukin 4 (IL-4) with or without interleukin (IL-13) polarizes macrophages towards the M2 phenotype. M1 macrophages can be further switched to M2, generating the M1-M2 phenotype, through the addition of IL-4 and IL-13. Until relatively recently, it was believed that M2 macrophages were the pro-angiogenic phenotype and M1 macrophages were anti-angiogenic. However, in a recent study Graney et al. determined how macrophages of different phenotypes influenced engineered blood vessels *in vitro* [10]. Using the same tissue-engineered blood vessels that will be used in this study it was found that while M1 macrophages caused endothelial cells to upregulate genes associated with early stages of angiogenesis, M2 macrophages caused endothelial cells to upregulate genes associated with later stages of angiogenesis. These results, in combination with other studies, suggest that both M1 and M2 macrophage phenotypes act in a sequential manner to regulate angiogenesis —reviewed in [11]—.

As discussed previously, it is important for a M1 to M2 transition to occur for proper implant integration. For this, various researchers have tried to develop different strategies to stimulate M2 activation — as has already been reviewed in the introduction —. One approach could be the use of tissue engineering blood vessels, with which, it will not only promote the M1 to M2 transition, but also help with integration of tissue-engineered constructs by anastomosing with the host vasculature. In concordance with the hypothesis that endothelial cells are able to induce M2 phenotype, He et al. described that direct contact with endothelial cells *in vitro* directed macrophage differentiation towards M2-like phenotype [12]. In a similar trend Njock et al. showed that indirect co-culture of endothelial cells with human monocytes drived an anti-inflammatory macrophage behavior [13]. Furthermore, this interaction is considered to be affected by Notch signaling [14, 15] .

However, how blood vessels, and engineered blood vessels in particular, regulate macrophage phenotype in return is not understood in detail yet. Therefore, the goal of this study is to test the hypothesis that the crosstalk with blood vessels

promote M2 polarization of macrophages. With that perspective, we formed a 3D tri-culture model of in vitro tissue engineered blood vessel network by coculturing human adipose microvascular endothelial cells (HAMECs), mesenchymal stromal cells (MSCs) in a 3D porous collagen scaffold as previously described [10]. Once immature blood vessels were formed, undifferentiated (M0) and differentiated macrophages (M1, M2 and M1M2) were seeded into the scaffold for 24 hours. The phenotypical change exerted by tissue-engineered blood vessels was determined using the general macrophage marker CD45 and common M1 (PD-L1, CD38, HLA-DR, CD80 and CCR7) and M2 (CD163, CXCR4, CD206 and CD209) flow cytometry macrophage markers and the results were processed by single cell analysis, specifically using dimensionality reduction algorithm (TriMap) and clustering analysis (FlowSOM).

2. Material and Methods

2.1. Cell culture

2.1.2. Primary human monocyte-derived macrophages

Freshly isolated primary human monocytes from healthy donors were purchased from the University of Pennsylvania Human Immunology Core (Philadelphia, PA). The monocytes were seeded in a concentration of $1x10^6$ cells/ml in non-cell treated 24 well plates (Falcon, Cat No: 351147) for 5 days in RPMI 1640 media (Thermo Scientific, Cat No: 11875119), supplemented with 10 % heat-inactivated human serum (Sigma Aldrich, Cat No: H3667), 1 % penicillin/streptomycin (Thermo Scientific, Cat No: 15140122), and 20 ng/mL macrophage colony stimulating factor (M-CSF) (Peprotech, Cat No: 300-25). The media was replenished at day 3.

On day 5, macrophages were either kept undifferentiated (M0) or they were further differentiated towards M1, M2 and M1M2 phenotypes. For M1 activation 100 ng/ml IFNγ (Peprotech, Cat No: 300-02) and 100 ng/mL LPS (Sigma-Aldrich, Cat No: L2654) were added; for M2 activation 40 ng/ml IL-4 (Peprotech, Cat No: 200-04) and 20 ng/mL IL-13 (Peprotech, Cat No: 200-13) and for M1M2 activation cells were treated for the first 24 hours with M1 activation media and for the next 24 hours with M2 differentiation media. On day 7, all macrophages were washed to remove polarizing stimuli. To confirm the polarization of the macrophages, n=3 biological

replicates per donor for a total of five donors were scrapped and stained for the flow cytometry panel as described in 2.3. All macrophages were maintained in a humidified chamber at 37 ºC and 5 % of CO_2 during culture.

2.1.3. Endothelial cells

HAMECs (ScienCell, Cat No: 7200) were cultured at 5000 cells/cm^2 in endothelial cell medium (ScienCell, Cat No: 1001) supplemented with 5% of fetal bovine serum (ScienCell, Cat No: 0025), 1 % of endothelial cell growth supplements (ScienCell, Cat No: 1052) and 1 % of antibiotic solution (ScienCell, Cat No: 0503). When cells reached 90 % of confluency, they were subcultured using TrypLE Express (Gibco, Cat. No: 12604-021). All cells were maintained in a humidified chamber at 37 ºC and 5 % of CO_2 during culture. Endothelial cells were used within six passages.

2.1.4. MSCs

Adipose tissue mesenchymal stromal cells (AT-MSCs) were purchased from ATCC® (ATCC®, Cat. No: PCS-500-011). Cells were seeded in 175cm^2 T-flasks (Corning Life Science, Cat No: 431080) and cultured in Mesenchymal Stem Cell Basal Medium (ATCC®, Cat. No: PCS-500-030™), supplemented with the Mesenchymal Stem Cell Growth kit (ATCC®, Cat. No: PCS-500-040™) and 1 % antibiotic/antimycotic solution (GIBCO, Cat No:15140-122). Cells were maintained at 37 ºC, 5 % CO_2, passaged when reaching 90 % confluency using TrypLE Express (Gibco, Cat. No: 12604-021) and neutralized with complete media. AT-MSCs were used within six passages.

2.2. Development of tissue-engineered blood vessels

Size 100 cm^2 Surgifoam (Ethicon, Cat No: 1975) collagen scaffold was cut using an 8 mm diameter biopsy punch (Fisher Scientific, Cat No: NC9324386), and soaked in complete media for 1 hour. To create tissue-engineering blood vessels, 300,000 endothelial cells and 60,000 AT-MSCs were seeded directly into the constructs in the complete media for endothelial cells as previously described [10]. To facilitate cell attachment into the scaffold, the cells were incubated for 45 minutes in a humidified incubator at 37 ºC and 5 % CO_2. Subsequently, the scaffolds were

immersed in media containing 50 % endothelial cell complete media and 50 % of AT-MSCs complete media. On day 3, 240,000 of M0, M1, M2a or M1M2 primary human macrophages were seeded directly onto the scaffolds — alone, with blood vessels, with endothelial cells or with MSCs —. All samples were incubated for 45 minutes to allow cell attachment and then the scaffolds were immersed in media containing 50 % of endothelial cell complete media and 50 % of AT-MSCs complete media. This media supported macrophage variability after 1 day *in vitro* via live death flow cytometry staining.

2.3. Scaffold digestion and flow cytometry

After 24 hours of seeding macrophages into the engineered blood vessels constructs, vascularized scaffolds were washed in 1X DPBS containing Ca^{2+} and Mg^{2+} (Thermo Scientific, Cat No: 14040133) and placed into 24 well plates. Collagenase IV (Worthington, Cat No: #LS004188) was reconstituted with DPBS containing Ca^{2+} and Mg^{2+} to a concentration of 5 mg/mL. 500 mL of Collagenase IV was added to each scaffold and were incubated at 37 ºC for 30 minutes on a Thermo Scientific Tube Revolver/Rotator set to 12 rpm with oscillation.

After the scaffolds were digested, complete media was added to each sample to reduce the enzymatic activity. In order to remove the undigested scaffold pieces, each sample was filtered using 70 mm filter caps (Bel-Art, Cat No: H136800040). After, the samples were centrifuged at 400 x g for 5 minutes the supernatant was aspirated, and cells were re-suspended in PBSs without Ca^{2+} and Mg^{2+} to start flow cytometry staining.

Cells were stained with the Live/Death fixable Aqua (Invitrogen, Cat No: L34957) according to the kit instruction and incubated for 20 minutes in room temperature. Afterwards the cells were washed with running buffer —PBS, 0.5 % BSA (Sigma-Aldrich, Cat No: A2153) and 2 mM ethylenediaminetetraacetic acid (EDTA) (Sigma-Aldrich, Cat No: E9884) — and centrifuged at 400 x g for 5 minutes. Subsequently, cells were blocked with FcR of blocking reagent (BD, Cat No: 564219) at a 0.02 mg/mL concentration for 5 min at room temperature. Finally, cells were stained with anti-CD45-APCVio770 (Miltenyi Biotech, Cat No: 130-110-635), anti-CD206-VioBlue (Miltenyi Biotech, Cat No: 130-100-034), anti-CD209-PEVio770 (Miltenyi Biotech, Cat No: 130-109-591), anti-CD163-APC (Miltenyi Biotech, Cat

No: 130-112-129), anti-CXCR4-PEVio615 (Miltenyi Biotech, Cat No: 130-109-848), anti-CCR7-BB515 (BD, Cat No: BDB565869), anti-CD80-PE (Biolegend, Cat No: 305208), anti-HLADR-PerCPVio700 (Miltenyi Biotech, Cat No: 130-111-793), CD38-BrillantViolet605 (Biolegend, Cat No: 303532), anti-PDL1-BrillantViolet711 (Biolegend, Cat No:329722) and incubated for 45 minutes at 4 ºC. Then cells were washed and re-suspended in running buffer. Cells were analyzed using a BD Fortessa Flow Cytometer (BD Bioscience, Franklin Lakes, NJ) in the Flow Cytometry Facility at Sidney Kimmel Cancer Center at Jefferson (Philadelphia, PA).

2.4. Flow citometry analysis

Data was acquired using BD FACSDiva™ software and analyzed using FlowJo™ flow cytometry data analysis software. The main goal of this study was to identify what macrophage phenotypic population were induced upon co-cultured with tissue-engineered blood vessels. For that aim, a combination of manually gating population and clustering algorithm was used to differentiate new macrophage populations and study how differently the macrophages behaved when co-cultured with blood vessels

For manual gating, each of the target clean population (Singlets / live / $CD45^+$ cells, aka macrophages) the median fluorescent intensity (MFI) of the M1-related markers (CCR7, CD80, HLA-DR, CD38, PDL1) and M2-related markers (CD206, CD209, CD163, CXCR4) was analyzed.

Single cell analysis was conducted by a combination of large-scale dimensionality reduction using triplets (TriMap) and Flow Cytometry self-organizing map (FlowSOM) algorithms. TriMap is an algorithm which produces 2 parameters (Y, X) and redistributes all the events in a two-dimensional (2D) space taking into account the multidimensional relationship between all the events. In order to compare different data sheet, all the data was concatenate into a single file. To do that, firstly, the target population — Singlets / live / $CD45^+$ cells, aka macrophages — was downsampled, to equalize the number of events. Then, all down sampled population was concatenated into a single file and the dimensionality reduction algorithm (TriMap) was ran. TriMap was used as it gives an idea about global structure of the data, which is not obtained in the case of the most commonly known t-distribution stochastic neighborhood embedding (tSNE) and Uniform Manifold Approximation

and Projection (UMAP) algorithm, while keeping the complexity of the data, which is lost in the case of the principal component analysis (PCA) [16].

Subsequently, clustering analysis was conducted to group cells into that have similar intensity for each of the markers analyzed. FlowSOM was chosen because it tends to group similar cell groups into large meta-clusters and because of its high precision, coherence and stability [17]. Then, those clusters were gated based in the different experimental conditions to determinate the percentage and que number of macrophages of each experimental group that composed each of the clusters. Finally, to evaluate the similarity between different clusters, Euclid algorithm was used to get the Taylor Index. Taylor index gives the information about the distance from one cluster to another in the dimensional space [18]. How well the cluster are differentiated from one to another – the higher the index value the higher the distance between two clusters and the less likely two clusters are related to each other.

3. Results

3.1. Validation of the flow cytometry panel

Throughout this manuscript, general macrophage marker (CD45), different M1 (HLA-DR, CD80, CCR7, CD38 and PD-L1) and M2 (CD206, CD209, CD163 and CXCR4) common markers were used to illustrate how blood vessels affected macrophage phenotype by flow cytometry. Towards that end, it was necessary to validate all the markers presented in this study. Therefore, primary human peripheral blood monocytes were isolated from five human donors, differentiated into macrophages (M0) and further polarized into M1, M2 or M1M2 phenotypes for 48 hours (Figure 1A).

Traditional flow cytometry analysis demonstrated that CD45 general macrophage marker exhibited no significant differences ($p > 0.05$) between the distinct phenotypes and also showed a high intensity in all of them. Furthermore, CD45 was only expressed in macrophages not in blood vessels, MSC or endothelial cells and this provided us the opportunity to analyze only the macrophages while not considering the blood vessels, endothelial cells and MSCs (Figure 1B). Regarding M2 markers, both CD206 and CD209 markers were upregulated in M2 macrophages

($p < 0.001$) compared with other macrophages phenotypes (Figure 1C). With respect to CXCR4, M1M2 macrophages demonstrated a significant upregulation compared with M2 macrophages ($p < 0.01$). However, CD163 was upregulated in M1 and M1M2 macrophages compared to M2 macrophages ($p < 0.05$) although the intensity of the marker was not high in none in none of them. This could be due to CD163 is a common marker for another subpopulation of M2 macrophages, known as M2c, which is obtained by the stimulation of M0 with IL-10 [19] (Supplementary Figure 1).

With respect of M1 markers, both M1 and M1M2 macrophages showed a significant upregulation ($p < 0.001$) of PD-L1, CD80, CD38 and HLA-DR compared to M2 and M0 (Figure 1D). However, an upregulation in any of the different phenotypes in CCR7 marker was not observed ($p > 0.05$). This also occurred when Spiller et al. measured the CCR7 expression in M0, M1 and M2 macrophages and the flow cytometry histogram did not show a strong difference between phenotypes [8]. Also, it is worth mentioning that in this study, CCR7 antibody was attached to APC fluorophore which has a brightness index of 5, whereas in our case, it was used along with FITC which has a brightness index of 1.

Dimensionality reduction analysis (TriMAP) was performed to further analyze the expression of the markers within the different macrophage phenotypes (Figure 1E). In dimensionality reduction visualization graph, it could be noticed that M1 and M1M2 macrophages were located in similar places within the graph (up on the left), suggesting similar expression profiles, whereas M0 and M2 macrophages were located down on the right. Subsequently, FlowSOM clustering analysis was conducted. Clustering analysis grouped cells that had similar marker expression (Figure 1F). As expected, M1 macrophages tended to be in clusters enriched in M1 markers, whereas M2 macrophages were in clusters enriched in M2 markers (Figure 1G).

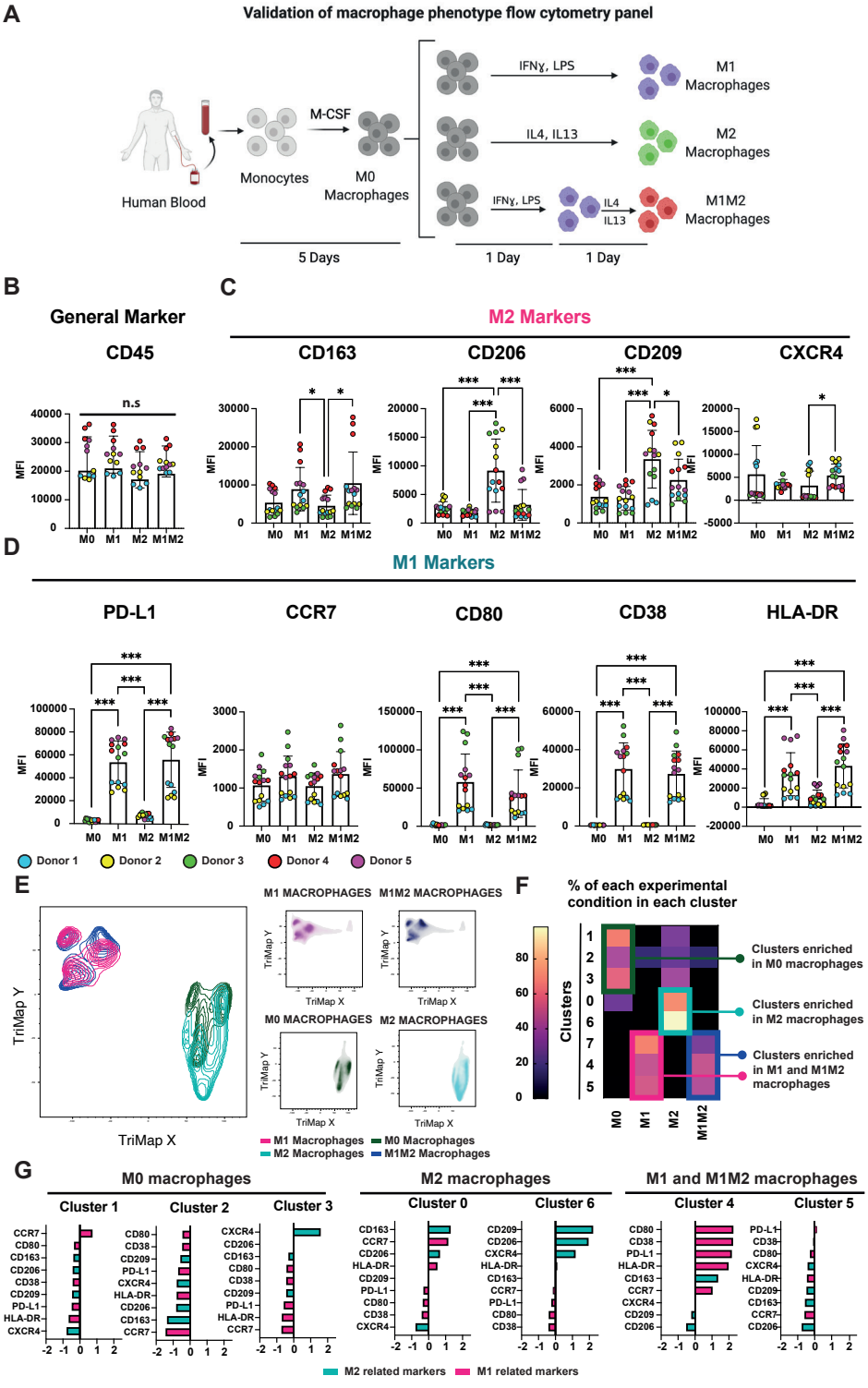
A
Validation of macrophage phenotype flow cytometry panel
Human Blood
Monocytes
M-CSF
M0 Macrophages
IFNγ, LPS
M1 Macrophages
IL4, IL13
M2 Macrophages
IFNγ, LPS
IL4
IL13
M1M2 Macrophages
5 Days
1 Day
1 Day
B
General Marker
CD45
n.s
MFI
M0 M1 M2 M1M2
C
M2 Markers
CD163
CD206
CD209
CXCR4
D
M1 Markers
PD-L1
CCR7
CD80
CD38
HLA-DR
Donor 1
Donor 2
Donor 3
Donor 4
Donor 5
E
TriMap Y
TriMap X
M1 MACROPHAGES
M1M2 MACROPHAGES
M0 MACROPHAGES
M2 MACROPHAGES
M1 Macrophages
M0 Macrophages
M2 Macrophages
M1M2 Macrophages
F
% of each experimental condition in each cluster
Clusters
Clusters enriched in M0 macrophages
Clusters enriched in M2 macrophages
Clusters enriched in M1 and M1M2 macrophages
G
M0 macrophages
M2 macrophages
M1 and M1M2 macrophages
Cluster 1
Cluster 2
Cluster 3
Cluster 0
Cluster 6
Cluster 4
Cluster 5
M2 related markers
M1 related markers

Figure 1: Validation of the human macrophage phenotype flow cytometry Panel. (A) Primary human peripheral blood monocytes were isolated from 5 human donors, differentiated into macrophages (M0) and further polarized into M1, M2 or M1M2. (B) Median fluorescent intensity (MFI) of the general macrophage marker CD45. (C) MFI of associated M1 markers (HLA-DR, CD80, CCR7, CD38 and PD-L1) (D) MFI associated M2 markers (CD206, CD209, CD163, CXCR4). Data in (B), (C) and (D) represents mean ± SD with n=3 technical replicates from five human donors. (E) Localization of M0 (dark green), M1 (pink), M2 (light green), M1M2 (dark blue) macrophages in TriMap plots. Phenotype groups shown collectively (left) and individually (right) (F) Heat map showing the percentage of cells within a given phenotype group in each cluster.(G) Z-scores showing the relative expression of each marker in clusters composed mainly of M0 (clusters 1,2 and 3), M2 (clusters 0 and 6), M1 and M1M2 (clusters 4 and 5) macrophages. One way ANOVA with Tukey post hoc analysis. *** $p < 0.001$ ** $p < 0.01$, * $p < 0.05$.

3.2. M0 macrophages show high plasticity and upregulate M2 markers when co-cultured with blood vessels

To determine how M0 macrophage phenotype was altered when co-cultured with blood vessels, primary human monocytes were isolated from human blood and differentiated towards M0 macrophage (Figure 2B). Endothelial cells and MSCs, which acted as support cells to facilitate the formation of stable blood vessels, were co-cultured together on 8 mm compressed Surgifoam sponges to start blood vessel formation. Previous studies from our group using the same methodology have shown that after 3 days, immature vessel formation could be already be noticed [10]. After 3 days of co-culture, human derived M0 macrophages were seeded in the scaffold, and changes in macrophage phenotype were assessed after one day via flow cytometry. To determine if these differences were solely due to blood vessels, macrophages were seeded in 3D scaffold alone, or with just MSCs or endothelial cells to use as controls. Using these controls and clustering analysis, it was possible to let aside the macrophages that did not change from the baseline, macrophages that only switched due to the co-culture in the 3D scaffold or due to endothelial cells or mesenchymal stromal cells.

Traditional flow cytometry analysis demonstrated that macrophages upregulated CD163 ($p < 0.001$), CD38 ($p < 0.001$), HLA-DR ($p < 0.05$), CD80 ($p < 0.05$), CCR7 ($p < 0.001$) and downregulated CD209 ($p < 0.01$) and PDL1

($p < 0.001$) markers when compared to the baseline (Figure 2B, Supplementary Figure 2). Furthermore, co-culture with blood vessels caused an upregulation of most M2 markers and downregulation of M1 markers, respectively, compared with macrophages co-cultured alone in the scaffold. Specifically, macrophages co-cultured with blood vessels upregulated CD163 ($p < 0.01$ and $p < 0.001$, when compared to macrophages co-cultured in the scaffold alone or with endothelial cells, respectively). CXCR4 ($p < 0.001$) and CD206 ($p < 0.001$) were also upregulated compared to when co-cultured alone in the 3D scaffold. In regards of M2-associated marker expression, CD209 was downregulated when compared to co-culturing macrophages alone in the 3D scaffold ($p < 0.01$), or with endothelial cells ($p < 0.001$) or MSCs ($p < 0.01$). Regarding M1-associated markers, compared to macrophages co-cultured alone in the scaffold and with endothelial cells, there was a downregulation of the PDL1 marker ($p > 0.001$). Likewise, there was an upregulation of the CD38 ($p > 0.001$) marker when compared with macrophages co-cultured with MSCs.

The previous traditional flow cytometry analyses took into account all the macrophages within the scaffold. To make sure only the macrophages that are affected particularly by the blood vessels were analyzed, and the influence of seeding them on the 3D system or with MSCs and endothelial cells were negated, the data was processed by single cell analysis using clustering analysis and visualization of the data was done by dimensionality reduction (TriMap). The clustering analysis allowed to group cells that showed similar marker expression into the same cluster. Therefore, FlowSOM was used and all the data were clustered in 20 different clusters. Clusters 12, 14 and 17 were enriched in macrophages in baseline, clusters 0, 1, 2, 3 and 7 were enriched in macrophages seeded in the 3D scaffold and clusters 4, 5, 6, 8, 9, 10, 11, 13, 15, 16, 18 and 19 were enriched in macrophages co-cultured with cells, either endothelial or MSCs, or with the blood vessels (Figure 2C). It is to be noted that being “enriched” indicated twice the number of macrophages in a specific experimental condition than in the other clusters.

Subsequently, the distance between every 2 clusters — known as Taylor index — were measured. If two clusters were very close together, the similarity was high and the color is darker in the heatmap, whereas if the cluster were farther, they were less similar and correspondingly brighter in the heatmap (Supplementary Figure 3). In this part, the focus was solely on the comparison between cluster 2, 10 and 19, that was where most macrophages were located when cultured alone in the

scaffold (cluster 2) or when co-cultured with blood vessels and MSCs (cluster 10) or endothelial cells (cluster 19) (Figure 2D). Even the distance value between the 3 clusters was not very high; cluster 10 and 2 were the less similar ones, whereas cluster 10 and 19 were the most similar ones (Figure 2E), which could also be noticed in the TriMap. Macrophages in cluster 10 and 19 were closer to each other than cluster 2, in the TriMAP (Figure 2F).

Furthermore, it was pertinent to analyze the composition of the main clusters already mentioned. Cluster 2, which CD209 was highly expressed, became enriched with macrophages co-cultured in the 3D collagen scaffold. Macrophages co-cultured with either blood vessels or MSCs were predominantly found in cluster 10, which was mostly upregulated in M2 markers CD163, CD206 and CD209. Finally, cluster 19 was enriched in macrophages co-cultured with endothelial cells in which also M2 markers were upregulated but to a lesser extent than in cluster 10 (Figure 2G).

3.3. M1 macrophages showed reduced plasticity and downregulation of most of the M1 common markers

To determine how pro-inflammatory M1 macrophage phenotype changed when co-cultured with blood vessels, primary human monocytes were isolated from human blood and differentiated towards M0 macrophages via administration of M-CSF for 5 days. M0 macrophages were further differentiated towards M1 by addition of LPS and IFNγ for 48 hours. To assess whether these differences were just because of the blood vessels, macrophages were seeded in 3D scaffold alone, or with just MSCs or endothelial cells to use as controls (Figure 3A).

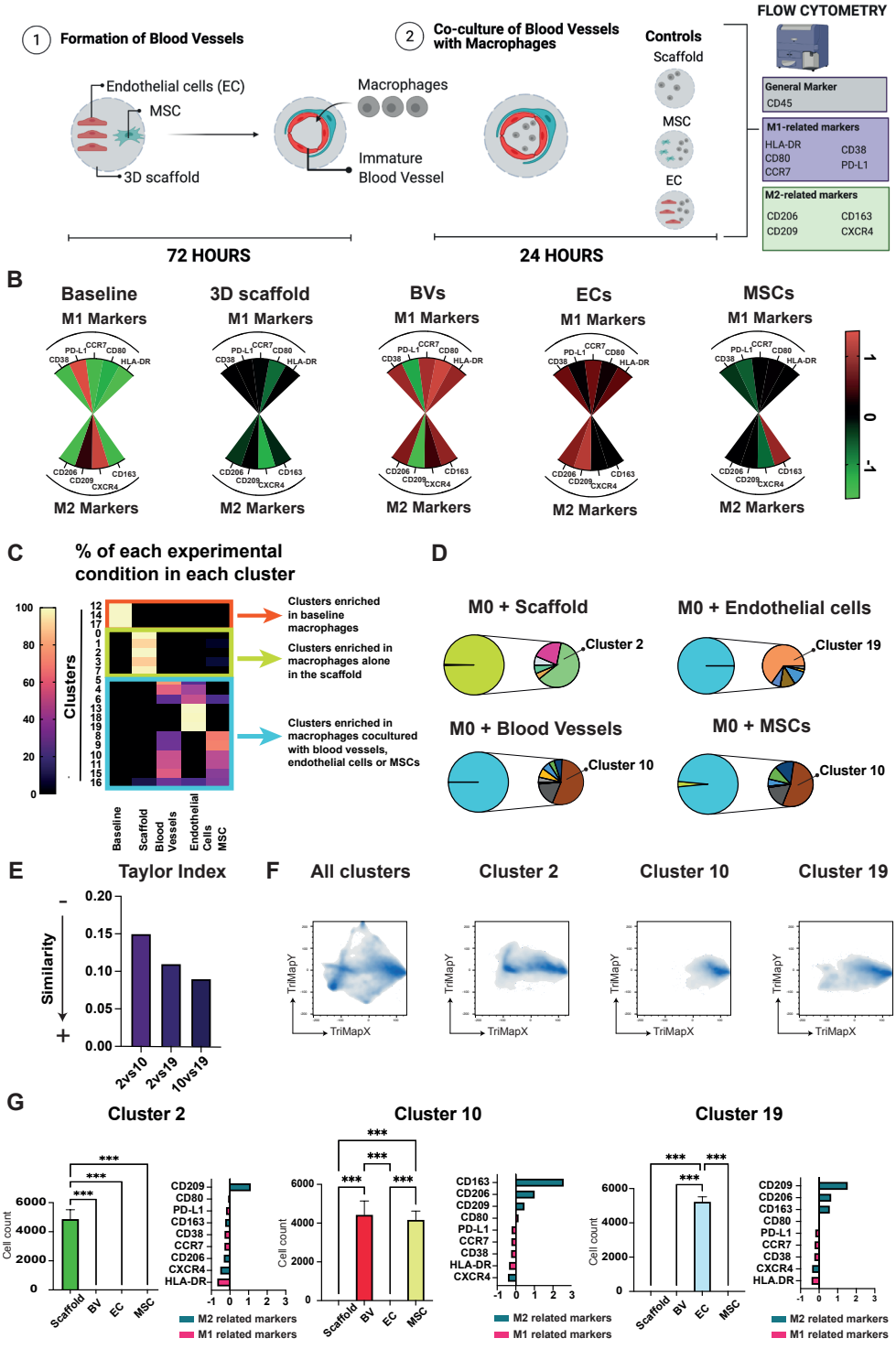
A
1 Formation of Blood Vessels
Endothelial cells (EC)
MSC
3D scaffold
Macrophages
Immature Blood Vessel
2 Co-culture of Blood Vessels with Macrophages
72 HOURS
24 HOURS
Controls
Scaffold
MSC
EC
FLOW CYTOMETRY
General Marker
CD45
M1-related markers
HLA-DR
CD80
CCR7
CD38
PD-L1
M2-related markers
CD206
CD209
CD163
CXCR4
B
Baseline
3D scaffold
BVs
ECs
MSCs
M1 Markers
M2 Markers
PD-L1
CCR7
CD80
CD38
HLA-DR
CD206
CD209
CD163
CXCR4
C
% of each experimental condition in each cluster
Clusters
Baseline
Scaffold
Blood Vessels
Endothelial Cells
MSC
Clusters enriched in baseline macrophages
Clusters enriched in macrophages alone in the scaffold
Clusters enriched in macrophages cocultured with blood vessels, endothelial cells or MSCs
D
M0 + Scaffold
Cluster 2
M0 + Endothelial cells
Cluster 19
M0 + Blood Vessels
Cluster 10
M0 + MSCs
Cluster 10
E
Taylor Index
Similarity
2vs10
2vs19
10vs19
F
All clusters
Cluster 2
Cluster 10
Cluster 19
TriMapX
TriMapY
G
Cluster 2
Cluster 10
Cluster 19
Cell count
Scaffold
BV
EC
MSC
M2 related markers
M1 related markers

Figure 2: Crosstalk between undifferentiated (M0) macrophages and tissue-engineered blood vessels. (A) *In vitro* tissue-engineered human blood vessels were generated by co-culture of endothelial cells and MSCs on 3D collagen scaffolds. Changes in macrophage phenotype were observed one day after macrophage seeding. (B) A comparison of the Z-score value of M1 (CD38, PD-L1, CCR7, CD80, HLA-DR) and M2 (CD206, CD209, CXCR4, CD163) phenotype markers in each experimental condition. (C) Heat map showing the percentage of macrophages from each experimental condition that are within each cluster. (D) Pie charts showing how macrophages in the different experimental conditions are located in clusters enriched in baseline macrophages (orange), macrophages alone in the 3D scaffold (light green), or macrophages co-cultured with cells and blood vessels (light blue). The attached pie chart shows the exact cluster location of macrophages in the different experimental conditions. (E) Taylor index representing the similarity between the different clusters. (F) Localization of all clusters, cluster 2, 10, and 19 in the TriMap plots. (G) Bar graphs showing the exact composition of the main clusters and Z-scores representing the relative expression of each marker in each of these clusters. Data in (H) represents mean ± SD with n = 3 biological replicates. BV, blood vessels. ECs, endothelial cells. MSCs, mesenchymal stromal cells. Statistical significance: One way ANOVA with Tukey post hoc analysis *** $p < 0.001$.

The traditional flow cytometry analysis demonstrated that macrophages upregulated CD163 ($p < 0.001$), CD206 ($p < 0.01$) and CD209 ($p < 0.01$) M2-related markers and CCR7 ($p < 0.01$) M1-related marker in comparison to the baseline. Furthermore, they downregulated most of the M1-related markers PDL1 ($p < 0.001$), CD38 ($p < 0.01$) and HLA-DR ($p < 0.001$) when compared to the baseline. Co-culturing with blood vessels mostly upregulated M2 markers and downregulated M1 markers when compared with the 3D controls — macrophages in the 3D scaffold alone, macrophages co-cultured with either MSCs or endothelial cells—. Specifically, macrophages co-cultured with blood vessels upregulated CD163 ($p < 0.01$ and $p < 0.05$) when compared to macrophages co-cultured in the scaffold alone or with endothelial cells, respectively. Macrophages upregulated CD209 marker expression ($p < 0.05$) when compared to macrophages co-cultured in the scaffold alone or with endothelial cells. Regarding M1-associated markers, compared to macrophages co-cultured alone in the scaffold and with endothelial cells, there was a downregulation of the CD38 and HLA-DR markers. Likewise, there was a downregulation of the CD38 ($p > 0.001$) marker when compared with macrophages co-cultured in the scaffold alone. Interestingly, no differences are observed in any of the markers ($p > 0.05$) when macrophages were co-cultured with either blood vessels or mesenchymal stromal cells (Figure 3B, Supplementary Figure 4).

Regarding single cell analysis, we found that clusters 2, 15, 16 were enriched in macrophages in baseline, clusters 7, 9 and 12 were enriched in macrophages seeded in the 3D scaffold and clusters 1, 3, 4, 5, 6, 8, 10, 11, 13, 14, 17, 18 and 19 were enriched in macrophages co-cultured with cells, either endothelial or MSCs, or with the blood vessels (Figure 3C). It was noticed that in clusters enriched with macrophages in the baseline or in clusters enriched in macrophages in the 3D scaffold, the macrophages that were co-culture with cells or blood vessels were also found, indicating the low plasticity of M1 macrophages (Figure 3D). This is, however, not the case for M0 and M2 macrophages, where plasticity seemed to be higher (Figure 2D and Figure 4D, respectively).

Subsequently, the distance between every 2 clusters were measured, which is the Taylor Index (Supplementary Figure 5). We only focused on cluster 0, 3 and 14, that were where most macrophages tend to migrate when cultured alone in the 3D scaffold or co-cultured with blood vessels, MSCs or endothelial cells (Figure 3D). Regarding the similarity between the clusters, cluster 0 and cluster 14, and cluster 0 and 13 were the ones that were more distant to each other indicating more differences than cluster 3 and 14 (Figure 3E), which can also be noticed in the TriMap. Macrophages in cluster 13 and 14 were located closer in the TriMap than cluster 0, which located in the far left of the graph (Figure 3F).

Thereafter, it was necessary to analyze how macrophages in the different conditions —co-cultured alone in the scaffold, with MSCs and endothelial cells or blood vessels— were organized within the clusters. Macrophages co-cultured in the 3D collagen scaffold were mostly located in cluster 0 which is upregulated in HLA-DR, CD163 and CD38 markers. Macrophages co-cultured with either blood vessels, endothelial cells and MSCs were mainly located in cluster 14 in which a mixture of both M1 (CD80 and CCR7) and M2 markers (CD206 and CXCR4) were expressed. Finally, macrophages co-cultured with endothelial cells and MSCs were also located in cluster 3 in which CXCR4, CCR7 and to a lesser extent CD209 were expressed (Figure 3G).

3.4. M2 macrophages showed high plasticity and upregulation of M1 and M2 markers

To determine how pro-regenerative M2 macrophages changed when co-cultured with blood vessels, primary human monocytes were isolated from a human donor and differentiated towards M0 macrophages via administration of M-CSF for 5 days. M0 macrophages were further differentiated towards M2 by addition of IL-4 and IL-13 for 48 hours. To assess whether these differences were just because of the blood vessels, macrophages were seeded in 3D scaffold alone, or with just MSCs or endothelial cells to use as controls (Figure 4A).

Traditional flow cytometry analysis demonstrated that macrophages co-cultured with blood vessels upregulated CD163 ($p < 0.001$), CD206 ($p < 0.001$), CD38 ($p < 0.001$), HLA-DR ($p < 0.001$) and CCR7 ($p < 0.05$) and downregulated CXCR4 ($p < 0.001$) and PD-L1 ($p < 0.001$) when compared to the baseline. Furthermore, macrophages co-cultured with blood vessels upregulated CD163 ($p < 0.001$, $p < 0.01$ and $p < 0.01$) when compared to macrophages co-cultured in the scaffold alone, with endothelial cells or MSCs, respectively. Macrophages downregulated CD209 marker expression ($p < 0.001$) when compared to macrophages co-cultured in the scaffold alone, with endothelial cells or with MSCs. Regarding M1-associated markers, compared to macrophages co-cultured alone in the scaffold, with endothelial cells and with MSCs, there was an upregulation of the CD38 and HLA-DR markers ($p < 0.001$) (Figure 4B, Supplementary Figure 6).

Regarding single cell analysis and clustering analysis, we found that clusters 16 and 17 were enriched in macrophages in baseline. Clusters 0, 1 and 7 were enriched in macrophages seeded in the 3D scaffold and clusters 2, 3, 4, 5, 6, 8, 9, 10, 11,12, 13, 14, 15, 18 and 19 were enriched in macrophages co-cultured with endothelial, MSCs, or with blood vessels (Figure 4C). It was noticed that in clusters enriched with macrophages in the baseline or also in macrophages in the 3D scaffold, macrophages that were co-culture with MSCs, endothelial cells or blood vessels were not nearly discernible (Figure 4D). This also happened for M0 macrophages but not with M1 and M1M2. This could indicate that the plasticity of M0 and M2 macrophages was higher than that of the M1 and M1M2 macrophages (Figure 2D, Figure 3F and Figure 5F).

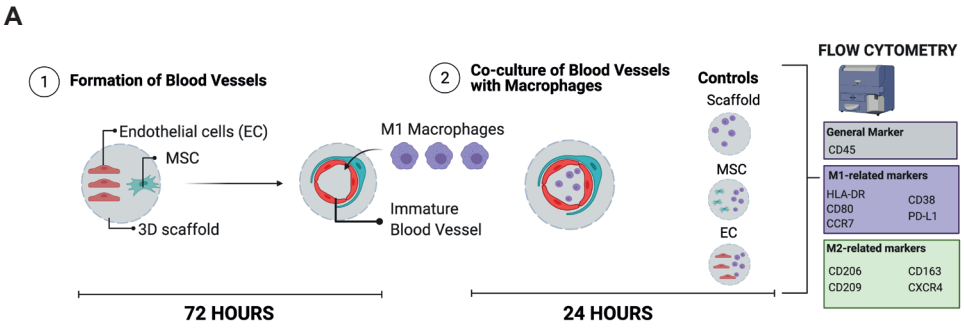
A
1 Formation of Blood Vessels
Endothelial cells (EC)
MSC
3D scaffold
M1 Macrophages
Immature Blood Vessel
2 Co-culture of Blood Vessels with Macrophages
Controls
Scaffold
MSC
EC
FLOW CYTOMETRY
General Marker
CD45
M1-related markers
HLA-DR
CD38
CD80
PD-L1
CCR7
M2-related markers
CD206
CD163
CD209
CXCR4
72 HOURS
24 HOURS

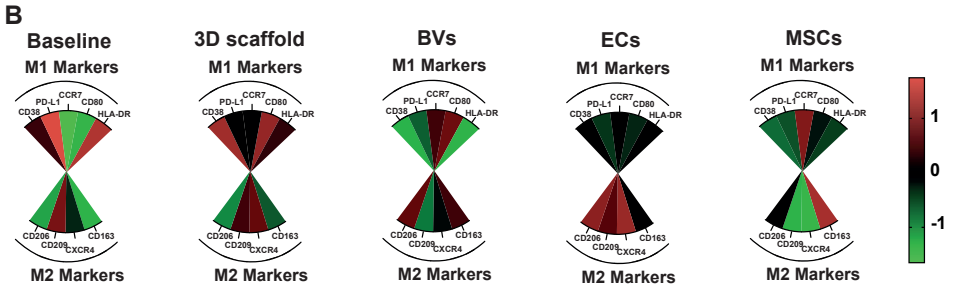
B
Baseline
3D scaffold
BVs
ECs
MSCs
M1 Markers
M2 Markers
CCR7
PD-L1
CD80
CD38
HLA-DR
CD206
CD209
CD163
CXCR4
1
0
-1

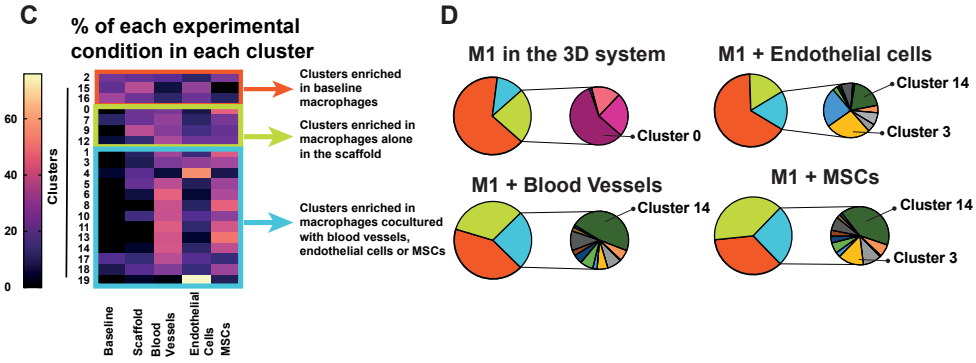
C
% of each experimental condition in each cluster
Clusters
Clusters enriched in baseline macrophages
Clusters enriched in macrophages alone in the scaffold
Clusters enriched in macrophages cocultured with blood vessels, endothelial cells or MSCs
Baseline
Scaffold
Blood Vessels
Endothelial Cells
MSCs
D
M1 in the 3D system
Cluster 0
M1 + Endothelial cells
Cluster 14
Cluster 3
M1 + Blood Vessels
Cluster 14
M1 + MSCs
Cluster 14
Cluster 3

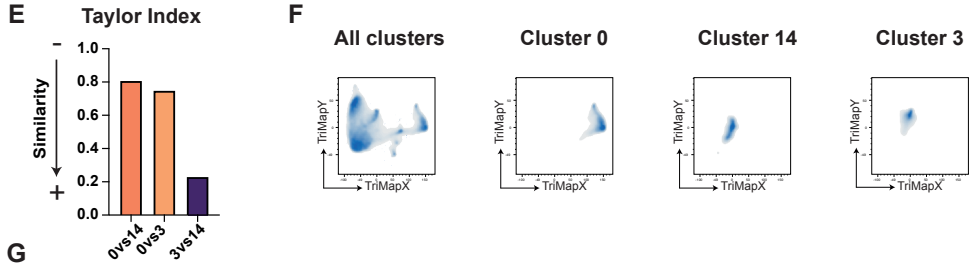
E
Taylor Index
Similarity
0vs14
0vs3
3vs14
F
All clusters
Cluster 0
Cluster 14
Cluster 3
TriMapY
TriMapX

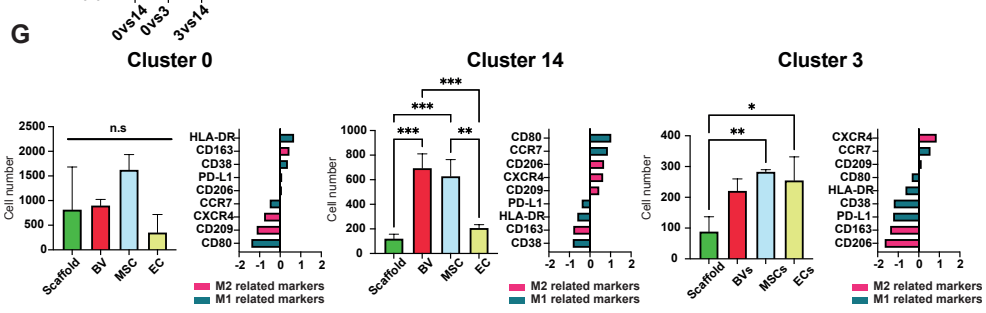
G
Cluster 0
Cluster 14
Cluster 3
Cell number
n.s
Scaffold
BV
MSC
EC
BVs
MSCs
ECs
M2 related markers
M1 related markers

Figure 3: Crosstalk between pro-inflammatory M1 macrophages and tissue-engineered blood vessels. (A) *In vitro* tissue-engineered human blood vessels were generated by co-culture of endothelial cells and MSCs on 3D collagen scaffolds. After 3 days, M1 macrophages were seeded. Changes in macrophage phenotype were observed one day after macrophage seeding. (B) A comparison of the Z-score value of M1 (CD38, PD-L1, CCR7, CD80, HLA-DR) and M2 (CD206, CD209, CXCR4, CD163) phenotype markers in each experimental condition. (C) Heat map showing the percentage of macrophages from each experimental condition that are within each cluster. (D) Pie charts showing how macrophages in the different experimental conditions are located in clusters enriched in baseline macrophages (orange), macrophages alone in the 3D scaffold (light green), or macrophages co-cultured with cells and blood vessels (light blue). The attached pie chart shows the exact cluster location of macrophages in the different experimental conditions. (E) Bar-graphs showing the similarity between clusters 0, 14 and 3, which are the clusters where most of the macrophages converge to. (F) Localization of all clusters, cluster 0, 3 and 14 in TriMap plots. (G) Bar graphs showing the exact composition of the main clusters and Z-scores showing the relative expression of each marker in each of these clusters. Data in (G) represents mean ± SD with n=3 bilogical replicates. BV, blood vessels. ECs, endothelial cells. MSCs, mesenchymal stromal cells. One way ANOVA with Tukey post hoc analysis Statistical significance: *** $p < 0.001$ ** $p < 0.01$, * $p < 0.05$.

Regarding the similarity between the clusters, cluster 0 and cluster 13, cluster 0 and 9, and cluster 0 and 4 are the ones that were more distant indicating that they demonstrated more differences than the other clusters (Figure 4E), which could also be noticed in the TriMap. Macrophages in clusters 3,4, 9, 13 and 19 were located closer in the TriMap than cluster 0, which was located in the far left of the graph (Figure 4F, G).

Thereafter, we analyzed how macrophages in the different conditions, co-cultured alone in the scaffold, with MSCs, endothelial cells or blood vessels were organized. Cluster 0 was enriched in macrophages alone in the 3D scaffold, which was upregulated in CD209, PD-L1 and CD80 markers (Figure 4G). Macrophages co-cultured with either blood vessels and MSCs mostly were located in cluster 9 in which a mixture of both M1 (CD80) and M2 markers (CD206 and CD163) were expressed. Macrophages co-cultured with blood vessels specifically were found in cluster 3 that was upregulated in CD38, CD206 and HLA-DR. Macrophages co-cultured with MSC specifically also were mostly found in cluster 4 that was upregulated in CD80, CD209 and CXCR4. Finally, Macrophages co-cultured with endothelial cells were found in cluster 13 and 19 clusters enriched in M2 markers. CD209, CD206 and CD209 were

upregulated in cluster 13 and CD209 and CXCR4 in cluster 19.

3.5. M1M2 macrophages showed little plasticity and downregulation of M1 and upregulation of M2 markers

To determine how M1M2 macrophage phenotype changed when co-cultured with blood vessels, primary human monocytes were isolated from human blood and differentiated towards M0 macrophages via administration of M-CSF for 5 days. M0 macrophages were further differentiated towards M1M2 by addition of IFNγ and LPS for 24 hours, followed by addition of IL-4 and IL-13 for 24 hours. To assess whether these differences were just because of the blood vessels, macrophages were seeded in 3D scaffold alone, or with just MSCs or endothelial cells to use as controls (Figure 5A).

Traditional flow cytometry analysis demonstrated that macrophages co-cultured with blood vessels upregulated CD163 ($p < 0.001$), CD206 ($p < 0.001$), and CCR7 ($p < 0.05$) and downregulated CXCR4 ($p < 0.001$), CD209 ($p < 0.01$), PD-L1 ($p < 0.001$) and HLA-DR ($p < 0.05$) when compared to the baseline. Furthermore, macrophages co-cultured with blood vessels upregulated CD163 ($p < 0.05$) and CD206 ($p < 0.01$) when compared to macrophages co-cultured in the scaffold alone. Macrophages downregulate CD209 ($p < 0.001$) and CXCR4 ($p < 0.05$, $p < 0.01$ and $p < 0.01$) marker expression when compared to macrophages co-cultured in the scaffold alone, with endothelial cells or with MSCs, respectively. Regarding M1-associated markers, compared to macrophages co-cultured alone in the scaffold and with endothelial cells there was a downregulation of HLA-DR markers ($p < 0.01$ and $p < 0.05$, respectively). Compared macrophages co-cultured with MSCs there was an upregulation of CD38 ($p < 0.05$) marker and a downregulation of CD80 ($p < 0.01$) marker (Figure 5B, Supplementary Figure 8).

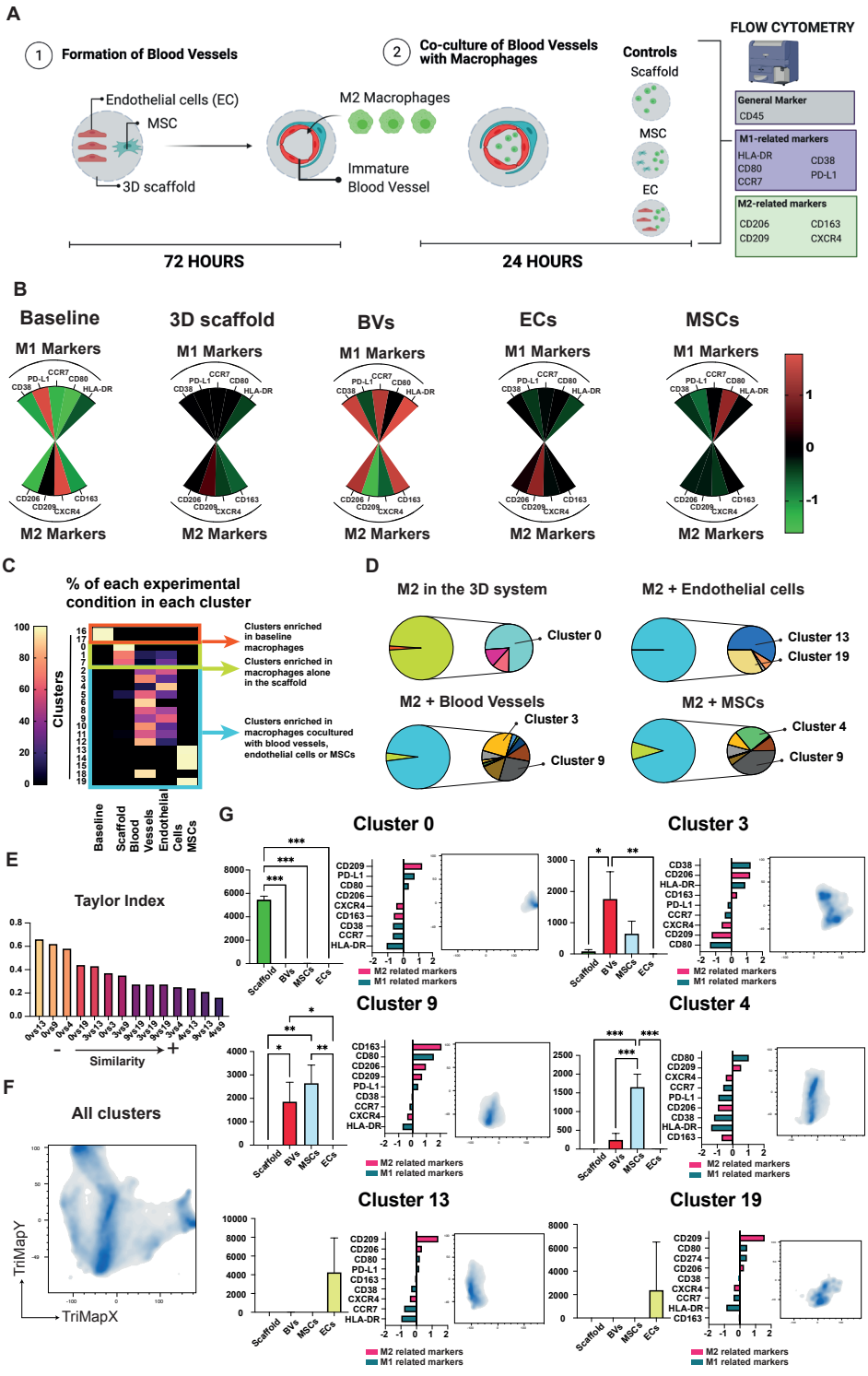
A
1 Formation of Blood Vessels
Endothelial cells (EC)
MSC
3D scaffold
2 Co-culture of Blood Vessels with Macrophages
M2 Macrophages
Immature Blood Vessel
72 HOURS
24 HOURS
Controls
Scaffold
MSC
EC
FLOW CYTOMETRY
General Marker
CD45
M1-related markers
HLA-DR
CD38
CD80
PD-L1
CCR7
M2-related markers
CD206
CD163
CD209
CXCR4
B
Baseline
3D scaffold
BVs
ECs
MSCs
M1 Markers
M2 Markers
C
% of each experimental condition in each cluster
Clusters
Clusters enriched in baseline macrophages
Clusters enriched in macrophages alone in the scaffold
Clusters enriched in macrophages cocultured with blood vessels, endothelial cells or MSCs
Baseline
Scaffold
Blood Vessels
Endothelial Cells
MSCs
D
M2 in the 3D system
Cluster 0
M2 + Endothelial cells
Cluster 13
Cluster 19
M2 + Blood Vessels
Cluster 3
Cluster 9
M2 + MSCs
Cluster 4
Cluster 9
E
Taylor Index
Similarity
F
All clusters
TriMapY
TriMapX
G
Cluster 0
Cluster 3
Cluster 9
Cluster 4
Cluster 13
Cluster 19
Scaffold
BVs
MSCs
ECs
M2 related markers
M1 related markers

Figure 4: Crosstalk between regenerative M2 macrophages and tissue-engineered blood vessels. (A) *In vitro* tissue-engineered human blood vessels were generated by co-culture of endothelial cells and MSCs on 3D collagen scaffolds. Changes in macrophage phenotype were observed one day after macrophage seeding. (B) A comparison of the Z-score value of M1 (CD38, PD-L1, CCR7, CD80, HLA-DR) and M2 (CD206, CD209, CXCR4, CD163) phenotype markers in each experimental condition. (C) Heat map showing the percentage of macrophages from each experimental condition that are within each cluster. (D) Pie charts showing how macrophages in different experimental conditions are located in clusters enriched in baseline macrophages (orange), macrophages alone in the 3D scaffold (light green), or macrophages co-cultured with cells and blood vessels (light blue). The attached pie charts show the exact cluster location of macrophages in the different experimental conditions. (E) Bar-graphs showing the similarity between clusters 0, 3, 9, 13 and 19 which are the clusters where most of the macrophages converge to. (F) Localization of all clusters in the TriMap plot. (G) Bar graphs showing the exact composition of the main clusters, Z-scores showing the relative expression of each marker in each of these clusters and the location of each of the clusters in the TriMap. Data in (G) represents mean ± SD with n=3 biological replicates. BV, blood vessels. ECs, endothelial cells. MSCs, mesenchymal stromal cells. One way ANOVA with Tukey post hoc analysis Statistical significance: *** $p < 0.001$ ** $p < 0.01$, * $p < 0.05$.

Regarding single cell data analysis, we found that clusters 11, 12, 13, 14 and 16 were enriched in macrophages in baseline, clusters 2, 3, 4, 5, 6, 7, 17, 18 and 19 were enriched in macrophages seeded in the 3D scaffold and clusters 0, 1, 5, 8, 9, 10 and 15 were enriched in macrophages co-cultured with endothelial cells, MSCs, or with blood vessels (Figure 5C). We noticed that in clusters enriched with macrophages in the baseline or also in macrophages in the 3D scaffold, the macrophages that were co-culture with MSCs, endothelial cells or blood vessels were also found (Figure 5F). The same trend occurred in M1 macrophages but did not occur with M0 and M2 macrophages. This may indicate that the plasticity of M0 and M2 macrophages was higher than that of the M1 and M1M2 macrophages (Figure 2F, Figure 3F and Figure 4F).

Subsequently, the distance between the clusters was analyzed. Cluster 0 and cluster 15, cluster 0 and 3, cluster 3 and 5, cluster 5 and 15 were the ones that were more distant meaning that were more different than the other clusters (Figure 5E), which could also be noticed in the TriMap. Macrophages in clusters 0 and 5 and 3 and 15 were located closer in the TriMap than cluster 0 and 15, 0 and 13, and 3 and 15 (Figure 5F and 5G).

Thereafter, we analyzed how macrophages in the different conditions, co-cultured alone in the scaffold, with MSCs, endothelial cells or blood vessels were organized. Cluster 3 was enriched in macrophages co-cultured in the 3D collagen scaffold, which was upregulated in all M2-related markers but CXCR4. Macrophages co-cultured with either blood vessels, endothelial cells and MSCs were found in cluster 0 in which a mixture of both M2 (CD163, CD206) and M1 markers (CD38) were expressed. Macrophages co-cultured with blood vessels specifically were also found in cluster 5, which was CD206 was upregulated. Finally, macrophages co-cultured with endothelial cells or MSC were also found in cluster 15 that was upregulated in CXCR4 and CD80 (Figure 5H).

3.6. Pre-polarization state of macrophages affected their crosstalk with Blood Vessels.

From section 3.2 to 3.5 we described how each macrophage phenotype (M0, M1, M2 and M1M2) changed when co-cultured with tissue engineered blood vessels comparing it when seeded in the scaffold alone or when co-cultured with endothelial cells or MSCs. In this section, we made a comparison between the different pre-polarization states (M0, M1, M2, M1M2). Towards this, we performed the same analysis as mentioned before, however, instead of adding the groups of macrophages co-cultured alone in the scaffold, macrophages co-cultured with either blood vessels, MSCs or endothelial cells, we run the single cell analysis with the different macrophage pre-polarization states (M0, M1, M2, M1M2) co-cultured with the blood vessels all together. This approach enabled us to compare the role of the pre-polarization state of the macrophages towards their blood vessel response (Figure 6A).

Traditional flow cytometry analysis showed that different pre-polarized macrophages were affected alternatively when co-cultured with blood vessels. However, there was a general upregulation of the CD163 ($p < 0.001$) and CD206 ($p < 0.001$) M2 markers and a downregulation of CD209 ($p < 0.001$ for M0, M2 and M1M2 macrophages and $p < 0.01$ for M1 macrophages) compared to each baseline state (Supplementary Figure 10). Interestingly, there were no differences between the intensity of the CD163 marker for any of the macrophages co-cultured with blood vessels. Also, irrespective of their pre-polarization state, all macrophages highly upregulated CD163 expression (Figure 6B, Supplementary Figure 11).

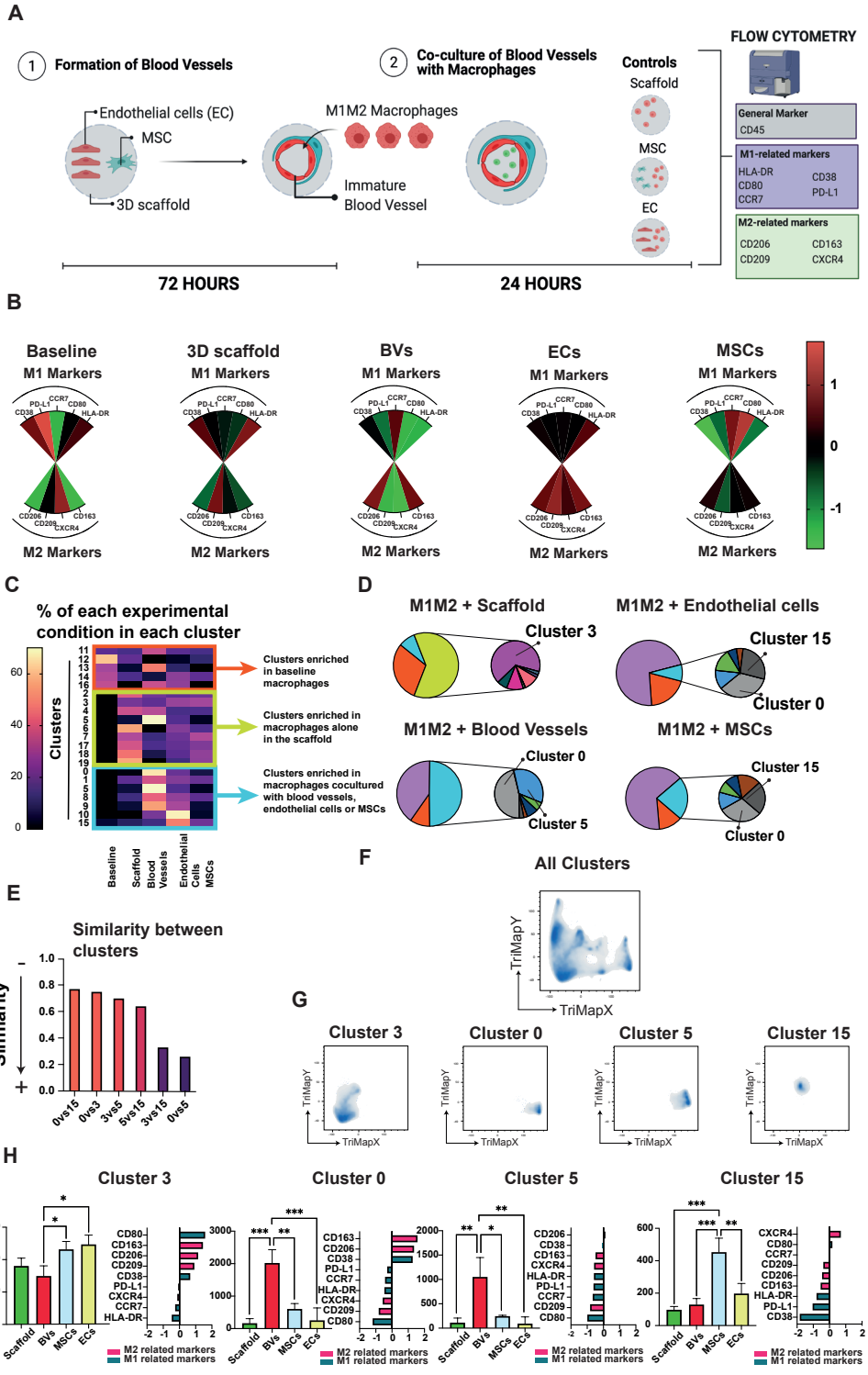
A
1 Formation of Blood Vessels
Endothelial cells (EC)
MSC
3D scaffold
2 Co-culture of Blood Vessels with Macrophages
M1M2 Macrophages
Immature Blood Vessel
Controls
Scaffold
MSC
EC
FLOW CYTOMETRY
General Marker
CD45
M1-related markers
HLA-DR
CD80
CCR7
CD38
PD-L1
M2-related markers
CD206
CD209
CD163
CXCR4
72 HOURS
24 HOURS
B
Baseline
3D scaffold
BVs
ECs
MSCs
M1 Markers
M2 Markers
C
% of each experimental condition in each cluster
Clusters
Clusters enriched in baseline macrophages
Clusters enriched in macrophages alone in the scaffold
Clusters enriched in macrophages cocultured with blood vessels, endothelial cells or MSCs
Baseline
Scaffold
Blood Vessels
Endothelial Cells
MSCs
D
M1M2 + Scaffold
Cluster 3
M1M2 + Endothelial cells
Cluster 15
Cluster 0
M1M2 + Blood Vessels
Cluster 0
Cluster 5
M1M2 + MSCs
Cluster 15
Cluster 0
E
Similarity between clusters
Similarity
0vs15
0vs3
3vs5
5vs15
3vs15
0vs5
F
All Clusters
TriMapY
TriMapX
G
Cluster 3
Cluster 0
Cluster 5
Cluster 15
H
Cluster 3
Cluster 0
Cluster 5
Cluster 15
Scaffold
BVs
MSCs
ECs
M2 related markers
M1 related markers

Figure 5: Crosstalk between M1M2 macrophages and tissue-engineered blood vessels. (A) *In vitro* tissue-engineered human blood vessels were generated by co-culture of endothelial cells and MSCs on 3D collagen scaffolds. After 3 days, M1M2 macrophages were seeded. Changes in macrophage phenotype were observed one day after macrophage seeding. (B) A comparison of the Z-score value of M1 (CD38, PD-L1, CCR7, CD80, HLA-DR) and M2 (CD206, CD209, CXCR4, CD163) phenotype markers in each experimental condition. (C) Heat map showing the percentage of macrophages from each experimental condition that are within each cluster. (D) Pie charts showing how macrophages in the different experimental conditions are located in clusters enriched in baseline macrophages (orange), macrophages alone in the 3D scaffold (light green), or macrophages co-cultured with cells and blood vessels (light blue). (E) Bar-graphs showing the similarity between clusters 0, 3, 5 and 15 which are the clusters where most of the macrophages converge to. (F) Localization of all clusters in the TriMap plot (G) Localization of cluster 3, cluster 0, cluster 5 and cluster 15 in the TriMap plot. (H) Bar graphs showing the exact composition of the main clusters (Cluster 0, Cluster 3, Cluster 5 and Cluster 15), Z-scores showing the relative expression of each marker in each of these clusters. Data in (H) represents mean ± SD with n=3 biological conditions. BV, blood vessels. ECs, endothelial cells. MSCs, mesenchymal stromal cells. One way ANOVA with Tukey post hoc analysis Statistical significance: *** $p < 0.001$ ** $p < 0.01$, * $p < 0.05$

Regarding single cell analysis, we found that clusters 4, 17 and 18 were enriched in macrophages in baseline, clusters 8, 11, 13, 15 and 19 were enriched in macrophages seeded in the 3D scaffold and clusters 0, 1, 2, 5, 6, 7, 9, 10, 12, 14 and 16 are enriched in macrophages co-cultured with the blood vessels (Figure 6C). Regarding the similarity between the clusters, cluster 0 and 14, cluster 0 and 10, and cluster 0 and 12, are the ones that were more distant indicating more differences than between other clusters (Figure 6E), which can also be noticed in the TriMap. Macrophages in clusters 0 and 5 are located further to the right compared to the other clusters indicating their similarity to each other but difference with the other clusters (Figure 6G, Supplementary Figure 11).

Furthermore, it was imperative to analyze how different macrophage phenotypes co-cultured with blood vessels were organized. M0 macrophages were mostly located in cluster 10 and 14 which were characterized by a high expression of CXCR4, CCR7, CD209, CD80 and CD209, CD80 (Figure 6H, I). M1 macrophages mostly migrate to cluster 12 in which a mixture of both M2 (CD209, CD163) and M1 markers (CD38, CD274, CD80) were expressed. M2 macrophages were mostly located in cluster 5, which was upregulated in the M2 markers CD206 and CD163.

Finally, M1M2 macrophages were also located in cluster 0, upregulated in CD38, CD274 and HLA-DR, and cluster 12, upregulated in CD209, CD163, CD38, CD274 and CD80. Interestingly, it seems that M1M2 macrophages shared a common cluster, cluster number 12, with the M1 macrophages while also were located in cluster 0. Cluster 0 and cluster 5, which was the cluster where M2 macrophages were, was very close to each other indicating similarity.

4. Discussion

Macrophages are key regulators in wound healing process. Their high plasticity allows them to switch phenotypes depending on the environmental stimuli. During normal wound healing process, macrophages switch from a pro-inflammatory M1 phenotype towards a pro-regenerative M2 phenotype. Even though this transition is crucial for the wound healing to be terminated, the precise mechanism of this transition is yet unclear. During biomaterial implantation, this transition and subsequently implant integration can be impaired —reviewed in [11] —. For this reason, researchers have been trying to facilitate this step by promoting M1 to M2 shift within the host vasculature. One of the strategies is to add tissue-engineered blood vessels to the biomaterial [3, 10]. The addition of tissue-engineered blood vessels not only will help with the M2 polarization of macrophages, but it will also anastomose with the host vasculature and, thereby promote implant integration. It has been shown that endothelial cells skew macrophage phenotype towards an M2 phenotype [12, 14, 15]. Furthermore, it has been studied that macrophages reciprocally promote vascularization [10]. However, the impact of tissue-engineered blood vessels on macrophage phenotype is not yet well studied. In this study we showed that, regardless of the pre-polarization state of macrophages, all of them exhibited an upregulation of M2 common markers. However, each different pre-polarization state did show a different expression pattern of the other markers, thereby demonstrating that pre-polarization state does have an influence in the crosstalk with the tissue-engineered blood vessels. These results are important because they could help in understanding not only the importance of pre-polarization states of macrophages but also the importance of the timing on the vascularize biomaterial implantation, to help in the overall implant outcome.

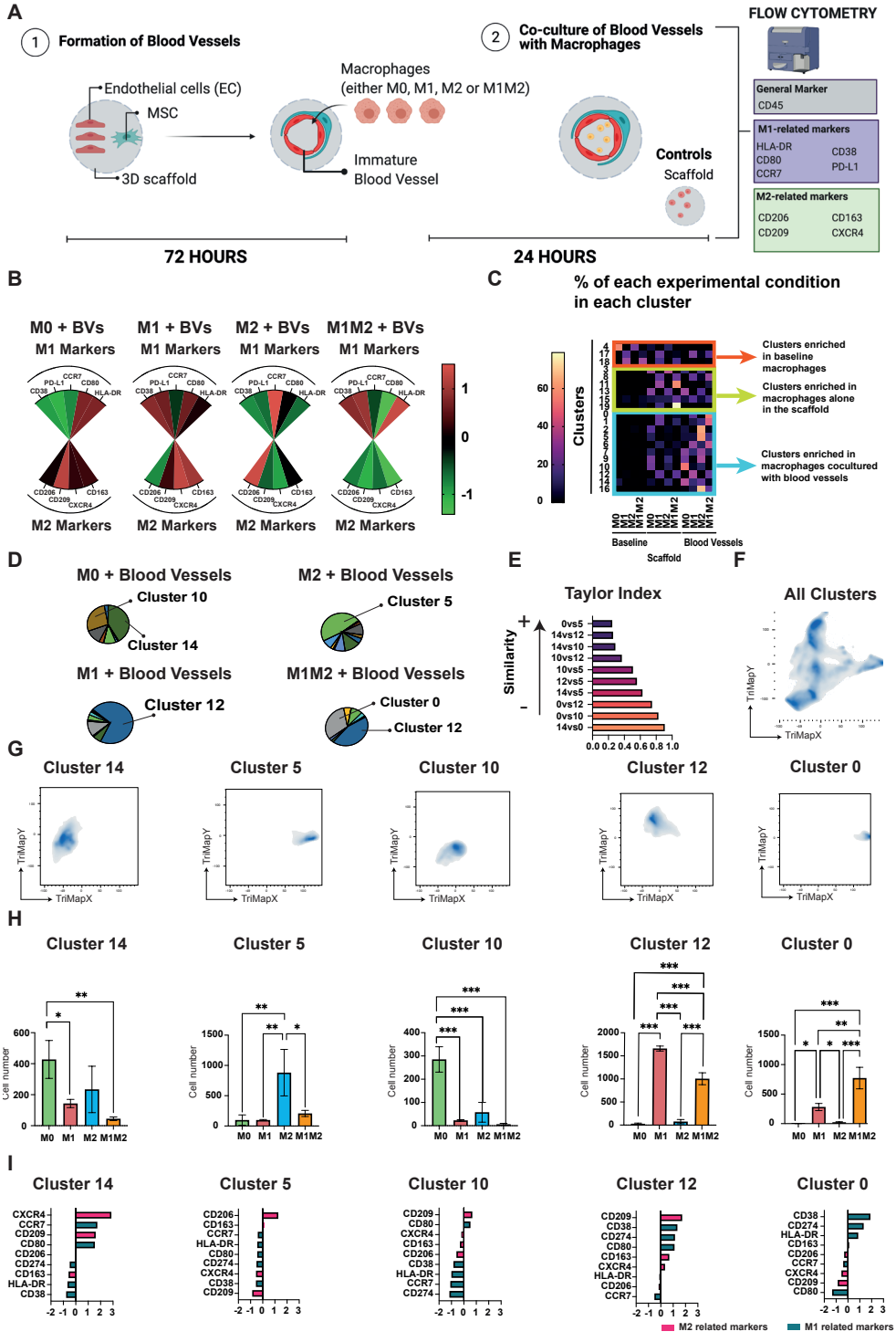
A
1 Formation of Blood Vessels
Endothelial cells (EC)
MSC
3D scaffold
Macrophages
(either M0, M1, M2 or M1M2)
Immature
Blood Vessel
72 HOURS
2 Co-culture of Blood Vessels with Macrophages
Controls
Scaffold
24 HOURS
FLOW CYTOMETRY
General Marker
CD45
M1-related markers
HLA-DR
CD38
CD80
PD-L1
CCR7
M2-related markers
CD206
CD163
CD209
CXCR4
B
M0 + BVs
M1 + BVs
M2 + BVs
M1M2 + BVs
M1 Markers
M2 Markers
C
% of each experimental condition in each cluster
Clusters
Clusters enriched in baseline macrophages
Clusters enriched in macrophages alone in the scaffold
Clusters enriched in macrophages cocultured with blood vessels
Baseline
Blood Vessels
Scaffold
D
M0 + Blood Vessels
Cluster 10
Cluster 14
M2 + Blood Vessels
Cluster 5
M1 + Blood Vessels
Cluster 12
M1M2 + Blood Vessels
Cluster 0
Cluster 12
E
Taylor Index
Similarity
F
All Clusters
TriMapY
TriMapX
G
Cluster 14
Cluster 5
Cluster 10
Cluster 12
Cluster 0
H
Cell number
M0 M1 M2 M1M2
I
M2 related markers
M1 related markers

Figure 6: Crosstalk between pre-polarized macrophages and tissue-engineered blood vessels. (A) *In vitro* tissue-engineered human blood vessels were generated by co-culture of endothelial cells and MSCs on 3D collagen scaffolds. After 3 days, macrophages (M0, M1, M2 or M1M2) were added. Changes in macrophage phenotype were observed one day after macrophage seeding. (B) A comparison of the Z-score value of M1 (CD38, PD-L1, CCR7, CD80, HLA-DR) and M2 (CD206, CD209, CXCR4, CD163) phenotype markers in each experimental condition. (C) Heat map showing the percentage of macrophages from each experimental condition that are within each cluster. (D) Pie charts showing how macrophages in the different experimental conditions are located in different clusters. (E) Taylor Index showing the similarity between clusters 0, 5, 10, 12 and 14 which are the clusters where most of the macrophages converge to. (F) Localization of all clusters in the TriMap plot. (G) Location of each of the main clusters in the TriMap (cluster 0, cluster 5, cluster 10, cluster 12 and cluster 14). (H) Bar graphs showing the exact composition of the main clusters. (I) Z-scores showing the relative expression of each marker in each of these clusters. Data in (H) represents mean ± SD with n=3. BV, blood vessels. ECs, endothelial cells. MSCs, mesenchymal stromal cells. One way ANOVA with Tukey post hoc analysis. Statistical significance: *** $p < 0.001$ ** $p < 0.01$, * $p < 0.05$.

The upregulation of this two M2 markers have been seen to help in both early and late stage of angiogenesis. This is in accordance with previous studies that have shown that endothelial cells and blood vessels caused macrophages to upregulate M2 markers. CD206, also known as mannose receptor C type 1 (MRC1) is a cell-surface protein abundantly presented mostly in M2 macrophages. Its main function is in endocytosis and phagocytosis and plays an important role in immune homeostasis by scavenging unwanted mannoglycoproteins. CD206 has also be linked with the vascular remodeling and pruning [20]. Furthermore, different studies have demonstrated that CD206 positive macrophages are related to a higher micro vessel count indicating that CD206 macrophages stimulate angiogenesis [21, 22]. CD163 is a member of the scavenger receptor super family class B. It is a receptor of the hemoglobin and haptoglobin complex which is recognized for clearance by receptor mediated endocytosis [23]. CD163 marker also has MMP-9, which is associated with extracellular matrix remodeling, thus helping in the early steps of capillary sprouting. Also, CD163 macrophages promotes intimal angiogenesis and vascular permeability [24].

When M0 macrophages were co-cultured with the tissue-engineered blood vessels, we noticed that only M2 markers were upregulated (CD206, CD209 and

CD163). However, recently, O'Brien et al. reviewed the importance of the timing of the macrophage transition [11]. It has been already described that early treatment with M2 macrophages leads to impaired integration and fibrous capsule formation [25]. For this reason, there is a need to tightly control the temporal activation of the macrophage transition. Therefore, it is important to avoid early M2 macrophage stimulation or addition. Taking this into account, adding the engineered tissue in the early phase of the wound healing could mean a too early transition towards and M2 phenotype and resulting in capsule formation and subsequent impairment in implant integration [26, 27]. Interestingly, when either M1, M2 and M1M2 macrophages were co-cultured with the blood vessels not only M2 markers were upregulated but different M1 markers, suggesting a possible mixed phenotype. Further experiments could help in understanding which will be the best timing for the implantation of the engineered tissue.

M0 and M2 macrophages phenotypes showed a high differentiation capacity with more than 90 % of macrophages switching phenotypes whereas M1 or even M1M2 macrophages were less plastic with only the 25 % and 15-50 % of macrophages changed phenotypes when cultured either in the scaffold alone, with cells or blood vessels. Interestingly, in the case of M0, M1 and M2 macrophages, the effect of the blood vessels was mainly driven by the presence of MSCs while in the case of M1M2 macrophages their phenotypical change was independent to the one exerted by endothelial cells and MSCs. This comes in concordance of several studies that have described how MSCs are able to promote the polarization of macrophages towards a M2 phenotype which is characterized by an increased production of IL-10 and high expression of CD163 and/or CD206 markers [28-30] and reviewed in [31].

When the analysis of the different macrophage pre-polarization states, taken together, were performed, we observed that M1 and M1M2 macrophages shared cluster 12 location. Furthermore, M1M2 macrophages were also widely observed in cluster 0. Moreover, M1M2 were also enriched in cluster 0 whose distance to cluster 5 was the shortest. Cluster 5 was mostly enriched with M2 macrophages. This could mean that M1M2 macrophages share more similarities to M2 macrophages than observed initially and that tissue engineered blood vessels would promote the perfect timing in the M1-M2 transition. Clustering is essentially grouping cells in discrete defined populations but does not provide any information about the temporal relationships between different clusters. However, using pseudo time analysis it

could be analyzed if those cluster are related to each other in continuous paths or different maturation states [32].

There are some limitations to this study. Firstly, even though previous studies have shown that donor-to-donor variability did not play a major role in affecting macrophage phenotype when culturing in different biomaterials, it would be important to show if there is donor-to-donor variability when co-cultured with blood vessels [33]. Additionally, analyzing some proangiogenic growth factors secreted by macrophages, such us vascular endothelial growth factor (VEGF), tumor necrosis factor (TNF), fibroblast growth factor (FGF), transforming growth factor beta (TGFβ1), could help in learning the mechanism from which macrophages develop their angiogenic capacity. [34]. As mentioned previously, macrophages may also form the initial blood networks using their extracellular matrix remodeling properties as MMP-9. Interestingly, there is a strong expression of MMP9 in M2 macrophages, but none so in M0 or M1 macrophages [35]. Being able to analyze the level of this protease in the different groups could also provide an insight of the macrophage function in the angiogenesis process [36]. Besides to their paracrine role in angiogenesis, macrophages can also physically interact with endothelial cells and help in anastomosis of vascular sprouts [10, 37]. Imaging these interactions could also help us to elucidate the physical crosstalk between macrophages and blood vessels.

5. Conclusions

In summary, we have characterized four macrophage phenotypes (M0, M1, M2, M1M2) in the context of crosstalk with tissue-engineered-blood vessels. We found evidence that all phenotypes commonly upregulate CD206 and CD163 M2 markers to a similar extent while also upregulating different M1 markers to a different extent depending on their pre-polarization state. Describing the phenotypical switch of macrophages when co-cultured with tissue engineered blood vessels could help us in deterining the exact implantation time of the tissue engineering construct to prevent implant rejection.

6. References

1. Langer, R. and J.P. Vacanti, Tissue-Engineering. Science, 1993. 260(5110): p. 920-926.
2. Landau, S., et al., Tropoelastin coated PLLA-PLGA scaffolds promote vascular network formation. Biomaterials, 2017. 122: p. 72-82.
3. Ben-Shaul, S., et al., Mature vessel networks in engineered tissue promote graft–host anastomosis and prevent graft thrombosis. Proceedings of the National Academy of Sciences, 2019. 116(8): p. 2955.
4. Mosser, D.M. and J.P. Edwards, Exploring the full spectrum of macrophage activation. Nature Reviews Immunology, 2008. 8(12): p. 958-969.
5. Kubota, Y., et al., M-CSF inhibition selectively targets pathological angiogenesis and lymphangiogenesis. Journal of Experimental Medicine, 2009. 206(5): p. 1089-1102.
6. Hirose, N., et al., The local injection of peritoneal macrophages induces neovascularization in rat ischemic hind limb muscles. Cell Transplantation, 2008. 17(1-2): p. 211-222.
7. Liu, S.X., et al., Trajectory analysis quantifies transcriptional plasticity during macrophage polarization. Scientific Reports, 2020. 10(1): p. 12273.
8. Spiller, K.L., et al., Sequential delivery of immunomodulatory cytokines to facilitate the M1-to-M2 transition of macrophages and enhance vascularization of bone scaffolds. Biomaterials, 2015. 37: p. 194-207.
9. Smith, T.D., et al., Regulation of macrophage polarization and plasticity by complex activation signals. Integrative Biology, 2016. 8(9): p. 946-955.
10. Graney, P.L., et al., Macrophages of diverse phenotypes drive vascularization of engineered tissues. Science Advances, 2020. 6(18): p. eaay6391.
11. O'Brien, E.M., G.E. Risser, and K.L. Spiller, Sequential drug delivery to modulate macrophage behavior and enhance implant integration. Advanced Drug Delivery Reviews, 2019. 149-150: p. 85-94.
12. He, H., et al., Endothelial cells provide an instructive niche for the differentiation and functional polarization of M2-like macrophages. Blood, 2012. 120(15): p. 3152-3162.
13. Njock, M.-S., et al., Endothelial cells suppress monocyte activation through secretion of extracellular vesicles containing antiinflammatory microRNAs. Blood, 2015. 125(20): p. 3202-3212.
14. Outtz, H.H., et al., Notch1 controls macrophage recruitment and Notch signaling is activated at sites of endothelial cell anastomosis during retinal angiogenesis in mice. Blood, 2011. 118(12): p. 3436-3439.
15. Pabois, A., et al., Notch signaling mediates crosstalk between endothelial cells and macrophages via Dll4 and IL6 in cardiac microvascular inflammation. Biochemical Pharmacology, 2016. 104: p. 95-107.
16. Wang, Y., et al., Understanding how dimension reduction tools work: An empirical approach to deciphering t-SNE, UMAP, TriMAP, and PaCMAP for data visualization. arXiv pre-print server, 2020.
17. Liu, X., et al., A comparison framework and guideline of clustering methods for mass cytometry data. Genome Biology, 2019. 20(1): p. 297.
18. Hartigan, P.M., Algorithm AS 217: Computation of the dip statistic to test for unimodality. Journal of the Royal Statistical Society. Series C (Applied Statistics), 1985. 34(3): p. 320-325.
19. Lurier, E.B., et al., Transcriptome analysis of IL-10-stimulated (M2c) macrophages by next-generation sequencing. Immunobiology, 2017. 222(7): p. 847-856.
20. DeFalco, T., et al., Yolk-sac–derived macrophages regulate fetal testis vascularization and morphogenesis. Proceedings of the National Academy of Sciences, 2014. 111(23): p. E2384.
21. Sun, D., et al., $CD86^{+}/CD206^{+}$ tumor-associated macrophages predict prognosis of patients with intrahepatic cholangiocarcinoma. PeerJ, 2020. 8: p. e8458.
22. Sakurai, E., et al., Macrophage depletion inhibits experimental choroidal neovascularization.

Investigative Ophthalmology & Visual Science, 2003. 44(8): p. 3578-3585.
23. Kristiansen, M., et al., Identification of the haemoglobin scavenger receptor. Nature, 2001. 409(6817): p. 198-201.
24. Guo, L., et al., CD163+ macrophages promote angiogenesis and vascular permeability accompanied by inflammation in atherosclerosis. Journal of Clinical Investigation, 2018. 128(3): p. 1106-1124.
25. Jetten, N., et al., Anti-inflammatory M2, but not pro-inflammatory M1 macrophages promote angiogenesis in vivo. Angiogenesis, 2014. 17(1): p. 109-118.
26. Nassiri, S., et al., Relative expression of proinflammatory and antiinflammatory genes reveals differences between healing and nonhealing human chronic diabetic foot ulcers. Journal of Investigative Dermatology, 2015. 135(6): p. 1700-1703.
27. Mirza, R. and T.J. Koh, Dysregulation of monocyte/macrophage phenotype in wounds of diabetic mice. Cytokine, 2011. 56(2): p. 256-264.
28. Giri, J., et al., CCL2 and CXCL12 derived from mesenchymal stromal cells cooperatively polarize IL-10^{+} tissue macrophages to mitigate gut injury. Cell Reports, 2020. 30(6): p. 1923-1934.e4.
29. Witte, S.F.H.d., et al., Immunomodulation By Therapeutic Mesenchymal Stromal Cells (MSC) Is Triggered Through Phagocytosis of MSC By Monocytic Cells. Stem Cells, 2018. 36(4): p. 602-615.
30. Luz-Crawford, P., et al., Mesenchymal stem cell-derived interleukin 1 receptor antagonist promotes macrophage polarization and inhibits B cell differentiation. Stem Cells, 2016. 34(2): p. 483-492.
31. Weiss, A.R.R. and M.H. Dahlke, Immunomodulation by mesenchymal stem cells (MSCs): mechanisms of action of living, apoptotic, and dead MSCs. Frontiers in Immunology, 2019. 10(1191).
32. Melsen, J.E., et al., A Comprehensive workflow for applying single-cell clustering and pseudotime analysis to flow cytometry data. The Journal of Immunology, 2020. 205(3): p. 864.
33. Witherel, C.E., et al., Response of human macrophages to wound matrices in vitro. Wound Repair and Regeneration, 2016. 24(3): p. 514-524.
34. Cheyne, C.D., H. Tay, and W.D. Spiegelaere, The complex TIE between macrophages and angiogenesis. Anatomia, Histologia, Embryologia, 2020. 49(5): p. 585-596.
35. Zajac, E., et al., Pro-angiogenic capacity of MMP-9 produced by different types of inflammatory leukocytes is determined by the levels of TIMP-1 complexed with the MMP-9 proenzyme. The FASEB Journal, 2012. 26(S1): p. 48.9-48.9.
36. Zajac, E., et al., Angiogenic capacity of M1- and M2-polarized macrophages is determined by the levels of TIMP-1 complexed with their secreted proMMP-9. Blood, 2013. 122(25): p. 4054-4067.
37. Lucas, T., et al., Differential roles of macrophages in diverse phases of skin repair. The Journal of Immunology, 2010. 184(7): p. 3964.

SUPPLEMENTARY FIGURES

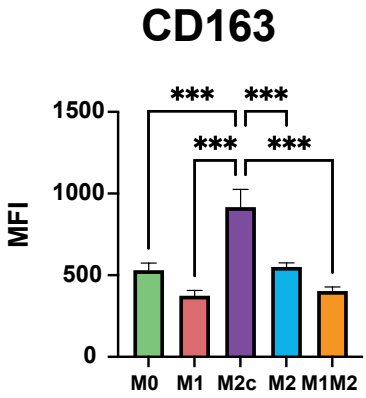

Supplementary Figure 1: Median Fluorescent Intensity (MFI) of the Associated M2c Marker CD163. Data represents mean ± SD with n=3. One way ANOVA with Tukey post hoc analysis. *** p < 0.001 ** p < 0.01, * p < 0.05.

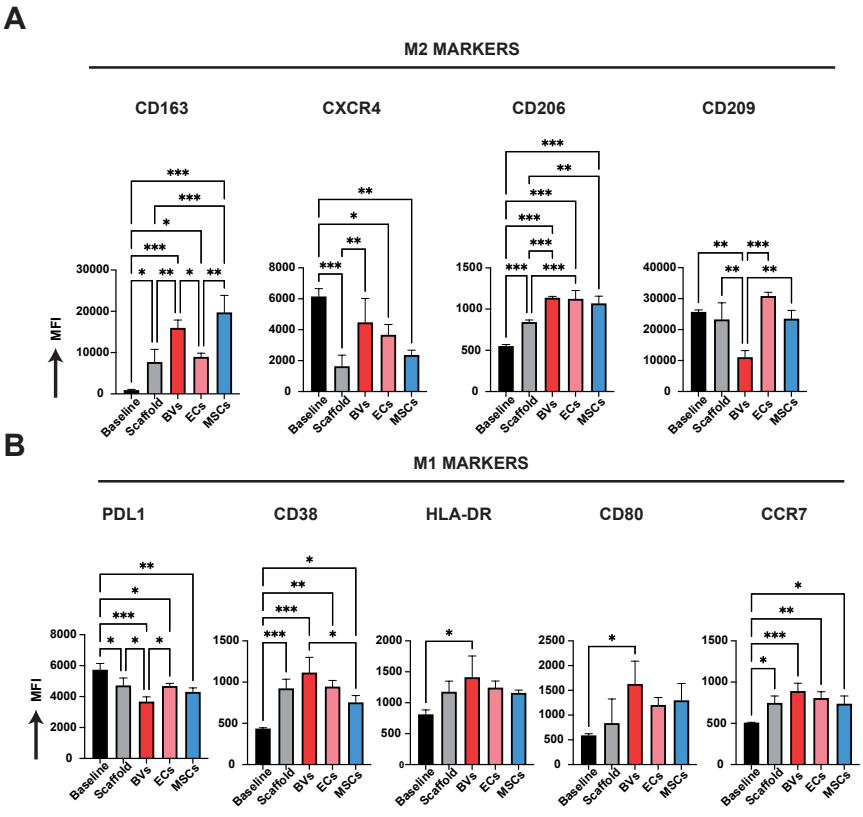

Supplementary Figure 2: Crosstalk between Undifferentiated (M0) Macrophages and 3D Collagen Scaffold, Tissue-Engineered Blood Vessels, Endothelial Cells and MSCs (A) Median fluorescent intensity (MFI) of associated M2 markers (CD163, CXCR4, CD206, CD209). (B) MFI of associated M1 markers (PDL1, CD38, HLA-DR, CD80, CCR7). Data in (A, B) represents mean ± SD with n=3 biological replicates. Statistical significance: One way ANOVA with Tukey post hoc analysis *** $p < 0.001$ ** $p < 0.01$, * $p < 0.05$.

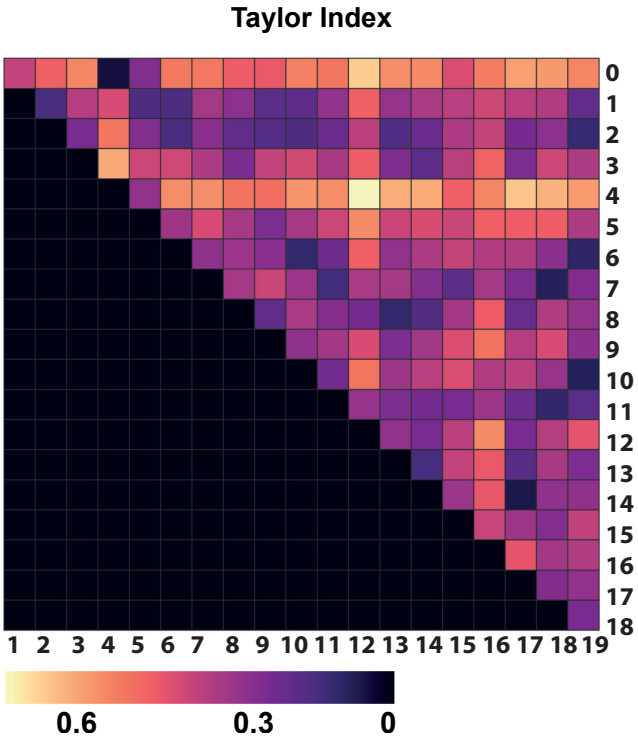

Supplementary Figure 3: Taylor Index showing the distance between every 2 clusters. If the distance between two cluster is low, they are similar to each other, and darker on the heatmap. If the distance between two clusters is high, they are different from each other, and lighter on theheatmap.

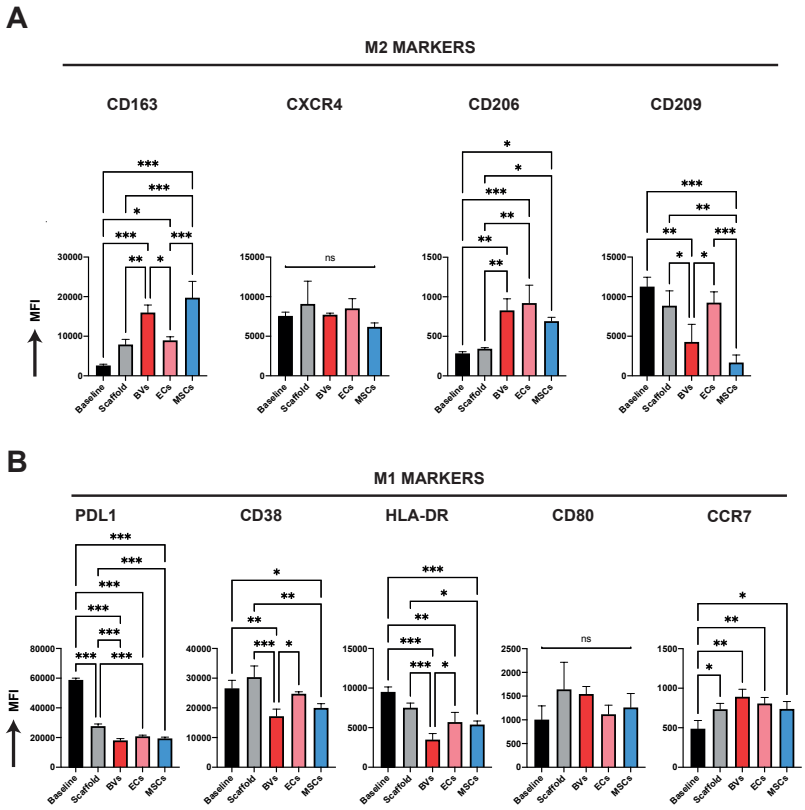

Supplementary Figure 4: Crosstalk between pro-Inflammatory M1 macrophages and tissue-engineered blood essels (A) Median fluorescent intensity (MFI) of associated M2 markers (CD163, CXCR4, CD206, CD209). (B) MFI of associated M1 markers (PDL1, CD38, HLA-DR, CD80, CCR7). Data in (A,B) represents mean ± SD with n=3 biological replicates. Statistical significance: *** $p < 0.001$ ** $p < 0.01$, * $p < 0.05$.

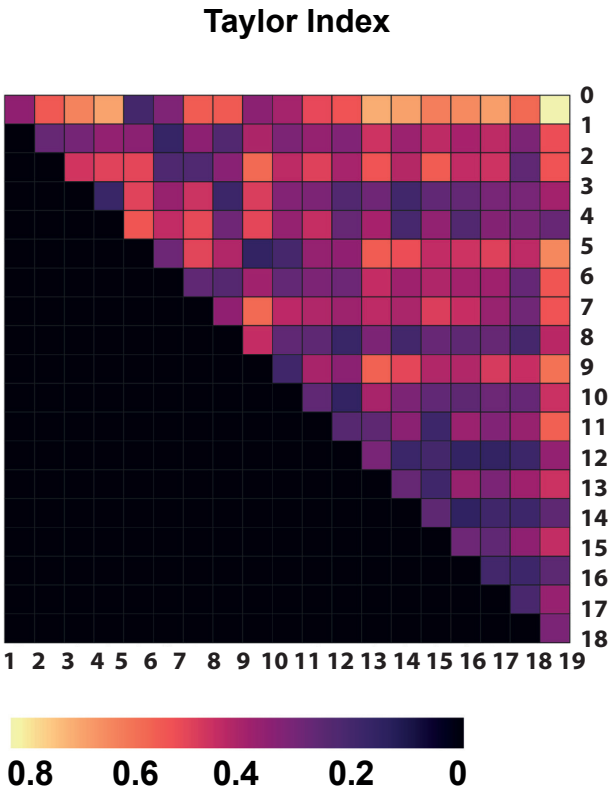

Supplementary Figure 5: Taylor Index showing the distance between every 2 clusters. If the distance between two cluster is low, they are similar to each other, and darker on the heatmap. If the distance between two clusters is high, they are different from each other, and lighter on theheatmap.

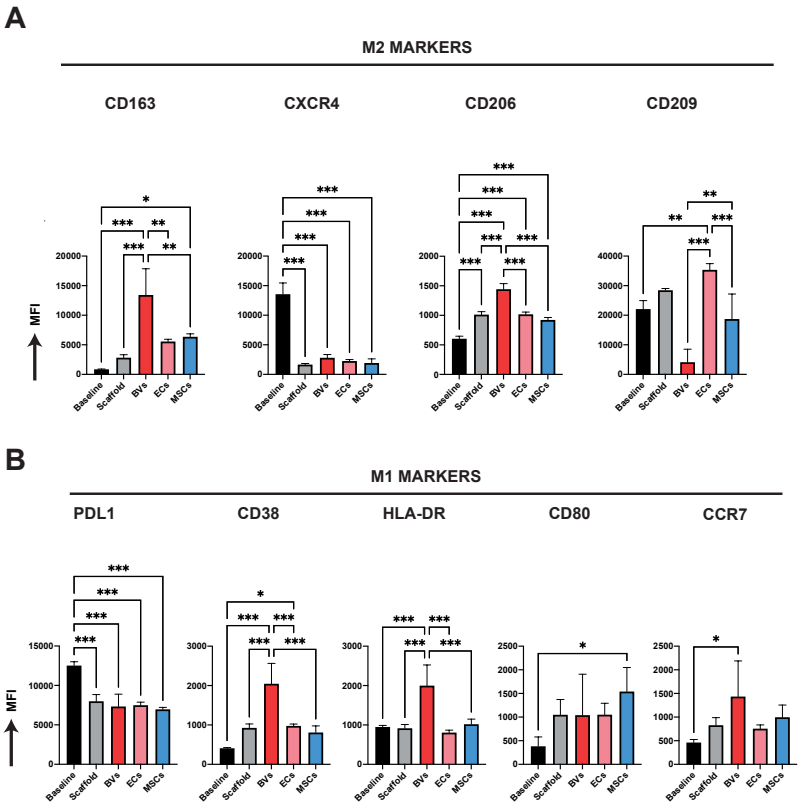

Supplementary Figure 6: Crosstalk between regulatory M2 macrophages and tissue-engineered blood vessels. (A) Median fluorescent intensity (MFI) of associated M2 markers (CD163, CXCR4, CD206, CD209). (B) MFI of associated M1 markers (PDL1, CD38, HLA-DR, CD80, CCR7). Data in (A, B) represents mean ± SD with n=3. Statistical significance: *** $p < 0.001$ ** $p < 0.01$, * $p < 0.05$.

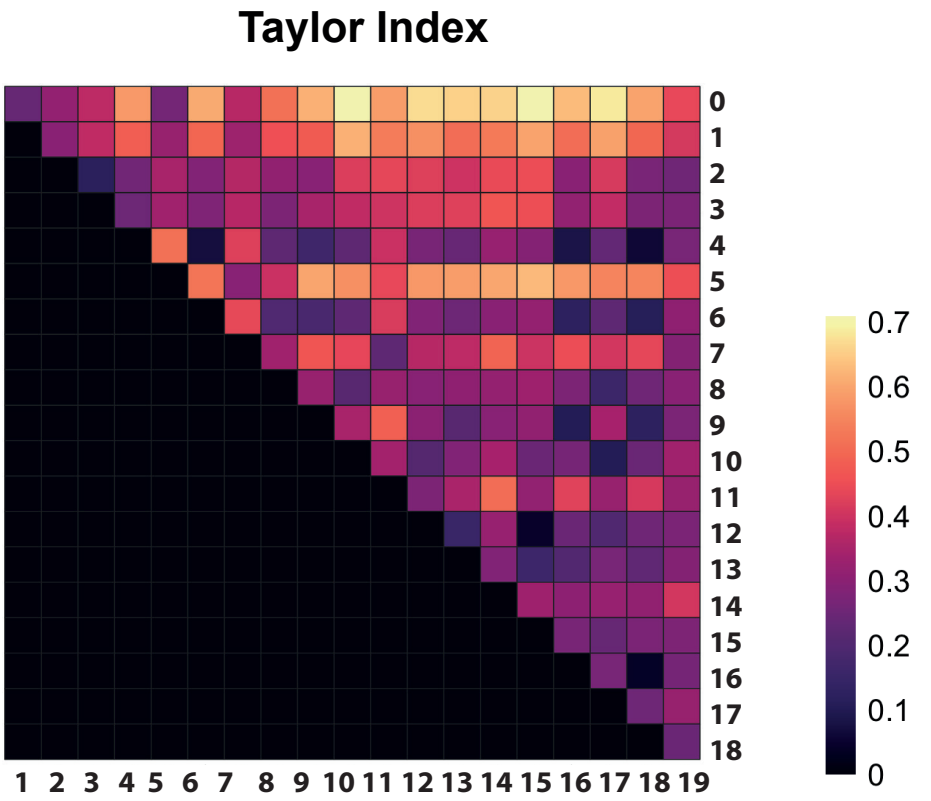

Supplementary Figure 7: Taylor Index showing the distance between every 2 clusters. If the distance between two cluster is low, they are similar to each other, and darker on the heatmap. If the distance between two clusters is high, they are different from each other, and lighter on theheatmap.

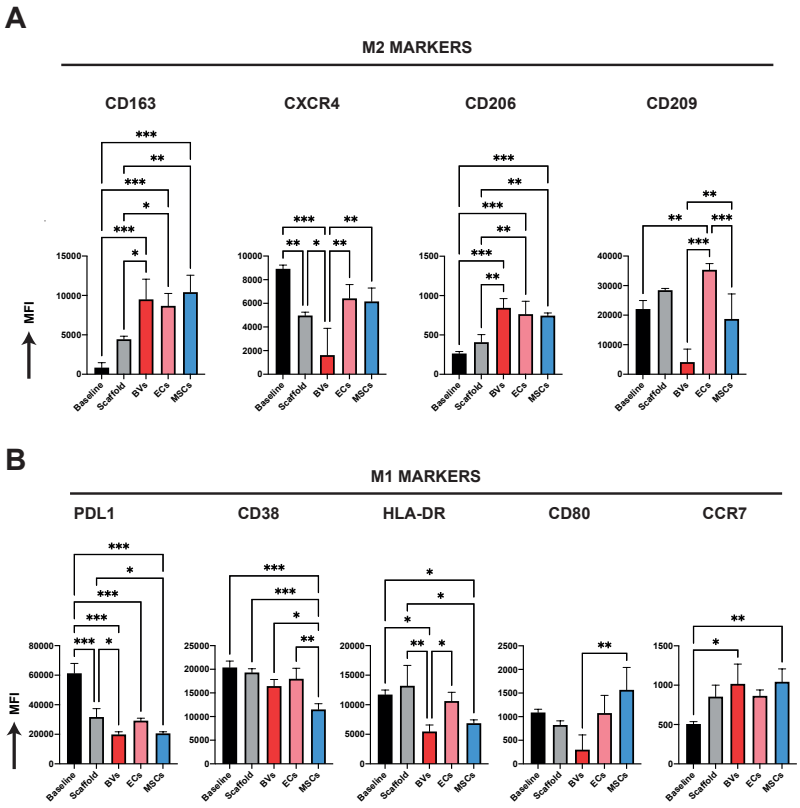

Supplementary Figure 8: Crosstalk between regulatory M1M2 macrophages and tissue-engineered blood vessels. (A) Median fluorescent intensity (MFI) of associated M2 markers (CD163, CXCR4, CD206, CD209). (B) MFI of associated M1 markers (PDL1, CD38, HLA-DR, CD80, CCR7). Data in (A, B) represents mean ± SD with n=3. Statistical significance: *** $p < 0.001$ ** $p < 0.01$, * $p < 0.05$.

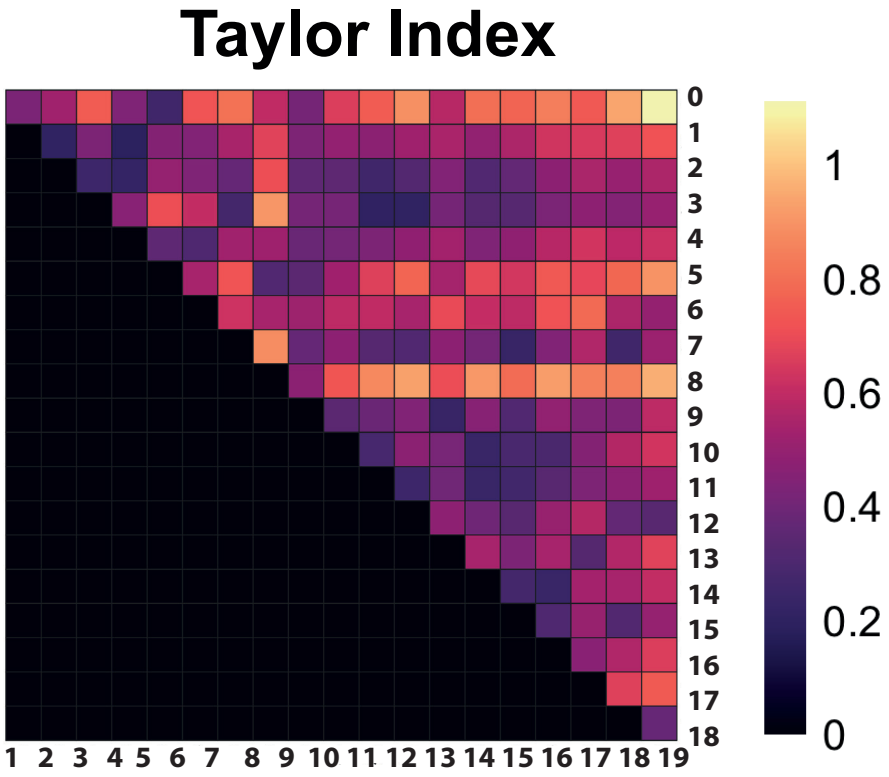

Supplementary Figure 9: Taylor Index showing the distance between every 2 clusters. If the distance between two cluster is low, they are similar to each other, and darker on the heatmap. If the distance between two clusters is high, they are different from each other, and lighter on theheatmap.

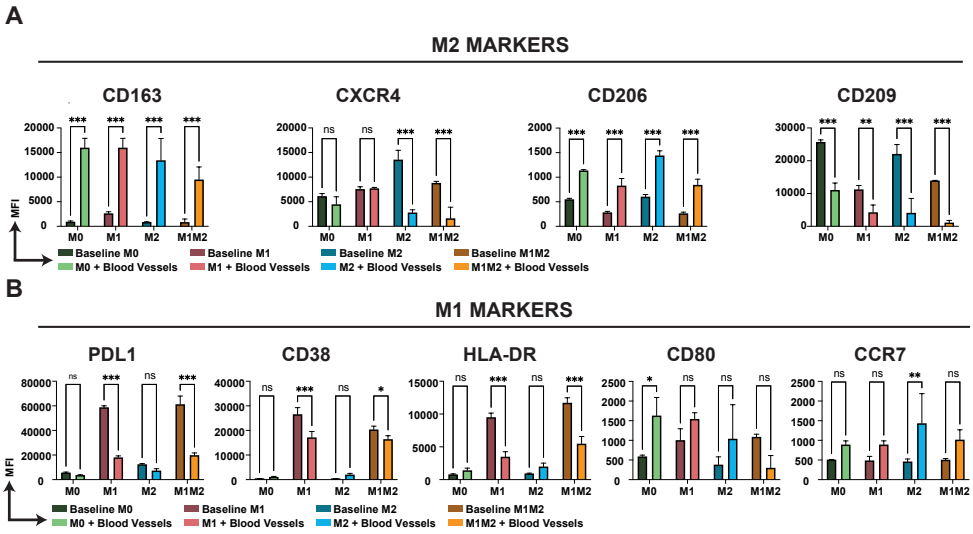

Supplementary Figure 10: Crosstalk between Pre-Polarized Macrophages and Tissue-Engineered Blood Vessels compared with the baseline. (A) Median fluorescent intensity (MFI) of associated M2 markers (CD163, CXCR4, CD206, CD209). (B) MFI of associated M1 markers (PDL1, CD38, HLA-DR, CD80, CCR7). Data in (A, B) represents mean ± SD with n=3. Statistical significance: *** $p < 0.001$ ** $p < 0.01$, * $p < 0.05$.

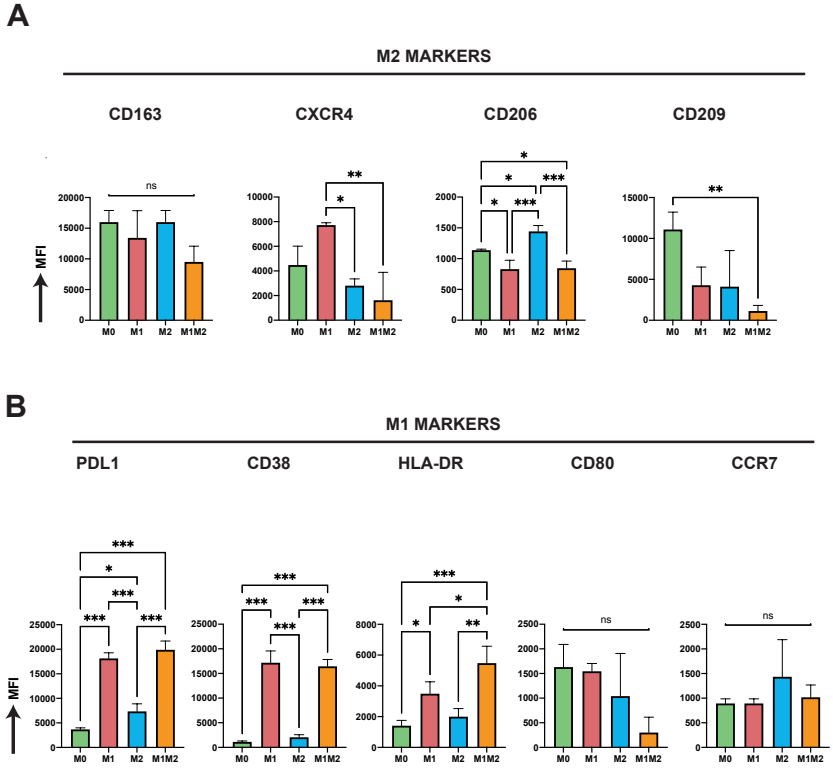

Supplementary Figure 11: Crosstalk between Pre-Polarized Macrophages and Tissue-Engineered Blood Vessels. (A) Median fluorescent intensity (MFI) of associated M2 markers (CD163, CXCR4, CD206, CD209). (B) MFI of associated M1 markers (PDL1, CD38, HLA-DR, CD80, CCR7). Data in (A, B) represents mean ± SD with n=3. Statistical significance: *** p < 0.001 ** p < 0.01, * p < 0.05.

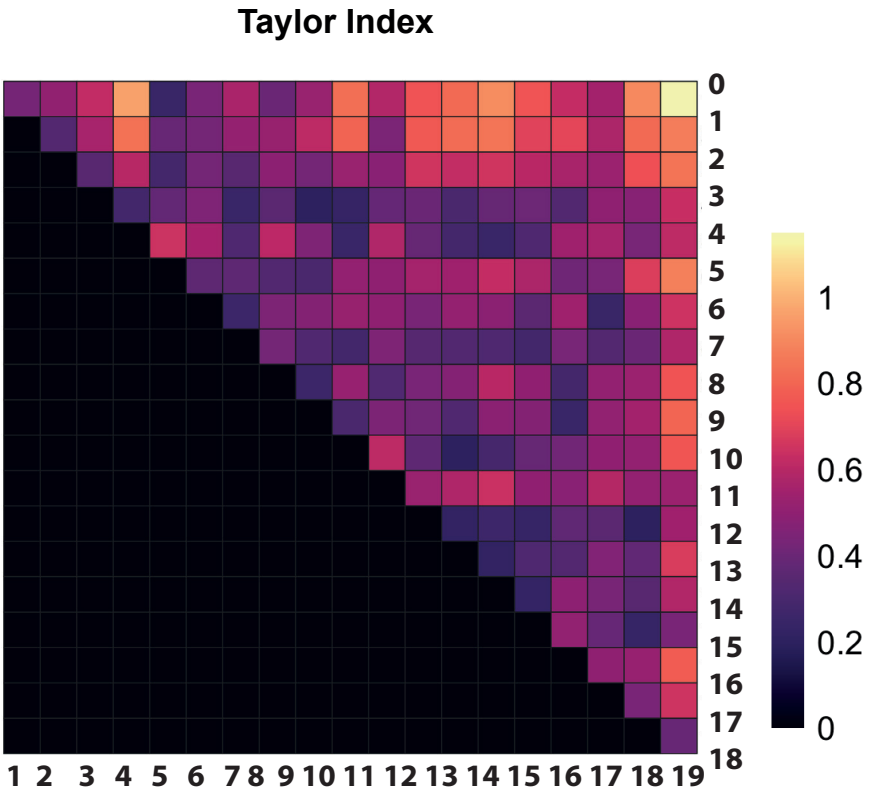

Supplementary Figure 12: Taylor Index showing the distance between every 2 clusters. If the distance between two cluster is low, they are similar to each other, and darker on the heatmap. If the distance between two clusters is high, they are different from each other, and lighter on theheatmap.

5

General Discussion

5. General Discussion

Organ transplantation has made significant strides in last fifty years. Improvements in immunosuppression therapies and novel developments in transplant procedures have markedly reduced the risk of implant rejection (1). However, there is one main challenge that still needs to be addressed: the shortage of human organs available for transplantation (2). Therefore, it is observed that the rate at which transplants are performed cannot keep up with the organ demand. Data from the annual report of the Organ Procurement and Transplantation Network/ Scientific Registry of Transplant Recipients (OPTN/SRTR) states that demands for transplant has continue to rise in the last years while the organ donations do not. For example, in 2019, 39,718 transplants — from 19,267 donors — were performed, while 112,568 people were on the national transplant waiting (Figure 1). As a possible solution to this problem, investigators have attempted to engineer every tissue and organ comprising the body by means of tissue engineering (3)

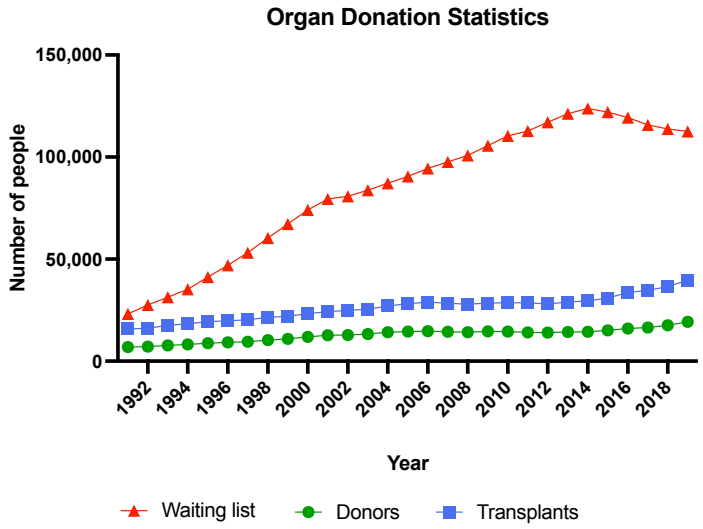

Figure 1: Organ donation statistics. The red, blue and green lines represent the individuals on the waiting list, the number of transplants being performed and the number of donors, respectively, for the corresponding years as labeled. Data obtained from the 2019 report of the Organ Procurement and Transplantation Network/ Scientific Registry of Transplant Recipients (OPTN/SRTR)

Tissue-engineering *is an interdisciplinary field that applies the principles of engineering and the life science towards the development of biological scaffolds that restore, maintain, or improve tissue function* (3). The main objective of tissue engineering is to repair and regenerate unfunctional organs and tissues by a combination of autologous or allogeneic cells with tissue-inducing substances such as cytokines or growth factors, placed on or within a scaffold, also named biomaterial (3). This scaffold/biomaterial serves as a support to guide tissue formation, creating an appropriate microenvironment that helps in the regeneration process.

For many years, inert biomaterials have been pursued with the main aim of evading the immune response and graft rejection. However, the current school of thought focuses on biomaterial design to facilitate immune-response modulation and integration with the host tissue, pointing out a paradigm shift from using immune-inert biomaterials (Figure 2).

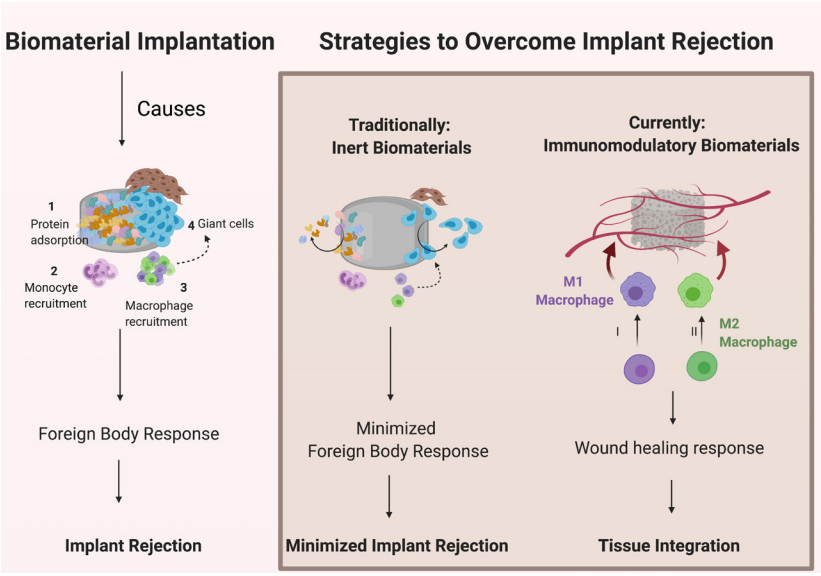

Figure 2: Biomaterial implantation and strategies to overcome implant rejection

Regardless of the fact that the biomaterial may be inert or less invasive, all implantation results in a host injury followed by a foreign body reaction that eventually causes implant rejection or integration. Host response following biomaterial implantation can be summarized in four main events: coagulation and

inflammation, proliferation and remodeling — with or without scar tissue formation — (4). Conventionally, the inert biomaterials have been engineered to have as minimal host response as possible. However, currently, there has been a paradigm shift and biomaterials are being designed such that they interact with host to produce an immune response which is helpful and constructive —reviewed in (5) and (6)—. In order to design the right biomaterials, it is important to know the process that occurs after the biomaterial implantation.

The first step of inflammation is protein adsorption, followed by platelet adhesion, activation and initiation of the blood-clotting cascade leading to a provisional fibrin matrix. Neutrophils are the first immune cells that arrive to the wound side. After 1-3 days, monocytes are recruited to the site of injury and differentiate into macrophages, which are crucial for coordinating both early and late events (4). Neutrophils undergo apoptosis and are removed via phagocytosis by macrophages — a process called efferocytosis — that serves to regulate macrophage behavior. Macrophages play a significant role in the entire tissue repair process. It has been observed that clearly discernible macrophage phenotypes develop in at least two sequential phases, as the normal healing proceeds. In the initial inflammatory phase, mostly pro-inflammatory M1 macrophages are present, whereas in the second stage is characterized by macrophages with a distinct pro-regenerative M2 phenotype (7, 8). Furthermore, the M2 population is considerably diverse, where different physiologically relevant stimuli cause phenotypically discernible macrophages (9, 10). Moreover, M2-type macrophages may derive from the infiltration of newly arriving monocytes — M0 to M2 macrophages — at later stages of wound healing, or they may derive from M1 macrophage repolarization — M1 to M2 macrophages — (11, 12).

Although both M1 and M2 macrophage phenotypes are needed for proper biomaterial-tissue integration, their modulation and inflammatory response development plays a major role in such process. The regulation of this early inflammatory phase and subsequent transition into a reparative state is mandatory for biomaterial integration and acceptance, since a chronic proinflammatory phase will lead to foreign body reaction and rejection of the implant. With respect to biomaterial implantation, an inability of macrophages to phagocytose the biomaterial induce repeated inflammation. During this chronic inflammatory response, macrophages agglutinate together to form multinucleated giant cells, which deposit a fibrous matrix

around the implant isolating it from the rest of the body hindering implant integration with host tissue (4). For this reason, it is important to try to overcome this chronic inflammation by interacting with the immune response. This is necessary to promote the aforementioned transition and to minimize the fibrous matrix development surrounding the implant, as much as possible.

While the detailed mechanisms regulating macrophage functions during tissue healing are still poorly understood, their critical roles in both the response to biomaterials and in tissue repair mark macrophages as a primary target when designing immunomodulatory strategies for biomaterial integration. Besides innate immune cells, adaptive immune cells, in particular T cells, also have been targeted to a lesser extent than macrophages (13).

To try to facilitate the M1-M2 transition in macrophages, multiple works have tried to develop a comprehensive understanding of the interaction between biomaterial properties and macrophage phenotype, concentrating on stimulating M2 activation by different means: (i) enhancing recruitment of M2-biased monocytes/macrophages, (ii) stimulating M2 phenotypes, (iii) and/or sequentially promoting M1 phenotype followed by a transition towards M2 phenotype. These effects have been achieved through different strategies, such as: manipulation of biomaterial properties, the addition of bioactive proteins or drugs, or the inclusion of immunomodulatory cell types, such as, mesenchymal stromal cells (MSCs) (Figure 3).

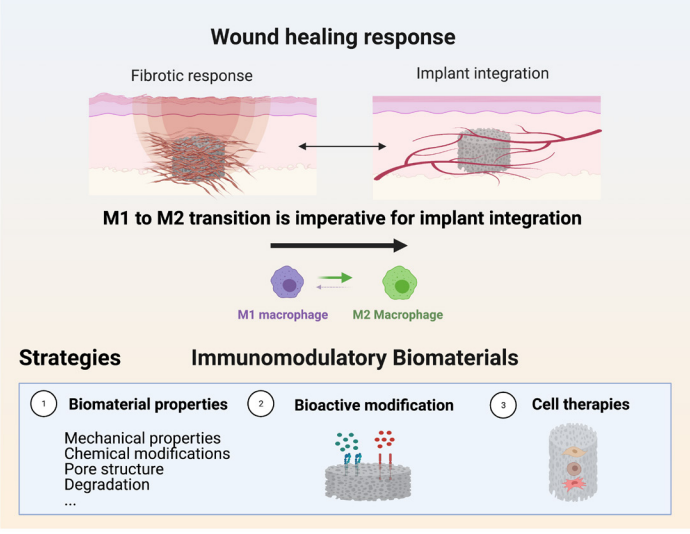

Figure 3: Design strategies for biomaterials that achieve implant integration

In this thesis, we focused on the last abovementioned strategy which is the inclusion of immunomodulatory cells to help with implant integration. We hypothesized that the use of MSCs could represent a beneficial strategy to gain control over implant integration by their immunomodulatory properties. However, as the isolation procedures of the popularly used source of MSCs are painful and invasive for the patients, we propose the use of a rather lesser-known source of MSCs: the hair follicle.

Along with stimulating tissue regeneration by immunomodulation, the current design strategies aim to develop a better understanding of the crosstalk between components of the immune system, stem/progenitor cells and other cells which play a role in the overall healing process — e.g. endothelial cells —. A critical component of the wound healing process is the development of an adequate blood supply, which not only provides cells with oxygen and nutrients but also removes the waste products. Biomaterial implantation results in disruption of the host vasculature, whose inability to quickly vascularize the implanted biomaterial may lead to lack of oxygen and nutrients. This may subsequently lead to impaired integration and function. As an initial step to overcome this problem, Levenberg et al. were the first ones growing tissue-engineered blood vessels *in vitro* and proved their effectiveness of anastomosing with the host vasculature *in vivo* (14, 15). However, like all implanted biomaterials, engineered tissues will interact with the innate immune system upon implantation.

As it has already being mentioned, the primary cells of the innate immune response, macrophages, are important for wound healing and biomaterial-tissue interaction, in this case, also by tightly monitoring the angiogenesis process. In fact, wound healing is considerably negatively influenced by the lack of macrophages (16), whereas their exogenous addition boosts angiogenesis (9, 17). However, the angiogenic effects mediated by the changes in macrophage phenotype that normally occur over time are still poorly understood. Recently, Graney et al. — using the same tissue-engineered model of human blood vessel formation used in this doctoral thesis — studied macrophage-blood vessel crosstalk *in vitro* (9). Firstly, they demonstrated that co-culture with pro-inflammatory M1 macrophages caused the upregulation of genes related to early stages of angiogenesis, such as sprouting. Also, M2 macrophages caused endothelial cells to upregulate genes associated with

later stages of angiogenesis, such as regulation of pericyte differentiation and vessel maturation. These results, in combination with numerous other studies, suggest that M1 and M2-type macrophages act sequentially to regulate angiogenesis — for review see (18) — However, the way in which blood vessels — especially engineered blood vessels — regulate macrophage phenotype is not yet totally understood.

With this perspective in mind, the goals of the doctoral thesis were:

- Firstly, to characterize a lesser-known MSCs from a more accessible and less invasive mesenchymal niche: the Hair Follicle.

- Secondly, to study the immunomodulatory capacities of those hair follicle-derived MSCs (HF-MSC) compared to the adipose MSCs (AT-MSCs), which are known to have the strongest immunomodulatory capacity.

- Thirdly, to analyze the implication of tissue-engineered blood vessels in macrophage phenotype switch.

All these points taken together are shown in Figure 4

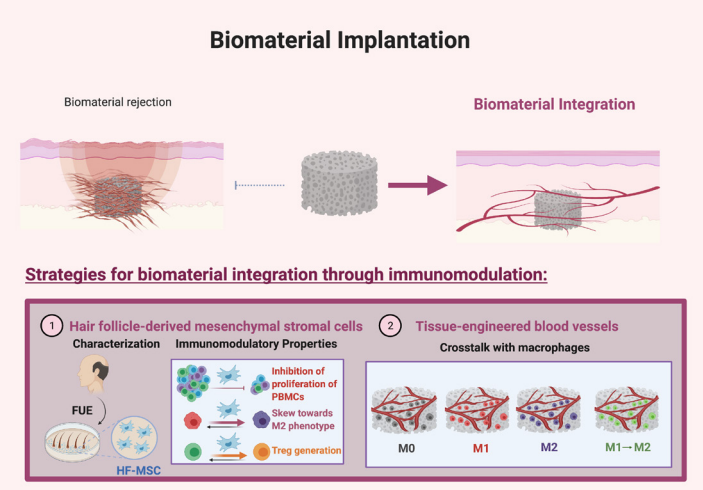

Figure 4: Schematic representation of the work performed in the doctoral thesis. FUE, follicular unit extraction. HF-MSC, hair follicle derived mesenchymal stromal cells. PBMCs, peripheral blood mononuclear cells. Treg, regulatory T lymphocyte

MSCs are now being even more broadly used for their immunomodulatory properties — for review, see (18) —. In particular, they exhibit low immunogenicity even in allogeneic transplants, and they have the capacity to inhibit immune cell proliferation. In addition, crosstalk with macrophages induces a unique macrophage phenotype sometimes referred to as MSC-educated macrophages (19-21). Consequently, macrophage phenotype and subsequently biomaterial integration could be modulated by MSC-based therapies.

Unlike many other cells that are only found in specific tissues, MSCs can be harvested from almost every tissue using their plastic-adherence properties. Historically, bone marrow was the first source from which MSCs were obtained (BM-MSCs) (22). Nevertheless, in the past decade, researchers have been able to isolate MSCs from other tissue sources, such as umbilical cord, placenta, adipose tissue, kidney, liver, lung and dental tissue (23, 24). Interestingly, MSCs which have different sources of origin generally demonstrate diverse properties and differentiation capacities (25). Recently, AT-MSCs have been utilized to almost the same extent as BM-MSCs, as these MSCs — with respect to bone marrow — can be more easily accessed in patients, are safer to harvest and provide a greater cell yield (26, 27). However, it should be noted that harvesting these cells from both origins —AT-MSCs and BM-MSCs— is relatively painful and invasive for the patient, not only during the operation but also in the post-operative phase. Moreover, in the particular case of AT-MSCs, a recent study has demonstrated that these cells are dysfunctional and undergo early senescence when harvested from obese patients (28). This and other similar conditions can also alter their “stemness” and secretome profiles, thus hindering their immunomodulatory properties (29, 30). Therefore, with the mentioned drawbacks in mind, in the present thesis we explored an alternative and relatively less known niche of MSCs, the hair follicle.

To assess the possible use of these cells, we first did a thorough characterization of the cells. The characterization consisted of a description of the exact anatomical location, study of their freshly isolated phenotype, stemness properties, immunoevasiveness and immunomodulatory responsiveness. In the second part of the study, we assessed their immunomodulatory potential comparing it to the most used AT-MSCs.

The hair follicle is one the main appendages of the skin and the niche of two different stem cells: epidermal-origin stem cells and dermal origin MSCs. To ensure that the cells we are studying were from mesenchymal and not from epidermal origin, an immunohistochemistry analysis was conducted. For that, we used a common marker for MSCs, CD90. As expected, and in concordance of previous studies, most of the CD90^{+} stained section was in the lower part of the hair follicle, where the dermal papilla/dermal cup is localized (Figure 5A) (31-33). One of the main characteristics of HF-MSCs is their possible neural differentiation capacity which other MSCs from different origins lack. This could be attributed to the hypothesis that these cells have their origin in the neural crest. In order to prove this concept, we analyzed the presence of three neural markers that are presented in cells with neural crest origin — SOX-2, CD271 and CD56—. Our results indicated that at least 96 % of the CD90^{+} cells co-expressed at least one of the three neural markers (Figure 5B). Interestingly, once the cells were cultured in vitro, CD271 expression decreased rapidly, whereas CD56 and SOX-2 expression were gradually lost over subsequent cell passages. In addition, significant variability amongst patients were observed. To try to overcome this variability, and to maintain consistency and for a thorough comparison, cell pools of no more than 5 different patients were used during the whole study.

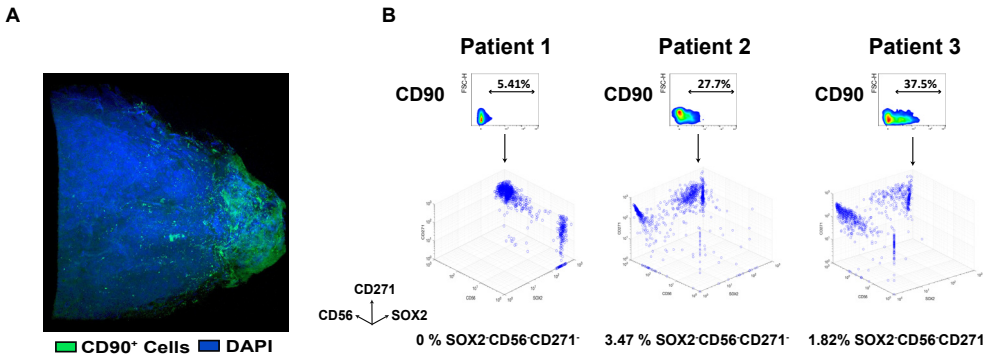

Figure 5: Isolation of HF-MSCs and neural origin characterization of freshly harvested HF-MSCs. (A) Immunohistochemistry of the hair follicle showing the MSC marker CD90 in green and DAPI in blue. (B) expression of the MSC marker (CD90) and neural markers (CD271, SOX2 and CD56) in freshly harvested hair follicle cells. Density plot representation of the CD90 variation with respect to FSC-H for the three different patients and three-dimensional representation of the intensity of neural markers, SOX2 (x-axis), CD56 (y-axis) and CD271 (z-axis) after the CD90 gaiting.

In 2006, the International Society for Cellular Therapy (ISCT) proposed 3 minimal criteria to define human MSCs (Figure 6A). Our HF-MSCs satisfied the necessary criteria to be termed as MSCs, in at least 10 passages (Figure 6B-J). Firstly, the HF-MSCs were able to adhere to plastic and proliferate (Figure 6B, C). Secondly, they were positive for the specific MSC markers — CD105, CD73 and CD90 — and negative for the non-specific MSC-markers — CD45, CD34, CD14 and CD20 — (Figure 6D). Finally, they possessed the capacity to differentiate to osteoblast, adipocytes and chondroblast, which was proven by tissue-specific staining and expression of specific genes (Figure 6E-J).

The immunomodulatory capacity of MSCs have been associated with the activity of indoleamine 2,3-dioxygenase (IDO), among many other compounds of their secretome (34). A strong expression of IDO, resulting in further immunoproliferation inhibition, has been noticed, when MSCs have been pretreated — licensed — with interferon gamma (IFNγ) (24, 35) (Figure 7A). Therefore, in order to study the immunomodulatory performance of the HF-MSCs, these cells were licensed with IFNγ for 72 hours followed by subsequent quantitative reverse transcription polymerase chain reaction (RT-qPCR) and Western Blot analysis (Figure 7B and 7C, respectively). HF-MSCs showed a good responsiveness to the pro-inflammatory stimulus, expressing comparable levels of IDO at both passage 2 and passage 10, thereby demonstrating their ability to retain the IDO responsiveness even when cultured for prolonged time spans *in vitro*.

Another important characteristic of the MSCs is their immunoevasiveness, meaning the incapacity of inducing an immune response. One of the principal explanations has been related with their inability to express major histocompatibility complex class II molecule (MHC-II) — reviewed in (36) —. In inflammatory environments, however, it has been reported that MSCs of various origins begin to express MHC-II molecules, consequently resulting in a loss of their signature evasiveness (37). Importantly, we observed that HF-MSCs, even though they started expressing MHC-II molecule when licensed with IFNγ, shower lower expression than AT-MSCs. (Figure 8). This could be attributed to the hair being an immunoprivileged organ, where the deviation of immune response is observed to favor tolerance. Also, multiple physiological processes are consistently maintained by a variety of processes that limit foreign antigen recognition (38). Thus, considering the limited number of cells available for autologous use, HF-MSCs may be a suitable allogenic alternative for MSC-based cell therapy.

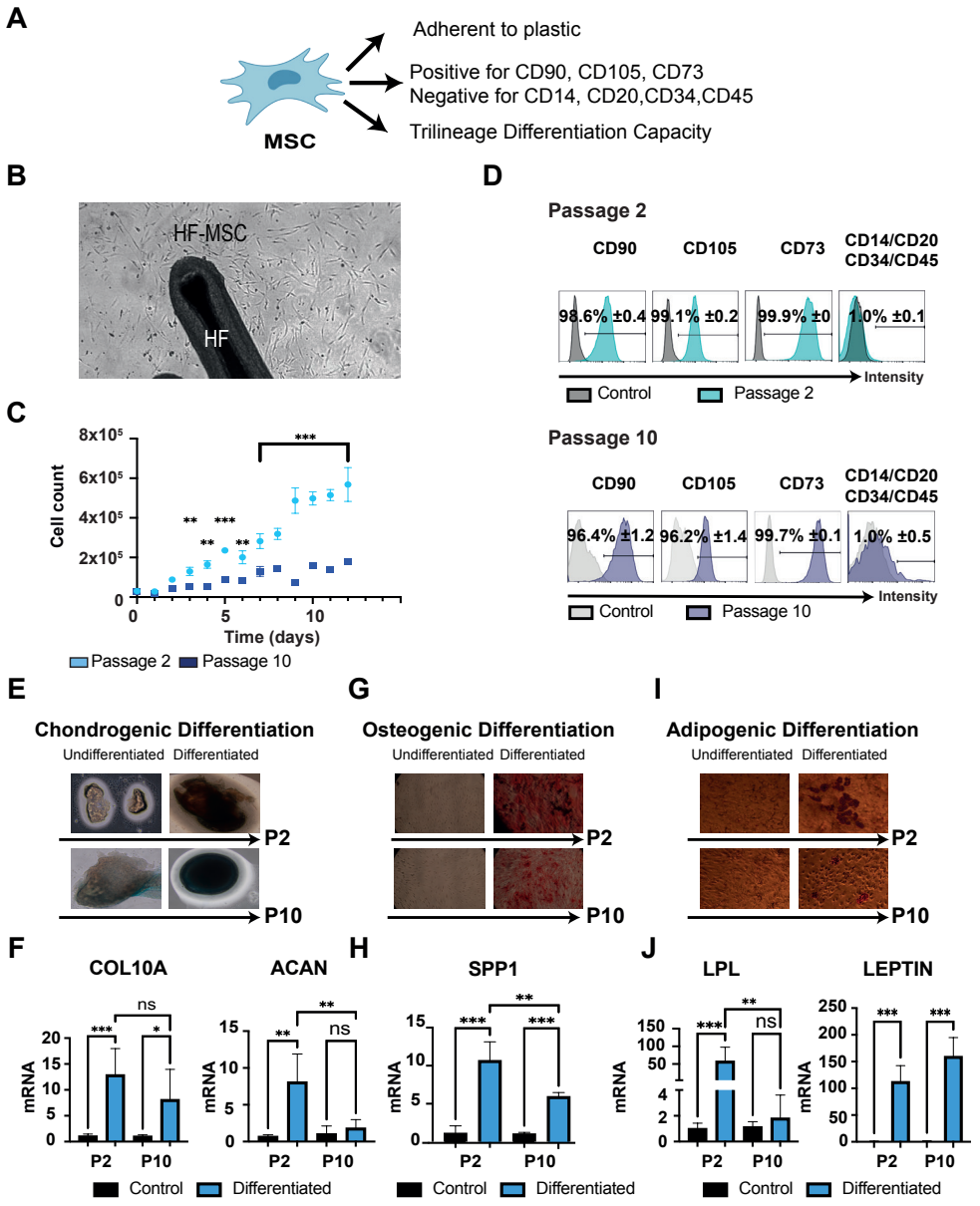

Figure 6: Characterization of minimal criteria to define MSCs. (A) A schematic representation of the MSCs and their necessary properties. (B) Microscopic image representing the capacity of the HF-MSCs to adhere to plastic (C) Graphical representation of the proliferation potential of HF-MSCs at both passage 2 and passage 10. Each datapoint represents the mean for 3 wells ± SD. Statistical significance: *** $p < 0.001$ ** $p < 0.01$, * $p < 0.05$. (D) Cells cultured at passage 2 and passage 10 were harvested and labelled with antibodies against the following cell surface proteins CD90, CD105, CD73, CD14, CD20,

(Figure 6 continue) CD34, CD45. Flow cytometry histograms of cells at P2 (teal) and P10 (dark blue) are shown. Gray histograms indicate isotype control for each antibody. Each datapoint represents the mean for 3 wells ± SD. (E-J) Trilineage differentiation of cells at both passage 2 and passage 10. (E) Chondrogenic differentiation capacity of HF-MSC after 21 days with the differentiation medium. Blue color represents the secretion of cartilage specific proteoglycans visualized with Alcian blue. (F) Chondrogenic differentiation was further confirmed by COL10A and ACAN gene expression. (G) Osteogenic differentiation capacity of HF-MSCs after 21 days with the differentiation medium. Deposition of calcified nodules was visualized by Alizarin Red staining. (H) Osteogenic differentiation was further confirmed by SPP1 gene expression. (I) Adipogenic differentiation capacity of HF-MSCs after 21 days with the differentiation medium. Red color indicates the staining of lipid vesicle-forming adipocytes by Oil Red staining. (J) Adipogenic differentiation was further confirmed by LPL and LEPTIN gene expression. Each datapoint represents the mean for at least 3 biological replicates ± SD. Statistical significance: *** $p < 0.001$ ** $p < 0.01$, * $p < 0.05$. MSC, mesenchymal stromal cells. P2, passage 2. P10, passage 10. HF-MSC, hair follicle-derived mesenchymal stromal cell.

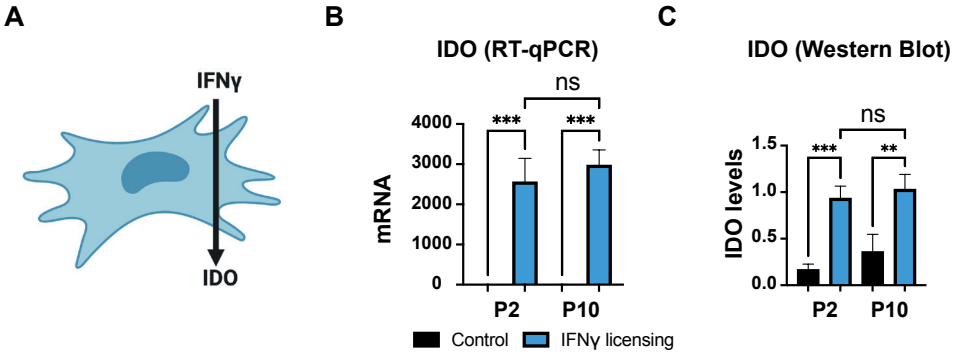

Figure 7: Effect of IFNγ licensing on HF-MSCs immunomodulatory responsiveness. (A) In humans, IFNγ induces expression of IDO in MSCs, which is a key molecule to drive their immunomodulatory capacity. (B, C) Histogram representation of IFNγ dependent relative IDO gene expression levels in HF-MSCs, as characterized by RT-qPCR(B) Western Blot (C). Each datapoint represents the mean for at least 3 biological replicates ± SD. Statistical significance: *** $p < 0.001$ ** $p < 0.01$, * $p < 0.05$, ns ($p > 0.05$) no significance. IFNγ, interferon gamma. IDO, indoleamine 2,3-dioxygenase.

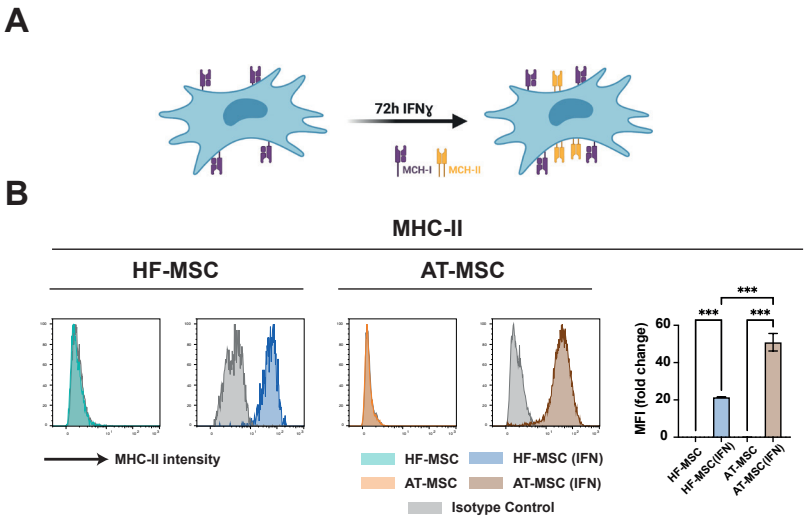

Figure 8: Effect of IFNγ licensing on HF-MSCs immunoevasiveness compared to AT-MSCs. (A) MSCs upregulate their MHC-II expression in pro-inflammatory environments. (B) Flow cytometry histograms showing MSCs positively stained for MHC-II on unstimulated and IFNγ-licensed HF-MSCs (light blue unstimulated, dark blue stimulated with IFNγ) and AT-MSCs (light orange unstimulated, dark orange stimulated with IFNγ). Bar graphs showing the MFI of MHC-II in each group. Each datapoint represents the mean for at least 3 biological replicates ± SD. Statistical significance: *** $p < 0.001$. IFNγ, interferon gamma. MHC-II, major histocompatibility class II molecule. HF-MSCs, hair follicle derived mesenchymal stromal cells. AT-MSCs, adipose tissue derived mesenchymal stromal cell. MFI, median fluorescence intensity.

Stemness, per the ISCT definition, and the immunomodulatory responsiveness could be observed even in passage 10, even though the proliferation rate had considerably reduced. This could play an important role in as MSCs have been observed to lose their ability to differentiate and immunomodulate much earlier than passage 10 (39). Using these properties, the necessary yield could be obtained without MSCs losing their quality.

Once HF-MSCs were characterized and analyzed for their responsiveness to IFNγ and their immunoevasiveness, the next step was to assess their immunomodulatory reach. Towards this end, AT-MSCs have been considered as a reference, given that they are considered the most immunomodulatory MSCs (29). First, by means of co-culture experiments, the influence of both MSCs on the proliferation of Concanavalin A activated peripheral blood mononuclear cells (PBMCs) was examined and compared (Figure 9).

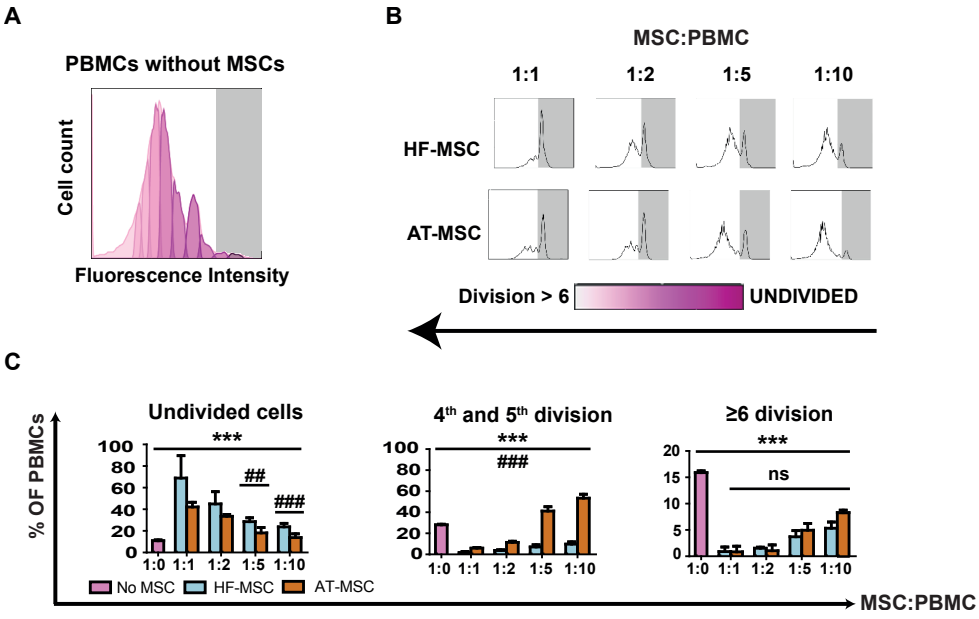

Figure 9: Immunomodulatory effects of HF-MSCs and AT-MSCs in concanavalin A-stimulated PBMCs. (A) Flow cytometry histogram showing the proliferation profile of PBMCs without MSCs after 5 days of co-culture. Undifferentiated cells are represented by the vertical grey bars in the figure. (B) Flow cytometry histograms showing the proliferation profiles of the PBMCs after 5 days of co-culture with different ratios (1:1, 1:2, 1:5, 1:10) of either AT-MSC or HF-MSCs. (C) Percentages of PBMCs remaining undivided, undergoing 4 and 5 division and undergoing more than or 6 divisions. Statistical significance: *** $p < 0.001$ and ** $p < 0,01$ when compared against PBMCs without MSCs; ### $p < 0.001$ and ## $p < 0.01$ when compared HF-MSCs with AT-MSCs; ns: not significant differences, $p>0.05$. PBMCs, peripheral blood mononuclear cells. MSC, mesenchymal stromal cells. HF-MSCs, hair follicle-derived mesenchymal stromal cells. AT-MSCs, adipose tissue-derived mesenchymal stromal cells.

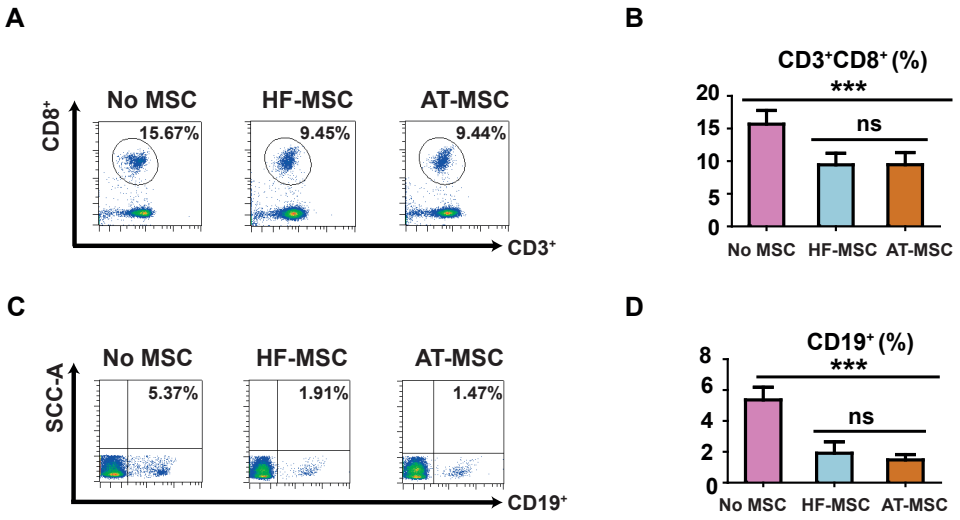

Figure 10: Immunomodulatory effects of HF-MSCs and AT-MSCs in concanavalin A-stimulated PBMCs. (A) Flow cytometry dot plot depicting the populations of $CD3^+CD8^+$ T lymphocytes (B) and their relative percentages when PBMCs were cultured alone (no MSCs), with HF-MSCs or with AT-MSCs. (C) Flow cytometry dot plot representing the populations of $CD19^+$ B lymphocytes (D) and their relative percentages when PBMCs were cultured alone (no MSCs), with HF-MSCs or with AT-MSCs. Each datapoint represents the mean for at least 3 biological replicates ± SD. Statistical significance: *** $p < 0.001$ when compared with PBMCs without MSCs; ns: not significant differences, $p > 0.05$. PBMCs, peripheral blood mononuclear cells. MSC, mesenchymal stromal cell. HF-MSCs, hair follicle-derived mesenchymal stromal cells. AT-MSCs, adipose tissue-derived mesenchymal stromal cells.

The results demonstrated a dose-dependent suppressive effect of both MSCs. Interestingly, HF-MSCs exerted a more powerful inhibition than AT-MSCs when co-cultured at lower MSC:PBMC ratios (Figure 9C).

On subsequent evaluation of the influence of these cells on specific lymphoid populations, we noticed that there was a considerable lowering of $CD3^+CD8^+$ T lymphocytes and $CD19^+$ B cells' percentages (Figure 10)

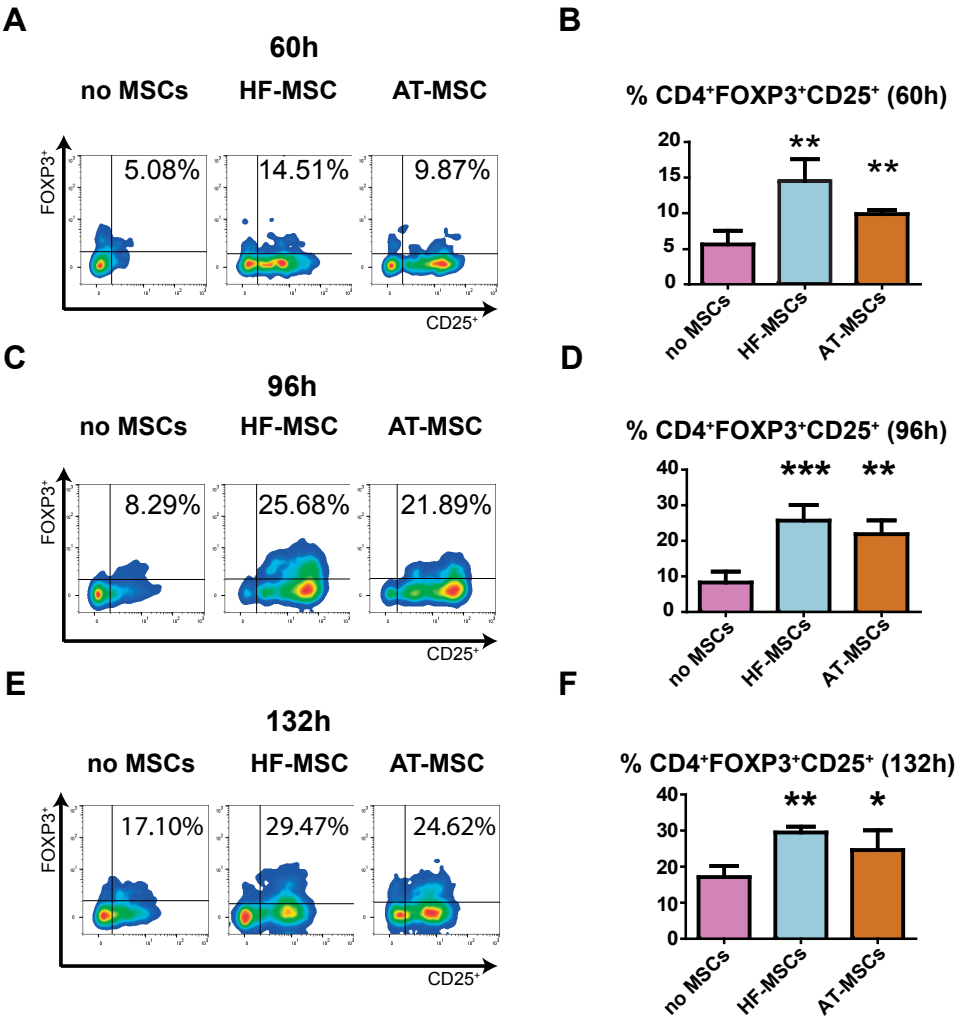

Figure 11: Effect of HF-MSC and AT-MSCs on induction of $CD4^+CD25^+FOXP3^+$ T regulatory lymphocyte from $CD4^+$ T lymphocytes. (A-F) Dot plots (A, C, E) and their bar-graph representations (B, D, F) exhibiting the percentages of $CD4^+CD25^+FOXP3^+$ cells under T regulatory induction conditions when cultured alone, with HF-MSCs or AT-MSCs during (A, B) 60h, (C, D) 96h and (E, F) 132h. Each datapoint represents the mean for at least 3 wells ± SD. Statistical significance: *** $p < 0.001$, ** $p < 0.01$ and *$p < 0.05$ when compared against T lymphocytes without MSCs. PBMCs, peripheral blood mononuclear cells. MSC, mesenchymal stromal cells. HF-MSCs, hair follicle-derived mesenchymal stromal cells. AT-MSCs, adipose tissue-derived mesenchymal stromal cells.

Furthermore, HF-MSCs induced the generation of $CD4^+CD25^+FOXP3^+$ T regulatory lymphocytes for over a period of 132 h to the same extent as AT-MSCs (Figure 11). $CD4^+CD25^+FOXP3^+$ T regulatory lymphocytes are a specialized suppressor T lymphocyte subpopulation that play a critical role in self-tolerance and immune homeostasis. Consequently, this tendency of the HF-MSCs to promote T-cell regulatory differentiation and inhibit activated B and T cell response allows them to be considered favorably for a variety of immune-mediated diseases. This is especially important in the cases where adaptive immunity is influential, such as, graft-versus-host disease (GvHD), inflammatory bowel disease (IBD) or multiple sclerosis (MS) (40-42).

As for the innate immunity, MSCs have been reported to be able to influence the formation of M2 macrophage phenotypes both *in vivo* and *in vitro*, which is an important mechanism in anti-inflammation or the induction of immune tolerance (9, 51-53). Specifically, a recent study has shown that MSCs located in the outer root sheath of the hair follicle have the ability to suppress the proinflammatory cytokines TNFγ and IL-12p40 while stimulating the production of anti-inflammatory cytokine IL-10 and the expression of the CD163 marker in M1 macrophages (43).

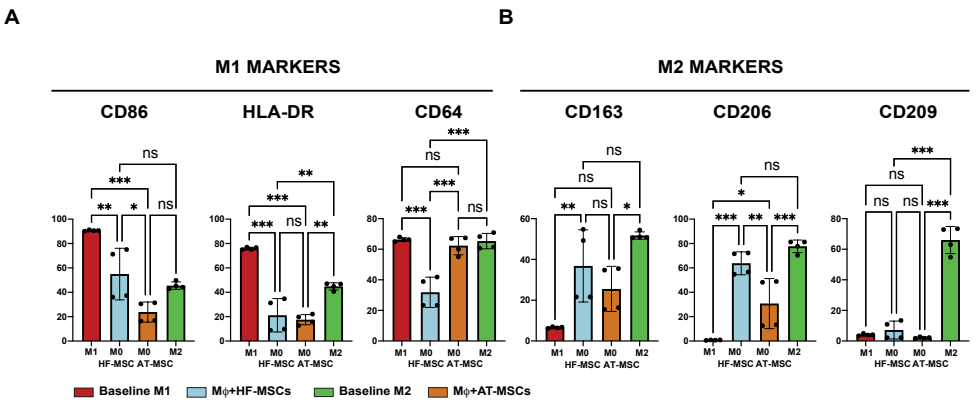

Figure 12: Effect of HF-MSCs and AT-MSCs on the modulation of undifferentiated (M0) macrophages phenotype. (A,B) Bar-graphs showing percentage of cells positive for either (A) M1 related phenotypic markers CD86, MHC-II and CD64 or (B) M2 related phenotypic markers CD163, CD206 and CD209 expression when M0 macrophages were co-cultured with HF-MSCs (light blue) or AT-MSCs (orange). Each datapoint represents the mean ± SD of 4 wells. Statistical significance: *** $p < 0.001$ and ** $p < 0.01$ and * $p < 0.05$ when compared with macrophages without MSCs; ns: not significant differences, $p > 0.05$. PBMCs, peripheral

(Figure 12 continued) blood mononuclear cells. Mϕs macrophages. HF-MSCs, hair follicle-derived mesenchymal stromal cells. AT-MSCs, adipose tissue-derived mesenchymal stromal cells.

To observe if our cells demonstrated the same ability, we co-cultured the HF-MSCs and AT-MSCs with undifferentiated primary human (M0) macrophages. Interestingly, our HF-MSCs were able to skew these macrophages towards a more regulatory — M2 — phenotype, acquiring marker expression profiles resembling those of the M2 baseline— low expression levels of M1 markers CD86, MHC-II and CD64, and higher values of M2-like markers, mostly CD163 and CD206 —. This is in accordance with the work published by Cutler et al. and Witte et al. who already described that MSCs have the ability to induce the expression of the regulatory markers CD163 and CD206 on monocytes (21, 44). Furthermore, when directly compared to AT-MSCs, HF-MSCs demonstrated a superior performance, as they were the only MSC type able to reduce significantly the CD64 M1 marker and upregulating CD163 and CD206 M2 markers to the same levels shown by the M2 control group (Figure 12).

It was also desired to determine whether the polarization state have an influence on the crosstalk between MSCs and macrophages. To understand that, we co-cultured the HF-MSCs and AT-MSCs with pro-inflammatory (M1) macrophages. As described in Figure 13, HF-MSCs, better than AT-MSCs, switched M1 macrophages into more M2-like phenotype. Although both MSC types succeeded in downregulating some M1-related markers, only HF-MSCs were able to downregulate CD64 marker and upregulate both CD163 and CD206 markers. This has important consequences

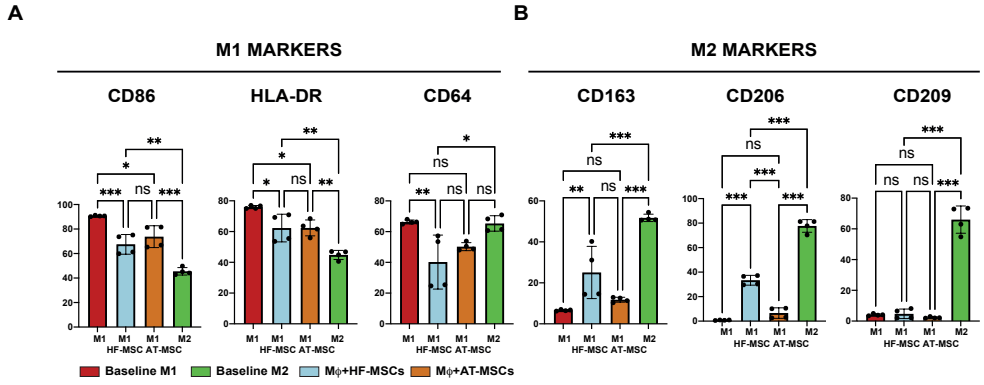

Figure 13: Effect of HF-MSCs and AT-MSCs on the modulation of M1 macrophage phenotype. (A,B) Bar-graphs showing percentage of cells positive for either (A) M1 related phenotypic markers CD86, MHC-II and CD64 or (B) M2 related phenotypic markers CD163, CD206 and CD209 expression when M1 macrophages were co-cultured with HF-MSCs or AT-MSCs. Each datapoint represents the mean ± SD of 4 wells. Statistical significance: ***p < 0.001 and ** p < 0.01 and * p < 0.05 when compared with macrophages without MSCs; ns: not significant differences, p > 0.05. PBMCs, peripheral blood mononuclear cells. Mϕs, macrophages. HF-MSCs, hair follicle-derived mesenchymal stromal cells. AT-MSCs, adipose tissue-derived mesenchymal stromal cells.

when chronic inflammation occurs, because the transition to the regenerative phenotype M2 from the pro-inflammatory M1 is absolutely essential for healing. If this transition is not smooth, healing is impaired, especially, something that is seen in the case of chronic wounds (45). Evidence has further reinforced the importance of MSCs in modulating macrophage phenotype from M0 and M1 to subsequently M2 (20, 46, 47). This study also demonstrates the addition of HF-MSCs facilitates a transition to a M2 phenotype. However, the expression of M1 markers can still be noticed, indicating the presence of M1 macrophages or at least and hybrid M1/M2 phenotype. The importance of the transition from an M1 to an M2 phenotype was reviewed by O'Brien et al. (17). Furthermore, in a recent study Witherel et al. determined that this hybrid M1/M2 macrophages encourage the production of less fibrotic extracellular matrix compared to a more predominant M2 macrophage phenotype (48). This could be helpful in our ultimate goal, as lowering the fibrotic extracellular matrix is critically important in achieving implant integration.

In summary, the cells obtained from the lower dermal sheath/dermal papilla of human hair follicles expressed specific neural markers such as CD56, CD271 and SOX-2 upon extraction. In addition, HF-MSCs maintained sufficient stemness properties for at least 10 passages, including standard phenotypic markers, trilineage differentiation and proliferative capacity. Moreover, these cells demonstrated a responsiveness to the pro-inflammatory cytokine IFNγ, while maintaining their immuno-privileged status. Also, HF-MSCs demonstrate immunomodulatory ability comparable with AT-MSCs. Besides, they also exhibit important advantages such as ease of access, painless, non-invasive harvesting procedures and low infection risk for donors. Therefore, it can be concluded that the use of HF-MSCs might be a plausible strategy to promote implant integration by skewing immune cells — such as T lymphocytes and macrophages — towards a regenerative phenotype.

Considering this, the next strategy that we presented in this thesis was the use of pre-vascularized biomaterials to help their integration by anastomosing with the host vasculature and possibly switching macrophage phenotype towards a more regenerative — M2— phenotype. As mentioned previously, it is well known that macrophages are key regulators in orchestrating the success or failure of the integration of tissue-engineered constructs. Also, it is understood that macrophages are very plastic cells that are able to switch their phenotypes depending on their milieu. For this reason, it was imperative to analyze the phenotype switch when macrophages were co-cultured with tissue-engineered blood vessels (49-51). Therefore, the goal of the next study was to test the hypothesis that the crosstalk with blood vessels will skew macrophage phenotype towards a more regenerative phenotype.

For that, common M1 (HLA-DR, CD80, CD38, PD-L1 and CCR7) and M2 (CD163, CXCR4, CD206 and CD209) markers were used to analyze how their expression changed during the co-culture of different macrophage phenotypes — M0, M1, M2 and M1M2 — with tissue-engineered blood vessels. Towards that end, it was crucial to validate all the markers presented in this study (Figure 14). Therefore, primary human peripheral blood monocytes were isolated from five human donors, differentiated into macrophages (M0) and further polarized into, M1, M2 or M1M2 phenotypes (Figure 14A). Even though most of the M1 markers were upregulated in M1 macrophages and M2 common markers were upregulated in M2 macrophages, there were some exceptions. Regarding M2 markers, CXCR4 and CD163 did not show an upregulation in M2 macrophages (Figure 14C). Concerning CXCR4, an elevated expression was noticed in M1M2 macrophages, when compared with M2s. CXCR4 is well known marker expressed in macrophages with potent angiogenic behavior (52, 53). For this reason, we expect that co-culture with tissue-engineered blood vessels could result in a higher expression of CXCR4. Furthermore, CD163 was upregulated in M1 and M1M2 macrophages as compared to standalone M2 macrophages.

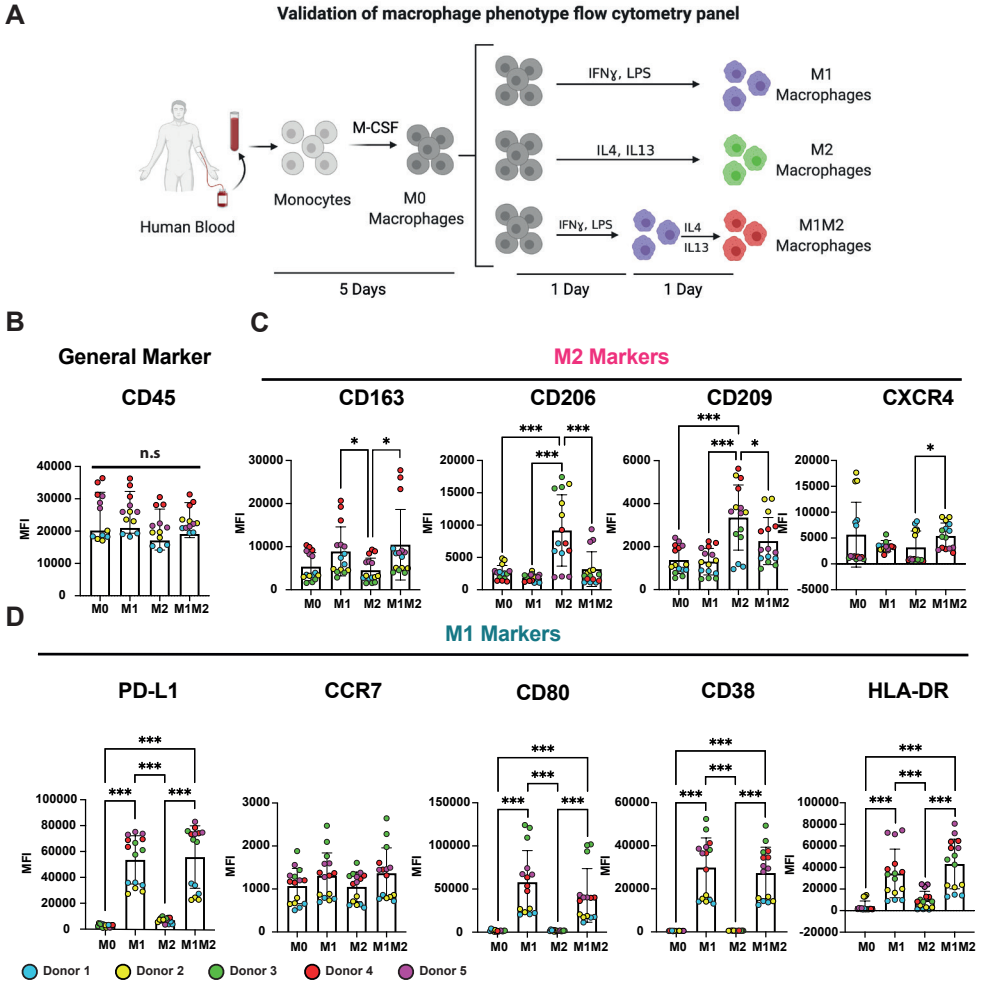

Figure 14: Validation of the human macrophage phenotype flow cytometry panel. (A) Primary human peripheral blood monocytes were isolated from 5 human donors, differentiated into macrophages and polarized into M0, M1, M2 or M1M2. (B) Median fluorescent intensity (MFI) of the general macrophage marker CD45. (C) MFI of associated M2 markers (CD163, CD206, CD209 and CXCR4) (D) MFI associated M1 markers (PD-L1, CCR7, CD80, CD38 and HLA-DR). Data in (B), (C) and (D) represents mean ± SD with n=3 biological replicates from five human donors. Statistical significance: *** $p < 0.001$ ** $p < 0.01$, * $p < 0.05$.

It was also observed that none of the marker intensities were high in any of the macrophages. CD163 is a common marker for another subpopulation of M2 macrophages, known as M2c, which is obtained by the stimulation of M0 with the IL-10 cytokine (10). M2c macrophages have been shown to have a high phagocytic activity and also secrete high levels of matrix metalloproteinases-7, -8, and -9, which have been related to vascularization by breaking down of the basement membrane and extracellular matrix (11, 54, 55). The reason of adding this marker is because, it has been described that crosstalk with endothelial and MSCs switch macrophages towards an M2 phenotype mostly upregulating markers such as CD163. Even though our baseline phenotype did not highly express CD163, our hypothesis was that the crosstalk with tissue-engineered blood vessels will end up upregulating its expression. On the other hand, regarding the CCR7 common M1 marker, a noticeable difference was not observed between the groups, not in the traditional flow cytometry analysis, nor in the clustering analysis in the 5 donors. This could be due to the changes were so minimum that it could not be appreciated in the analysis (Figure 14D). This also occurred when Spiller et al. measured the CCR7 expression in M0, M1 and M2 macrophages and the flow cytometry histogram did not show a strong difference between phenotypes (11). Also, it should be noted that in the abovementioned study, CCR7 antibody was attached to APC fluorophore that has a brightness index of 5, whereas in our case, it was used along with FITC which has a brightness index of 1. However, at gene expression level, CCR7 has been shown to be high in M1 compared to M2 (56).

After the validation of the common M1 and M2 markers, we analyzed how undifferentiated, M0, macrophages changed when co-cultured with tissue-engineered blood vessels (Figure 15). For that, primary human monocytes were isolated from human blood and differentiated towards M0 macrophages by addition of M-CSF for 5 days. Endothelial cells and MSCs — which act as support cells to facilitate the formation of blood vessels — were co-cultured together on 8mm compressed porous collagen scaffolds to start blood vessel formation. Previous studies using the same approach, have described that after 3 days of co-culture, immature blood vessel formation could be already noticed in the construct (9). After 3 days of co-culture, human derived M0 macrophages were seeded within the scaffold, and changes in macrophage phenotype were assessed after one day of the co-culture via flow cytometry. To determine whether these differences were just because of blood vessels, macrophages were seeded in 3D scaffold alone, or with just MSCs or

endothelial cells to use as controls. Each of the variables were separately analyzed to determine their contribution to the isolated phenotype, in comparison to the rest of the variables considered together. Using these controls and clustering analysis, it was possible to let aside the macrophages that did not change from the baseline, macrophages that only switched due to the co-culture in the 3D scaffold or due to endothelial cells or MSCs alone.

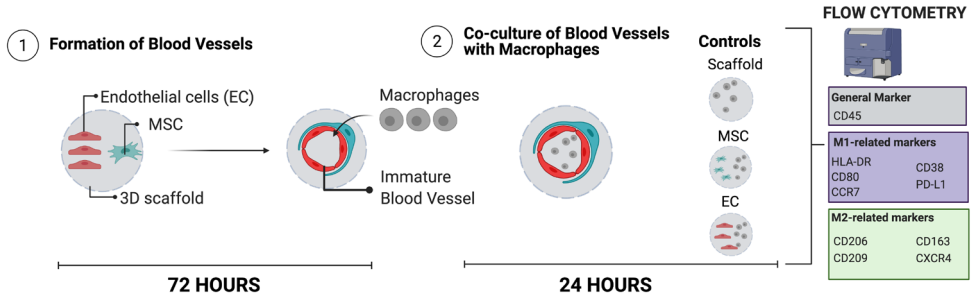

Figure 15: Crosstalk between undifferentiated M0 macrophages and tissue-engineered blood vessels. *In vitro* tissue-engineered human blood vessels were generated by co-culture of endothelial cells and MSCs within 3D collagen scaffolds. After 3 days, M0 macrophages were added to either the acellular 3D scaffold, the 3D scaffold with engineered blood vessels, the 3D scaffold with the endothelial cells or the 3D scaffold with MSCs. Changes in macrophage phenotype were observed one day after macrophage seeding.

The traditional flow cytometry analysis showed that when co-cultured with the blood vessels both M1 and M2-related markers were upregulated (Figure 16). This suggested that a hybrid macrophage phenotype was formed. In order to further analyze this phenotype, we analyzed the data using single cell analysis, more specifically clustering and dimensionality reduction analysis.

Dimensionality reduction analysis, large-scale dimensionality reduction was performed using triplets (TriMap). This algorithm gave us an idea about global structure of the data, which is not obtained in the case of the most commonly known t-distribution Stochastic Neighborhood Embedding (tSNE) and Uniform Manifold Approximation and Projection (UMAP) algorithm, while keeping the complexity of the data, which is lost in the case of the Principal Component Analysis (PCA) (57). On the other hand, clustering enabled us to take into consideration only the macrophages that were affected by the blood vessels. The clustering analysis allows to group cells that show similar marker expression. For that, Flow Cytometry self-organizing map (FlowSOM) was used and all the data were clustered in 20 different

clusters (Figure 17A). Clusters 12, 14 and 17 were enriched in macrophages in baseline, clusters 0, 1, 2, 3 and 7 were enriched in macrophages seeded in the 3D scaffold and clusters 4, 5, 6, 8, 9, 10, 11, 13, 15, 16, 18 and 19 were enriched in macrophages co-cultured with cells, either endothelial or MSCs, or with the blood vessels. Particularly, macrophages seeded in the scaffold alone were found mostly in cluster 2, macrophages co-cultured with either blood vessels or MSCs in cluster 10 and macrophages co-cultured with endothelial cells in cluster 19 (Figure 17B).

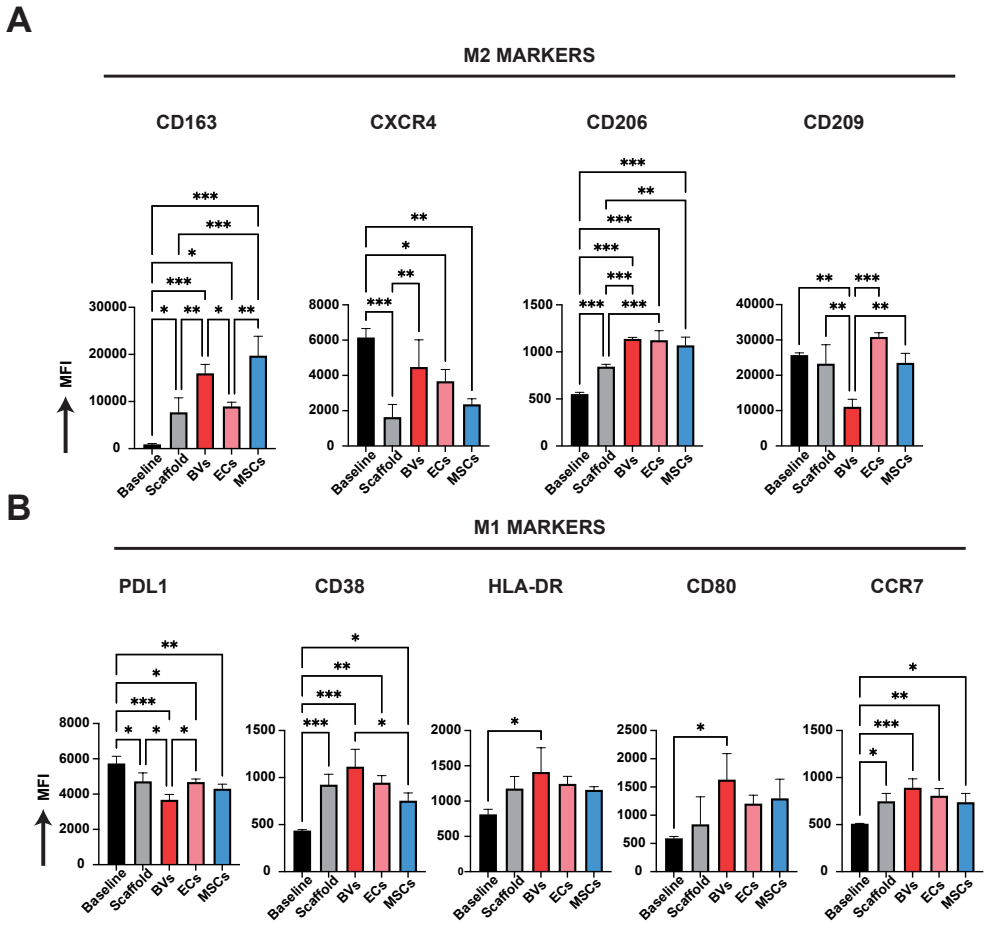

Figure 16: Crosstalk between undifferentiated (M0) macrophages and 3D collagen scaffold, tissue-engineered blood vessels, endothelial cells or MSCs (A) Median fluorescent intensity (MFI) of associated M2 markers (CD163, CXCR4, CD206, CD209). (B) MFI of associated M1 markers (PDL1, CD38, HLA-DR, CD80, CCR7). Data in (A, B) represents mean ± SD with n=3. Statistical significance: One way ANOVA with Tukey post hoc analysis *** $p < 0.001$ ** $p < 0.01$, * $p < 0.05$. BVs, blood vessels. ECs, endothelial cells. MSCs, mesenchymal stromal cells. MFI, median fluorescent intensity.

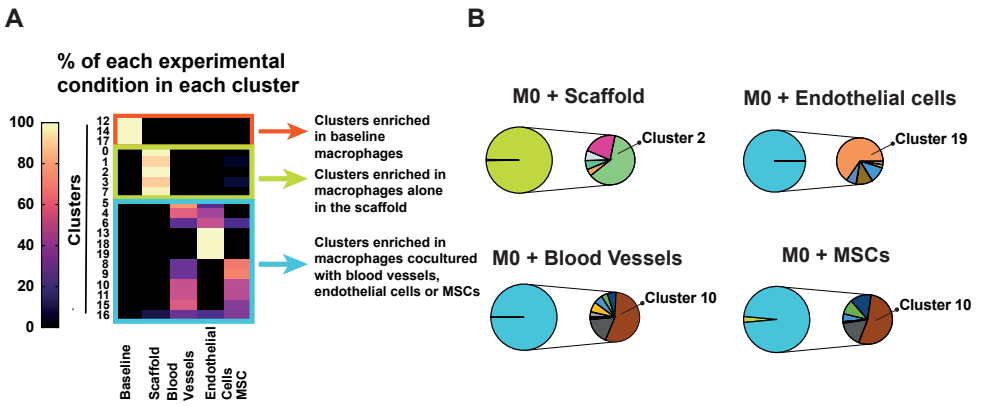

Figure 17: Clustering analysis of macrophages in the baseline, seeded in the 3D collagen scaffold, or co-cultured with tissue-engineered blood vessels, endothelial cells or MSCs. (A) Heat map showing the percentage of macrophages from each experimental condition that are within each cluster. (B) Pie charts showing how macrophages in the different experimental conditions are located in clusters enriched in baseline macrophages (orange), macrophages alone in the 3D scaffold (light green), or macrophages co-cultured with cells and blood vessels (light blue). The attached pie chart shows the exact cluster location for most macrophages in the different experimental conditions. MSCs, mesenchymal stromal cells.

To evaluate the similarity between different clusters Euclid algorithm was used to get the Taylor Index. Taylor index gives the information about the distance from one cluster to another in the dimensional space (58). How well the cluster are differentiated from one to another — the higher the Taylor index value —the higher the distance between two clusters and the less likely two clusters are related to each other (Figure 18A). Even the distance value between the 3 clusters is not very high; cluster 10 and 2 are the less similar ones, whereas cluster 10 and 19 are the most similar ones (Figure 18B), which can also be noticed in the dimensionality reduction map. Macrophages in cluster 10 and 19 are more concentrated than cluster 2, in the dimensionality reduction map (Figure 18C).As we have mentioned before, macrophages co-cultured in the 3D collagen scaffold mostly were located in cluster 2, where CD209 was highly expressed. Macrophages co-cultured with either blood vessels or MSCs were mostly located in cluster 10 which was upregulated in several M2 markers — CD163, CD206 and CD209 —. Finally, macrophages co-cultured with endothelial cells were located in cluster 19 in which also M2 markers were upregulated but to a lesser extent than in cluster 10 (Figure 19).

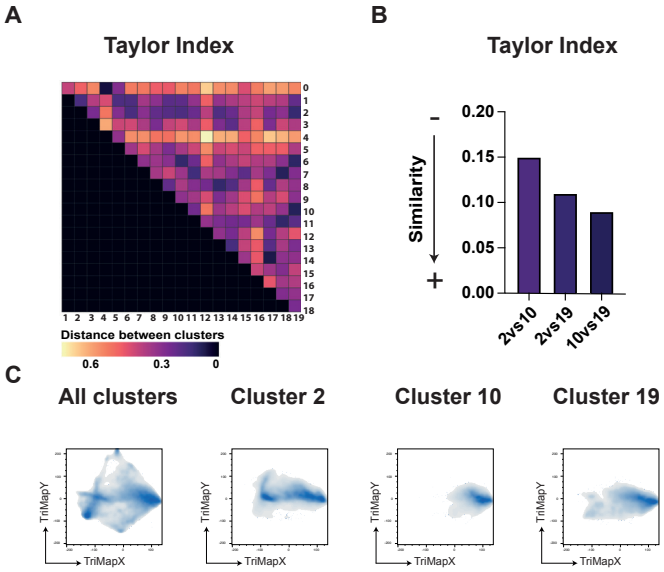

Figure 18: Taylor index and dimensionality reduction analysis (TriMAP) of M0 macrophages in the baseline, seeded in the 3D collagen scaffold, or co-cultured with tissue-engineered blood vessels, endothelial cells or MSCs. (A) Taylor index showing the similarity between every 2 clusters. (B) Bar-graphs showing the similarity between clusters 2, 10 and 19, which are the clusters where most of the macrophages converge to. (C) Localization of all clusters, cluster 2, 10, or 19 in TriMap plots.

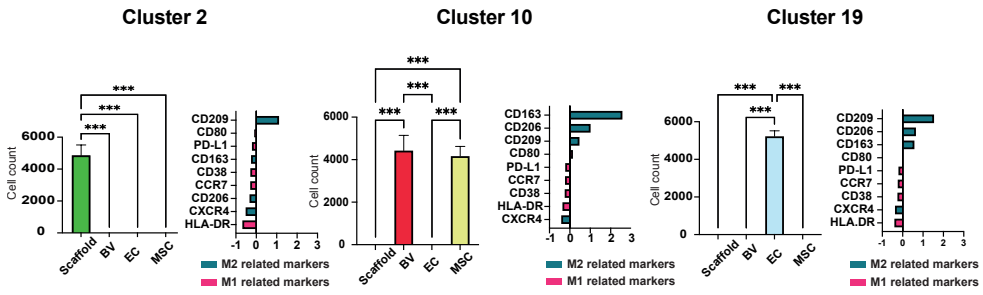

Figure 19: Composition of the main clusters when M0 macrophages were seeded in the 3D collagen scaffold, or co-cultured with tissue-engineered blood vessels, endothelial cells or MSCs. Bar graphs showing the exact composition of the main clusters (cluster 2, cluster 10 and cluster 19) and Z-scores showing the relative expression of each marker in each of these clusters. Data represents mean ± SD with n=3 biological replicates. BV, blood vessels. EC, endothelial cells. MSC, mesenchymal stromal cells. Statistical significance: *** $p < 0.001$ ** $p < 0.01$, * $p < 0.05$.

To determinate if the pre-polarization state has an effect in the macrophage-blood vessel crosstalk we followed the same approach with pre-polarized M1, M2 and M1M2 macrophages. Using this procedure, we observed that both M0 and M2 macrophages phenotypes showed a high differentiation capacity with more than 95 % of macrophages changing phenotypes whereas M1 and M1M2 macrophages were less plastic with only the 25 % and 50 % of macrophages switching phenotypes when cultured in the presence of blood vessels, respectively (Figure 20).

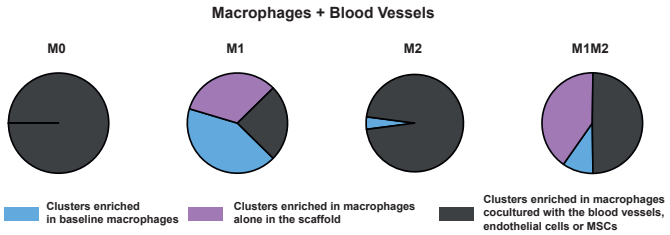

Figure 20: Pie charts showing how different pre-polarized macrophages (M0, M1, M2 and M1M2) tend to migrate to different clusters after the co-culture with blood vessels.

Interestingly, in the case of M0, M1 and M2 macrophages, the effect of the blood vessels seems that was driven by the MSCs — cluster 10 for M0, cluster 14 for M1 and cluster 3 and 9 for M2 —, whereas in the case of M1M2 the effect was independent to the one exerted by endothelial cells and MSCs — cluster 5 and 0 for M1M2 — (Figure 21). This comes in concordance of several studies that have described how MSCs are able to promote the polarization of macrophages towards a M2 phenotype which is characterized by an increased production of IL-10 and high

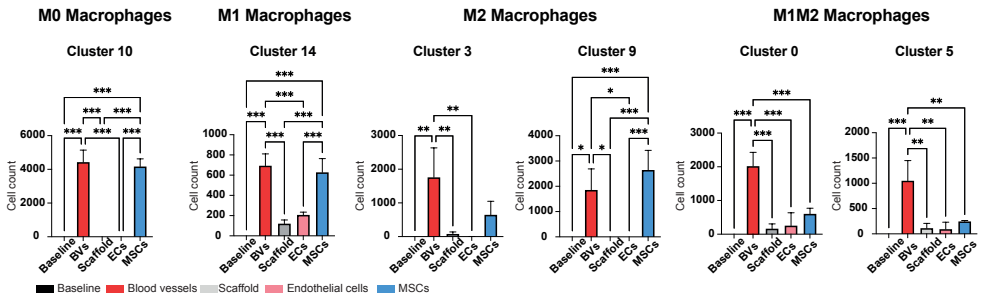

Figure 21: Composition of the main clusters when M0, M1, M2 or M1M2 macrophages were co-cultured with tissue-engineered blood vessels. BVs, blood vessels. ECs, endothelial cells. MSCs, mesenchymal stromal cells. Data represents mean ± SD with n=3 biological replicates. Statistical significance: *** $p < 0.001$ ** $p < 0.01$, * $p < 0.05$.

expression of CD163 and/or CD206 markers (59-61) and reviewed in (62).

When M0 macrophages were co-cultured with the tissue-engineered blood vessels, we noticed that only M2 markers were upregulated (CD206, CD209 and CD163) (Figure 22). However, recently, O'Brien et al. reviewed the importance of the timing of the macrophage transition (17). It has been already described that early treatment with M2 macrophages leads to impaired integration and fibrous capsule formation (55). For this reason, there is a need to tightly control the temporal activation of the macrophage transition. Therefore, it is important to avoid early M2 macrophage stimulation or addition (63, 64). Interestingly, when either M1, M2 and M1M2 macrophages were co-cultured with the blood vessels not only M2 markers were upregulated but also different M1 markers, suggesting a possible mixed phenotype. In the case of M1 and M1M2 macrophages the high expression of most M1 markers expressed in the baseline was mostly lost, however, some residual M1 expression was still observed suggesting a transition from the pro-inflammatory

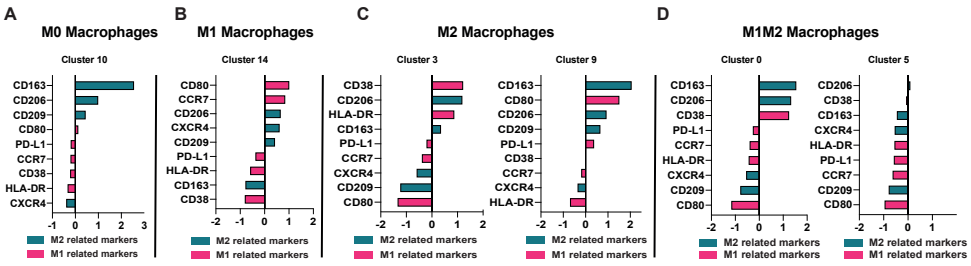

Figure 22: Composition of the clusters enriched in macrophages co-cultured with blood vessels. (A-D) Z-scores showing the relative expression of each marker in each of these clusters that are enriched in M0, M1, M2, M1M2 macrophages co-cultured with the blood vessels. Data represents mean ± SD with n=3 biological replicates

phenotype towards a more regulatory one.

Until now, we have described how each macrophage phenotype (M0, M1, M2 and M1M2) changed when co-cultured with tissue-engineered blood vessels, by comparing it when they were seeded in the scaffold alone or when they were co-cultured with endothelial cells or MSCs separately. In the following section, we changed the approach such that the comparison between the different pre-polarization states (M0, M1, M2, M1M2) co-cultured with the blood vessels together in the same analysis (Figure 23). Towards this, we performed the same study as mentioned before, however, instead of adding the groups of macrophages co-cultured

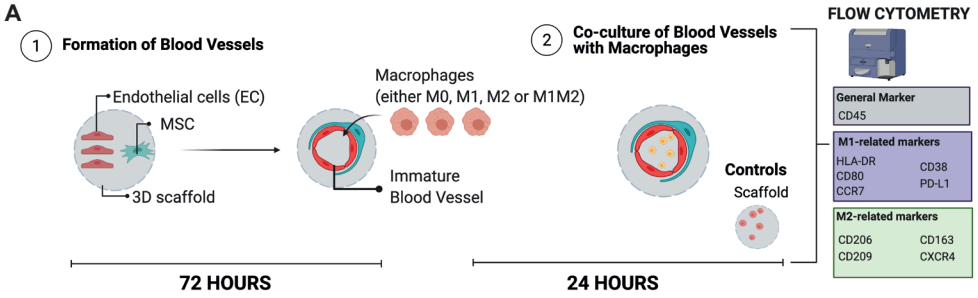

Figure 23: Schematic of the study. *In vitro* tissue-engineered human blood vessels were generated by co-culture of endothelial cells and MSCs on 3D collagen scaffolds. Primary human peripheral blood monocytes were differentiated into macrophages (M0) and polarized into M1, M2 or M1M2. After 3 days, M0, M1, M2 or M1M2 macrophages were added to either the acellular 3D scaffold or the 3D scaffold with engineered blood vessels. Changes in macrophage phenotype were observed one day after macrophage seeding by flow cytometry analysis.

alone in the scaffold, macrophages co-cultured with either blood vessels, MSCs or endothelial cells, we run the single cell analysis with the different macrophage pre-polarization states (M0, M1, M2, M1M2) co-cultured with blood vessels or within the scaffold alone. This approach enabled us to compare how each pre-polarization state responded to the crosstalk with blood vessels.

The analysis showed that, each of the different macrophages were found in different clusters —M0 to clusters 14 and 10, M1 to cluster 12, M2 to cluster 5 and M1M2 to cluster 0 and 12— and each of these clusters expressed different M1 and M2 markers (Figure 24).

Interestingly, M1 and M1M2 macrophages shared cluster location in cluster 12 (Figure 25A). Moreover, M1M2 are found also in cluster 0, which has the shortest distance from the cluster 5 — an M2 cluster — of all the clusters analyzed (Figure 25B, C, D). This could mean that M1M2 macrophages share more similarities with M2 macrophages than was initially observed. Clustering is essentially grouping cells in discrete defined populations regarding their markers expression profiles, but does not give information about the temporal relationships between clusters. However, using pseudo-time analysis, it could be analyzed (65). This could mean that tissue -engineered blood vessels would promote the perfect timing in the M1-M2 transition.

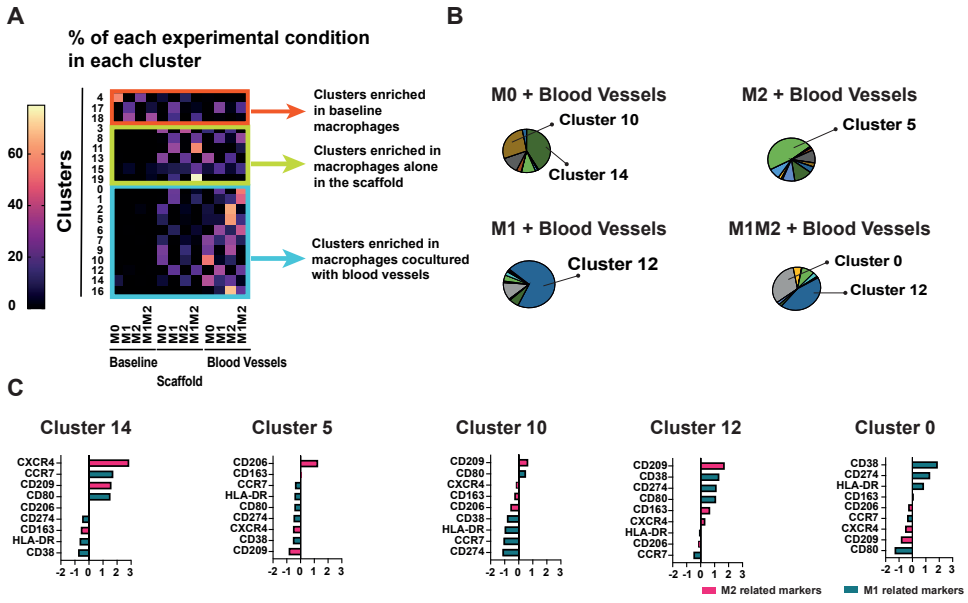

Figure 24: Clustering and cluster composition analysis of M0, M1, M2 or M1M2 macrophages in the baseline, seeded in the 3D collagen scaffold, or co-cultured with tissue-engineered blood vessels. (A) Heat map showing the percentage of macrophages from each experimental condition that are within each cluster enriched in baseline macrophages (orange), macrophages alone in the 3D scaffold (light green), or macrophages co-cultured with cells and blood vessels (light blue). (B) Pie charts showing how macrophages in the different experimental conditions are located in different clusters. (C) Z-scores showing the relative expression of each marker in each of these clusters that are enriched in M0, M1, M2, M1M2 macrophages co-cultured with the blood vessels. Data represents mean ± SD with n=3 biological replicates.

In summary, we showed that macrophages with distinct phenotypes all upregulated M2 markers (CD206 and CD163) when co-cultured with tissue engineered blood vessels. However, they did also upregulate different markers depending on their pre-polarization state. With this perspective, we are allowed to state that pre-polarization state influenced the crosstalk outcome with blood vessels. Interestingly, our data suggested that blood vessels influenced macrophages to take on phenotypes that are beneficial for both early and late angiogenesis. Moreover, the clustering and dimensionality reduction analysis showed that the phenotypical change occurring in M0, M1 and M2 macrophages was exerted mostly by the MSCs

presented in the blood vessels, whereas in the case of the M1M2 macrophages the effect was independent. Lastly, analyzing all the macrophage phenotype together, we found out that the M1M2 macrophage phenotype could be a temporal transition between M1 and M2 phenotype. This finding could suggest that tissue-engineered blood vessels would promote the perfect timing in the M1 to M2 transition. This could help in macrophage transition towards a more regenerative phenotype and

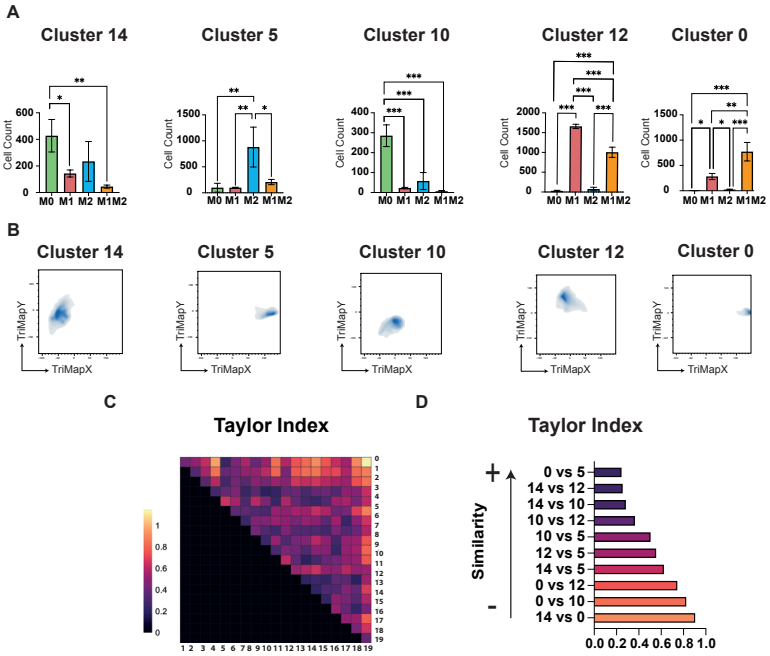

Figure 25: Cluster composition and similarity between the clusters. (A) Composition of the main clusters. (B) Localization of cluster 14, 5, 10, 12 and 0 in TriMap plots. (C) Taylor index showing the similarity between every 2 clusters. (D) Bar-graphs showing the similarity between clusters 14, 5, 10, 12 and 0, which are the clusters where most of the macrophages converge to. Data in (A) represents mean ± SD with n=3 biological replicates. Statistical significance: *** $p < 0.001$ ** $p < 0.01$, * $p < 0.05$.

eventually helping in the biomaterial integration.

Ultimately, in this doctoral thesis we have focused on the study of two different strategies to try to improve implant integration through interacting with the host immune system. Therefore, with our results, we can conclude that both strategies can have an important developmental impact towards the implementation of immunomodulatory techniques and could have important consequences for tissue engineering.

REFERENCES

1. Wadström J, Ericzon B-G, Halloran PF, Bechstein WO, Opelz G, Serón D, et al. Advancing transplantation: new questions, new possibilities in kidney and liver transplantation. Transplantation. 2017;101(2).
2. Dangi A, Yu S, Luo X. Emerging approaches and technologies in transplantation: the potential game changers. Cell Mol Immunol. 2019;16(4):334-42.
3. Langer R, Vacanti JP. Tissue-Engineering. Science. 1993;260(5110):920.
4. Anderson JM, Rodriguez A, Chang DT. Foreign body reaction to biomaterials. Semin Immunol. 2008;20(2):86-100.
5. Franz S, Rammelt S, Scharnweber D, Simon JC. Immune responses to implants – A review of the implications for the design of immunomodulatory biomaterials. Biomaterials. 2011;32(28):6692-709.
6. Huyer LD, Pascual-Gil S, Wang Y, Mandla S, Yee B, Radisic M. Advanced strategies for modulation of the material–macrophage interface. Adv Funct Mater. 2020:1909331.
7. Kim B-S, Tilstam PV, Springenberg-Jung K, Boecker AH, Schmitz C, Heinrichs D, et al. Characterization of adipose tissue macrophages and adipose-derived stem cells in critical wounds. PeerJ. 2017;5:e2824.
8. Daley JM, Brancato SK, Thomay AA, Reichner JS, Albina JE. The phenotype of murine wound macrophages. Journal of Leukocyte Biology. 2010;87(1):59-67.
9. Graney PL, Ben-Shaul S, Landau S, Bajpai A, Singh B, Eager J, et al. Macrophages of diverse phenotypes drive vascularization of engineered tissues. Science Advances, 2020. 6(18)
10. Lurier EB, Dalton D, Dampier W, Raman P, Nassiri S, Ferraro NM, et al. Transcriptome analysis of IL-10-stimulated (M2c) macrophages by next-generation sequencing. Immunobiology. 2017;222(7):847-56.
11. Spiller KL, Nassiri S, Witherel CE, Anfang RR, Ng J, Nakazawa KR, et al. Sequential delivery of immunomodulatory cytokines to facilitate the M1-to-M2 transition of macrophages and enhance vascularization of bone scaffolds. Biomaterials. 2015;37:194-207.
12. Rao AJ, Gibon E, Ma T, Yao Z, Smith RL, Goodman SB. Revision joint replacement, wear particles, and macrophage polarization. Acta Biomaterialia. 2012;8(7):2815-23.
13. Zhang DKY, Cheung AS, Mooney DJ. Activation and expansion of human T cells using artificial antigen-presenting cell scaffolds. Nature Protocols. 2020;15(3):773-98.
14. Ben-Shaul S, Landau S, Merdler U, Levenberg S. Mature vessel networks in engineered tissue promote graft–host anastomosis and prevent graft thrombosis. Proceedings of the National Academy of Sciences. 2019;116(8):2955.
15. Kubota Y, Takubo K, Shimizu T, Ohno H, Kishi K, Shibuya M, et al. M-CSF inhibition selectively targets pathological angiogenesis and lymphangiogenesis. Journal of Experimental Medicine. 2009;206(5):1089-102.
16. Hirose N, Maeda H, Yamamoto M, Hayashi Y, Lee G-H, Chen L, et al. The local injection of peritoneal macrophages induces neovascularization in rat ischemic hind limb muscles:. http://dxdoiorg/103727/000000008783906919. 2008.
17. O'Brien EM, Risser GE, Spiller KL. Sequential drug delivery to modulate macrophage behavior and enhance implant integration. Advanced Drug Delivery Reviews. 2019;149-150:85-94.
18. Le Blanc K, Ringdén O. Immunomodulation by mesenchymal stem cells and clinical experience. Journal of Internal Medicine. 2007;262(5):509-25.
19. Kim J, Hematti P. Mesenchymal stem cell–educated macrophages: A novel type of alternatively activated macrophages. Experimental Hematology. 2009;37(12):1445-53.
20. Németh K, Leelahavanichkul A, Yuen PST, Mayer B, Parmelee A, Doi K, et al. Bone marrow

stromal cells attenuate sepsis via prostaglandin E2–dependent reprogramming of host macrophages to increase their interleukin-10 production. Nature Medicine. 2009;15(1):42-9.
21. de Witte SFH, Luk F, Sierra Parraga JM, Gargesha M, Merino A, Korevaar SS, et al. Immunomodulation by therapeutic mesenchymal stromal cells (MSC) is triggered through phagocytosis of MSC by monocytic cells. Stem Cells. 2018;36(4):602-15.
22. Friedenstein AJ, Chailakhjan RK, Lalykina KS. The development of fibroblast colonies in monolayer cultures of guinea-pig bone marrow and spleen cells. Cell Proliferation. 1970;3(4):393-403.
23. Andrzejewska A, Lukomska B, Janowski M. Concise Review: mesenchymal stem cells: from roots to boost. Stem Cells. 2019;37(7):855-64.
24. Shi Y, Wang Y, Li Q, Liu K, Hou J, Shao C, et al. Immunoregulatory mechanisms of mesenchymal stem and stromal cells in inflammatory diseases. Nature Reviews Nephrology. 2018;14(8):493-507.
25. Elahi KC, Klein G, Avci-Adali M, Sievert KD, MacNeil S, Aicher WK. Human mesenchymal stromal cells from different sources diverge in their expression of cell surface proteins and display distinct differentiation patterns. Stem Cells International. 2016;2016:5646384.
26. Yin JQ, Zhu J, Ankrum JA. Manufacturing of primed mesenchymal stromal cells for therapy. Nat Biomed Eng. 2019;3(2):90-104.
27. Strioga M, Viswanathan S, Darinskas A, Slaby O, Michalek J. Same or not the same? Comparison of adipose tissue-derived versus bone marrow-derived mesenchymal stem and stromal cells. stem cells and development. 2012;21(14):2724-52.
28. Conley SM, Hickson LJ, Kellogg TA, McKenzie T, Heimbach JK, Taner T, et al. Human obesity induces dysfunction and early senescence in adipose tissue-derived mesenchymal stromal/stem cells. Frontiers in Cell and Developmental Biology. 2020;8(197).
29. Rady D, Abbass MMS, El-Rashidy AA, El Moshy S, Radwan IA, Dörfer CE, et al. Mesenchymal stem/progenitor cells: the prospect of human clinical translation. Stem Cells International. 2020;2020:8837654.
30. Serena C, Keiran N, Ceperuelo-Mallafre V, Ejarque M, Fradera R, Roche K, et al. Obesity and type 2 diabetes alters the immune properties of human adipose derived stem cells. Stem Cells. 2016;34(10):2559-73.
31. Fernandes KJL, McKenzie IA, Mill P, Smith KM, Akhavan M, Barnabé-Heider F, et al. A dermal niche for multipotent adult skin-derived precursor cells. Nature Cell Biology. 2004;6(11):1082-93.
32. Waters JM, Richardson GD, Jahoda CAB. Hair follicle stem cells. Seminars in Cell & Developmental Biology. 2007;18(2):245-54.
33. Owczarczyk-Saczonek A, Krajewska-Włodarczyk M, Kruszewska A, Banasiak Ł, Placek W, Maksymowicz W, et al. Therapeutic potential of stem cells in follicle regeneration. Stem Cells International. 2018;2018:1049641.
34. Martin I, Galipeau J, Kessler C, Le Blanc K, Dazzi F. Challenges for mesenchymal stromal cell therapies. Science Translational Medicine. 2019;11(480):eaat2189.
35. Zimmermann JA, Hettiaratchi MH, McDevitt TC. Enhanced immunosuppression of T cells by sustained presentation of bioactive interferon-γ within three-dimensional mesenchymal stem cell constructs. Stem Cells Translational Medicine. 2017;6(1):223-37.
36. Ankrum JA, Ong JF, Karp JM. Mesenchymal stem cells: immune evasive, not immune privileged. Nature Biotechnology. 2014;32(3):252-60.
37. Gonzalez-Pujana A, Igartua M, Santos-Vizcaino E, Hernandez RM. Mesenchymal stromal cell based therapies for the treatment of immune disorders: recent milestones and future challenges. Expert Opinion on Drug Delivery. 2020;17(2):189-200.
38. Niederkorn JY. See no evil, hear no evil, do no evil: the lessons of immune privilege. Nature Immunology. 2006;7(4):354-9.

39. Pokrywczynska M, Maj M, Kloskowski T, Buhl M, Balcerczyk D, Jundził A, et al. Molecular aspects of adipose-derived stromal cell senescence in a long-term culture: A potential role of inflammatory pathways. Cell Transplantation. 2020;29:0963689720917341.
40. Lee H-J, Kim S-N, Jeon M-S, Yi T, Song SU. ICOSL expression in human bone marrow-derived mesenchymal stem cells promotes induction of regulatory T cells. Sci Rep. 2017;7:44486-.
41. English K, Ryan JM, Tobin L, Murphy MJ, Barry FP, Mahon BP. Cell contact, prostaglandin E2 and transforming growth factor beta 1 play non-redundant roles in human mesenchymal stem cell induction of $CD4^{+}CD25^{High}FoxP3^{+}$ regulatory T cells. Clinical & Experimental Immunology. 2009;156(1):149-60.
42. Maccario R, Podestà M, Moretta A, Cometa A, Comoli P, Montagna D, et al. Interaction of human mesenchymal stem cells with alloantigen-induced T lymphocyte activation favors the differentiation of $CD4^{+}$ T cell subsets expressing CD25 and/or CTLA4 molecules. Blood. 2004;104(11):2123-.
43. Li H, Masieri FF, Schneider M, Kottek T, Hahnel S, Yamauchi K, et al. Autologous, Non-Invasively Available Mesenchymal Stem Cells from the Outer Root Sheath of Hair Follicle Are Obtainable by Migration from Plucked Hair Follicles and Expandable in Scalable Amounts. Cells. 2020;9(9).
44. Cutler AJ, Limbani V, Girdlestone J, Navarrete CV. Umbilical cord-derived mesenchymal stromal cells modulate monocyte function to suppress T cell proliferation. The Journal of Immunology. 2010;185(11):6617.
45. Santos-Vizcaino E, Salvador A, Vairo C, Igartua M, Hernandez RM, Correa L, et al. Overcoming the inflammatory stage of non-healing wounds: *In vitro* mechanism of action of negatively charged microspheres (NCMs). Nanomaterials. 2020;10(6).
46. Zhang Q-Z, Su W-R, Shi S-H, Wilder-Smith P, Xiang AP, Wong A, et al. Human gingiva-derived mesenchymal stem cells elicit polarization of M2 macrophages and enhance cutaneous wound healing. Stem Cells. 2010;28(10):1856-68.
47. Melief SM, Schrama E, Brugman MH, Tiemessen MM, Hoogduijn MJ, Fibbe WE, et al. Multipotent stromal cells induce human regulatory T cells through a novel pathway involving skewing of monocytes toward anti-inflammatory macrophages. Syem Cells. 2013;31(9):1980-91.
48. Witherel CE, Sao K, Brisson BK, Han B, Volk SW, Petrie RJ, et al. Regulation of extracellular matrix assembly and structure by hybrid M1/M2 macrophages. Biomaterials. 2021;269:120667.
49. Badylak SF, Valentin JE, Ravindra AK, McCabe GP, Stewart-Akers AM. Macrophage phenotype as a determinant of biologic scaffold remodeling. Tissue Eng Pt A. 2008;14(11):1835-42.
50. Graney PL, Roohani-Esfahani S-I, Zreiqat H, Spiller KL. In vitro response of macrophages to ceramic scaffolds used for bone regeneration. J Roy Soc Interface. 2016;13(120):20160346.
51. Graney PL, Ben-Shaul S, Landau S, Bajpai A, Singh B, Eager J, et al. Macrophages of diverse phenotypes drive vascularization of engineered tissues. Science Advances. 2020;6(18):eaay6391.
52. Hur J, Choi J-I, Yun J-Y, Yoon C-H, Jang JH, Im S-G, et al. Highly angiogenic CXCR4+CD31+ monocyte subset derived from 3D culture of human peripheral blood. Biomaterials. 2013;34(8):1929-41.
53. Seeger Florian H, Rasper T, Koyanagi M, Fox H, Zeiher Andreas M, Dimmeler S. CXCR4 expression determines functional activity of bone marrow–derived mononuclear cells for therapeutic neovascularization in acute ischemia. Arteriosclerosis, Thrombosis, and Vascular Biology. 2009;29(11):1802-9.
54. Spiller KL, Anfang RR, Spiller KJ, Ng J, Nakazawa KR, Daulton JW, et al. The role of macrophage phenotype in vascularization of tissue engineering scaffolds. Biomaterials. 2014;35(15):4477-88.
55. Jetten N, Verbruggen S, Gijbels MJ, Post MJ, Winther MPJD, Donners MMPC. Anti-inflammatory M2, but not pro-inflammatory M1 macrophages promote angiogenesis in vivo. Angiogenesis. 2014;17(1):109-18.
56. Hind LE, Lurier EB, Dembo M, Spiller KL, Hammer DA. Effect of M1–M2 polarization on the motility and traction stresses of primary human macrophages. Cell Mol Bioeng. 2016;9(3):455-65.

57. Wang Y, Huang H, Rudin C, Shaposhnik Y. Understanding how dimension reduction tools work: An empirical approach to deciphering t-SNE, UMAP, TriMAP, and PaCMAP for data visualization. arXiv pre-print server. 2020.
58. Hartigan PM. Algorithm AS 217: Computation of the dip statistic to test for unimodality. Journal of the Royal Statistical Society Series C (Applied Statistics). 1985;34(3):320-5.
59. Giri J, Das R, Nylen E, Chinnadurai R, Galipeau J. CCL2 and CXCL12 Derived from mesenchymal stromal cells cooperatively polarize IL-10^{+} tissue macrophages to mitigate gut injury. Cell Reports. 2020;30(6):1923-34.e4.
60. Witte SFHd, Luk F, Parraga JMS, Gargesha M, Merino A, Korevaar SS, et al. Immunomodulation by therapeutic mesenchymal stromal cells (MSC) is triggered through phagocytosis of MSC by monocytic cells. Stem Cells. 2018;36(4):602-15.
61. Luz-Crawford P, Djouad F, Toupet K, Bony C, Franquesa M, Hoogduijn MJ, et al. Mesenchymal stem cell-derived interleukin 1 receptor antagonist promotes macrophage polarization and inhibits B cell differentiation. Stem Cells. 2016;34(2):483-92.
62. Weiss ARR, Dahlke MH. Immunomodulation by mesenchymal stem cells (MSCs): mechanisms of action of living, apoptotic, and dead MSCs. Frontiers in Immunology. 2019;10(1191).
63. Nassiri S, Zakeri I, Weingarten MS, Spiller KL. Relative expression of proinflammatory and antiinflammatory genes reveals differences between healing and nonhealing human chronic diabetic foot ulcers. J Invest Dermatol. 2015;135(6):1700-3.
64. Mirza R, Koh TJ. Dysregulation of monocyte/macrophage phenotype in wounds of diabetic mice. Cytokine. 2011;56(2):256-64.
65. Melsen JE, van Ostaijen-ten Dam MM, Lankester AC, Schilham MW, van den Akker EB. A comprehensive workflow for applying single-cell clustering and pseudotime analysis to flow cytometry data. The Journal of Immunology. 2020;205(3):864.

6

Conclusions

Conclusions

Experimental results prompt us to make the following conclusions from the doctoral thesis:

1. The stromal cells obtained from the lower dermal sheath/ dermal papilla of human hair follicles (HF-MSCs) expressed neural markers (CD56, SOX-2, CD271) and maintained their stemness properties for at least 10 passages. This indicates that HF-MSCs could be used for at least 10 passages without losing their stemness capacity. Furthermore, HF-MSCs can be obtained via painless, less invasive, and lower infection risk harvesting procedure comparing to the most studied sources of MSCs — bone marrow and adipose tissue—.
2. HF-MSCs showed responsiveness to the pro-inflammatory cytokine IFNγ while retaining immune-privilege status better than adipose tissue-derived mesenchymal stromal cells (AT-MSCs). This attribute could be very useful considering the limited number of cells available for autologous use, HF-MSCs could be a suitable allogeneic alternative for MSC-based cell therapy.
3. Importantly, HF-MSCs exhibited immunomodulatory properties at least comparable to those of AT-MSCs, regarding the interaction with cells of both the innate and adaptative immune systems. Considering all the advantages mentioned above, we were able to conclude that HF-MSCs can be an important and feasible alternative over AT-MSCs, thereby making it a highly probable and potential candidate for implant integration.
4. The co-culture of macrophages with tissue-engineered blood vessels demonstrated the complexity of macrophage phenotype that does not come in concordance with the traditional and simplistic M1 and M2 classification; macrophages co-cultured with blood vessels upregulated both M1 and M2-related markers.
5. With respect to M0, M1 and M2 macrophages, it was observed that the effect of blood vessels was primarily driven by MSCs. This reinforces the immunomodulatory role MSCs have in the innate immune response.
6. The addition of tissue-engineered blood vessels to the biomaterial resulted in skewing undifferentiated (M0) and macrophages from different pre-polarization states (M1, M2 and M1M2) towards a more regenerative, M2 phenotype. Furthermore, each pre-polarization state also upregulated distinct M1 markers. This finding could suggest that tissue-engineered blood vessels could promote the perfect M1 to M2 transition and eventually helping with biomaterial integration.